HAL
archives-ouvertes.fr

Innovative and integrated approach for environmentally efficient aircraft design and operations

Sylvain Prigent

▶ **To cite this version:**

Sylvain Prigent. Innovative and integrated approach for environmentally efficient aircraft design and operations. Optimization and Control [math.OC]. ISAE - Institut Supérieur de l'Aéronautique et de l'Espace, 2015. English. <NNT : 2015ESAE0014>. <tel-01379914>

HAL Id: tel-01379914

https://hal.archives-ouvertes.fr/tel-01379914

Submitted on 12 Oct 2016

HAL is a multi-disciplinary open access archive for the deposit and dissemination of scientific research documents, whether they are published or not. The documents may come from teaching and research institutions in France or abroad, or from public or private research centers.

L'archive ouverte pluridisciplinaire **HAL**, est destinée au dépôt et à la diffusion de documents scientifiques de niveau recherche, publiés ou non, émanant des établissements d'enseignement et de recherche français ou étrangers, des laboratoires publics ou privés.

Université Fédérale
Toulouse Midi-Pyrénées

THÈSE

En vue de l'obtention du

DOCTORAT DE L'UNIVERSITÉ DE TOULOUSE

Délivré par :

Institut Supérieur de l'Aéronautique et de l'Espace

Présentée et soutenue par :
Sylvain PRIGENT
le jeudi 17 septembre 2015

Titre :
Approche novatrice pour la conception et l'exploitation d'avions écologiques

Innovative and integrated approach for environmentally efficient aircraft design and operations

---

École doctorale et discipline ou spécialité :
ED MITT : Domaine Mathématiques : Mathématiques appliquées

Unité de recherche :
Equipe d'accueil ISAE-ONERA MOIS

Directeur/trice(s) de Thèse :

M. Pierre MARECHAL (Directeur de thèse)
Mme Aude RONDEPIERRE (Co-directrice de thèse)

Jury :
M. Christian BES, Professeur d'Université, ICA - Président du jury
M. Pierre MARECHAL, Professeur des universités, IMT - Directeur de thèse
Mme Aude RONDEPIERRE, Maître de conférence, IMT - Co-directrice de thèse
M. Abdel LISSER, Professeur d'Université, Paris Sud - Rapporteur
M. Peppino TERPOLILLI, Chercheur mathématicien, Total - Rapporteur
M. Laëtitia ANDRIEU, Chef de groupe EDF-R&D
M. Térence BAYEN, Maître de conférence, Montpellier 2
Mme Patricia KLOTZ, Ingénieur de recherche, ONERA

"Anytime you have a 50-50 chance of getting something right, there's a 90% probability you'll get it wrong."
Andy Rooney

"Essentially, all models are wrong, but some are useful."
George Box

Remerciements

Ces trois années se terminent alors qu'elles me semblaient tout juste avoir commencé. Je tiens à remercier profondément toutes les personnes que j'ai côtoyées de près ou de loin pendant cette aventure. Ce travail n'aurait pas été possible sans leur inébranlable soutien, leurs judicieux conseils, leur éternelle sympathie et leur patience. Je leur suis très reconnaissant, pour l'ensemble indénombrable des richesses qu'ils m'ont apportées, autant sur le plan professionnel que sur le plan personnel.

Je remercie vivement mes encadrants, Thierry Druot et Mathieu Belleville du coté industriel, Aude Rondepierre et Pierre Maréchal du coté académique, sans qui tout cela aurait été réduit à l'ensemble vide. Je remercie Thierry qui m'a fait confiance dès le début et qui m'a permis de vivre cette merveilleuse aventure. Merci Thierry et Mathieu pour votre patience, votre pédagogie, votre disponibilité, et vos nombreux conseils. Merci Aude pour ton soutien, ton écoute et toute la motivation que tu m'as apportée. Merci à toi et Pierre pour vos conseils, votre aide précieuse dans le développement de ce travail. Merci à tous les quatre pour votre encadrement et vos encouragements, vous avez été pour moi une source inépuisable de connaissances et de motivation.

Je remercie sincèrement les rapporteurs, Abdel Lisser et Peppino Terpolilli, pour le temps et l'attention qu'ils ont apportés à la relecture de cette thèse et pour leur travail en tant que rapporteurs.

Mes remerciements s'adressent également à Christian Bes, Laëtitia Andrieu, Terence Bayen et Patricia Klotz qui ont accepté de participer au jury. J'en suis très honoré.

Je remercie Jean-Baptiste Hiriart-Urruty pour ses relectures et son aide précieuse.

Je remercie la société Airbus, et en particulier Messieurs Philippe Escarnot, Jean-Jacques Mirat, Jaime-Jacques Genty-De-La-Sagne, Laurent Marin, pour leur accueil au sein des avant-projets et leur contribution à l'excellent déroulement de cette thèse.

Je suis tout particulièrement reconnaissant envers Mattia Padulo qui m'a permis d'apprendre énormément sur l'univers incertain de cette thèse. Merci également pour ta précieuse aide sur les travaux que nous avons menés ensemble.

J'associe à ces remerciements chaque personne qui m'a accompagné de près ou de loin pendant la thèse. Merci à tous mes collègues des avant-projets pour leur constant soutien, leur disponibilité, leur sympathie et leur bonne humeur. J'ai beaucoup appris à vos

côtés, et je vous suis très reconnaissant quant à l'ambiance de travail. Merci Catherine, Céline, Michel, Jessie, Sole, Christophe, Sergio, Cécile, Yann, Antoine, Renaud, Matthieu, Stéphane, Guillaume, Philippe, Julien, Gilles, Thierry, Eric, Claire(s), Marylène, Mickaël. Un remerciement particulier à mes compagnons de box, Manuel, Markus, Jérôme(s), Paul, Martin. Merci Olive pour les magnifiques dessins Catia, pour la maquette 3D et pour tes encouragements. Merci également à Manon, qui m'a supporté lors de la conférence OPT-i 14.

Je remercie sans égal Marie-Julie, de m'avoir encouragé au quotidien, et d'avoir toujours cru en moi. Je remercie profondément mes parents Pierrette et Michel et ma sœur Maïlys pour leurs encouragements, et pour tout ce qu'ils ont fait pour moi. Je tiens aussi à remercier sincèrement Christian et Valérie pour leur soutien et le cadre de vie qu'ils m'ont permis d'avoir pendant ces trois années. Je remercie enfin toute ma famille et tous mes amis, qui m'ont soutenu de près ou de loin et qui ont surtout toujours cru en moi.

Pour toutes ces raisons, et surtout toutes celles que j'oublie de citer, je vous dédicace ce manuscrit.

Summary

Since the 50s, the air traffic is in constant growth. The actors of air transport - the engine manufacturers, the aircraft manufacturers, and the airlines - are focused on issues of their own business. This sometimes proves to be restrictive. Moreover, objectives of reduction of the climatic impact of the aviation recently appeared and must be taken into account in the preliminary aircraft design phase.

During this phase, the aircraft manufacturer studies the performances of various configurations. This study is modeled as a deterministic multidisciplinary optimization under constraints. The criteria are the minimization of the fuel consumption, the global operating cost of the aircraft or the maximum take-off weight (which measures the global efficiency of the aircraft). The constraints are defined by the specifications. The degrees of freedom of this optimization are generally the wing area and the engine size. These studies are sometimes based on very simplified models. The reasons are mostly the computation time and the lack of knowledge on the approached concepts.

This thesis introduces a new holistic approach of the aircraft design optimization problem: we aggregate into the classical models, more accurate models of the propellant part and the trajectory. For that purpose, we first familiarize with the existing models in order to understand the interactions between the involved disciplines. We then validate the integration of the more accurate models in the existing tools, by matching it with existing aircrafts. A contribution of this thesis is to integrate parameters of the engine and of the mission into the usual degrees of freedom. The study of the results presents the benefits brought by this new approach.

We also incorporate the climate impact to the optimization objectives.

Also, during the preliminary aircraft design phase, innovative technologies are studied, which can be integrated into the propellant system of the aircraft, into its aerodynamic system, or into its geometry. We select some of them in order to obtain the configuration with the best possible performances. We suggest applying the holistic approach to a concept of aircraft with an hybrid fuel-electric propulsion system. The corresponding models are presented and are added to the existing ones, after validation by the experts. The results of this optimization are compared with those of a conventional aircraft satisfying the same specifications.

All the studies led until now are deterministic. Until now, the uncertainties around the models are taken into account by margins, which are based on engineer know-how. It can sometimes lead to unexpected disappointing performances. So, we introduce a new approach which consists in carefully taking into account these uncertainties. For that purpose, we list, compare and select methods of uncertainty management which could be applied to our design problem. This is done according to criteria such as the computa-

tion time, the accuracy, and the hypotheses on the models. We then suggest solving a chance constrained optimization of the hybrid aircraft concept, by taking into account the uncertainties coming from the evolution of the technologies required by the hybridization.

Finally, this thesis presents a new approach of aircraft preliminary design via robust optimization. We suggest finding an optimal plane of which the performances are satisfied whatever the uncertainty. This approach is complementary to the chance constrained approach. The implementation of robust optimization requires a particular modeling of the problem which is described in this thesis.

Key words: Aircraft preliminary design modeling and optimization, uncertainty propagation, chance constrained optimization, robust optimization.

Résumé

Depuis les années 1950, le trafic aérien est en constante croissance. Les acteurs du transport aérien - les constructeurs de moteur, les avionneurs, et les compagnies aériennes - sont concentrés sur des enjeux propres à leur secteur d'activité, ce qui peut s'avérer restrictif. De plus, des objectifs de réduction de l'impact climatique de l'aviation sont apparus et vont devoir être pris en compte dès la phase préliminaire de conception d'avion.

Lors de cette phase, l'avionneur étudie les performances de nombreuses configurations. Cette étude est modélisée sous la forme d'un problème d'optimisation multidisciplinaire déterministe sous contraintes. Les critères sont la minimisation de la consommation de fuel, du coût global d'opération de l'avion ou de la masse maximale au décollage (qui mesure l'efficacité globale de l'avion). Les contraintes sont définies par le cahier des charges. Les degrés de liberté de cette optimisation sont généralement la surface de la voilure et la taille du moteur.

Ces études sont effectuées à partir de modèles parfois très simplifiés, soit par volonté de réduction du temps de calcul, soit par manque de connaissance sur les concepts abordés.

Cette thèse introduit une nouvelle approche holistique du problème d'optimisation de la conception d'avion: nous agrégeons aux modèles classiques, des modèles plus précis de la partie propulsive et de la trajectoire. Pour cela, nous nous familiarisons avec les modèles existants, pour comprendre les interactions entre les disciplines concernées. Nous validons ensuite l'intégration des modèles plus précis de moteur et de trajectoire aux outils existants, en se basant sur les données d'avions existants. Une contribution de cette thèse est d'intégrer aux degrés de liberté usuels, des paramètres de conception du moteur et des degrés de liberté de la mission. L'étude des résultats présente les gains apportés par cette nouvelle approche.

Cette thèse contribue également à ajouter la minimisation de l'impact climatique aux objectifs de l'optimisation. Une modélisation de cet impact est intégrée aux modèles.

Aussi, pendant la phase préliminaire de conception d'avion, des technologies innovantes sont étudiées, qui s'intègrent au système propulsif de l'avion, à son système aérodynamique, ou à sa géométrie. Nous en sélectionnons certaines afin de tirer de la configuration les meilleures performances. Nous proposons d'appliquer l'approche holistique à un concept d'avion à propulsion hybride électrique-fuel. Les modèles utilisés sont présentés et viennent compléter les modèles existants, après validation par des experts. Les résultats de cette optimisation sont comparés à ceux d'un avion conventionnel répondant au même cahier des charges.

Toutes les études menées jusqu'à présent sont déterministes. Les incertitudes autour des modèles utilisés ne sont pour l'instant prises en compte que par des marges basées sur le savoir-faire ingénieur. Cela peut parfois mener à des contre-performances inattendues.

Dans cette thèse, nous introduisons une nouvelle approche qui consiste à prendre en compte consciencieusement ces incertitudes. Pour cela, nous recensons, comparons et sélectionnons des méthodes de gestion des incertitudes qui pourraient s'appliquer à notre problème de conception, selon des critères de temps de calcul, de précision, et d'hypothèses sur les modèles. Nous proposons ensuite de résoudre une optimisation probabiliste du concept d'avion hybride, en prenant en compte les incertitudes liées à l'évolution des technologies nécessaires à l'hybridation.

Enfin, cette thèse présente une nouvelle approche d'optimisation robuste de la conception d'avion. Nous proposons de trouver un avion optimal dont les performances sont satisfaites quelle que soit l'incertitude présente. Cette approche est complémentaire à l'approche probabiliste. L'application de ces méthodes d'optimisation robuste nécessite une modélisation particulière du problème qui est décrite dans cette thèse.

Mots clés : Modélisation et optimisation de la conception avion, propagation des incertitudes, optimisation sous contraintes en probabilité, optimisation robuste.

Principales contributions classées par domaine

Dans le domaine de la conception préliminaire d'avions :

- Nous proposons une nouvelle approche globale du problème d'optimisation du dimensionnement préliminaire d'avion. Une des principales innovations est d'intégrer, pas à pas, un nouveau modèle de moteur, un nouveau modèle de trajectoire et un modèle d'impact climatique, aux modèles utilisés jusqu'à présent.

- Nous incorporons des nouvelles variables de design au problème d'optimisation: aux deux variables classiques, la surface de la voilure et la poussée du moteur, nous ajoutons le "wing aspect ratio" de la cellule avion, le "by-pass ratio" du moteur, l'altitude de croisière, le mach de vol, ainsi que les vitesses de montée et descente pour ce qui concerne la trajectoire. Cette intégration est validée par une comparaison des résultats de l'optimisation en ajoutant progressivement les nouvelles variables de design.

- Nous proposons une configuration d'avion innovante dont l'impact climatique serait réduit par rapport à un avion conventionnel. Pour cela, nous fournissons une étude d'une configuration d'avion à propulsion hybride (électricité-fuel), en la comparant à une configuration d'avion classique respectant le même cahier des charges. Nous résolvons le problème d'optimisation du dimensionnement de ces deux configurations, et nous comparons les solutions obtenues pour les trois critères suivants : l'impact climatique, le cout global d'opération de l'avion et la masse maximale au décollage de l'avion (critère qui mesure l'efficacité globale de l'avion).

Dans le domaine des méthodes dédiées à l'optimisation du dimensionnement d'avion :

- Nous avons intégré dans un outil de dimensionnement avion une méthode de différenciation automatique, qui permet d'atteindre une meilleure précision dans le calcul des gradients en comparaison aux méthodes de type différences finies.

- Nous avons comparé et sélectionné des méthodes d'optimisation adaptées au problème de dimensionnement d'avion : selon la qualité des modèles ou le nombre de variables de design, nous avons implémenté dans l'outil des algorithmes basés sur les gradients et des algorithmes de type heuristiques.

Dans le domaine des incertitudes :

- Nous avons développé une nouvelle famille de lois de probabilité, nommée Beta-Mystique, qui englobe plusieurs familles de distributions uni-modales.

- Nous proposons une étude détaillée de méthodes de propagation des incertitudes à travers les modèles. Les critères de comparaison sont la précision des méthodes, le cout de calcul et les informations disponibles sur les modèles. Cette étude générale nous permet de sélectionner une méthode adaptée à la résolution du problème de dimensionnement d'avion sous incertitude.

Dans le domaine des méthodes d'optimisation sous incertitudes appliquées au dimensionnement d'avion :

- Nous proposons une approche basée sur une optimisation sous contraintes en probabilités du problème du dimensionnement d'avion. Pour cela nous utilisons une méthode nommée S.O.R.A., par-dessus laquelle nous adaptons des techniques permettant de calculer des bornes précises sur les probabilités, afin d'obtenir une meilleure solution.

- Nous appliquons cette méthode à l'optimisation sous contrainte en probabilités de la configuration d'avion hybride, en résolvant le problème suivant : trouver l'année à partir de laquelle l'avion hybride sera aussi performant qu'un avion conventionnel avec une probabilité de 95%.

- Nous abordons une approche d'optimisation robuste du problème du dimensionnement avion, dont la solution satisfait les contraintes pour toutes les réalisations des variables incertaines.

Contents

List of Figures

List of Tables

Acronyms

AET	=	Airbus Equivalent Thrust
$APGWP$	=	Air Pulsed Global Warming Potential
APU	=	Auxiliary Power Unit
ATC	=	Air Traffic Control
BLI	=	Boundary Layer Ingestion
BPR	=	By-Pass Ratio
BRQ	=	Bivariate Reduced Quadrature
$ClbVz$	=	Climb Vertical Speed
CAS	=	Calibrated Air Speed
COC	=	Cash Operating Cost
$CrzVz$	=	Cruise Vertical Speed
DOC	=	Direct operating Cost
$dofs$	=	Degrees of freedom
FPR	=	Fan Pressure Ratio
HTP	=	Horizontal Tail Plane
IAS	=	Indicated Air Speed
ISA	=	International Standard Atmosphere
$LDSPEED$	=	LanDing Speed
$LEEA$	=	Low Emission Effect Aircraft
LoD	=	Lift Over Drag
$MADS$	=	Mesh Adaptive Direct Search
MLW	=	Maximum Landing Weight
$MTOW$	=	Maximum Take-off Weight
$MZFW$	=	Maximum Zero Fuel Weight
MWE	=	Manufacturer Weight Empty
$Npax$	=	Number of Passengers
OPR	=	Overall Pressure Ratio
OWE	=	Operator Empty Weight
SAR	=	Specific Air Range
SFC	=	Specific Fuel Consumption
$SiMCAD$	=	Simple Models for Conceptual Aircraft
$SLSThrust$	=	Sea Level Static Thrust
$StepMisMTOW$	=	Step-Mission Maximum Take-off Weight
$SORA$	=	Sequential Optimization Reliability Assessment
$T4$	=	Temperature out of the turbine
TAS	=	True Air Speed
TLR	=	Top Level Requirements

$TOFL$	=	Take-Off Field Length
TTC	=	Time To Climb
URQ	=	Univariate Reduced Quadrature
$Vcas$	=	Calibrated AirSpeed
VTP	=	Vertical Tail Plane
$WingAR$	=	Wing Aspect Ratio

Pour Olga et Aimé,

Introduction

Air traffic has been regularly growing for the last seven decades. The current number of passengers per year is around 3 billions and, according to the lower predictions, this number is expected to double over the next fifteen years. The main three commercial actors of air transport - the engine manufacturers, the aircraft manufacturers, and the airlines - are focused on issues of their own business. This sometimes proves to be restrictive, since there is no global consideration of all the interactions between the engine, the airframe and the airline operations (trajectory). The aircraft design process deeply involves these three drivers. This process starts with the conceptual design phase, generally followed by the preliminary design phase. During the conceptual phase, engineers and researchers define an aircraft configuration involving new innovative concepts. This can be minimal changes with respect to the existing aircraft, e.g. add wingtip fence to improve the aerodynamic performances of the aircraft. This can also be more important changes, as completely defining a new aircraft configuration, e.g. with the flying wing concept. These innovative technologies can be integrated into the propulsion system of the aircraft, into its aerodynamic system, or into its geometry. The preliminary design phase consists in stating some numerical values on the so defined configuration, with respect to the available knowledge on the used concepts.

The frame of this thesis is straddling the conceptual and the preliminary design phase. During the preliminary phase, the aircraft manufacturer studies and compares the performances of various aircraft configurations. The objective is to determine the design parameters that will lead to the best aircraft with respect to well-selected specifications and requirements. The specifications (number of seats, range) are the results of a market analysis since the objective is to sell as many aircraft as possible. The requirements can be operational, in order to ensure fly-ability, best performances and safety. They can also be regulatory, e.g. to avoid repeating past incidents.

The preliminary design studies are multi-disciplinary, involving aerodynamics, thermodynamics, geometries, weights, structures, etc. At the beginning of the study, a wide design space is explored, which can become more complex after down-selection of a few candidates. Finally, the aircraft design study is modeled as a deterministic multidisciplinary optimization under constraints. The most often used criteria are the minimization of:

- the fuel consumption over a representative mission, or
- the global operating cost of the aircraft, which takes into account charges, the fuel, maintenances and the flight crew costs, or
- the maximum take-off weight of the aircraft, which measures the global efficiency of the aircraft.

The constraints are defined by the specifications and the requirements. They can be landing speed limitations, take-off field limited length, limited time to climb, etc. The degrees of freedom of this optimization are generally the wing area and a parameter that drives the engine size and power, namely the sea-level static thrust. This choice is due to the main impact of these two parameters on the aircraft performances and criteria, via the used models. It is also due to the simplicity and fastness to handle a bi-dimensional optimization.

Moreover, as for all human activities, air transportation gets more and more challenged by competition and ecological matters. New regulatory objectives of reduction of the aviation climate impact recently appeared. This represents a new challenge for the aircraft designers that must be accounted for in the preliminary phase.

This thesis introduces a new holistic approach of the aircraft design optimization problem: we aggregate into the classical simple models, more accurate models of the propulsion system part and of the trajectory part. For that purpose, we first familiarize ourselves with the existing models in order to understand the interactions between the involved disciplines. We then validate the integration of the more accurate models in the existing tools, by matching them with existing aircraft. We also incorporate a climate impact model related to the finest trajectory model. This allows us to add a measure of the climate impact to the classical criteria of the optimization.

The following step of this thesis has been to integrate step-by-step additional parameters of the airframe, parameters of the engine and of the mission additionally to the two usual degrees of freedom (the wing area and the sea-level static thrust). We select a conventional aircraft configuration to which we apply the step-by-step approach. This aims at validating the results at each addition of degrees of freedom. It helps understanding the impact of the various design variables on the performances.

A contribution of this thesis is the proposal of new concept of aircraft namely a hybrid aircraft, with a hybrid fuel-electric propulsion system. We suggest applying the holistic approach to the preliminary design of this concept.

All the previously mentioned studies, and aircraft design process in general, are deterministic. In practice, the uncertainties around the models are taken into account by margins, which are based on engineer know-how. It can sometimes lead to unexpected disappointing performances, which are directly transformed into cost penalties for the aircraft manufacturer. So, we introduce in this thesis a new approach which consists in carefully taking into account these uncertainties, via robust design methodologies. The manuscript is divided into six parts:

Chapter one is dedicated to the conceptual and the preliminary aircraft design. The general context of this thesis, which is the future project office of Airbus, is presented. We underline its role in the aircraft design process. The classical models used to simulate this process are then described: the geometry, thermodynamics, aerodynamics, weights, missions and performances. The models developed in the frame of this thesis are introduced: the trajectory simulation, the finest engine and the environmental impact. Then, the hybrid aircraft configuration is described. The related models are built and validated by the experts. We underline the importance of studying the way of operating such an innovative concept, especially energy management. Finally, we propose improvements of

the first concept idea, in order to take benefit of all the detected synergies and opportunities.

Chapter two deals with the mathematical tools required to solve the aircraft design problem via the holistic approach. We first present an automatic differentiation method which has been implemented in the numerical tools. The objective is to obtain the function gradients with more accuracy than with finite differences techniques. We then introduce some classical optimization methods: gradient based, derivative free, and surrogate based.

Chapter three presents the step-by-step approach of the aircraft design optimization, with the introduction of the additional degrees of freedom. We first describe the steps of this approach. Then, it is applied to the conventional configuration, with an analysis of the results. Finally, we propose to apply this approach to the hybrid aircraft design optimization satisfying the same specifications. We add in parallel a step-by-step integration of the hybrid aircraft synergies presented in the first chapter. The conventional and hybrid aircraft are finally optimized in terms of the climate impact criterion. Results are compared.

Chapter four is dedicated to uncertainty management. We start with the general definitions on uncertainties that we choose to represent by random variables. Then, we introduce methods that we select to characterize the uncertainty. Finally, we propose a review of uncertainty propagation methods. For that purpose, we list, compare and select methods of uncertainty propagation which could be applied to our design problem, namely Monte-Carlo, Taylor expansion, quadrature and polynomial chaos expansion methods. This is done according to criteria such as the computation time, the accuracy, and the assumptions on the models. The selected methods are finally compared through numerical examples.

Chapter five presents a new approach of aircraft preliminary design via a chance constrained optimization. The introduction is dedicated to general information on robust design approaches. A numerical method namely SORA (Sequential Optimization Reliability Assessment) is described. We then propose an adaptation of this method to manage unconventional random variables. We assess the robustness thanks to a method of uncertainty propagation selected among the ones presented in the fourth chapter. We apply this robust optimization method to the hybrid aircraft design to answer the following question: according to a given criterion, what kind of hybrid aircraft will be reliably competitive and when can we expect it? The compared criterion are the fuel consumption, the global operating costs and the climate impact.

Chapter six presents the first works on another approach of a robust optimization of a conventional aircraft design. We suggest finding an optimal aircraft of which the performances are satisfied whatever the uncertainty. This approach is complementary to the chance constrained approach. The implementation of robust optimization requires a particular modeling of the problem which is described in this chapter.

This manuscript ends with the conclusion and the perspectives of the thesis.

Chapter 1

Conceptual Aircraft Design for Air Transportation

Contents

Air transportation is the mode of transport that has experienced the fastest growth in the last century. Starting with the first flight of Wright's brother in 1903, commercial air transport development really began in the late twenties and early thirties. Important advances were introduced in aircraft construction methods with the monocoque and the use of aluminum. At the same time the first airlines appear in Europe and in the U.S., followed by several Latin American carriers.

The world war II accelerated the development of aircraft, and hundred of airports were created. From the forties, technological evolutions impact the air transport with electronics devices (RADAR - 1944, GPS - 1993, ...), making it always safest, controlled, comfortable and also profitable. These innovations also helped to manage the growth of the number of flights around the world. At the same time, engines evolved with the research of the safest, the more silent, economical and powerful engine. Also in parallel, airlines kept looking for the best way of managing flight in order to make it more comfortable for the passenger, but also safest and more economical. The fuel price increase drove the engine manufacturers to pay more attention to the economical aspect via the engine fuel efficiency. This leads to one of the best compromise: the turbofans, that are powering most of the current commercial aircraft. This rising price also drove the airlines to be more careful on flight operations from the ground to the cruise altitude.

The continuous growth of air traffic number quickly brought the need for a more global organization of air transportation. It yielded the creation of several organizations: the Federal Aviation Administration (FAA) in the U.S., the European Aviation Safety Agency (EASA) or the Direction Générale de l'Aviation Civile (DGAC) in France. These organizations have the role to regulate and oversee all aspects of civil aviation in there country. However the most important of them is the International Civil Aviation Organization (ICAO). It is a specialized agency of the United Nations and it codifies the principles and techniques of international air navigation and fosters the planning and development of international air transport to ensure safe and orderly growth. One particular concern of ICAO is the environmental impact of aviation. It is reported in [132] that aviation is responsible for about 3.5% of the total radiative forcing of all anthropogenic emissions and scenarii say that it would likely rise to 5% (with a worst-case scenario of 15% of human emissions) by 2050.

To give a rough idea, the global airline industry performs today around 32 million commercial flights per year transporting 3 billion passengers and 50 million tonnes of freight. Airbus global market forecast in [6] predicts a traffic growth of around 4.7% per year from 2014 to 2033. As we can see in Figure 1.1, it means a global growth of around 250%. This evolution of air transportation leads to an evolution of the challenges. We can quote the following ones from [166], with their associated goals:

- quality and affordability, by reducing passenger charges, increasing passenger choice, reducing time to market,
- environment, by reducing CO_2 emission by 50%, NO_x emission by 80%, perceived external noise by 50%. These targets have been assessed by the Advisory Council for Aviation Research and Innovation in Europe (ACARE) in [42], and
- safety, by reducing accident rate by 80%, reducing human error and its consequences.

These challenges have then to be taken into account from the beginning of a new project of aircraft. This starting point is realized at Airbus Future Project Office. The objective

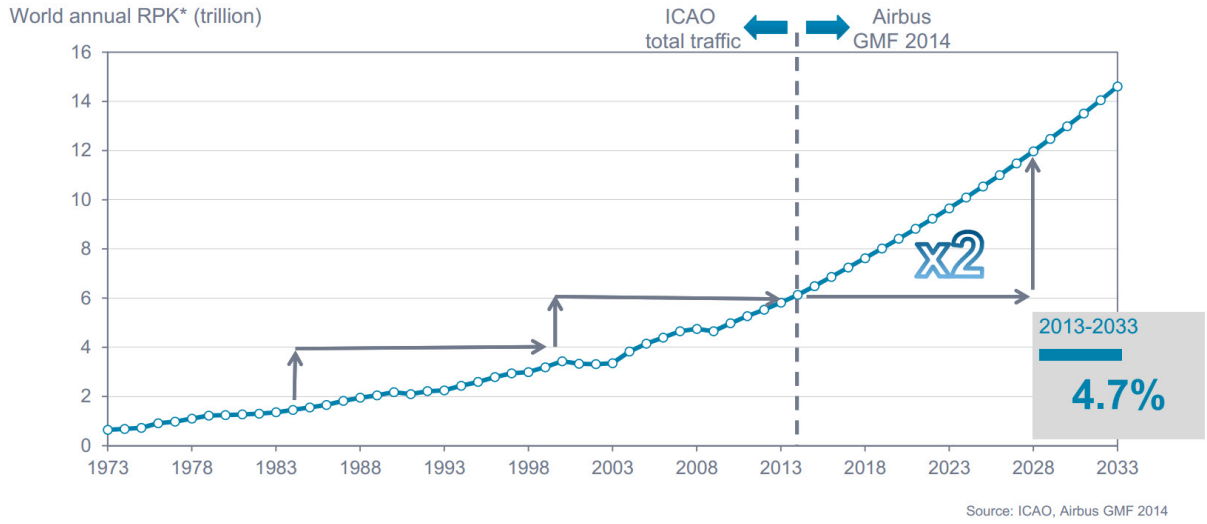

Figure 1.1: Airbus and ICAO global market forecast until 2033. Revenue passenger kilometres (RPK) is a measure of the volume of passengers carried by an airline, a revenue passenger-kilometre is flown when a passenger (excepted airline employees and babies) is carried one kilometre.

of this chapter is to present in a first part the process of aircraft conception, also called aircraft design, from a general point of view and with a particular focus on the role of future project office. The second part of the chapter is dedicated to the presentation of numerical models that have been selected for the preliminary design of new aircraft configurations.

1.1 Aircraft Conception

Aircraft conception is all but a simple task. From the idea of a new project to the industrialization, around 10 years are necessary. As a comparison, it is around 5 year for a car and around 1 year for a computer. The operating time is also huge comparing to daily life objects: the mean is around 30 years for an aircraft, whereas it is around 15 year for a car and 3 year for a computer. An example of duration of an aircraft project management is given in Figure 1.2. Aircraft conception is then a major project. Specific management approach has been created to carry out this project in optimal managing conditions. It is based on a project life management division that is called Maturity Gates (MG). The role of this steps is to follow and validate the project maturity. Figure 1.3 presents the typical maturity gates of a project of aircraft, with the corresponding steps that have to be reached.

1.1.1 Future Project Office

Airbus, like many other business entity, has to build and sell a range of products: its aircraft from the different families. From the short range to the long range type and with a various number of seats, we can find the four following families: the A320, the A330, the A350 and the A380. Figure 1.4 presents the diagram of the radius of action versus the number of seats with all current Airbus family products. Target a market segment

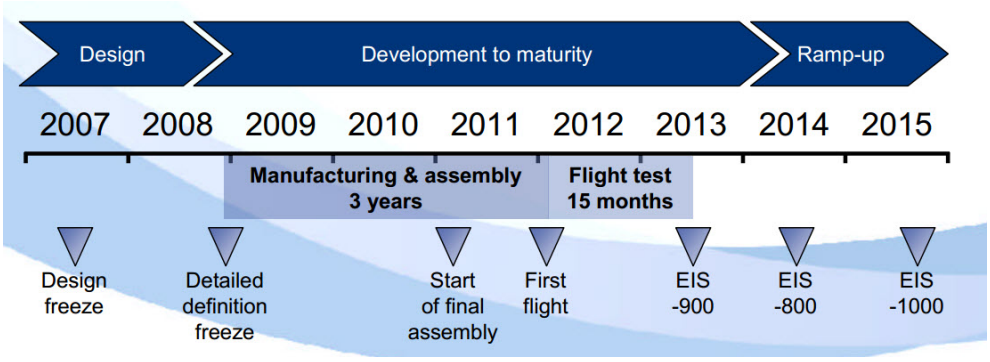

Figure 1.2: Example of an aircraft product life management.

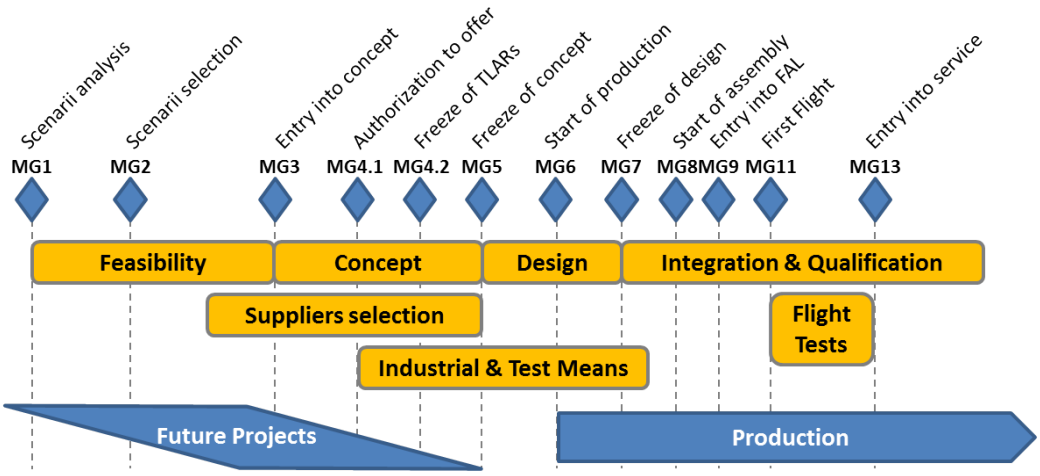

Figure 1.3: Aircraft design process with maturity gates (MG).

amounts to defining a number of characteristics, essentially the two previously mentioned, but also performances at takeoff, landing, climb, cruise, etc. The objective is to cover with all families of aircraft the market where we want to be present with the best performed products. For that, we are constantly on the lookout for a competitive threat, and looking for improvements in our product range.

Future project office role takes place at the very beginning of the project development. One of the main work of future project office is to assess the benefits and drawbacks of various aircraft configurations, to provide the technical arguments to the company strategy, and to propose the best configuration according to the required top level requirements. The design phase actually began before MG1. From then, the future project office is responsible for the following actions:

- scenario analysis (MG1),
- scenario selection (MG2),
- study of most attractive TLARs of the market and find out corresponding capabilities,

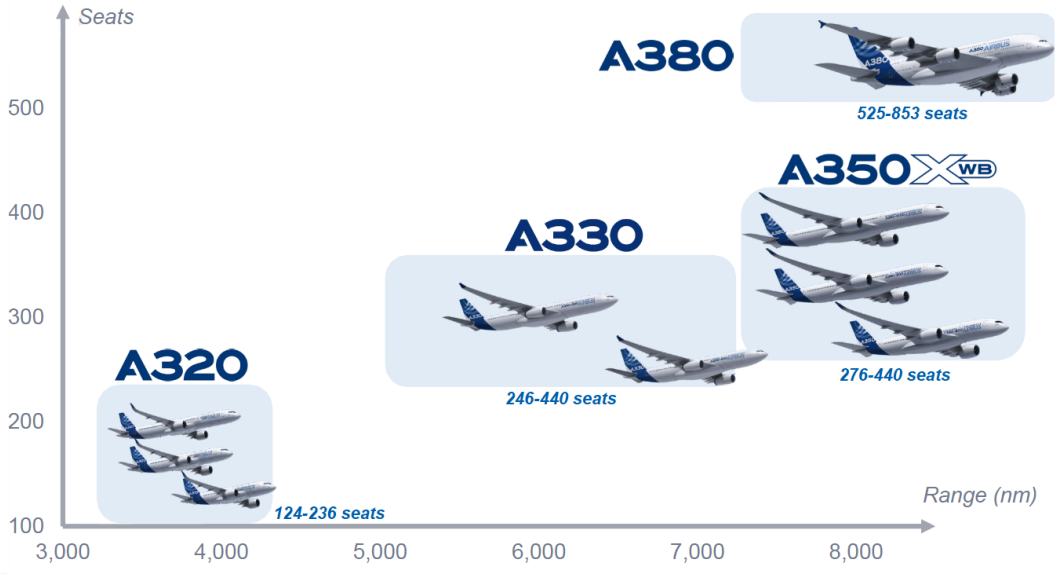

Figure 1.4: Airbus aircraft families market positioning.

- study and evaluation of all ideas with regards to best technologies available, by discussing with partners and customers,
- entry into concept (MG3),
- following first steps of concept.

During these phases, the future project department has various roles:

- technology watching, by monitoring worldwide the technical advances that could lead to promising applications, and by evaluating what would be the performances of an aircraft that embeds such technologies,
- competitor positioning watching (look for the aircraft that will rival with our products, compare the performances between our aircraft and the competition, ...),
- innovative platform, by studying innovative configurations in order to evaluate new technologies. All innovations that bring performances improvement are studied. Their interest is evaluated according to a global interaction of the following aspects: technicals (new material, flight command, cabin layout, ...), economical (fuel price, airlines strategies, ...), environmental (pollution, noise, rules, ...), and last but not least, safety,
- supporting development, by integrating general work from the whole engineering, and by helping to ensure the aircraft consistency and the satisfaction of cost and performance objectives,
- research, by participating in national and European research programs to promote innovation,

- design, by writing the specifications, by experimenting numerically aircraft missions and performances.

The integrator role of future project is a key of aircraft design: the best concept is often the one that will take benefit of all technologies together. Clearly, the goal is to manage the concept configuration in order that the sum of one improvement in the propulsive part and one in the aerodynamic part for instance is greater than these improvements taken separately. That is the integrator role of future project office: aerodynamics, propulsion, handling qualities are managed together to ensure the best efficient configuration. To illustrate this, Figure 1.5 represents some of the various innovative concept planes that have been studied by future project office.

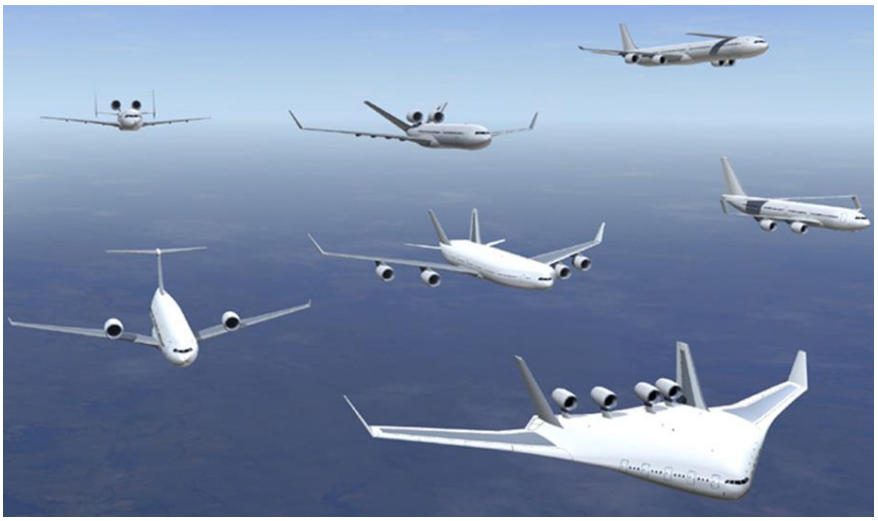

Figure 1.5: Examples of innovative aircraft configurations.

The evaluation of the performances of all these configurations is done thanks to models and processes of different levels. The choice of the models is often a trade between the accuracy on the results and the computation time. As an example, for the masses evaluation, we can find the three following levels of models:

- the more accurate level is considering each part of the aircraft (fuselage, wings, ...) as a structural mesh,
- the second level relies on semi-empirical modeling with a piece by piece estimate of the masses, based on a breakdown that can be more or less detailed,
- the last level, called level 0, consists in simple formulas to compute the weight of each main component (fuselage, wing, ...).

The models that we are going to introduce in Section 1.2 are considered of level 0. These models allows to evaluate the performances of a new aircraft in around 10 seconds, which is one of the main required constraint in order to put this design evaluation into an optimization loop.

1.1.2 Aircraft Design: A Multi-Disciplinary Optimization problem

As mentioned in Section 1.1.1, aircraft design involves the following disciplines: propulsion, aerodynamics, weights, handling qualities, etc. It can be completed by the non exhaustive list: electricity, controls, stress, structure, hydraulic, etc. One of the difficulty of aircraft design is to integrate all these disciplines and the corresponding various requirements. It is most of the time a question of trades. Requirements of a discipline can be constraints for another one, and interactions management is a key part of the design. Figure 1.6 is a well representative caricature that represents the ideal aircraft through each discipline view. At Airbus, specific departments are specialized in discipline. They are called the center of competences. Future project communicates with these different departments in order to integrate and validate concepts around the aircraft project. Like any product intended

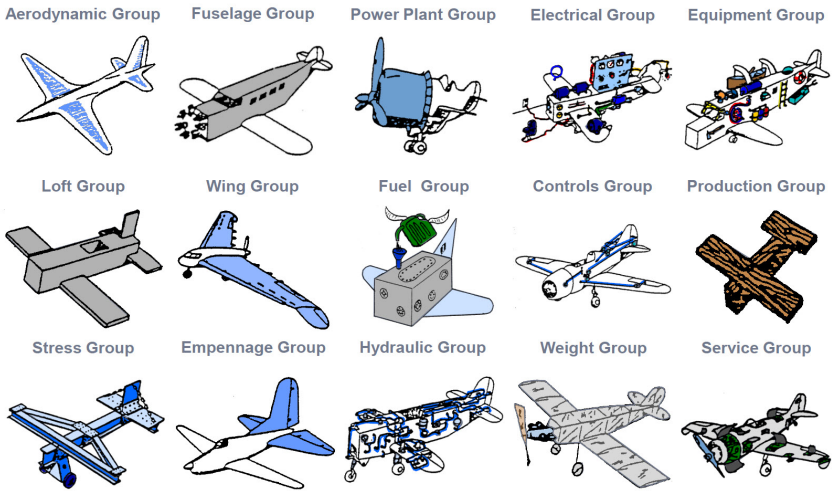

Figure 1.6: Caricature of aircraft design according to specific discipline.

for a market, an aircraft is responding to specific requirements. The main performance requirements of an aircraft are the following ones:

- number of seats,
- range and speed (Mach number),
- initial climb altitude,
- take-off field length,
- approach speed,
- landing distance,
- ...

The first three parameters of the above list are considered as specifications whereas the last ones are considered as operational constraints: they correspond to real needs for safety or operations. According to these specifications, an inverse problem has to be solved. The

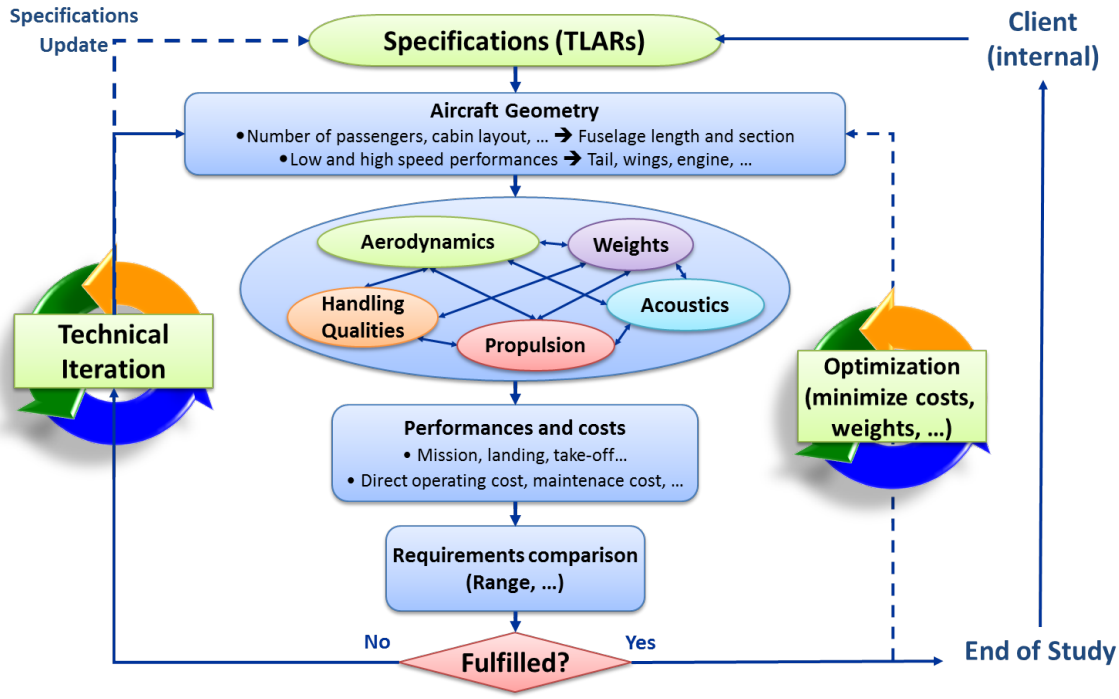

Figure 1.7: Future project iterative design process.

objective is to define an aircraft that fulfills all these required performances. It can be explained by Figure 1.7. It is important to note that these performances are function of the product. For instance, a short range aircraft has to be compatible with smaller airports, which may yields more binding landing and take-off field length requirements. Once these requirements are selected, what will drive the choice of the customer? The response has to be selected among parameters that impact its profits, but also its reputation. It can be one of the following:

- the fuel consumption,
- the operating cost of the aircraft,
- the environmental impact,
- the aircraft structural weight,
- a differentiation parameter (the biggest, the fastest, ...).

The aircraft design objective is then to optimize these parameters, for all the above mentioned one, optimize means minimize. The global aircraft design approach, from the requirements to the minimization of one of these criteria clearly defines a constrained multidisciplinary optimization problem.

A trade between the objectives can also be of interest. Indeed, in the case where two required criteria are conflicting, the corresponding optimized aircraft configurations can be very different. The idea can then be to present to the customer various optimized configurations, that balance both criteria. This allows to let him some freedom of choice and to decide what is the best trade between the criteria.

1.1.3 Aircraft: How to make it fly?

To make an aircraft fly, i.e. to reach a required altitude and speed, means that it has to generate sufficient aerodynamic lift to compensate its weight. At the same time, it is generating aerodynamic drag that has to be compensated by generating sufficient thrust to maintain the required altitude. This is summarized in Figure 1.8. The target is then a

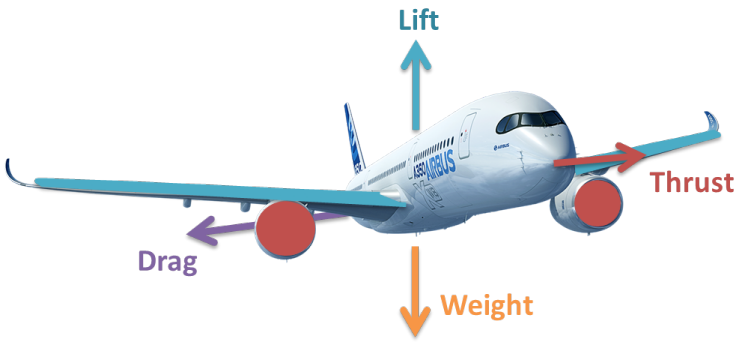

Figure 1.8: Aerodynamics of flight.

reduction of the weight and a reduction of the drag. However, it is not so simple, interactions between aircraft components have to be carefully studied. Schema from Figure 1.9 represents the cause-and-effect of the aircraft design for flying. It underlines the fact that any change in one actors of the flight will impact others. The design process objective is not only to find the right value for the design variable, for example the wing area and the engine size, but also to find the best ones according to the criteria. It also brings out the importance of models that will be used in the design process in order to account for the interactions with the right balance between accuracy and computational cost. All these

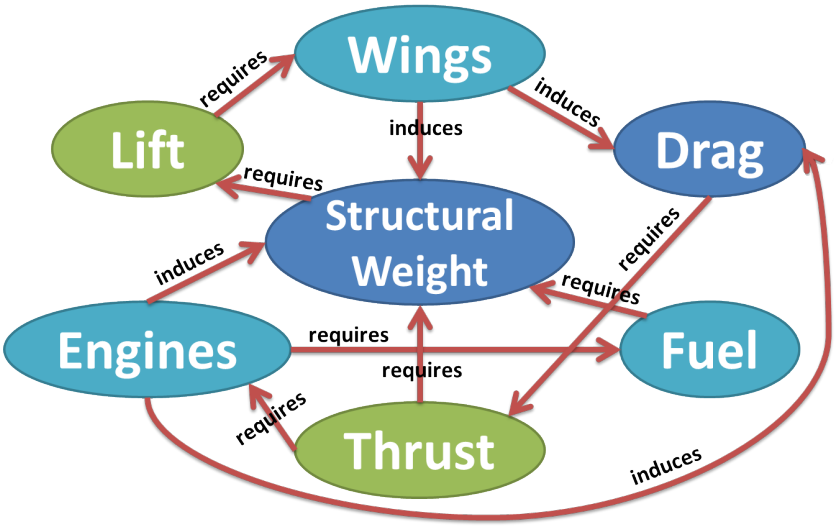

Figure 1.9: Cause-and-effect of aircraft design for flighting.

models are put together to obtain the aircraft design simulation toolbox. They will be presented in the following sections. The design process can now be implemented according to the specifications, the requirements and the criteria from Section 1.1.2, the design parameters, and also some hypothesis around promising technologies, such as in Figure 1.10. One of the important step in the design process is what is called the mass-mission loop.

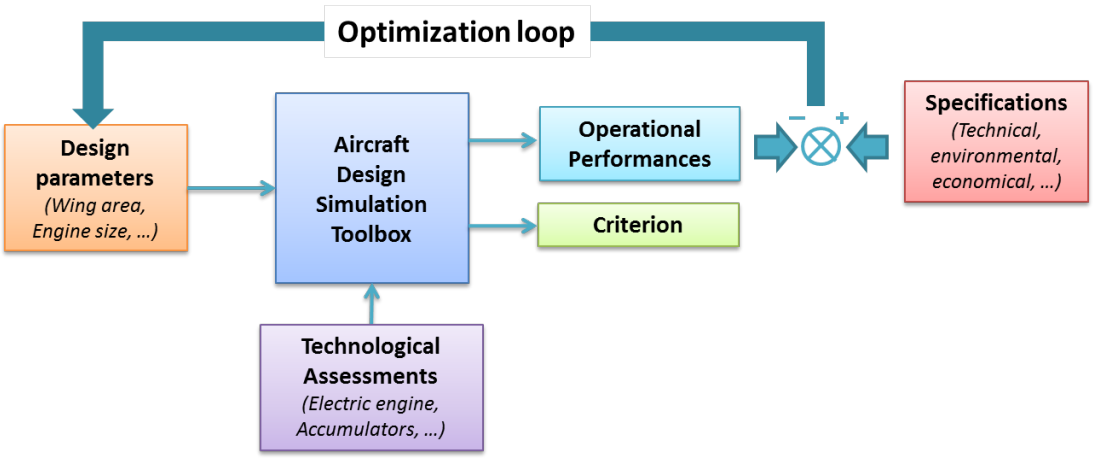

Figure 1.10: Aircraft Design Process.

It is presented in Section 1.2.5 and it illustrates the snowball effect that can result from an increase in the structural mass. This step of the design process well underlines the complexity of the aircraft design.

1.1.4 The important place of the engine

Engine has a very important part during the aircraft design: it represents more than 25% of the total mass of the aircraft and it gives the aircraft its propulsion power through the thrust, as well as all the necessary energies (electrical, hydraulic, thermal).

We can introduce here the "Supreme Propulsion System Family" (Figure 1.11). Engines can be designed with respect to various expectations that can be summarized by this figure. It is also important to underline that all these criteria (noise, cost, climatic impact, fuel efficient, fast) are most of the time contradictory and the best engine is highly depending on the aircraft needs and requirements. The main objective of engine manufacturers is then to reduce the difference between the different expectations (noise and consumption, silent and cheap, high speed and environmentally friendly...). The most used engine for commercial aircraft is the turbofan engine. It offers a good compromise between all the previously mentioned expectations. To define a turbofan, we first have to define what is a turbine engine [136]:

A turbine engine is a container with a hole in the back end, called nozzle, to let air inside the container escape, and thus provide propulsion. Inside the container is turbo-machinery to keep the container full of air under constant pressure.

Propulsion is the net force that results from unequal pressures. This force is called thrust. The following four steps are the basis of any internal combustion engine, with the corresponding engine section that is represented in Figure 1.12:

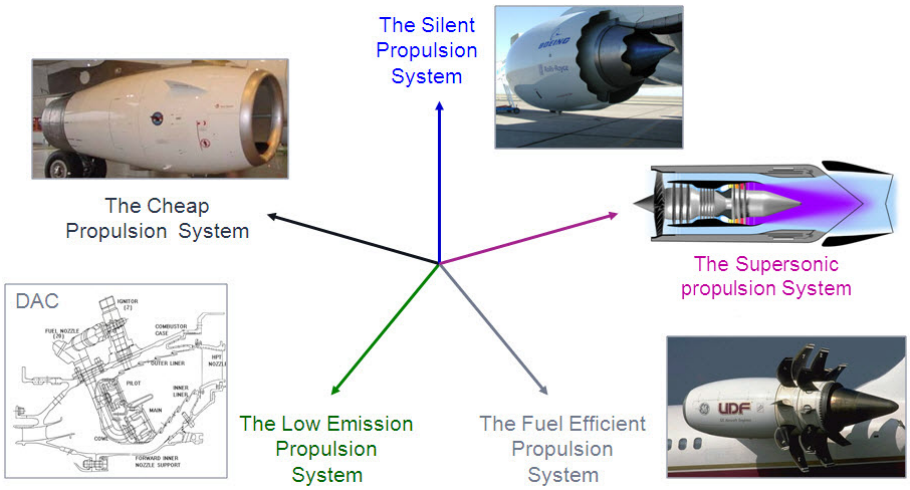

Figure 1.11: Supreme Propulsion System Family.

- intake of air by the inlet section,
- compression of the air, by the compressor section,
- combustion, where fuel is injected and burned to convert the stored energy, by the combustion section,
- expansion and exhaust, where the converted energy is put to use, by the exhaust section (turbine and nozzle).

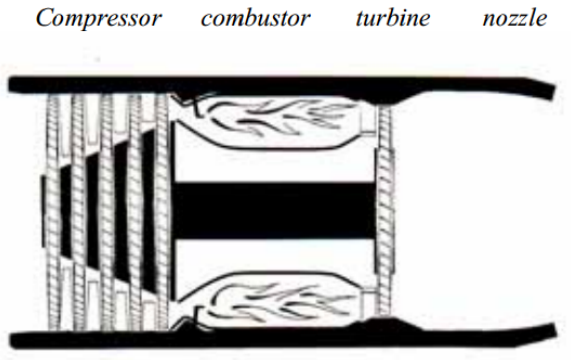

Figure 1.12: Basic layout of a jet propulsion turbine system [136].

A turbofan engine is then simply a turbine engine where the first stage compressor rotor is larger in diameter than the rest of the engine. Figure 1.13 represents a turbofan engine model. The larger stage is called the fan. Its principle is the following one [136]: the ambient air that passes through the fan can be divided into two flows, the one that goes through the compressor stage which is then compressed and processed through the engine cycle, and the one that does not pass through the core but instead passes along the outside

engine. This air is called the bypass air, and the ratio of bypass air over core air is called the bypass ratio (BPR). The total thrust is finally the sum of those from both the hot thrust provided by the core stream and the thrust provided by the bypass stream. Note that the turbofan configuration results from an optimization of a pressure ratio efficiency, that yields a highly performed engine. The engine design process is presented in Section 1.2.3,

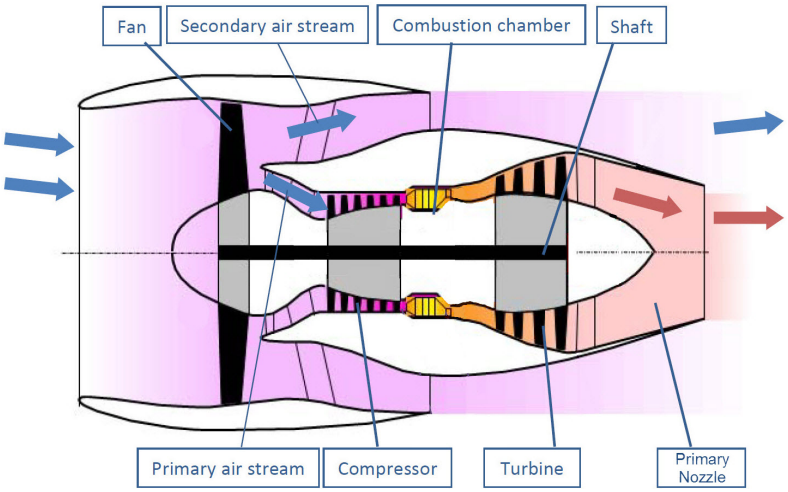

Figure 1.13: Single shaft turbofan engine simplified model.

with the main design parameters description. The aircraft whole design process is detailed in next section.

1.1.5 The importance of the trajectory

Basically, an aircraft is an aerodyne that is using its own velocity in the air to produce a force that counterbalance its weight. This way of flying requires that an engine produces the necessary thrust. The airflows around the aircraft, as well as inside the engines, are driven by aerodynamic laws, whilst the thrust and the fuel consumption are driven by thermodynamic laws. It is clear that interactions between the aircraft and the surrounding air mass are a key of air transport operations.

According to this, two parameters have a major impact on these interactions: the speed of the aircraft through the air and its flying altitude. The speed of the aircraft is represented by its Mach number:

$$\text{Mach} = \frac{v}{a} = \frac{v}{\sqrt{\gamma RT}}, \tag{1.1}$$

where v is the velocity of the moving aircraft, a is the speed of sound in the medium (in m/s), which depends on the temperature T (in K), the universal gas constant R (≈ 287.053 J/kg/K), and γ the adiabatic index ($\gamma = 1.4$ for the air). This latter relation is made assuming the air is an ideal gas. The temperature is assumed to follow the International Standard Atmosphere (ISA) rules (Figure 1.14), which are an average set of conditions set as an international reference. It also gives an average behavior of the pressure P (in Pa) (Figure 1.15) as a function of the altitude h (in m). The air density ρ (in kg/m^3) can be

computed via the formula:

$$\rho = \frac{P}{RT}. \tag{1.2}$$

The aerodynamic forces can be expressed as follows:

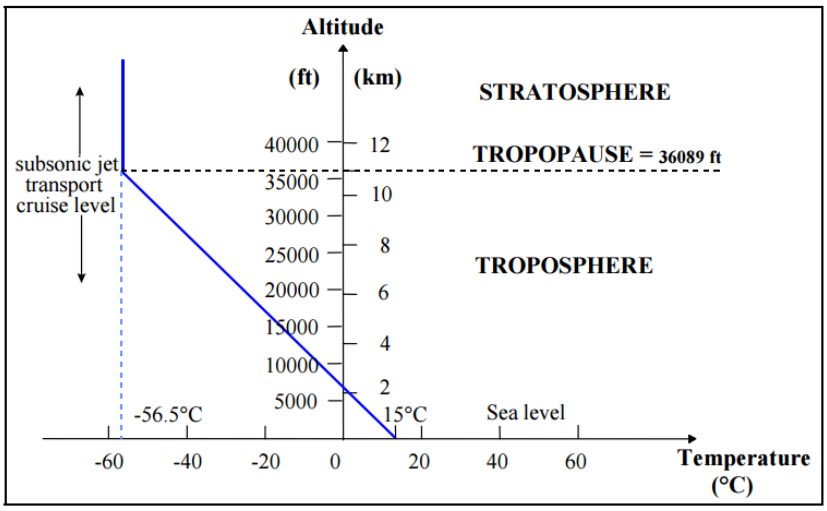

Figure 1.14: ISA temperature model.

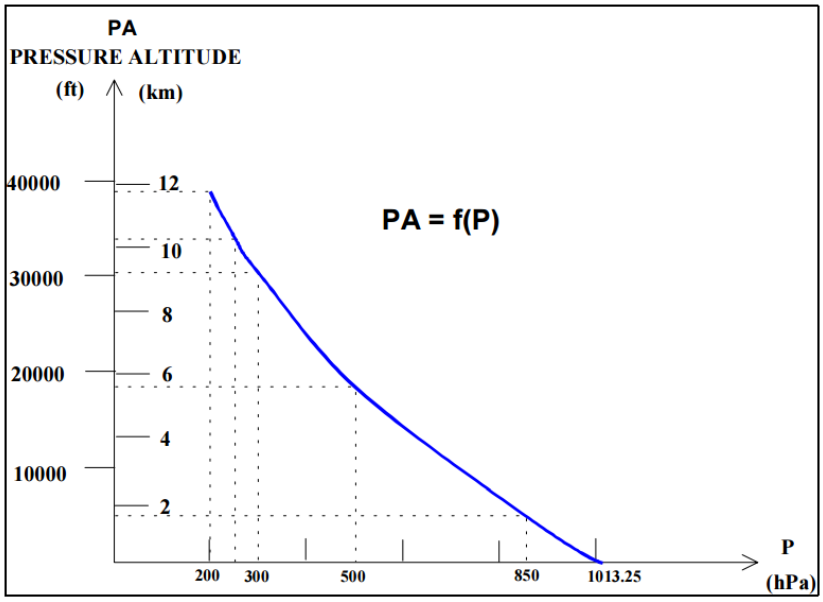

Figure 1.15: ISA pressure model.

$$F = \frac{1}{2} \underbrace{\rho}_{\text{atmosphere}} \times \underbrace{v^2}_{\text{speed}} \times \underbrace{S \times C}_{\text{shape and orientation}}, \tag{1.3}$$

$$= 0.7 \times P \times \text{Mach}^2 \times S \times C, \tag{1.4}$$

where ρ is the air density, v is the aircraft speed, P the pressure, S a constant value (in m^2) which allows the homogeneity of the formula, and C which is a coefficient that represents the force response to the shape submitted to the airflow. This response is of course depending on the shape itself but also of it orientation versus the airflow. For instance during the aircraft cruise, the lift has to counterbalance the weight, which leads in the following relation:

$$mg = \frac{1}{2}\rho \times v^2 \times S \times C_z, \tag{1.5}$$

$$= 0.7 \times P \times \text{Mach}^2 \times S \times C_z, \tag{1.6}$$

where C_z is the lift coefficient, mostly equal to 0.2 and is in practice fixed for a given cruise. Thanks to this relation, we can observe the strong link between the speed parameter (Mach) and the altitude of the aircraft z. When z increases, the air density ρ decreases, which means that to keep satisfying relation (1.5), the Mach has to increase.

The interactions between the running engine and the atmosphere are in turn very complex and beyond the scope of this study. Nevertheless, we can note at this stage that the turbofan engines show a maximal efficiency at a given speed and a given thrust which is in practice set to match the cruise conditions. Indeed, the cruise Mach is strongly limited by the speed of sound in the air. Let us present the case of an aircraft that is flying Mach 1, which is equal to the speed of sound. Crossing of the speed leads to a huge change of the nature of the airflow around the aircraft and consequently to important effects on the aircraft shape. For proof, we can compare the shape of the Concorde to the one of an A320, as presented in Figure 1.16. For the subsonic transport aircraft, the higher Mach

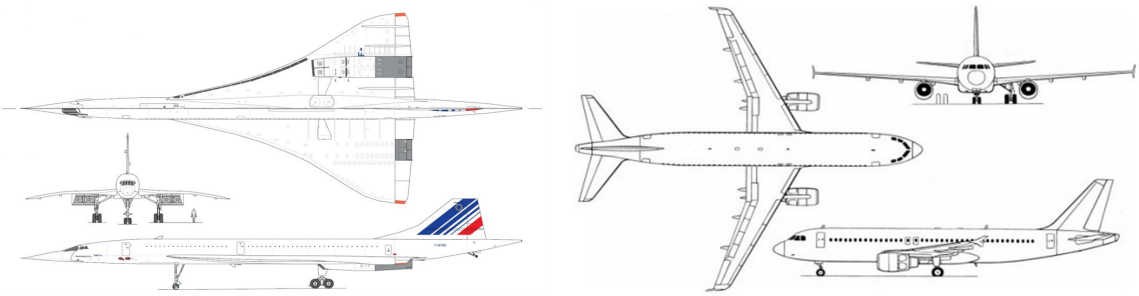

Concorde
Cruise Mach 2.04
Seats 120
Range 3900 NM

A320
Cruise Mach 0.78
Seats 150
Range 3300 NM

Figure 1.16: Concorde versus A320: a difference of shape.

that can be handled without a huge modification of the aircraft shape is around 0.85.

During the cruise, the other aerodynamic relation that involves the thrust and the drag is the following one:

$$\text{Thrust} = \frac{1}{2}\rho \times v^2 \times S \times C_x, \tag{1.7}$$

$$= 0.7 \times P \times \text{Mach}^2 \times S \times C_x, \tag{1.8}$$

where C_x is the drag coefficient. We observe that the thrust is increasing as a function of the square of the Mach number: the cost of the speed is considerable. This is why the interest is to fly high, such that ρ decreases. However, the engine need air to run properly then too high altitudes are not possible.

From all these interactions, it results that the trajectory of the aircraft (in green) in the 2D-map (altitude z,speed v) generally follows the path presented in Figure 1.17. It follows iso-ρv^2 and iso-Mach.

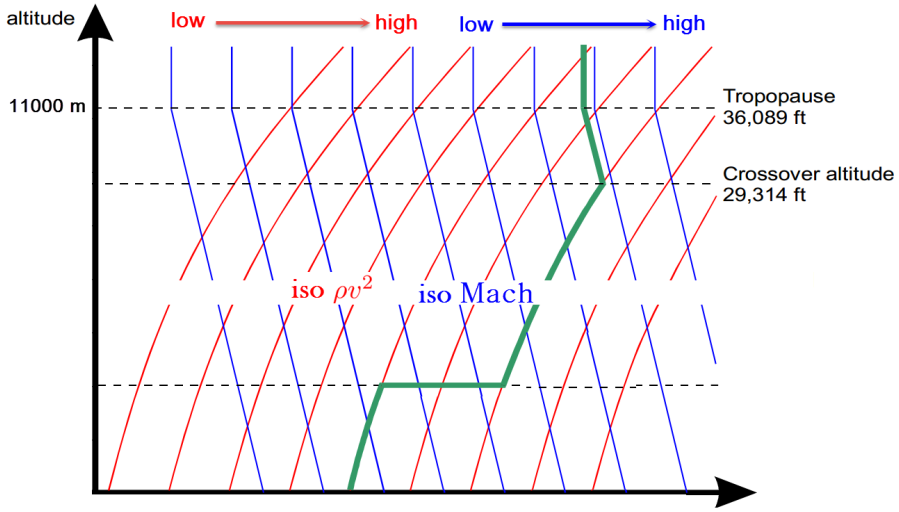

Figure 1.17: Resulting aircraft trajectory in (z,v)-map.

1.2 Aircraft Design Processes and Models

This section is devoted to the presentation of the models and processes of aircraft preliminary design. For more details see [22].

Let us recall that most important quantities for fly-ability are Wing and Engine: wings are generating the lift, and engines the thrust. Maximum Take-Off Weight, already mentioned in the previous section, directly influences the amount of mechanical structure, but also the required engine power and the cost of the aircraft. Classical Overall Aircraft Design (OAD) objective is to define consistent values for Wing Area, Engine Size and MTOW. The process presented at the end of this chapter consists in optimizing the global aircraft configuration taking as degrees of freedom not only these airframe design components but also some additional degrees of freedom of the trajectory and of the engine.

1.2.1 Aircraft Design Process description

The Overall Aircraft Design (OAD) process is the name of the global definition of the aircraft. The steps of this process are illustrated in Figure 1.18. The first step is the selection of the specifications and requirements: mainly the number of passengers, the range of the the aircraft, its required performances. An example of specifications for a short range aircraft is given in Tables 1.1 and 1.2. The design is generally optimized with respect to a

given criterion, for instance the fuel consumption, the MTOW, the operating cost, which have to be minimized. At the same time, the design variables are selected, the classical ones are the Wing Area and the Sea Level Static Thrust of the aircraft. From there, OAD numerical tools allow to compute a complete aircraft configuration with its performances. The overall aircraft design process then consists in finding the values of the design variables that allow the aircraft to satisfy the requirements, and which minimize the criterion. This optimization, which encompass the aircraft computation, is a deterministic mono-objective constrained optimization. This optimization process can also be represented with more

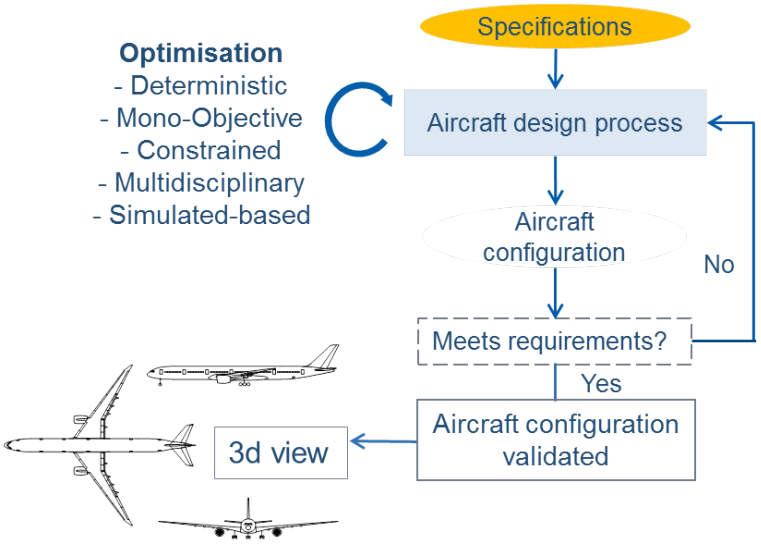

Figure 1.18: Overall Aircraft Design Process.

Table 1.1: An example of short range specifications and requirements.

Name	Value
Number of Passengers (Npax)	180
Design Range	2000 NM
Cruise Mach number	0.76
Wing Aspect Ratio	9
Number of Electrical Engine	0 or 1
Number of Thermal Engine	2
Engine By Pass Ratio	10
Top of climb Reference Altitude (ZpRef)	35000 ft
Engine Overall Pressure Ratio	40

details, as illustrated in Figure 1.19. Here we dissociate the design into subprocesses. The first one is the aircraft geometry computation according to design parameters and to requirements. The entire shape of the aircraft is designed through parametric models. At the same time the engine parameters are computed. The second step is the estimation of aerodynamic forces and structural masses with the mass-mission loop, detailed in Sec-

Table 1.2: An example of short range operational constraints.

Name	Value
Approach Speed (LdSpeed)	< 130 kt
Climb Vertical Speed Ceiling (ClbVz)	> 500 ft/min
Cruise Vertical Speed Ceiling (CrzVz)	> 300 ft/min
Take-Off Field Length 1 (at Sea Level) (TOFL1)	< 2000 m
Take-Off Field Length 2 (in High & Hot conditions) (TOFL2)	< 2500 m

tion 1.1.3. Once this loop is done, we have the complete aircraft description. Then the last step is the computation of its operational performances and of the criteria to minimize. This is a classical way of designing a new aircraft. One of the objective of this thesis was to

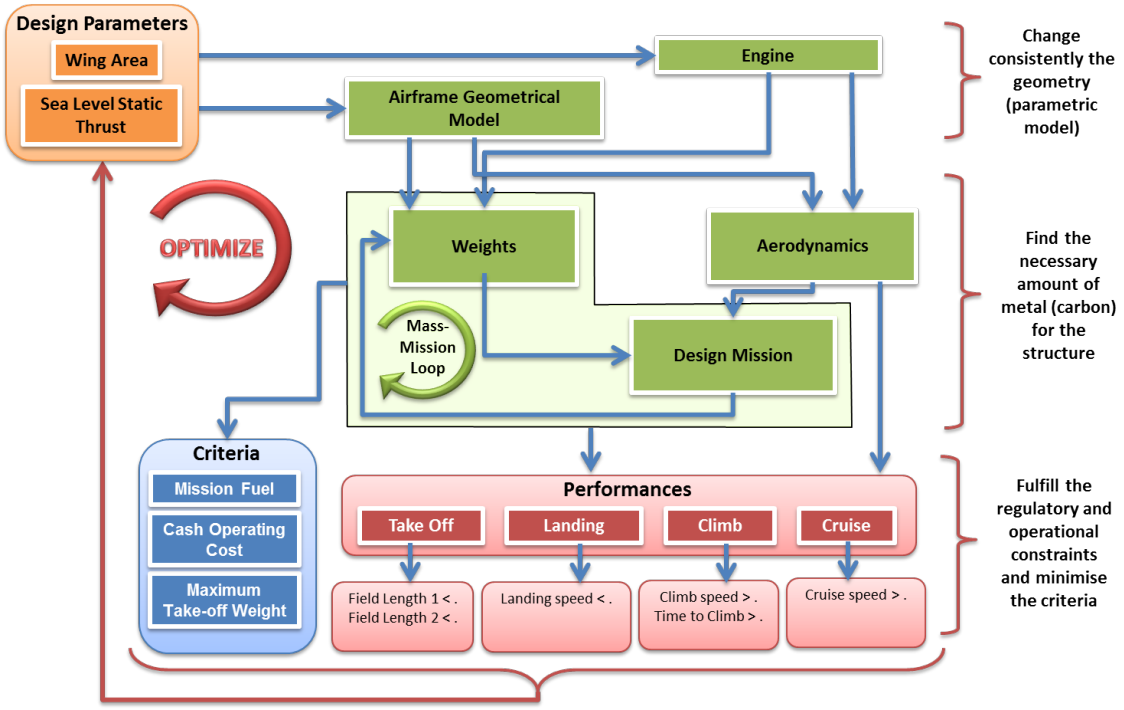

Figure 1.19: Aircraft Design Optimization Process.

integrate to the process semi-empirical models of a thermodynamic engine and of a detailed mission and to look for global optimum. This integration is developed in the last section.

The multidisciplinary aircraft preliminary design process is the interaction of different physics. Most important are the geometry, aerodynamics, weights, propulsion, trajectory, environmental impact, etc. Each discipline is modeled by intrinsic integer or real parameters, and also by various functions of all parameters. The design tool used during this thesis is an Airbus internal tool named OCCAM, which results of more than ten years of research and experiments [22, 12]. A complete description of these models can be found in [22]. It is based on semi-empirical models: some models are taken from physical laws, some others are extracted by regression from a database of around 60 aircraft. Interpolations are often

linear, or polynomials according to engineering intuitiveness and knowledge. The models are organized into a multi-layered toolbox as presented in Figure 1.20: the lower layer contains models computing aircraft components such as fuselage, wings, etc, and the higher layer contains processes for the optimization. Let us now have a more accurate look on the

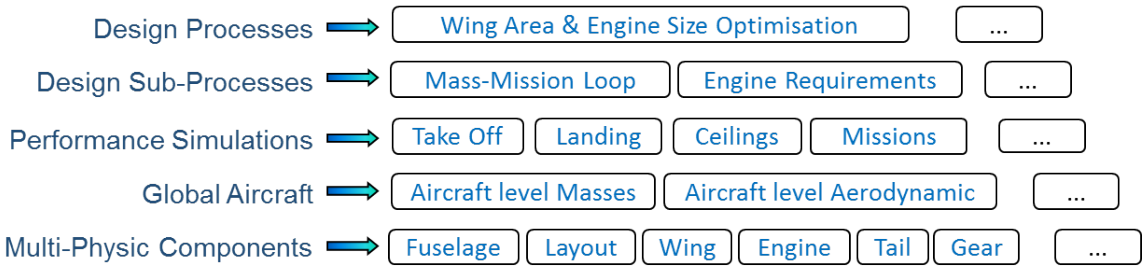

Figure 1.20: Aircraft Design: a multi-layers toolbox.

different boxes of Figure 1.19 by presenting their inputs, their outputs, and the parameters required for their computation. We present the geometry model, the aerodynamics model, the weights model, the engine model, the mission model and the performances model.

1.2.2 Geometry model

As presented in Figure 1.19, the first step in the aircraft configuration computation is the geometry. According to design parameters values and specifications, the geometry of the aircraft is computed: all the dimensions of the fuselage, the wings, the vertical and the horizontal tail-planes. It is represented by the diagram of Figure 1.21. Various concepts

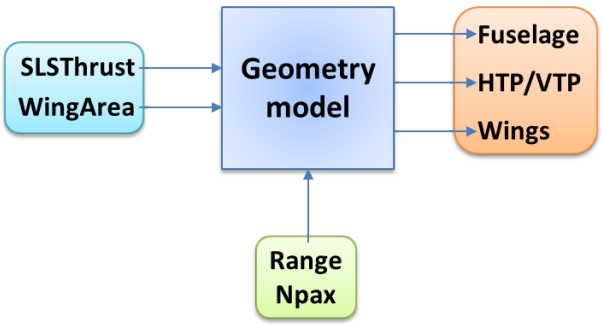

Figure 1.21: Geometry model inputs, outputs and parameters.

such as the ones presented in Figure 1.22 are integrated in the tool box and can be used. The different properties offered by these concepts can be then compared by designing aircraft with each of them. During the process, in parallel with the geometry, the engine parameters are computed.

1.2.3 Thermodynamic Turbofan Engine model

The objective of the engine model is to compute the fuel consumption, the thrust and the mass of the engine versus the required flight conditions. A scheme of a turbofan engine is

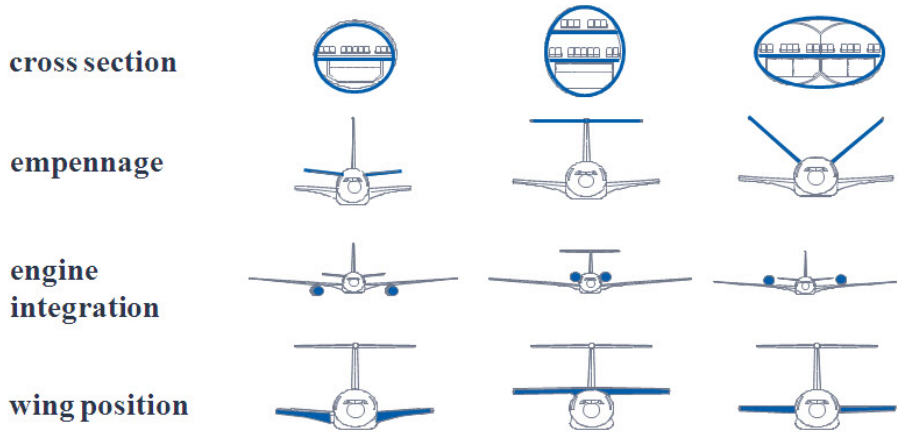

Figure 1.22: Examples of different concepts with variable geometry.

recalled in Figure 1.23. The input parameters of a turbofan engine are the following ones:

- A parameter that drives the size of the engine: the Sea Level Static Thrust, the maximum thrust that can be generated by the engine,
- Three parameters of the engine thermodynamic cycle:
  - the Overall Pressure Ratio (OPR), the ratio of total stagnation pressure between front and rear of the compressor line, a parameter of the thermodynamic cycle,
  - the By-pass Ratio (BPR), the ratio between the mass flow rate of air drawn in by the fan (cold flow) bypassing to the one passing through the engine core (hot flow),
  - the Fan Pressure Ratio (FPR), the ratio of the fan discharge pressure to the fan inlet pressure,

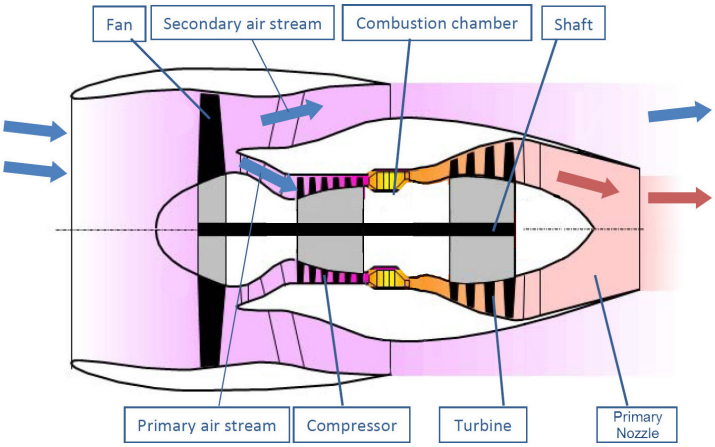

Figure 1.23: Turbofan engine simplified model.

- Four parameters that drive the engine maximum thrust given the flight phase (Take-Off, Climb, Cruise, Landing), with a value less or equal to 1.

The output are the weight of the engine, its nominal thrust F_n (N) and the Specific Fuel Consumption (SFC) ($kg/s/N$), as functions of flying confitions (Mach, altitude, temperature D_{isa}). This function will then be used for simulating the aircraft mission. The International Standard Atmosphere (ISA) is an atmospheric model of how the pressure and temperature of the Earth's atmosphere change over a wide range of altitudes. The variable D_{isa} is used to model a shift in the temperature as a function of the altitude (see Section 1.1.5). It is the simplest way to model the influence of the local weather conditions.

The engine model is summarized by the diagram of Figure 1.24. An engine is usually designed such that input design values minimize the engine SFC. It is representative of the engine fuel efficiency with respect to its thrust. It can be seen as a fuel consumption (kg/s) per unit of thrust (N). Once engine and geometry of the aircraft have been computed, we

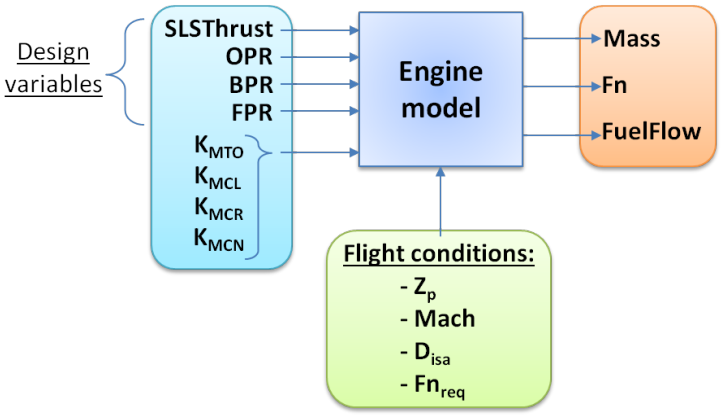

Figure 1.24: Engine model inputs, outputs and parameters.

can go to the next step of the process: computation of aerodynamics.

1.2.4 Aerodynamics model

The aerodynamics of the aircraft aims at producing the required lift and drag of the aircraft. The objective of the aerodynamics model is to compute the drag as a function of the required lift and of the flying conditions (Mach number, altitude, temperature D_{isa}). This function will then be used for the simulation of the aircraft design process.

Aerodynamics model is illustrated in Figure 1.25.

1.2.5 Weights and Mission model

Once the aerodynamics are evaluated, the following step is to compute the weights and the mission by running the mass-mission loop. This process is iterative as the mission requires the weights to be computed but the weights also require the amount of fuel and so the mission. Starting with hypothetic weights we solve the mass-mission loop process to obtain what is called a converged aircraft, satisfying mission and structural weights requirements. This is described hereafter.

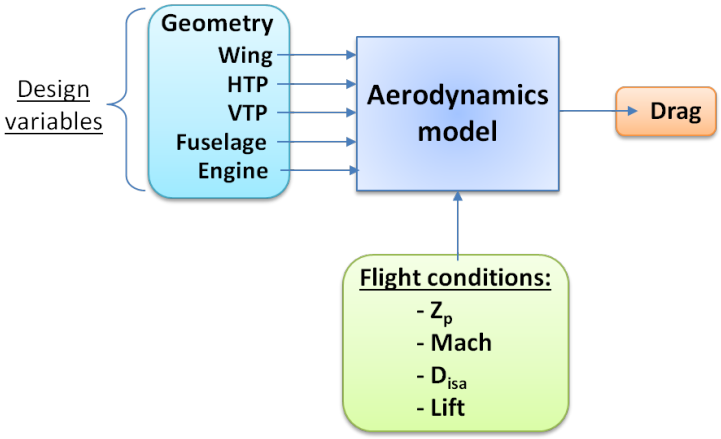

Figure 1.25: Aerodynamics model inputs, outputs and parameters.

For a classical aircraft, the manufacturer structural weights are broken down as in Figure 1.26. Of course this breakdown varies with respect to the passenger capacity, the range, the cruise speed. However, the order of magnitude remains similar. The objective

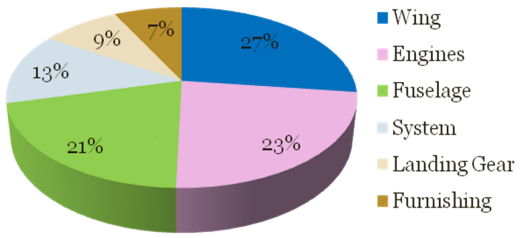

Figure 1.26: Repartition of the Manufacturer Weight Empty of a classical aircraft.

of weights model is to compute the following masses:

- the Manufacturer Weight Empty (MWE), which is detailed in Figure 1.26,
- the Operator Weigth Empty (OWE).

As presented in diagram from Figure 1.27, the inputs of the model are the geometry, the specifications (number of passengers for example), and the three following aircraft weights:

- Maximum Take-Off Weigth (MTOW), which is the maximum weight above which the aircraft is no longer allowed to take-off because of structural matters,
- Maximum Zero Fuel Weigth (MZFW),
- Maximum Landing Weight (MLW).

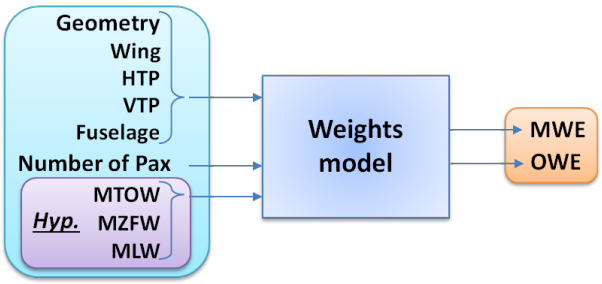

Figure 1.27: Weigths model inputs and outputs.

All these weights, called characteristic weights of the aircraft, are related, such as presented in Figure 1.28. The operator's items are the water, the food, the cabin crew and the cockpit crew. The equipment is composed of the galleys, the toilets, the storage structures and the seats. From a structural aspect and from the weights model, we know that the OWE can

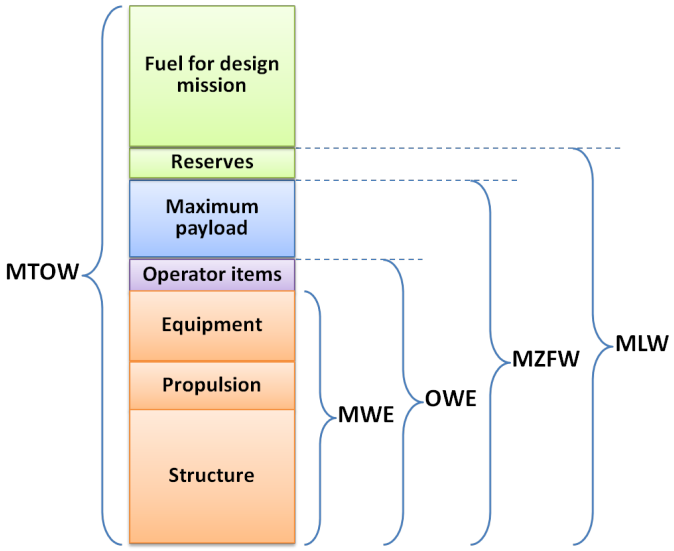

Figure 1.28: Characteristic weights of an aircraft.

only be computed by knowing the MTOW. We have:

$$\text{OWE} = f_1(\text{MTOW}).$$

As the two weights are unknown, a second equation is required to find the two weights. This second equation is based on the design mission range requirement: an aircraft is designed to perform a mission with a required range. The mission model is then necessary, and is presented in Figure 1.29. Its objective is to compute the fuel over a given mission, according to the weights of the aircraft, the speeds and altitudes. It yields the following equation:

$$\text{OWE} = \text{MTOW} - \text{Payload}_{mis} - \text{Fuel}_{mis} = f_2(MTOW),$$

where Payload_{mis} and Fuel_{mis} are respectively the payload and the fuel of the design mission. These two equations introduce the mass-mission loop process: its objective is to determine jointly the MTOW and the OWE of the aircraft. To illustrate this loop we

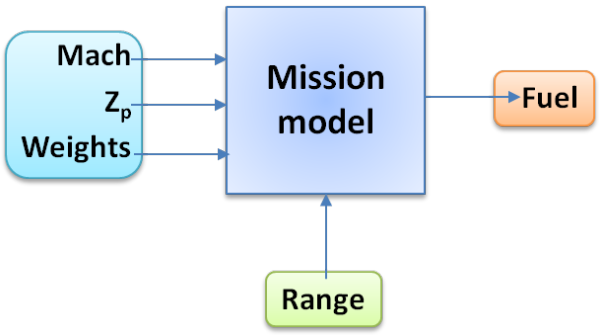

Figure 1.29: Mission model inputs, outputs and parameters.

can draw f_1 and f_2 in a graph that is presented in Figure 1.30. The two weights are the solution of a system such that:

- the aircraft has to be able to fly over the required mission distance the required amount of fuel,
- the structure is strong enough to sustain the load (aircraft, fuel and passengers).

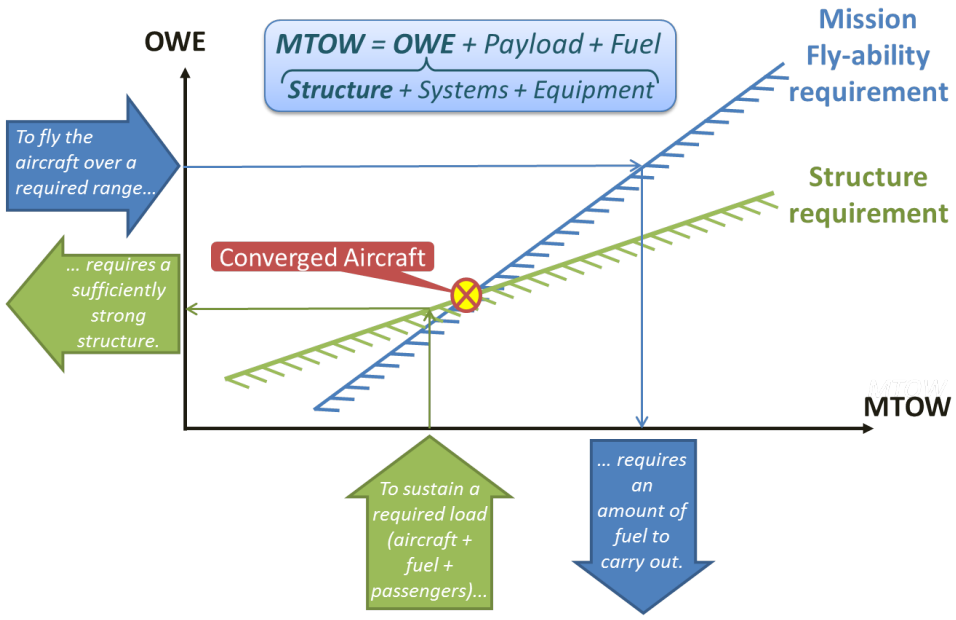

Figure 1.30: Aircraft Design Mass-Mission loop.

It implies a snowball effect, illustrated by the graph of Figure 1.31. For a given OWE to be flown over a given mission, the required MTOW can be read from the blue line. For

a given MTOW, a strong enough structure leads to the OWE that can be read from the green line. At the left of the intersection of the two lines, the MTOW is not sufficient to complete the mission and at the right the MTOW is exceeding the required one according to the OWE: the aircraft is overweighted. Then the ideal aircraft is the one that is at the intersection of the two lines. Now let us imagine that we change the OWE from a given delta. Then the new fly-able aircraft has to be at the new intersection and then it yields an even bigger delta of OWE. For example, for a typical long range aircraft: $1t$ additional

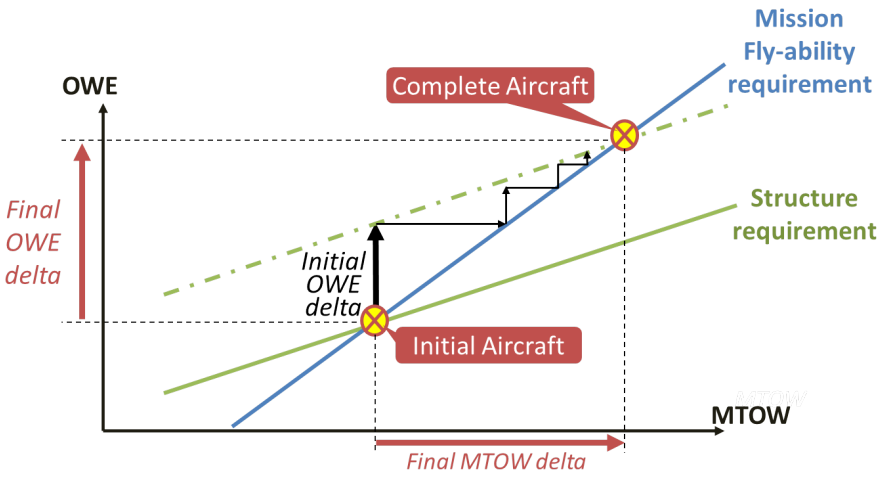

Figure 1.31: Aircraft Design Mass-Mission loop OWE versus MTOW: a snowball effect.

to the initial OWE, after the mass-mission loop is complete, leads to $1,4t$ additional to the OWE. The main effects are the additional amount of of fuel necessary to carry each additional kilogram of structure, and the additional amount of structural reenforcement required to each additional kilogram to take-off. This snowball effect is illustrated in Figure 1.32. Once the aircraft is converged, i.e. the mass-mission loop has converged, we

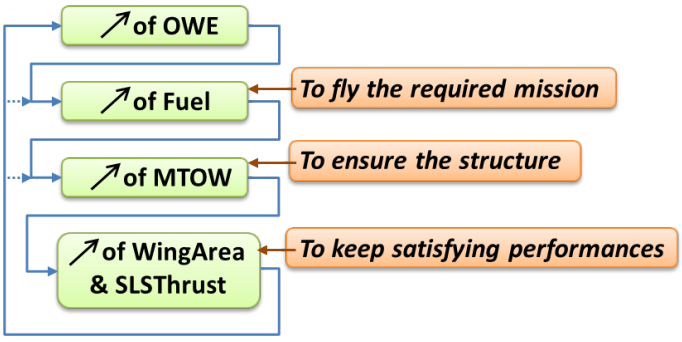

Figure 1.32: Aircraft Design Mass-Mission loop snowball effect.

can compute the other operational performances of the aircraft.

1.2.6 Performance models

Among these performances we can find the constraints that will have to be satisfied during the optimization process and also various of the criteria to be minimized.

1.2.6.1 Operational constraints

As mentioned in Section 1.2.1, aircraft design process is subject to various operational constraints, with the main objective of ensuring both the fly-ability and the safety. Regulatory constraints are often coming from the History of aviation: when a dangerous situation or an accident happened, a constraint was set in order to avoid this situation in the future. Nevertheless they are also defined by aviation infrastructures, particularly by the airports: a short range aircraft has to be designed to answer to regional airport operability that often have reduced runway length compare to international airports. To summarize, Figure 1.33 presents the constraints that we can find along the flight mission (see Table 1.2 that presents an example of values for a short range aircraft).

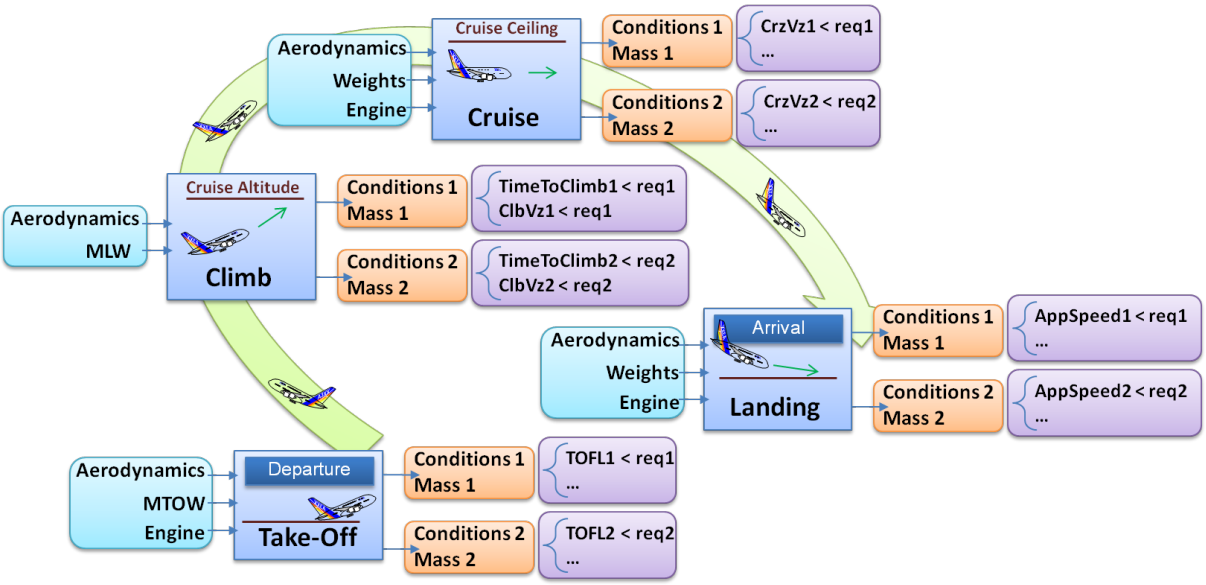

Figure 1.33: Performances model inputs, outputs and parameters.

1.2.6.2 Criteria

The aircraft design optimization can be driven by various objectives, the ones of interest in our case are presented in Figure 1.34. The Cash Operating Cost (COC) of the aircraft is detailed in Figure 1.35. It is based on a defined cost mission, that is well representative of the future use of the aircraft. We could have selected the Direct Operating Cost (DOC), that includes the following additional costs: insurance, aircraft price, CO_2, NO_x and noise charges, ramp handling, passenger handling, catering, and cabin crew. However doing so we would have considered hypothesis on the capital cost, and as it is an important unknown of the DOC, the COC remains an easier choice. The MTOW has already been presented in Section 1.2.5. In practice the MTOW is a big driver of the COC (but not the only one).

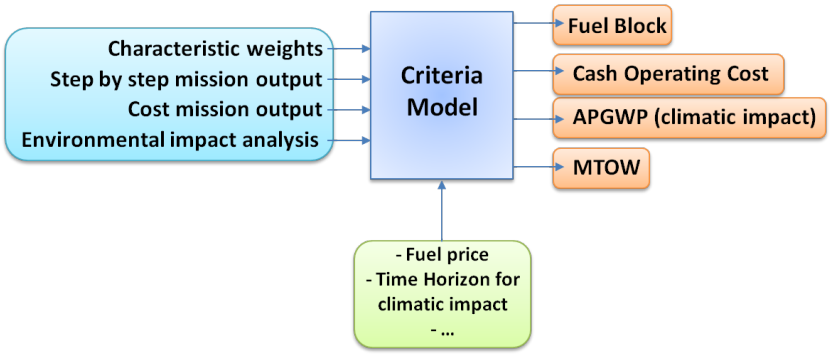

Figure 1.34: Criteria model inputs, outputs and parameters.

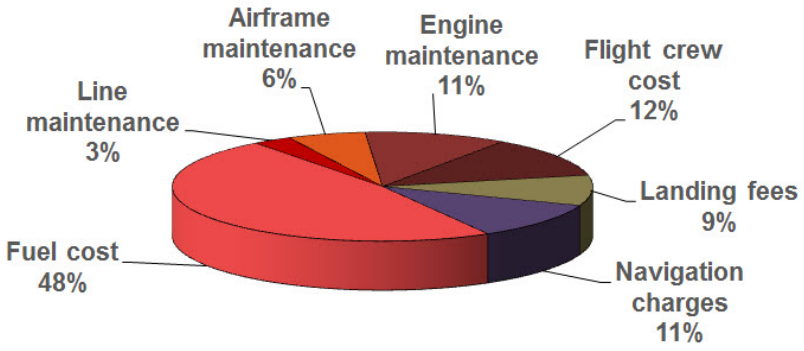

Figure 1.35: COC repartition for a single-aisle aircraft.

Hence as the COC is not always available, MTOW is most used as the aircraft design optimization objective.

The fule consumption can be evaluated on a shorter mission than the design mission. Typically, the same mission as for the cost evaluation is used. Let us note that the fuel is an other big driver of the cost.

The last objective is the Absolute Pulsed Global Warming Potential (APGWP) and is a measure of the climatic impact of the aircraft in our case. It is presented in detailed in the Section 1.3.3 with the environmental impact model.

The next section presents with more details the models that we used for our approach.

1.3 Models selection for the Overall Aircraft Design Process

Each model's way of operating has been presented in the previous section. The selection of each model is a question of trades that depend on the user willingness. One can requires an accurate way of solving aircraft design process. In this case accurate models will be required, which is directly traduced by a higher computation time. At our level one of the most important criteria is the computation time. On another side, the models have to give account from the concerned physics. A choice has to be done to select each model with enough accuracy to satisfy the physical representativeness of the models, but also to

maintain an affordable computing time.

Consistency between models is also very important: each of the interacting ones has to remain at a same level of accuracy. It would be a lost in computation time to merge accurate models with less accurate ones, as the global accuracy of the process will always be the one of lowest.

Classic overall aircraft design presented in Section 1.1.2 can be done with a very simplified engine model that does not take into account cycle parameters of the engine. The engine parameters are only driven by its SLSthrust and does not account for the thermodynamics. It makes the engine computation very simple but does not let any freedom of design or sensitivity to the type of engine. The mission model is also a simple one that does not model a step by step mission, which is particularly required to compute the climatic impact of the aircraft.

Several speeds are used to describe the flight trajectory and to define some operational constraints. The three following speeds will be used in the following sections:

- The Indicated Air Speed (IAS) is shown on the flight deck instrument.
- The True Air Speed (TAS) is the actual aircraft velocity relative to the airmass in which the aircraft is flying.
- The Calibrated Airs Speed (CAS) is a corrected IAS for instrument and position error.

Note that at sea level and a standard atmospheric pressure, with no wind effect, all the speeds are equal to the true speed of the aircraft relative to the earth surface.

Note also that the models that we used to run our studies are based on the very simplest models presented in the previous sections. However, we use little more sophisticated models, with a finer granularity level. This allows us to better appreciate and analyze the interactions between all the models and disciplines. All the models are described in [22].

1.3.1 Turbofan engine simple model

At future project level a software is dedicated to the design of engines. It is currently used by the expert engineers. However the computation of the engine design process with this software has two drawbacks according to our criteria:

- its number of design parameters is too high,
- its computational time is too high ($\approx$ 1 minute for one engine design, $\approx$ 20 secondes for one design point evaluation.

Then, a simplified model was required to satisfy our requirements. The objective is to introduce it in the overall aircraft design process. A Scilab version of a simple turbofan engine has been developed, based on [15], with a reduction of the number of design parameters. However, its computation time was still not fast enough.

The first idea was to build a meta-model of this simple version, with a given sample of the design parameters. The first step of this idea was to generate a sample that brings a satisfying accuracy of the meta-model. However, the required sample did not bring enough computational benefit compared to the initial model.

The second idea was then to build a semi-empirical model from the initial model. The modeling approach of the model, based on a required set of specifications, is fully described in Appendix A.

In order to validate the model, we have to define the flight envelope of the aircraft. The performances of the turbofan engine (thrust, power, fuel consumption, temperatures, shaft speeds etc.) are crucially dependent upon the local atmospheric conditions. During a flight, these conditions are varying. Then we define a flight envelope with ranges of Mach, pressure altitude and temperature where the engine will be operating according to the aircraft requirements. Figure 1.36 presents a typical flight envelope and more particularly in red the one we are going to use to proceed the validation tests.

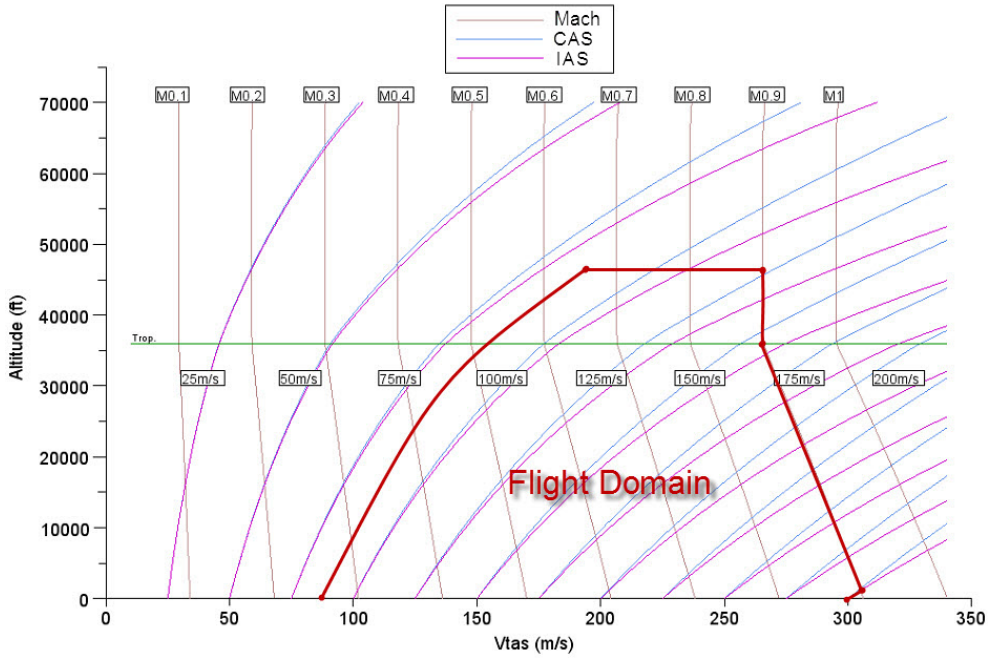

Figure 1.36: Aircraft Operational Envelope for Engine model validation.

After the engine model validation has been done, it can be integrated to the whole aircraft design process.

1.3.2 Operations modeling

Operation models cover various type of missions. The three following missions are fixed, with respect to operational requirements, and they allow to compute various performances of the aircraft. We find:

- the Cost mission is representative of the typical operating mission of the aircraft. Output are the different costs of the aircraft. In the case of a short range aircraft, it is 500 NM.

- The Nominal mission, also called the design mission, is the one used to run the mass-mission loop and to compute the aircraft performances.

- The Maximum Payload mission, the Zero Payload mission and the Maximum Fuel mission are also computed but not of interest in our case of study. These missions can be summarized in a simple diagram, namely the Payload-Range diagram. An example is presented in Figure 1.37. It illustrates the trade-off relationship between the payload and the range of an aircraft. The first line is the maximum range that can be reached at the maximum payload. At this maximum range, any further range is achieved only by reducing the payload and then increasing the fuel, which follows the following diagonal line. The last almost vertical line starts with the point at which the maximum fuel capacity is reached. From this point, only the payload can be reduced which leads to this slight increase of the range.

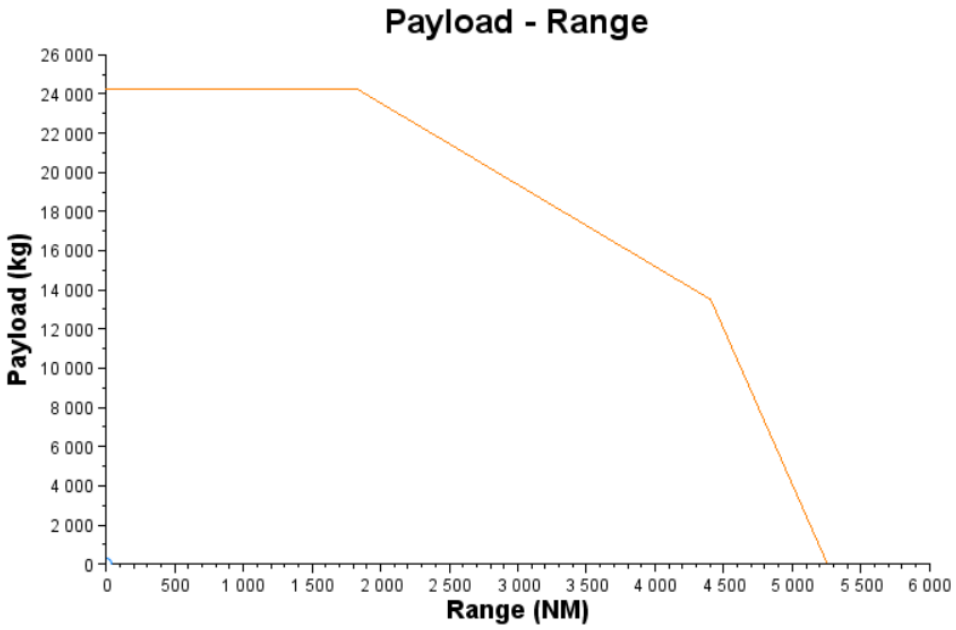

Figure 1.37: Example of a Payload-Range diagram.

These missions computation are all based on the Breguet-Leduc equation, that compute the range of an aircraft mission, according to the structure, the aerodynamics and the propulsion of the aircraft. This equation is given by:

$$Range = \frac{1}{g} \times \underbrace{\frac{L}{D}}_{\text{Aerodynamics}} \times \underbrace{\frac{V}{SFC}}_{\text{Propulsion system}} \times \underbrace{\ln\left(1 + \frac{FuelBurn}{OWE + Payload + Reserves}\right)}_{\text{Structure}}, \tag{1.9}$$

where:

- g is the gravity acceleration (m/s^2),
- $\frac{L}{D}$ is the Lift over Drag ratio,
- V is the ground speed, equivalent to the addition of the True AirSpeed (TAS) and the wind speed (m/s^2),

- SFC is the Specific Fuel Consumption ($kg/s/N$),
- OWE is the Operating Weight Empty (kg),
- $FuelBurn$ is the amount of fuel burned during the mission (kg),
- $Range$ (m).

Additionally to these missions, a more detailed model was required to compute the climatic impact and to integrate the engine model at different points of the trajectory. Then, Breguet-Leduc equation was not sufficient. So, we have used a step-by-step mission model which produces the whole trajectory of the aircraft along the mission and with an accurate value of the speed, the weight, the distance, the altitude at various points of the trajectory. This allows the computation of the climatic impact, with the models presented in Section 1.3.3.

However, the current air traffic is subject to many constraints, in order to keep air transport safe, fast and efficient. Among these constraints, aircraft trajectories must obey several standards for the three different flight phases: climb, cruise and descent. The step-by-step mission model has to fulfill the following operations according to the mission phase. These operations can be found in [5].

1.3.2.1 Climb

A climb is generally operated at a constant IAS and a constant Mach number. For instance a standard climb profile for the A320 family is : 250kt/300kt/Mach0.78. This example is

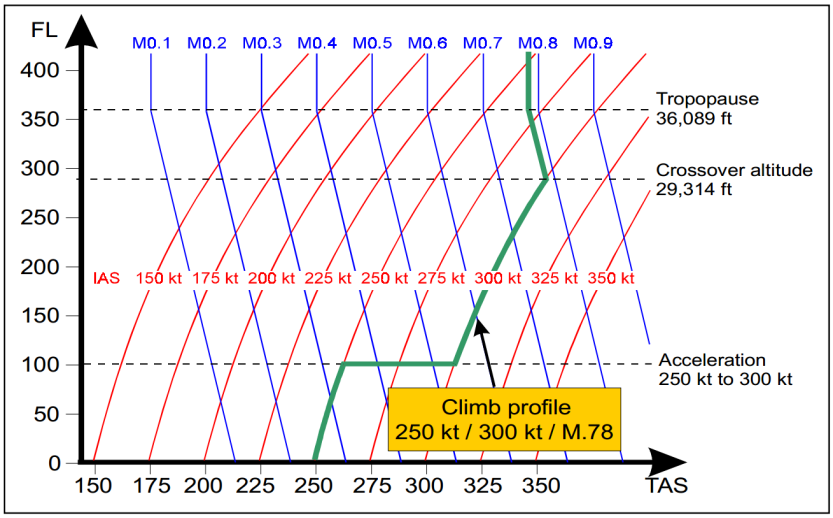

Figure 1.38: Example of standard climb profile for an A320, at given Mach/IAS Law [5].

presented in Figure 1.38, the three numbers correspond to the three following phases:

- Below 10,000 feet : climb is done at a constant IAS of 250 knots. This speed is limited by Air Traffic Management (ATC) laws.
- Between 10,000 feet and the crossover altitude : climb is done at a constant IAS of 300 knots. This phase is maintained as long as the Mach number remains under 0.78.

- Above the crossover altitude : climb is done at a constant Mach of 0.78. The crossover altitude is the altitude where 300 knots IAS is equal to Mach 0.78. This last phase is maintained until the cruise altitude is reached.

1.3.2.2 Cruise

Ideal cruise should coincide with optimum altitude, where the fuel consumption per distance unit is the lowest. As a general rule, this altitude is not constant. It increases as weight decreases during cruise. On the other hand, ATC restrictions require some constant levels of flight cruise: an aircraft must fly by segments of constant altitude. Consequently, the cruise phase is composed of several segments of increasing altitude: it is a step climb. The number of segments depends on the range of the mission. In the example of Figure

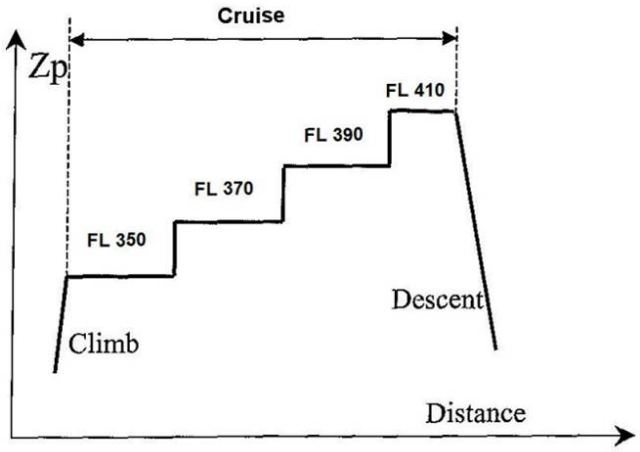

Figure 1.39: Example of standard cruise profile for an A320.

1.39, there are four segments. The altitude separation between two segments is 2000 feet. The operational altitudes of this flight are called FL for flight level and for instance FL350 is equivalent to a cruise at 35000 feet.

1.3.2.3 Descent

As for the climb phase, a descent is generally operated at a constant Mach number and a constant IAS, as presented in Figure 1.40. For instance, a standard descent profile for the A320 family is: Mach0.78/300kt/250kt, the reverse course of the climb.

1.3.3 Environmental impact modeling

Aircraft environmental impact is highly difficult to assess as it happened in various conditions, it implies chemistry, physics and an important amount of parameters. At the future project level, we choose a method developed in the frame of a European project named LEEA (for Low Emission Effect Aircraft) [89] presented in Figure 1.41. It evaluates the climatic impact of an aircraft as a function of several concrete parameters given in Table 1.3. Emission index of NO_x can be computed using Boeing2 method [14] in combination with the mission flight profile. LEEA takes into account contrail formation and chemi-

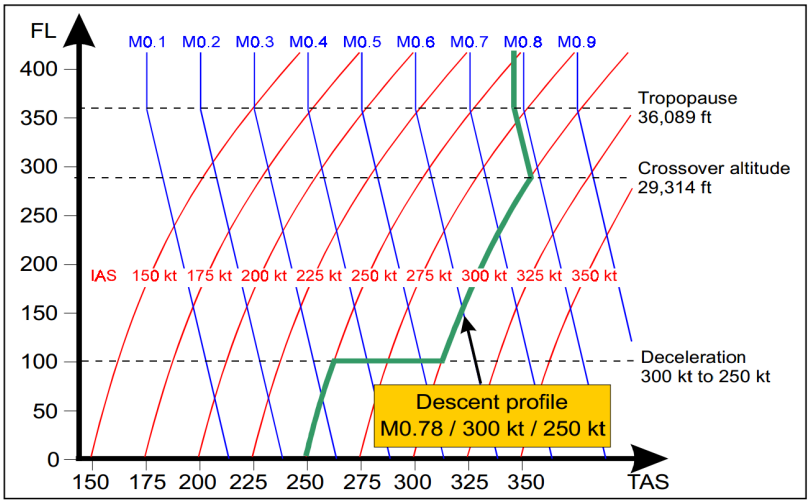

Figure 1.40: Example of standard descent profile for an A320, at given Mach/IAS Law [5].

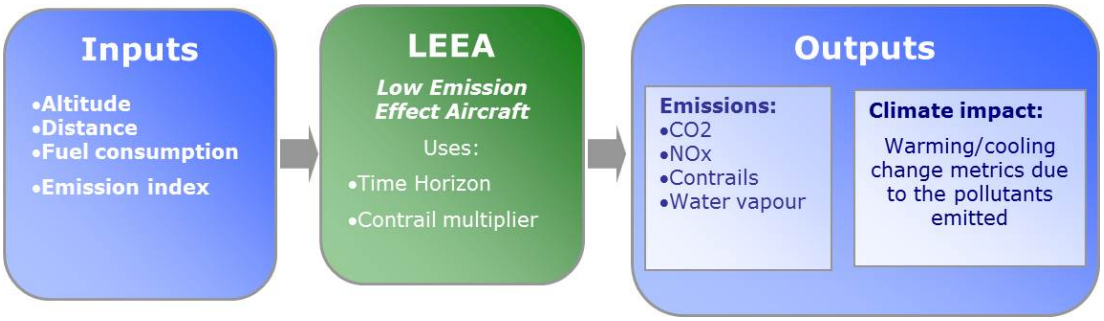

Figure 1.41: Environmental Impact LEEA modeling

Table 1.3: Description of LEEA input parameters

Name	Unit
Altitude of interest	ft
Distance flown	km
Fuel used	kg
NO_x Emission Index	g/kg

cal changes to the atmosphere. It considers the pollutants from Table 1.4 with the effect presented in the same table. It uses the same measures of climate impact as the Kyoto Protocol: the "Global Warming Potential", which is essentially the radiative forcing due to a pulse emission integrated forward over time. However four metrics were used and can be selected as output of LEEA method. They are presented in Table 1.5. The metrics calculate the climate effect integrated over a time period, named the 'Time Horizon'. In the literature on climate impact of aircraft, values are often between 20 and 100 years.

Table 1.4: LEEA: Pollutant and their effect

Pollutant	Effects	Warming or Cooling
Carbon dioxide	Greenhouse effect	Warming
Nitrogen oxides	Produce ozone Destroy pre-existing methane	Warming Cooling
Contrails	Reflect sunlight Reflect infrared	Cooling Warming
Water (vapour)	Greenhouse effect. Small effect in troposphere and larger effect in stratosphere	Warming

Here we choose 100 years. The effect of contrails is particularly uncertain. The contrail multiplier is thus included in LEEA and can be selected between 2 and 10. Usually the value of 5 is used, and it is the one we choose. In order to remain consistent with the most used metric, we select APGWP (see Table 1.5) as the environmental objective of the future aircraft design optimization.

Table 1.5: LEEA Four metrics

Metric	Units
Absolute Sustained Global Warming Potential (ASGWP)	$mW \cdot m^{-2} \cdot (km \cdot year^{-1}) \cdot year$
Absolute Pulse Global Warming Potential (APGWP)	$mW \cdot m^{-2} \cdot km^{-1} \cdot year$
Absolute Sustained Global Temperature Change Potential (ASGTP)	$mK \cdot (km \cdot year^{-1})^{-1}$
Absolute Pulse Global Temperature Change Potential (APGTP)	$mK \cdot km^{-1}$

1.3.4 Hybrid configuration modeling

Now the core of models have been introduced, we are going to present an innovative aircraft configuration based on an hybrid electric/fuel way of propelling the aircraft. This configuration is presented in Figure 1.42. We decide to keep a conventional configuration and to add an electric engine fan on the rear fuselage of the aircraft. In order to power the electric engine we first add accumulators. They can be placed in the airplane cargo hold for instance such that the handling qualities of the aircraft does not change. Secondly electric generators are placed in the turbofan engines so that we can take additional energy from the turbofan to power the electric fan. The idea is that an additional fan increases the global By-Pass Ratio of the propulsion system and thus improves the propulsion performances. An electric Ratio parameter is then introduced allowing to control the amount of energy given by the electric generators (as a part of the total thermal energy produced by the turbofan) to the electric engine. Then a big amount of work was done about how the

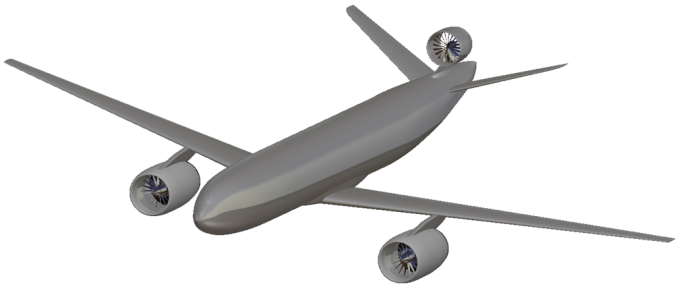

Figure 1.42: Hybrid Aircraft Configuration, version 1.

electric powered aircraft differs from the conventional aircraft. The objective is to take into account a maximum of the new possibilities brought by the hybridization. Clearly, it is not possible to envisage accumulators as a long term source of energy during the flight, as the additional weight of battery is really expensive. Hence it only can be considered as an additional source that can be used temporarily, with the idea of reducing thermal engine oversizing by compensation.

1.3.4.1 Electric engine and energy management

As illustrated in Figure 1.43 we propose the following use of the hybrid propelling as a function of the different flight phases:

- Before taxi-out battery are fully charged, and electric fan is not used during taxi-out.
- During the take-off the battery are used to power the electric fan, along with power coming from the turbofans. A constraint of take-off rating less or equal than 5 minutes of use of battery is set in order to limit its size.
- During the climb, if required the battery can be used to power the electric fan (for example at the top of climb, when more power is needed).
- During the cruise, the turbofans are used to charge the battery and power the electric fan.
- During the descent, the electric fan may be used to complete the battery charge, like a windmill.
- During the taxi-in, thermal engines can be off and accumulators power the electrical engine to drive the aircraft to the parking. It is a way of reducing fuel consumption, but also noise and emissions at the airport.
- In case one engine becomes inoperative, the battery are used to power the electric fan and limit the extra power required from the remaining thermal engine.

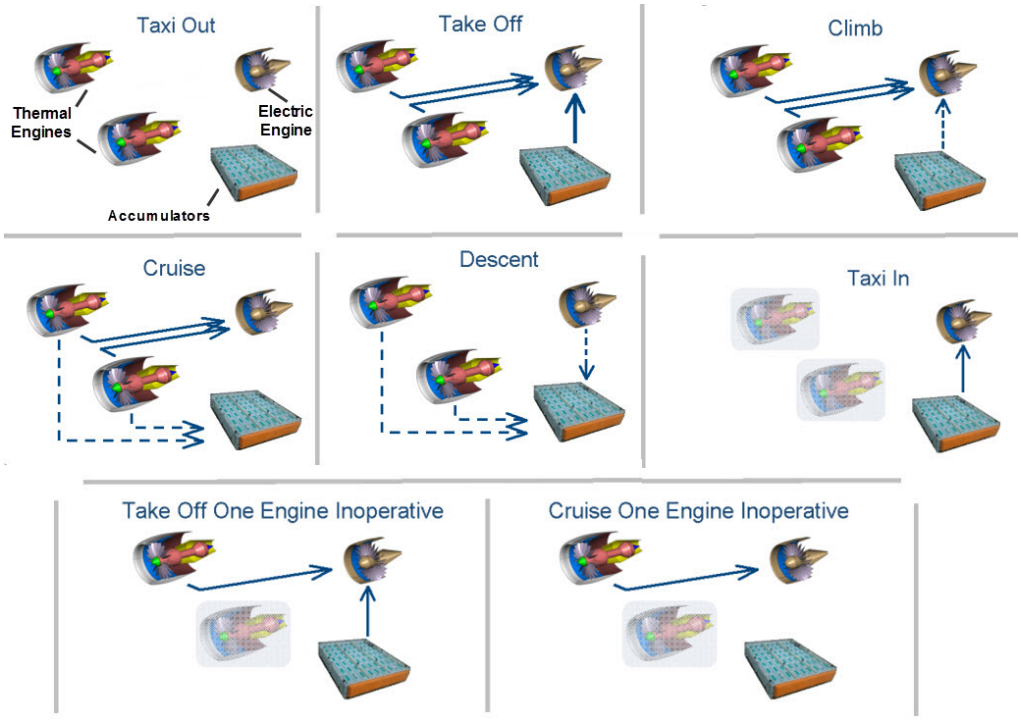

Figure 1.43: Energy Flows Management (blue arrows) for hybrid aircraft operations.

1.3.4.2 Hybrid Engine model

From this concept we need to build several models. The first one is the new propulsion model of the electric turbofan, presented in [15]. The others are the different mass penalty functions due to electric engine and accumulators. We finally modify the impacted functions from the classical aircraft design process. The last one is the operability of the electrical parts of the hybrid aircraft described in Figure 1.43. New parameters are required to manage the hybrid propulsion system. The first ones are presented in Table 1.6. The energy density is the amount of energy stored in a given system per unit mass and the power density is the amount of power per unit of mass. These values are set according to last technological assessments given by the electrical expert of airbus future project. We select as new design parameters, i.e. additional optimization degrees of freedom, the

Table 1.6: Description of the hybrid aircraft technological parameters.

Name	Value & Unit
Power Density of Electrical Engine	3.5 kW/kg
Power Density of Electrical Generator	3.5 kW/kg
Energy Density of Accumulators	350 Wh/kg

ones presented in Table 1.7: the electric Fan Power, the electric Ratio and the electric Fan Diameter. The diagram from Figure 1.44 illustrate the hybrid propulsion model, with the latter mentioned input, transfer links between the thermal engines, the electric fan and the

Table 1.7: Description of the hybrid propulsion design parameters.

Name	Bounds & Unit
Fan Power	$[1.5 - 4]$ MW
Generator Electric Ratio	$[1 - 10]$ %
Fan Diameter	$[1 - 3]$ m

battery and also the new outputs.

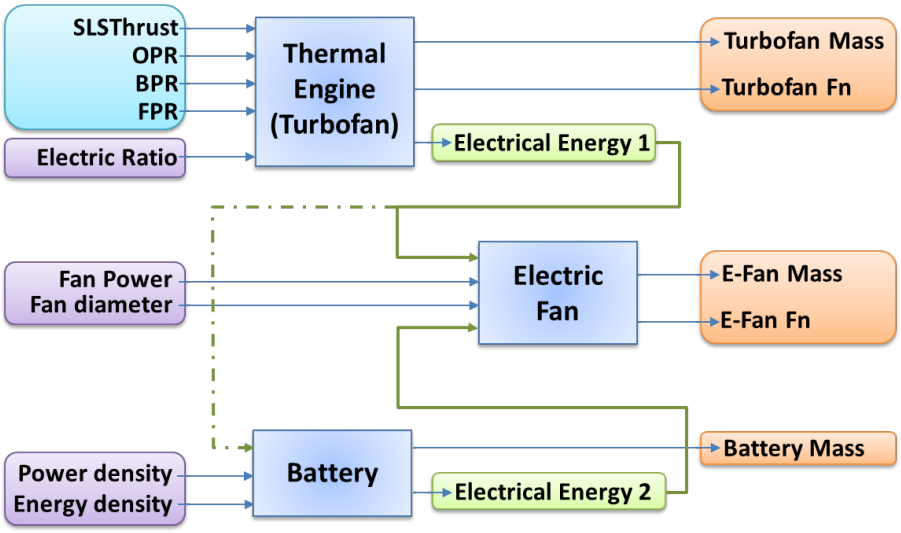

Figure 1.44: Hybrid propulsion model inputs, outputs and parameters.

1.3.4.3 Technologies evolution

Running the processes for the hybrid aircraft we logically observe that current technologies performances do not allow this configuration to be as efficient as the conventional configuration. The idea proposed is to add to the models some prediction functions of the technology improvement as a function of the year for the power density of electrical engine and the power density of electrical generator (EPD), and for the energy density of accumulators (EED). Thanks to some assumptions found in literature [158, 48], we propose for these two entities some evolution models as function of the year. It is represented in Figure 1.45. As the evolution is given with a prediction error, we will take it into account in our further studies. So we draw on the latter figure the 99% confidence interval for the evolution functions, with in green the upper bound and in red the lower bound.

1.3.4.4 Additional improvements of the hybrid aircraft concept

A first hybrid aircraft was designed as previously described. However the benefits in comparison to an equivalent classical configuration were not obvious. That makes us think

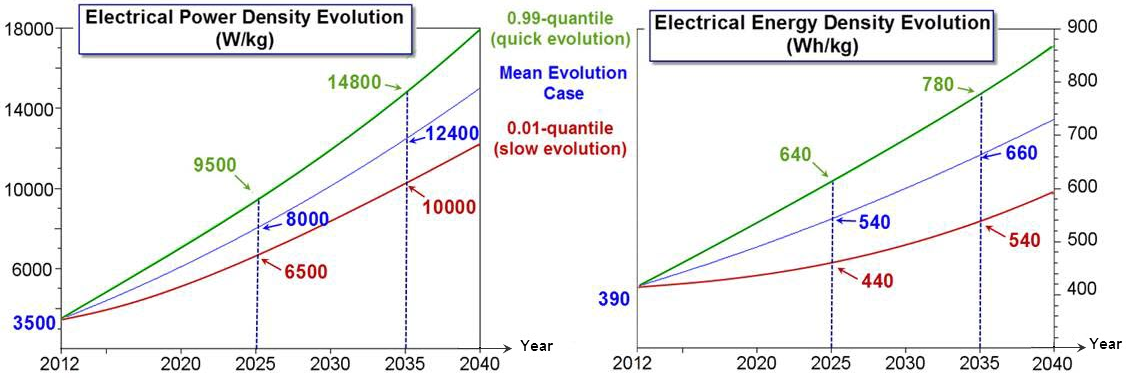

Figure 1.45: Prediction functions of electrical technologies evolution with their uncertainty (Gaussian distribution).

of what kind of additional synergies of the hybridization we could use to increase these benefits. The following strategies were selected:

- We choose a variable pitch electric fan, such that it can generate reverse thrust. Doing so, the thrust-reverser of the two thermodynamic turbofans could be removed. This improvement comes with a new constraint that ensures a minimal reverse thrust.

- We place the electric fan so that the carter of the fan could contribute to longitudinal and lateral stability of the airplane. Hence we can reduce the vertical and horizontal tail-planes size.

- We also can take advantage of the performance of a Boundary Layer Ingesting electric fan, by placing it at the rear fuselage such as presented in Figure 1.46. More details [134]. In our case we assume that it yields a decrease of 5% of the total Specific Fuel Consumption (SFC) of the propulsion system.

- Finally, to take more benefit of the battery system, we think of removing the Auxiliary Power Unit (APU) of the aircraft. It is usually used to provide energy for functions other than propulsion. However we assume that an additional 100 kg of battery were required to compensate this removal.

1.3.4.5 Final hybrid aircraft concept

Finally a last concept of hybrid aircraft has been selected. It is presented in Figure 1.47. It differs from the previous one by a reverse sweep of the wings and by the two thermal engines that are now placed at the rear fuselage. The idea is to compare the improvements of the hybridization of two different concepts. We will observe if the impact of the hybridization can be more beneficial depending on the configuration. Results are presented in Chapter 3.

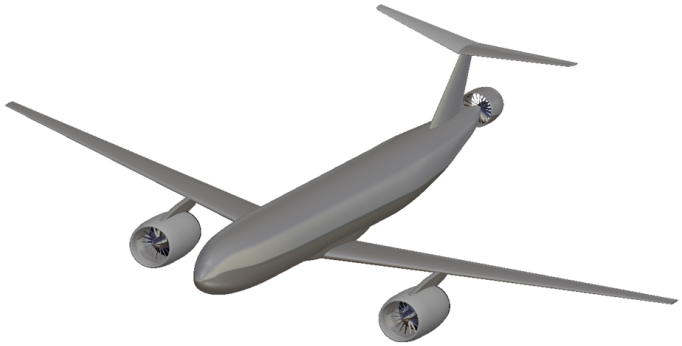

Figure 1.46: Hybrid aircraft configuration with additional improvements, version 2.

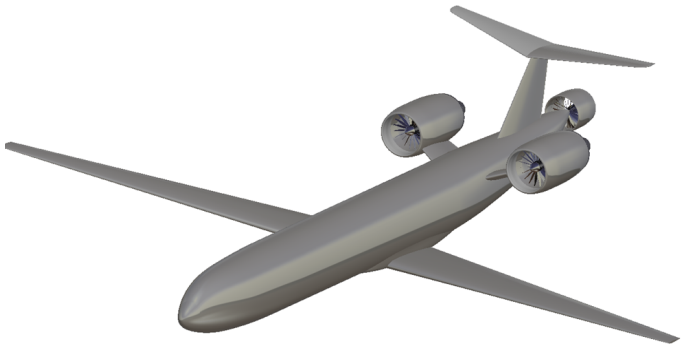

Figure 1.47: Final Hybrid aircraft configuration, version 3.

1.4 In summary

The integration of all models required an accurate analysis. We start by integrating the engine design to the overall aircraft design process. The first idea was to couple the engine design process such as presented in Figure 1.48: the objective is to solve the whole loop, where engine design is done according to thrust requirements that come from aircraft design, which is operated using engine design parameters. However two problems appear. First, there was a risk of non convergence of this loop, in particular because the two optimization processes are not minimizing the same criteria but they are sharing one common parameter, the engine SLSThrust. Secondly, there was a risk that the engine model is too simple to influence the performances of the whole design process.

The second idea was to put the engine design process at the same place as for the original aircraft design process as in Figure 1.19 and to merge both optimizations according to the final criteria. This method required a better understandability of the connections between the models but finally it results in a consistent physical behavior. However it also increases computation times. That is what makes us study some surrogate modeling method and surrogate based optimization (see Chapter 2).

Finally we add to the design the detailed step-by-step mission trajectory. The whole process can be represented in Figure 1.49, with in circle red the new models integrated to the overall aircraft design. Chapter 3 is dedicated to the application of this optimization

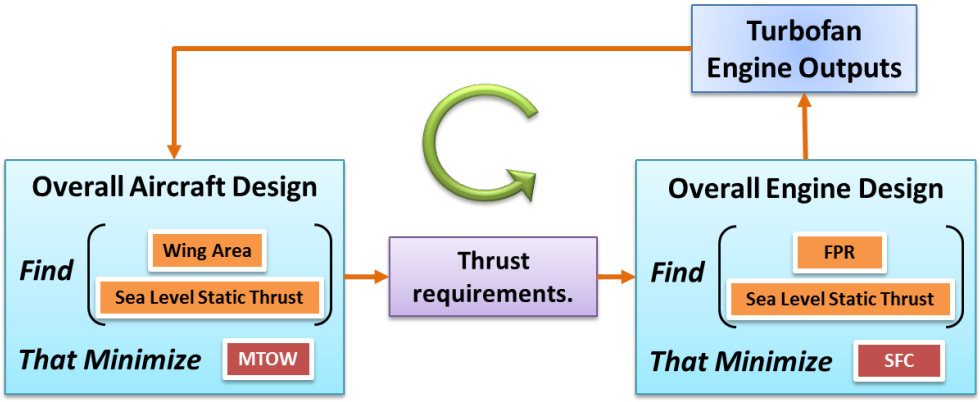

Figure 1.48: Overall Aircraft Design Optimization Process: first engine integration.

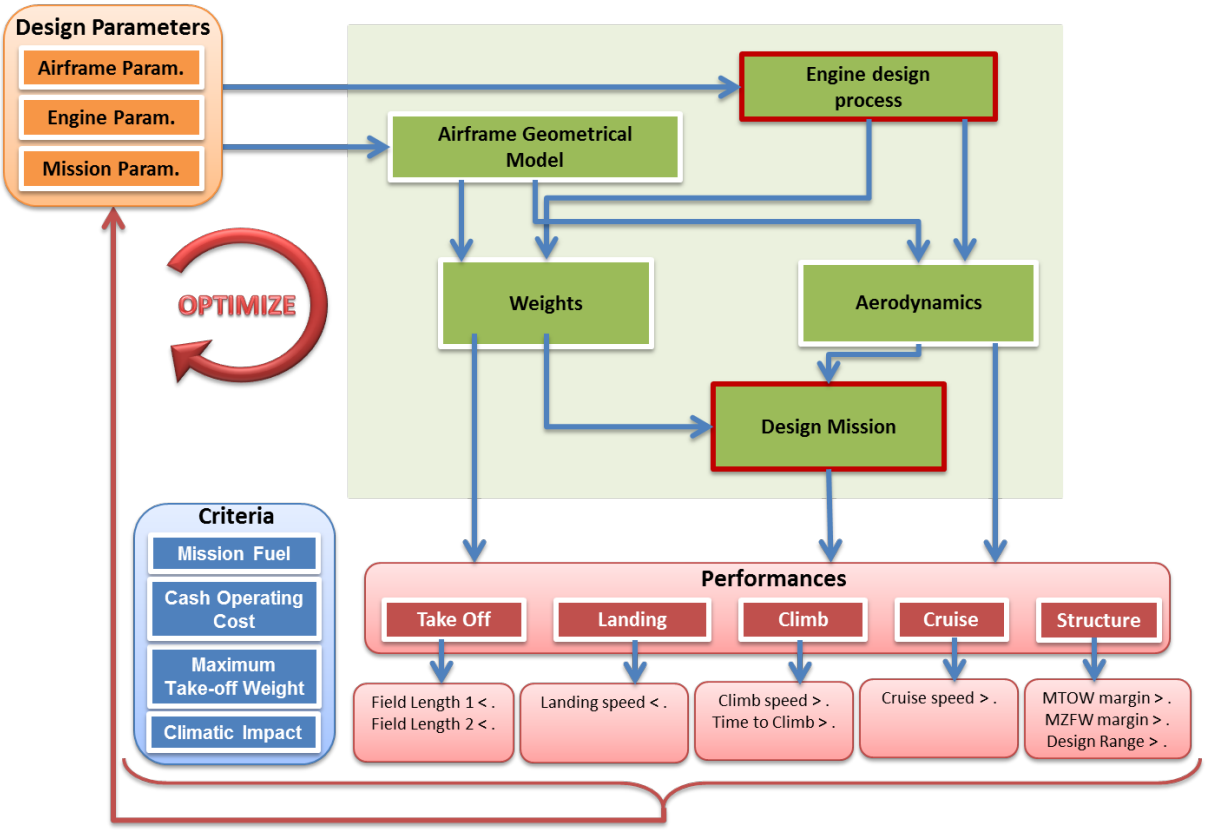

Figure 1.49: Enhanced Overall Aircraft Design Optimization Process.

process.

Chapter 2

Mathematical Tools

Contents

Aircraft preliminary design relies in a first part on modeling the whole process from requirements to evaluation of performances. The second part is to optimize this design, selecting objective and constraints from the performances. As mentioned in the previous chapter, optimizing a new aircraft configuration can be to minimize the block fuel along a given flight mission, with respect to operational constraints such as not to exceed a given length of take-off field, or a given approach speed. The new approach proposed in Chapter 1 leads to the integration and adaptation of optimization methods and mathematical tools. All along this chapter we will present these tools and methods, each of them responding to a specific need. In a first section, we briefly present useful tools of automatic differentiation field. The second section is dedicated to three surrogate modeling methods. Finally the last section deals with optimization methods. Two main categories are described: derivative-free optimization algorithms on the one hand, algorithms using gradients on the other hand. Multi-objective and Pareto front notions are finally addressed in the last section.

2.1 Automatic differentiation

Automatic differentiation appears to be a very useful tool to obtain gradients through the process of aircraft preliminary design. The idea comes first with the uncertainty propagation through the process (see Chapter 4). The main idea was to get at each step of the process, not only a value of a variable, but also its uncertainty. At the end, it comes with the need of gradient at each step of the process, and then with the implementation of some automatic differentiation tools.

Automatic differentiation dates back to the fifties. Papers from [23, 147, 75] give a good survey on the subject, relevant properties and examples of applications. The main principle of automatic differentiation is well summed up by the following definition [147]:

The basic idea behind the automation of differentiation is very simple: Once a code list has been obtained for the function considered, then the rules of elementary calculus can be applied to it line by line to give a list of instructions for evaluation of the derivative.

Benefits of automatic differentiation are to compute derivatives analytically and systematically, in particular without the numerical error inherent in finite difference approximations. Since the used models are black-box functions, this kind of numerical error is one of the limit in the use of gradient optimization tools. Automatic differentiation then brings a more accurate way to compute gradients. As a consequence, it paves the way to gradient-based optimization. The principle used to obtain gradient is presented in the following paragraph.

The objective is to apply automatic differentiation methods to the process of aircraft design, for which models are coded in Scilab language. To produce gradient as an output at the same level of each variables value we have to go into the line code.

Let $(x_1, \ldots, x_n)$ be the input vector of the process. The main steps towards automatic differentiation are illustrated on Figure 2.1 and are the following:

1. Create a new type of object such that each input or output variable in the process comes with a value and its gradient with respect to specific variables, namely here with respect to the variables $(x_1, \ldots, x_n)$. Scilab enables this via the *tlist* declaration.

2. Overload the basic operators and functions. Indeed, once a new type of variable is defined, the next step is that each operation and each function in the process

can automatically manage this new type of variable. Typically the most important operators to be overloaded are:

$$+, -, \times, /, \cos, \sin, \tan, \log, \exp, x \mapsto x^a, \min, \max, x \mapsto |x|.$$

3. Eventually, overload all functions involved in the process. In our case, they include vectorized operations, insertion, extraction, transposition, all logical operations, all operations on matrices. Overloading a function consists in adding a method to the function that enables it to deal automatically with the new type of variable.

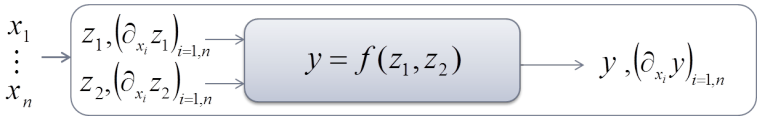

Figure 2.1: Automatic differentiation illustration.

Let us now consider the specific example illustrated in Figure 2.1. The objective is to obtain the gradient of the function f with respect to the input vector $\boldsymbol{x} = (x_1, \ldots, x_n)$. According to the chain rule, the gradient of f with respect to $\boldsymbol{x}$ is given by:

$$\nabla_{\boldsymbol{x}} f = \nabla_{z_1} f(z_1, z_2) \cdot \nabla_{\boldsymbol{x}} z_1 + \nabla_{z_2} f(z_1, z_2) \cdot \nabla_{\boldsymbol{x}} z_2. \tag{2.1}$$

As an illustration of what is happening into the gray box of Figure 2.1, we consider the example of the multiplication of z_1 by z_2, i.e. $f(z_1, z_2) = z_1 \times z_2$. Then the overloading of the operation $y = z_1 \times z_2$ is given by:

$$\begin{pmatrix} y \\ \partial_{x_1} y \\ \vdots \\ \partial_{x_n} y \end{pmatrix} = \begin{pmatrix} z_1 \times z_2 \\ z_1 \times \partial_{x_1} z_2 + z_2 \times \partial_{x_1} z_1 \\ \vdots \\ z_1 \times \partial_{x_n} z_2 + z_2 \times \partial_{x_n} z_1 \end{pmatrix}.$$

A careful attention has to be paid to the code: all the functions used with the new type of variable, have to be overloaded. We also have to overload all the operations dealing with a scalar. For instance if z_1 is a variable of the new type and a a scalar, the overloading of the operation $y = z_1 \times a$ is done the following way:

$$\begin{pmatrix} y \\ \partial_{x_1} y \\ \vdots \\ \partial_{x_n} y \end{pmatrix} = \begin{pmatrix} z_1 \times a \\ a \times \partial_{x_1} z_1 \\ \vdots \\ a \times \partial_{x_n} z_1 \end{pmatrix}.$$

The last step is then to declare each variable of the vector $(x_1, \ldots, x_n)$ as a new variable, where the gradient of x_i with respect to $\boldsymbol{x}$ is:

$$\nabla_{\boldsymbol{x}} x_i = (\partial_{x_1} x_i, \ldots, \partial_{x_i} x_i, \ldots, \partial_{x_n} x_i) = (0, \ldots, 0, 1, 0, \ldots, 0). \tag{2.2}$$

Doing this, at the end of the process, we obtain variables of the new type, i.e. with their value and their gradient with respect to $\boldsymbol{x}$. This is especially useful when we want to use

automatic differentiation for optimizing functions of the process, since we can provide the value and the gradient of the objective function.

Automatic differentiation can also be used to obtain the Hessian of each variable with respect to the input vector. The approach is the same:

1. Define a new object with a value, its gradient and its Hessian with respect to the input vector.
2. Overload functions and operations with corresponding methods to compute the Hessian.

For a function $f : (z_1, z_2) \mapsto f(z_1, z_2)$, and a process input vector $\boldsymbol{x} = (x_1, \ldots, x_n)$, the Hessian $H_{\boldsymbol{x}} f$ is computed as:

$$\begin{aligned} H_{\boldsymbol{x}} f = \nabla_{z_1} f(z_1, z_2) \cdot H_{\boldsymbol{x}} z_1 + \nabla_{z_2} f(z_1, z_2) \cdot H_{\boldsymbol{x}} z_2 + \partial^2_{z_2} f(z_1, z_2) \cdot \nabla_{\boldsymbol{x}} z_1 \nabla_{\boldsymbol{x}}^\top z_1 + ... \\ ... + \partial^2_{z_1} f(z_1, z_2) \cdot \nabla_{\boldsymbol{x}} z_2 \nabla_{\boldsymbol{x}}^\top z_2 + \partial^2_{z_1 z_2} f(z_1, z_2) \cdot (\nabla_{\boldsymbol{x}} z_1 \nabla_{\boldsymbol{x}}^\top z_2 + \nabla_{\boldsymbol{x}} z_2 \nabla_{\boldsymbol{x}}^\top z_1). \end{aligned}$$

As an illustration, let us consider again the example: $f(z_1, z_2) = z_1 \times z_2$. Then the Hessian of f is given by:

$$H_{\boldsymbol{x}} f = z_2 \cdot H_{\boldsymbol{x}} z_1 + z_1 \cdot H_{\boldsymbol{x}} z_2 + \nabla_{\boldsymbol{x}} z_1 \nabla_{\boldsymbol{x}}^\top z_2 + \nabla_{\boldsymbol{x}} z_2 \nabla_{\boldsymbol{x}}^\top z_1.$$

As previously done, each variable of the input vector has to be declared as a variable of the new type, with a value, its gradient and now its Hessian which is, in this case, the null matrix of dimension $n \times n$. This can be useful for second-order optimization algorithms. This technique will also be useful in the uncertainty propagation method, where the Taylor coefficients of the function f are required, see Chapter 4.

2.2 Surrogate modeling

In engineering and more particularly in aircraft design process, the evaluation of performances is generally expensive. For example, the evaluation of the fuel consumed by an aircraft over a given mission requires the computation of the geometry, of the weights, of the propulsion system and then of the trajectory of the aircraft with respect to some operational requirements. This involves nested solvers. To sum up, it takes time and computational resources. Moreover, the functions involved in an engineering process can also be hard to track: they can be discontinuous, non differentiable, and subject to noise. When an optimization has to be performed, it can quickly become untractable. Therefore we choose a practical handling of these functions by using surrogate models. This section describes various methods used to create surrogate models.

In a general way, meta-modeling consists in the following steps [159]:

- choosing a design of experiment for generating data,
- choosing a model to represent these data,
- fitting the model to the observed data,
- model validation.

We focus here on the choice of the model. Note that model validation techniques strictly depend on the choice of the modeling techniques. Most commonly used metrics for validation can be found in [175]. In the next sections, we present two different models: the Radial Basis Functions model and then the Kriging model. All the mentioned techniques rely on solving the scattered data interpolation problem:

Given data $(\boldsymbol{x}_i, y_i)_{i=1,\dots,N}$*, where* $\boldsymbol{x}_i \in \mathbb{R}^n$ *and* $y_i \in \mathbb{R}$*, find a (continuous) function* f *such that:*

$$f(\boldsymbol{x}_i) = y_i,\ i = 1, \dots, N. \tag{2.3}$$

2.2.1 Radial Basis Functions

Radial Basis Functions are generally used in scattered data interpolation problems. The main advantage of this approach is to cover a large class of interpolation functions, enabling to model various situations. Moreover a general theory, namely the radial basis function theory [32], ensures tractability of models and shows good convergence properties. An introduction and some examples can be found in [123].

Let us first introduce radial functions: a function $h : \mathbb{R}^n \to \mathbb{R}$ is called radial if there exists a function $\Phi : [0, +\infty) \to \mathbb{R}$ such that $h(\boldsymbol{x}) = \Phi(\|\boldsymbol{x}\|)$. A typical radial function is the Gaussian:

$$\Phi(\|\boldsymbol{x}\|) = \exp\left(-c^2\|\boldsymbol{x}\|^2\right),$$

where the parameter c can be tuned.

An interpolating function is defined as a linear combination of well selected radial basis functions $(h_j)_{j=1,\dots,M}$:

$$f(\boldsymbol{x}) = \sum_{j=1}^{M} c_j h_j(\boldsymbol{x}).$$

Solving the interpolation problem (2.3) leads to a system of linear equations of the form:

$$A\boldsymbol{c} = \boldsymbol{y}, \tag{2.4}$$

where the matrix A is given by $A_{i,j} = h_j(\boldsymbol{x}_i)$, $i = 1, \dots, N$, $j = 1, \dots, M$, $\boldsymbol{c} = [c_1, \dots, c_M]^\top$ and $\boldsymbol{y} = [y(\boldsymbol{x}_i), \dots, y(\boldsymbol{x}_N)]^\top$.

Note that the benefit of radial functions is that the interpolation problem becomes insensitive to the dimension n of the input space, since the functions are all univariate. The choice of the function depends on the user interpolation need but also on the resolution of the system (2.4). RBFs techniques used in our studies, are implemented in Scilab and described in [13].

2.2.2 Kriging

Kriging has its origins in geostatistics [74] with the research works of D.G. Krige [100] and has been formalized and developed thanks to [112]. Kriging was almost at the same time introduced in oceanology by [31] and called the Gauss-Markov interpolation method. The main idea is to estimate a function at a given point, by computing a weighted average

of the known values in the neighborhood of the point. The weights are related to spatial covariance values.

As interpolation, kriging has the following benefits:

- it first minimizes the variance of the estimation,
- it gives an estimate of the estimation error along with the estimate of the variable itself,
- it helps to compensate for the effects of data clustering treating clusters more like single points.

However kriging requires to specify a covariance model which may be difficult when data are sparse. An illustration of the use of kriging is presented in Figure 2.2 for estimating a function from $\mathbb{R}$ to $\mathbb{R}$. The error estimate helps to provide some confidence intervals, here

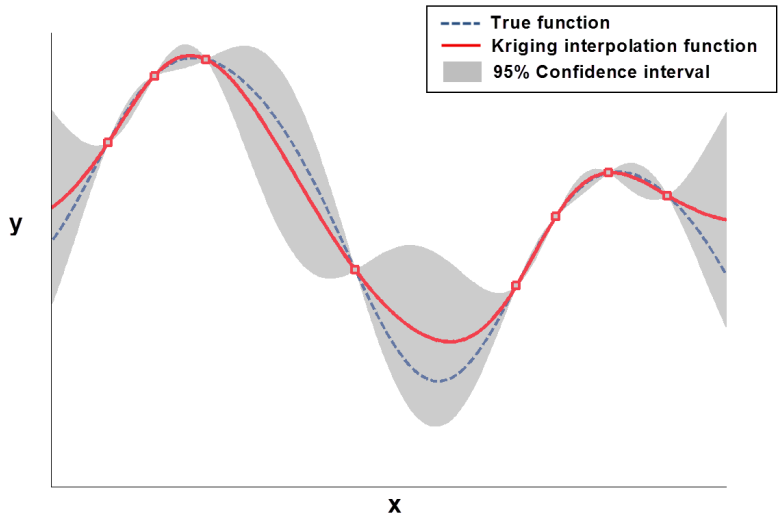

Figure 2.2: Kriging interpolation of a given function and its confidence interval.

the grey zone of the graphic. Basis of kriging methodology is presented in the following paragraph.

Let $y_i = y(x_i)$ be some given observations at points x_i, $i = 1, \ldots, N$. We can define the covariance function C of the process as a measure of how two variables are related. It is given by:

$$C(t) = \operatorname{cov}\left(y(x+t), y(x)\right),$$

where:

$$\begin{aligned}\operatorname{cov}\left(y_i, y_j\right) &= \mathrm{E}\left[\left(y_i - \mathrm{E}\left[y_i\right]\right)\left(y_j - \mathrm{E}\left[y_j\right]\right)\right] \\ &= \mathrm{E}\left[y_i y_j\right] - \mathrm{E}\left[y_i\right]\mathrm{E}\left[y_j\right]\end{aligned}$$

Assume that the covariance function C of the considered process, is known. The goal is to estimate $y_0 = y(x_0)$ at a point x_0 which is not available. The random variable y at any location can be written as:

$$y(x) = m(x) + \delta(x),$$

where $m(x)$ denotes a deterministic component, called the trend, and $\delta(x)$ denotes the stochastic component satisfying: $\mathrm{E}[\delta(x)] = 0$. The trend $m(x)$ is the expected value of $y(x)$.

There are three kinds of univariate kriging methods, depending on the knowledge of the statistics of the interpolated variable:

- simple kriging which assumes that the mean $m(x)$ is known and constant,
- ordinary kriging which assumes that the mean is unknown,
- universal kriging which assumes that the mean has a functional dependence on spatial location x (unstationary process).

The most frequently used method is the ordinary kriging and consists in computing an unbiased estimation y_0^* of the variable y_0 such that:

$$y_0^* = \sum_{i=1}^{N} \lambda_i y_i. \tag{2.5}$$

The weights λ_i are the unknowns of the following optimization problem: minimize the variance $\sigma_e^2 = \mathrm{var}\,[y_0^* - y_0]$ to obtain an unbiased estimator y_0^* of y_0. This constraint is equivalent to $\mathrm{E}\,[y_0^* - y_0] = 0$ and yields the constraint $\sum_{i=1}^{N} \lambda_i = 1$, so that we solve:

$$\min_{\lambda \in \mathbb{R}^N} \sigma_e^2 \quad \text{such that:} \quad \sum_{i=1}^{N} \lambda_i = 1.$$

Using the Lagrangian $L(\lambda, \mu) = \sigma_e^2 + 2\mu \left(\sum_{i=1}^{N} \lambda_i - 1 \right)$, we obtain:

$$\sigma_e^2 = \mathrm{var}\,[y_0] + \sum_{i=1}^{N} \sum_{j=1}^{N} \lambda_i \lambda_j \,\mathrm{cov}(y_i, y_j) - 2 \sum_{j=1}^{N} \lambda_i \,\mathrm{cov}(y_0, y_i). \tag{2.6}$$

This leads to solve the following system:

$$\begin{pmatrix} \sigma^2 & \mathrm{cov}(y_1, y_2) & \dots & \mathrm{cov}(y_1, y_N) & 1 \\ \mathrm{cov}(y_2, y_1) & \sigma^2 & \dots & \mathrm{cov}(y_2, y_N) & 1 \\ \vdots & \dots & \ddots & \vdots & \vdots \\ \mathrm{cov}(y_N, y_1) & \mathrm{cov}(y_N, y_2) & \dots & \sigma^2 & 1 \\ 1 & 1 & \dots & 1 & 0 \end{pmatrix} \cdot \begin{pmatrix} \lambda_1 \\ \lambda_2 \\ \vdots \\ \lambda_N \\ \mu \end{pmatrix} = \begin{pmatrix} \mathrm{cov}(y_1, y_0) \\ \mathrm{cov}(y_2, y_0) \\ \vdots \\ \mathrm{cov}(y_N, y_0) \\ 1 \end{pmatrix}$$

Observe that only the right part of the system depends on the point y_0 to estimate, and that the solution λ depends on the covariance function of the process. In practice, this

function is not known in advance. In the geostatistical literature, the covariance function is not often used and the semi-variogram function $\gamma(\cdot)$ is preferred [143]:

$$2\gamma(t) = \mathrm{E}\left[(y(x+t) - y(x))^2\right].$$

In the case of a stationary process, as in most of cases, the semi-variogram function is defined according to the covariance function by the relation:

$$2\gamma(t) = C(0) - C(t).$$

In practice the semi-variogram can be selected among a list of functions [47]: one of the most used is the Gaussian function, depending on the scale c_0 and the range a_0 parameters:

$$\gamma(t) = c_0 \left(1 - \exp\left(-\frac{t^2}{a_0^2}\right)\right).$$

In case of multivariate interpolation, cokriging has then be introduced, with the same rules as those for kriging. More informations about this method, can be found among many others in [102, 173]. These meta-modeling techniques will be used in Section 2.3.4 for surrogate based optimization. Before this, we make a review of the optimization methods that will be used in our aircraft design studies.

2.3 Optimization methods

Aircraft design problems and generally engineering complex problems, are frequently expressed as optimization problems. In this thesis we focus on continuous optimization problems, namely:

$$\left| \begin{array}{rl} \text{Minimize} & f(\boldsymbol{x}) \\ \text{s.t.} & \boldsymbol{x} \in \mathcal{C}, \end{array} \right. \tag{2.7}$$

where:

- f: $\mathbb{R}^n \to \mathbb{R}$ is the objective function, or the cost function, assumed at least continuous over its definition set,
- $\mathcal{C} \subset \mathbb{R}^n$ is the constraint set,
- $\boldsymbol{x} \in \mathbb{R}^n$ is the optimization variable.

In the case of aircraft design, the objective function can be the aircraft design mass, the fuel consumption over a mission or the climatic impact over a mission. Optimization parameters can be the wing area, the engine thrust, the flight speed and altitude, etc. In practical problems, the constraint set $\mathcal{C}$ is defined by:

$$\mathcal{C} = \{\boldsymbol{x} \in \mathbb{R}^n \mid g_1(\boldsymbol{x}) \leq 0, \ldots, g_L(\boldsymbol{x}) \leq 0, h_1(\boldsymbol{x}) = 0, \ldots, h_M(\boldsymbol{x}) = 0\}. \tag{2.8}$$

where the functions $h_i : \mathbb{R}^n \to \mathbb{R}$, $i = 1, \ldots, M$, and $g_j : \mathbb{R}^n \to \mathbb{R}$, $j = 1, \ldots, L$, are assumed at least continuous over their definition sets. Note that the inequality constraints defined by $g_j(x) \leq 0$, can include bound constraints $\boldsymbol{x}_{min} \leq \boldsymbol{x} \leq \boldsymbol{x}_{max}$. In some other problems,

$\mathcal{C}$ can be defined by an infinity of constraints, as for example in robust optimization, see Chapter 6.

In the case of aircraft design optimization, the constraint functions are representing operational constraints, as for instance maximal approach speed or lengths of landing and take-off field to respect.

The choice of the optimization method to solve Problem (2.7) depends widely on the properties of the objective function and of the constraint set. A good overview of optimization methods and algorithms from theory to practical aspects, can be found e.g. in [27]. Among all these methods, we can distinguish local and global methods. Local methods aims at finding a local minimum in the following sense:

Definition 2.1. *Let $f : X \subset \mathbb{R}^n \to \mathbb{R}$. The point $\boldsymbol{x}_0 \in X$ is called a local minimum point of f if there exists a neighborhood $\Omega \subset \mathbb{R}^n$ of $\boldsymbol{x}_0$ such that: $\forall \boldsymbol{x} \in \Omega \cap X$, $f(\boldsymbol{x}_0) \leq f(\boldsymbol{x})$.*

Global methods aim to find a global optimum if it exists:

Definition 2.2. *Let $f : X \subset \mathbb{R}^n \to \mathbb{R}$. The point $\boldsymbol{x}_0 \in X$ is called a global minimum point of f if: $\forall \boldsymbol{x} \in X$, $f(\boldsymbol{x}_0) \leq f(\boldsymbol{x})$.*

An example of a local and a global minimum is presented in Figure 2.3. Note that a local minimum becomes global when both the objective function and the constraint set are convex.

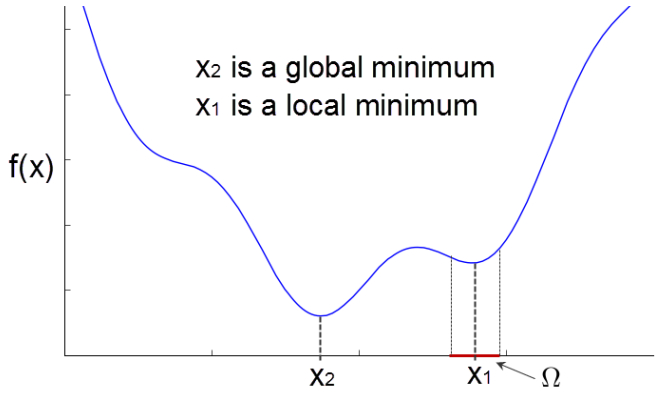

Figure 2.3: Illustration of a local and a global minimum of a function $f : \mathbb{R} \mapsto \mathbb{R}$.

In our engineering design problems, all functions result from black-box processes and so are not known analytically. This lack of knowledge leads to the incapacity to prove the existence of an optimal solution, whether local or global. The best that we can do is to test different methods and to compare the obtained solutions. Nevertheless, thanks to automatic differentiation techniques (see Section 2.1), the gradients of the involved functions are available, which enables us to use gradient-based optimization methods, see Section 2.3.1. Since the aircraft design problem is not necessarily convex, these methods only leads *a priori* to local minimum points which is an important but usual drawback. One way to improve the quality of a given solution, is to apply repeatedly the chosen algorithm, but there is no guarantee to eventually find a global minimum and the computational cost is multiplied.

Section 2.3.2 is dedicated to derivative free optimization or gradient free optimization methods. They have the main advantage to be robust and not to depend on the differentiability of the involved functions. It works fine in practice, but their computational time is quite heavy. Section 2.3.3 introduces multi-objective optimization with the Pareto front notion. It is useful in the case where several objectives have to be minimized at the same time. Finally this chapter ends with a brief presentation of a method of surrogate based optimization. When dealing with computationally expensive or noisy processes, these sequential methods provide interesting benefits.

2.3.1 Gradient Based methods

When the gradients of the objective and the constraint functions are available and satisfy some regularity properties, there exist various optimization methods to tackle Problem (2.7). Most of them are described in [27]. The following three methods have been numerically implemented and are used for solving aircraft design optimization:

- FSQP (for Feasible Sequential Quadratic Programming) provided by [184],
- DOT (for Design Optimization Tools) from [172],
- IPOPT (for Interior Point OPTimizer) from [174].

The first two methods belong to the class of sequential quadratic programming methods, and the third one is based on an interior point method. Before presenting briefly the methods, we start by a short recall of the necessary optimality conditions associated to Problem (2.7), namely the Karush-Kuhn-Tucker optimality conditions. These conditions are at the heart of SQP algorithms.

2.3.1.1 KKT optimality conditions

Let us consider a general optimization problem under functional constraints:

$$\min_{\boldsymbol{x}\in\mathbb{R}^n} f(\boldsymbol{x}) \text{ s.t. } \left| \begin{array}{l} g_i(\boldsymbol{x}) \leq 0, \quad i = 1,\dots,L, \\ h_i(\boldsymbol{x}) = 0, \quad i = 1,\dots,M. \end{array} \right. \tag{2.9}$$

where the functions $f, g_i, h_j : \mathbb{R}^n \to \mathbb{R}$, $i = 1,\dots,L$, $j = 1,\dots,M$, are assumed at least differentiable. The Karush-Kuhn-Tucker (KKT) conditions are the necessary conditions for a given point to be optimal [77] for the considered problem.

Let us introduce the well-known Lagrangian function associated to Problem (2.9):

$$L(\boldsymbol{x},\boldsymbol{\lambda}) = f(\boldsymbol{x}) + \sum_{i=1}^{L} \lambda_i^{(g)} \cdot g_i(\boldsymbol{x}) + \sum_{j=1}^{M} \lambda_j^{(h)} \cdot h_j(\boldsymbol{x}), \tag{2.10}$$

where the vector $\boldsymbol{\lambda} \in \mathbb{R}^{M+L}$, which is the concatenation of $\boldsymbol{\lambda}^{(g)}$ and $\boldsymbol{\lambda}^{(h)}$, is the Lagrange multiplier vector. The KKT conditions associated to (2.9) are:

Theorem 2.1. *Let x^* be an admissible point of the problem (2.9). Assume that the functions f,g,h are differentiable at x^* and that the constraints are qualified at x^*. If x^* is a local minimum point of f over the constraint set $\{x \in \mathbb{R}^n / g_i(x) \leq 0, i = 1,\dots,L,\ h_j(x) = 0, j = 1,\dots,M\}$ then there exists $\lambda = (\lambda^{(g)}, \lambda^{(h)}) \in \mathbb{R}^L \times \mathbb{R}^M$ such that:*

$$\nabla_{\boldsymbol{x}^*} L(\boldsymbol{x},\boldsymbol{\lambda}) \quad = \quad 0, \tag{2.11}$$

$$\lambda_i^{(g)} \cdot g_i(\boldsymbol{x}^*) = 0,\ \forall i = 1, \ldots, L, \tag{2.12}$$
$$h_j(\boldsymbol{x}) = 0,\ \forall j = 1, \ldots, M, \tag{2.13}$$
$$\lambda_i^{(g)} \geq 0,\ \forall i = 1, \ldots, L, \tag{2.14}$$

Condition (2.12) is referred to as the complementarity relations. Note that there exist several conditions of constraint qualification in the literature as the Slater conditions or the Mangasarian-Fromovitz conditions [27]. We here use the simplest one which is the following:

Proposition 2.1 (Sufficient condition for constraint qualification)**.** *The constraints of Problem (2.9) are said qualified at a point $x^* \in \mathbb{R}^n$ if the gradients of active constraints at x^*, namely:*

$$\{\nabla h_j(x^*); j = 1, \ldots, M\} \cup \{\nabla g_i(x^*); i = 1, \ldots, L\}$$

are linearly independent.

2.3.1.2 Sequential Quadratic Programming methods

Sequential Quadratic Programming (SQP) methods are iterative methods for nonlinear optimization [184] where the objective function is usually assumed twice continuously differentiable while the constraint functions only have to be continuously differentiable. They consist in replacing the initial optimization problem by a sequence of quadratic optimization problems under linear constraints that are easier to solve.

Let us consider the general nonlinear programming problem 2.9) and its Lagrangian L (2.10). At the current iterate $\boldsymbol{x}_k$, a SQP algorithm defines an appropriate descent direction $\boldsymbol{d}_k$ as the solution of the following quadratic programming subproblem:

$$\left| \begin{array}{ll} \min\limits_{\boldsymbol{d}} & L(\boldsymbol{x}_k, \lambda_k, \sigma_k) + \nabla L(\boldsymbol{x}_k, \lambda_k, \sigma_k)^\top \boldsymbol{d} + \frac{1}{2} \boldsymbol{d}^T \nabla^2_{xx} L(\boldsymbol{x}_k, \lambda_k, \sigma_k) \boldsymbol{d} \\ \text{s.t.} & g(\boldsymbol{x}_k) + \nabla g(\boldsymbol{x}_k)^\top \boldsymbol{d} \leq 0, \\ & h(\boldsymbol{x}_k) + \nabla h(\boldsymbol{x}_k)^\top \boldsymbol{d} = 0. \end{array} \right. \tag{2.15}$$

As any Newtonian method, the basic SQP method converges locally with a quadratic rate. The FSQP algorithm is even more sophisticated and combines linesearch and SQP method to compute a new descent direction, see [184] for more details.

2.3.1.3 An Interior Point method

This method [34, 176] consists in a primal-dual barrier approach: the idea is to encode the feasible set using a barrier function. The algorithm thus solves a constrained minimization problem such as Problem (2.16). Equality constraints and bound constraints on $\boldsymbol{x}$ do not appear anymore, they are reformulated into equivalent inequality constraints.

$$\left| \begin{array}{ll} \min\limits_{\boldsymbol{x} \in \mathbb{R}^n} & f(\boldsymbol{x}) \\ \text{s.t.} & g_i(\boldsymbol{x}) \leq 0, \quad i = 1, \ldots, L. \end{array} \right. \tag{2.16}$$

The Interior Point algorithm computes the solutions of a sequence of approximate minimization problems called *barrier problems*. Using a logarithm barrier function and for a

decreasing sequence of the barrier parameter $\mu > 0$, the associated approximated problem is:

$$\min_{\boldsymbol{x}} f_\mu(\boldsymbol{x}) := f(\boldsymbol{x}) - \mu \cdot \sum_{i=1}^{n} \ln\left(-g_i(\boldsymbol{x})\right). \tag{2.17}$$

As μ decreases to zero, the unconstrained minimizers of f_μ will approach the local constrained minimizer of f. The approximate problem (2.17) defines a sequence of unconstrained problems depending on the barrier parameter μ. These problems are easier to solve than the original constrained problem (2.16). The main benefits and improvements of this type of methods come from the resolution of the sequence of approximate problems. In particular, first order optimality conditions of Problem (2.17) are similar to the KKT conditions of Problem (2.16). See [34] for more details.

2.3.2 Derivative free optimization

Derivative free optimization was first motivated by the absence of computable derivatives in a lot of engineering optimization problems [45]. A main benefit of derivative free methods is to handle failing computation of the model functions, which sometimes happens in black-box computation. Various methods were developed; we focus here on direct search methods and heuristics methods.

2.3.2.1 Direct Search Methods

Direct search methods are characterized by the fact that they require neither explicit nor approximate derivatives. They first appeared in [87], with the following description:

We use the phrase "direct search" to describe sequential examination of trial solutions involving comparison of each trial solution with the "best" obtained up to that time together with a strategy for determining (as a function of earlier results) what the next trial solution will be.

This is discussed in [107] with a large overview of direct search methods between 1960 and 2000. The main advantage is the robustness of such algorithms and the main drawback is that they do not enjoy rapid local convergence. As [107] says:

A carefully chosen, carefully implemented direct search method can be an effective tool for solving many nonlinear optimization problems.

Global Pattern Search methods [164] then generalized these methods. They appeared mainly for solving non-linear optimization constrained or unconstrained problems. Among these methods, we first present the Nelder-Mead algorithm which has been modified to deal with non-linear constraints and then the Mesh Adaptive Direct Search algorithm, which brings several improvements to global pattern search methods.

2.3.2.1.a The Nelder-Mead algorithm and constraint management

The original method is also known as Downhill Simplex, Nonlinear Simplex or simply Nelder-Mead Simplex. It is due to [115] for solving non-linear optimization problems. The Nelder-Mead method uses the concept of a simplex: a simplex is defined as a convex hull

of $n+1$ vertices in a n-dimensional space, e.g. a line segment in dimension 1, a triangle in dimension 2. A complete description of the algorithm can be found in [76]. It performs geometrical operations (reflection, expansion, contraction) on some candidate vertices of the convex hull in order to move this convex hull in descent directions. Geometrical operations are illustrated in Figure 2.4. That is, the candidates are first reflected: if this makes

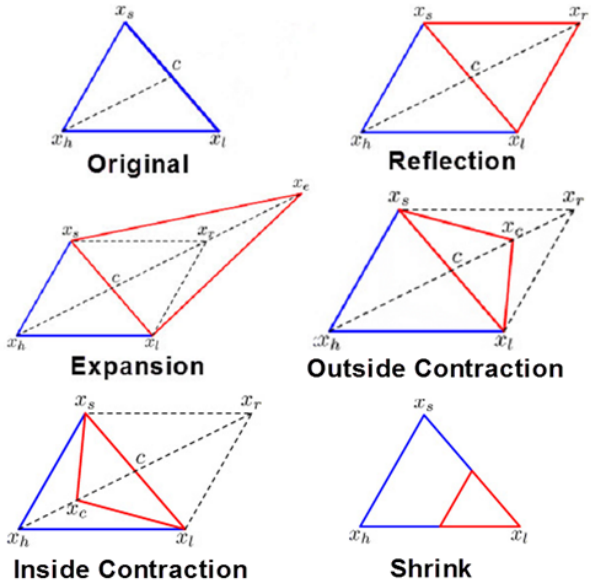

Figure 2.4: Geometrical operations performed by Nelder-Mead algorithm.

an improvement (i.e. a better function value), an expansion will be attempted. Otherwise, the polytope is reduced. By those geometrical operations, the polytope changes in volume and in form. The procedure can be summarized into the following basic steps:

- **Step 1**: Choose an initial polytope (i.e. $n+1$ vertices) of dimension n.
- **Step 2**: Take as a search direction $[X_h, X_0]$, the direction joining X_h (the vertex with the highest objective function value) and the centroid X_0 of all vertices excepted X_h.
- **Step 3**: If this direction behaves as a descent direction, we replace X_h by a chosen point in this direction. That point may be chosen closer (reflection) or the furthest possible (expansion) according to the results of the basic geometrical operations applied on X_h.
- **Step 4**: The polytope is eventually updated with the new vertices according to step 3, aiming to "move" it in the descent directions. It may also be reduced.
- **Step 5**: Stop if a stopping condition (number of steps, size of the polytope, ...) is satisfied otherwise return to step 2.

An illustration of this algorithm is presented in Figure 2.5. In dimension $n = 2$ the simplex is a triangle, and we can see its moves and size evolution until a solution is reached. At the end, the last polytope should be a small one, whose vertices are very close from each

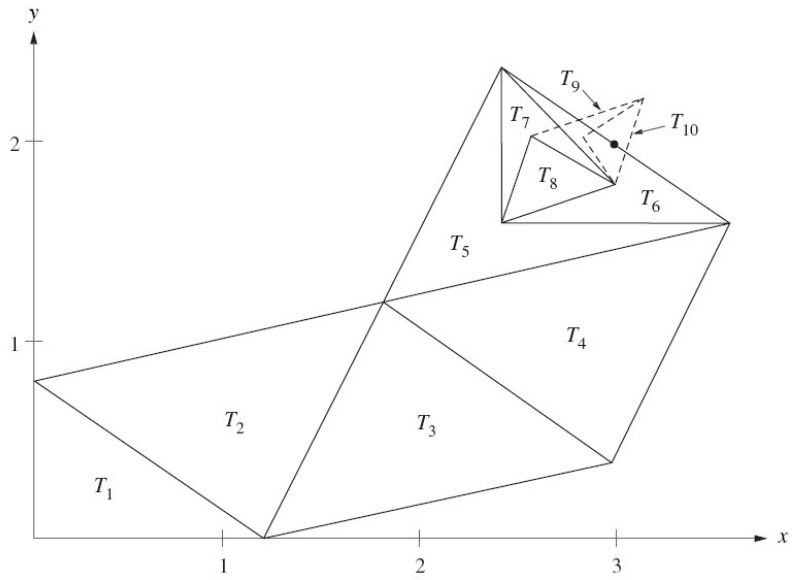

Figure 2.5: Example of Nelder-Mead algorithm: the sequence of triangles T_k converges to the point $(3, 2)$.

other, and so hopefully close to a local minimum.

In order to deal with constraints, we need to define a measure of *how much constraints are violated* in order to compare two unfeasible points. This measure/function has the following property: it gives a lowest value to the point the closest to the constraint boundary measured with euclidean norm $\|\cdot\|$, i.e. the point that violates "less" the constraint. We say that A is better than B if:

- the constraint measure of A is lower than that of B, in the case where both points are not satisfying constraints, or
- A satisfies the constraints but B does not, or
- both points satisfy the constraints, and the objective function at A is lower than the objective function at B.

Note that when the process fails, which means the computation of the objective or the constraint function produces an error, this algorithm handles it, assuming the unavailable point is worse than any other. Drawbacks of this algorithm is that it can sometimes be stuck in a local optimum. Moreover, convergence properties of the Nelder-Mead algorithm [101] are only proved for some strictly convex class of functions in dimensions 1 and 2.

2.3.2.1.b Mesh Adaptive Direct Search (MADS)

The Mesh adaptive direct search method has been introduced in [11]. The main improvement compared to basic global pattern search methods is that the local exploration of the space of variables is not restricted to a finite number of directions (as for instance for

Nelder-Mead algorithm). The analysis of [11] shows that the finite number of these directions, called poll directions, is one of the main limitations of the algorithm convergence. The main advantage is that MADS aims at ensuring an asymptotically dense set of poll directions. This yields some hierarchical proofs of convergence depending on properties of the function f and of the feasible region to first order stationary points but also to second order ones under reasonable conditions [3].

2.3.2.2 Meta-heuristic methods

Meta-heuristic methods date from the fifties, see [54] for more details. The term *Meta-heuristic* designates a computational method that optimizes a problem by iteratively trying to improve a candidate solution with regard to a given measure of quality. However, as for most of derivative free optimization algorithms, meta-heuristics do not guarantee that an optimal solution will be found.

The two meta-heuristic methods presented hereafter, are population based: we start with a population of individuals, that are some selected points among the domain of definition of our problem. At each iteration this population evolves in order to look for the "best" individual i.e. the optimal solution of the problem. The used functions are so dedicated to select, to evaluate and to add or to remove individuals from the population at each iteration.

The main benefit of these techniques is the search for global solutions, as the first population can cover the whole design space. One of the drawbacks is that they depend a lot on the different functions that are used to improve the individuals. Popular meta-heuristics include simulated annealing, particle swarm optimization, differential evolution and genetic algorithms [99, 41, 96]. We test most of these techniques and selected two of them for application to our study cases: genetic algorithms and differential evolution algorithms.

2.3.2.2.a Genetic Algorithms

A genetic algorithm is a search heuristic that mimics the process of natural evolution. It consists in generating solutions to optimization problems using techniques such as inheritance, mutation, selection, and crossover. The genetic algorithms method that we implement are based on the Non-Sorting-Genetic-Algorithms II [51], modified to deal with constraints.

The principle of genetic algorithms is presented in Figure 2.6. The blue points on the curve represent the initial population, the red points represent the worst individuals, and the yellow ones the best ones. Every step of the genetic algorithm has a particular function, as described in the following list:

Initialization: Many individual solutions are randomly generated to form an initial population. Occasionally, the initial individual solutions may be located in areas where optimal solutions are likely to be found. The population size depends on the nature of the problem.

Selection: During each successive generation, a proportion of the existing population is selected to breed a new generation. Individual solutions are selected through a fitness-based process, where fitter solutions (measured by a fitness function) are typically more likely to be selected.

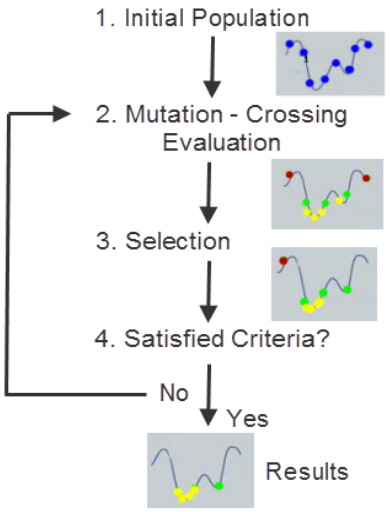

Figure 2.6: Genetic Algorithms: principle.

Reproduction (Cross-over and Mutation): The next step is to generate a second generation population of solutions from those selected through genetic operators: crossover and/or mutation. For each new solution to be produced, a pair of "parent" solutions is selected to produce a "child" solution using the above operators. A new solution is created which typically shares many of the characteristics of its "parents". New parents are selected for each new child, and the process continues until a new population of solutions of appropriate size is generated. These processes ultimately result in the next generation population of candidate solutions that is different from the initial generation and in average performs better in term of fitness.

Termination: This generational process is repeated until a termination condition has been reached. Common terminating conditions are:

- A solution is found that satisfies minimum criteria,
- Fixed number of generations reached,
- The highest ranking solution's fitness has reached a state such that successive iterations no longer produce better results.

The genetic algorithm used for our studies is based on the one from [12]. A careful attention has to be paid concerning the functions used to select, evaluate, or cross the individuals: the convergence of the algorithm strictly depends on these parameters. The best way to find the best combination of these parameters is unfortunately to test different values of them.

2.3.2.2.b Differential Evolution algorithms

Differential Evolution algorithms are search heuristic methods that belong to the class of evolutionary algorithms [54]. It is very similar to genetic algorithms [78]. It consists in the following:

1. randomly generate an initial population;
2. for each individual of this population, select three random individuals different from the first one;
3. create a new individual from these four individuals;
4. replace the first individual by the new one if it has better performances;
5. do step 2 to 4 until a stopping condition is satisfied.

The algorithm ultimately results in individuals with better performances in terms of a given objective function and constraint satisfaction. The basic algorithm was not specified for constrained optimization problems. Based on the basic algorithm [54], we implemented the same comparison process as for the Nelder-Mead algorithm: in order to deal with constraints, we introduce a function measuring the degree of constraint violation. However, even if it is known to be an efficient method, it does not guarantee the optimality of the solution. The main advantage is that tuning parameters of differential evolution algorithms is less sensitive than in the case of genetic algorithms.

Another interest of such population based techniques is the possibility to launch multi-objective optimization as described next.

2.3.3 Multi-Objective optimization: Pareto front

Multi-objective optimization (MOO) denotes the process that consists in optimizing simultaneously a collection of objective functions. A survey of MOO can be found in [110]. It allows an additional degree of freedom in comparison to single-objective optimization: solving a MOO problem will bring not an unique solution but a set of solutions. A consequence of this flexibility is the introduction of new concepts and then methods different from the one of classical single-objective optimization.

Let us recall the general form of a MOO problem:

$$\left| \begin{array}{ll} \min\limits_{\boldsymbol{x}\in\mathbb{R}^n} & \boldsymbol{F}(\boldsymbol{x}) = [f_1(\boldsymbol{x}), f_2(\boldsymbol{x}), \ldots, f_k(\boldsymbol{x})]^\top \\ \text{s.t.} & g_i(\boldsymbol{x}) \leq 0,\ i = 1, \ldots, L. \end{array} \right. \tag{2.18}$$

As mentioned above, solutions to multi-objective problems are not unique and then the notion of set of solution leads to the concept of Pareto optimality:

Definition 2.3. *A point $\boldsymbol{x}^* \in \mathbb{R}^n$ is Pareto optimal if and only if there does not exist another point $\boldsymbol{x} \in \mathbb{R}^n$ such that $\boldsymbol{F}(\boldsymbol{x}) \leq \boldsymbol{F}(\boldsymbol{x}^*)$, and $f_i(\boldsymbol{x}) < f_i(\boldsymbol{x}^*)$ for at least one function.*

Following this definition and given a set of individuals with a given allocation in solution space, a Pareto improvement is a change to a different allocation that makes at least one individual better without making any other individual worse. An allocation of individuals is defined as "Pareto efficient" or "Pareto optimal" when no further Pareto improvements can be made. This leads to the Pareto front definition: it is the set of individuals that are Pareto efficient. A representation of a Pareto front in dimension 2 is given in Figure 2.7. All points represent feasible solutions for f_1 and f_2 functions. Let us now consider a minimization problem. Point C is not on the Pareto front because it is worse than both

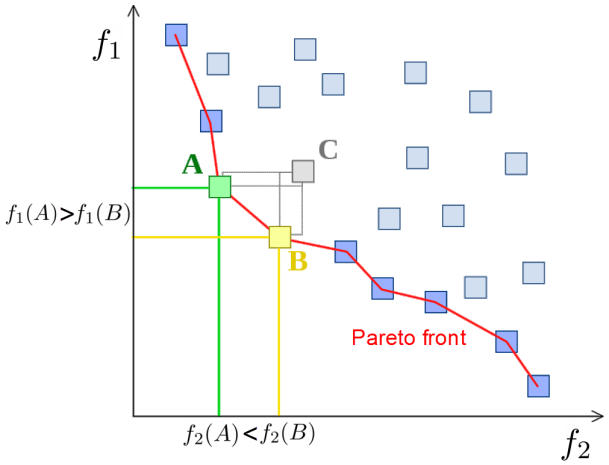

Figure 2.7: Pareto front illustration.

point A and point B. Points A and B are not worse than any other, and hence do lie on the Pareto front. In our study cases, the objective of MOO problem is to draw Pareto fronts. It is then the choice of the user to select a solution from this front, according to the importance of the different objectives. For more information and bibliography around MOO and its methods, one can see [110]. The method that we will use to draw Pareto front is based on genetic algorithms [50]. The evaluation of a large population of individuals is primordial in order to find the best ones in term of Pareto efficiency.

2.3.4 Surrogate Based Optimization

Surrogate based optimization (SBO) or Meta-model based Optimization (MBDO) main objective is to apply optimization algorithms to engineering problems where classical methods are not practical. For instance, it can be used when processes are noisy, or when function evaluations are too expensive. A comprehensive discussion around these techniques can be found in [144]. The standard engineering practice of SBO is the following one [28]:

- Choose a surrogate model f^* for f (among the techniques presented in Section 2.2 for example) and g_i^* for g_i, $i = 1, \ldots, L$ (sample the design space, build the metamodel, and validate the model).
- Solve the surrogate optimization problem to obtain a solution $\boldsymbol{x}^*$:

$$\min_{\boldsymbol{x} \in \mathbb{R}^n} f^*(\boldsymbol{x}) \text{ s.t. } \quad g_i^*(\boldsymbol{x}) \leq 0, \quad i = 1, \ldots, L. \tag{2.19}$$

- Compute $f(\boldsymbol{x}^*)$ to determine if improvements have been made over the last found best $\boldsymbol{x}$.

Techniques have improved this basic approach. The main ones use sequences of surrogates to identify promising regions in which the use of accurate surrogates leads to better behavior of the algorithms [157]. The objective is to determine whether or not the model has to be more accurate in a given design space region, with generally a high need of accuracy close to the optimum. Example of strategies are presented in Figure 2.8. An additional benefit

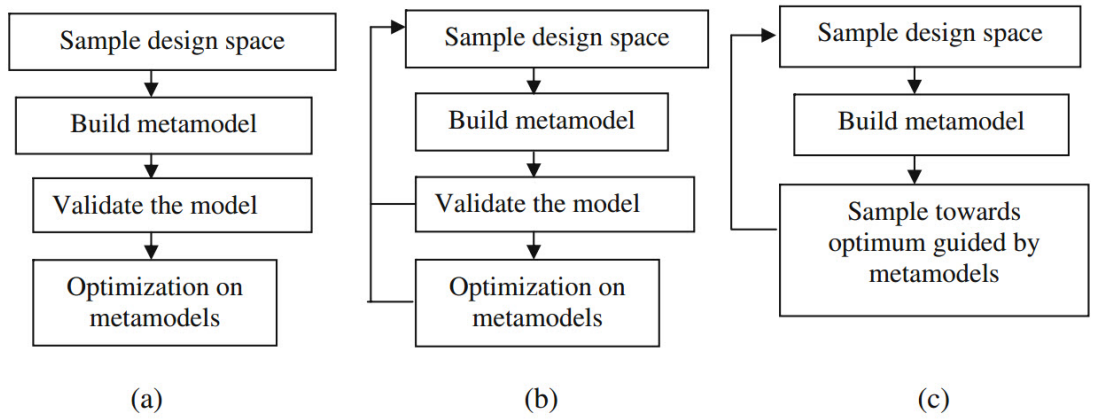

Figure 2.8: SBO algorithms with different strategies: (***a***) sequential basic approach, (***b***) Adaptive method [53], (***c***) Direct sampling method [175].

of such techniques is the low computational cost for solving the approximate optimization problem. However the refinement of the surrogate has to be carefully managed, and to be global enough not to drive the optimization to local optimum. A very interesting review of recent and promising techniques is proposed in [157].

Chapter 3

Preliminary Aircraft Design Deterministic Optimization

Contents

This chapter is dedicated to the deterministic optimization of the preliminary design of two types of aircraft. The first aircraft is a conventional short range aircraft, which specifications and requirements are presented in the first section. The second aircraft is the hybrid aircraft concept already presented in Chapter 1, Section 1.3.4. The optimization tools that will be used have been presented in Chapter 2. The models to which we refer are the ones described in Chapter 1.

The first section is dedicated to our step-by-step approach. The second section starts with the optimization of a conventional short range aircraft, from the simplest optimization with the two classical design variables, to an extend with 12 design variables. Several optimization objectives are studied and the focus is made on the description and the analysis of the results. Some conclusions are presented according to comparisons between the different optimizations.

In the second section, the optimization process is applied to an unconventional aircraft configuration, already presented in Chapter 1: an hybrid aircraft. The impact of the selected objective is also studied and by using the conventional aircraft as a baseline we explain the benefits of such a hybrid configuration.

3.1 A step-by-step approach

3.1.1 Baseline aircraft optimization

This section presents the approach that we select to solve the aircraft design optimization. First we choose a baseline aircraft, that is a short range aircraft with the specifications presented in Table 3.1. As mentioned in Chapter 1, the aircraft preliminary design is

Table 3.1: Description of the baseline aircraft specifications.

Name	**Value**
Number of Passengers (Npax)	180
Design Range	2000 NM
Cost Mission Range	500 NM
Cruise Mach number	0.76
Wing Aspect Ratio	9
Number of Turbofan Engine	2
Engine By Pass Ratio	9
Top of Climb altitude	35000 ft

subject to constraints, that are addressing operational needs for safety and operations. The more important ones, and the only ones that we will use in this study, are selected according to basic requirements of short range aircraft. They are presented in Table 3.2. From these requirements, we can formulate the usual aircraft design optimization problem, which is the following:

$$\left| \begin{array}{rl} \text{Minimize} & f(\mathbf{x}) \\ \text{s.t.} & \mathbf{x} \in \mathcal{C}, \end{array} \right. \tag{3.1}$$

where:

Table 3.2: Description of the aircraft design constraints.

Name	Value
Approach Speed (LdSpeed)	< 120 kt
Climb Vz Ceiling (ClbVz)	> 300 ft/min
Cruise Vz Ceiling (CrzVz)	> 100 ft/min
Take-Off Field Length 1 (TOFL1)	< 2000 m
Second segment limitation 1 (extTOFL1)	< 2000 m
Time-To-Climb	< 25 min

- the objective function f represents the maximum take-off weight of the aircraft, which is classically used at early stage of preliminary design as a measurement of the global efficiency of the aircraft,
- the constraint set

$$\mathcal{C} = \left\{ \boldsymbol{x} \in \mathbb{R}^n \mid g_1(\boldsymbol{x}) \leq G_1^{sup}, \ldots, g_l(\boldsymbol{x}) \leq G_l^{sup}, g_{l+1}(\boldsymbol{x}) \geq G_S^{inf}, \ldots, g_m(\boldsymbol{x}) \geq G_m^{inf} \right\}, \tag{3.2}$$

  where g_i are the operational constraints and requirements that are listed in Table 3.2,
- the design variables $\boldsymbol{x} \in \mathbb{R}^2$ usually are the wing area x_1 and the sea level static thrust (SLSthrust) x_2. This latter is a driver of the engine power and size through the corresponding models.

This allows to compute quickly an optimized aircraft. The optimization algorithm used in this case is a bi-dimensional pattern search which has been specifically tuned by engineers to be efficient on this particular problem. At the end of this step, we have a reference optimized aircraft. This one is the first aircraft to be optimized in Section 3.2.

3.1.2 Mass-mission loop release

The mass-mission loop has already been introduced in Chapter 1, Section 1.2.5. For a given design, its objective is too produce a converged aircraft such that the weights satisfy the mission range and the structural requirements. This is usually solved within the aircraft design process thanks to numerical solvers (*fsolve* from Scilab in our case). This is done at each aircraft evaluation: it has a non-negligible computational cost and it adds some risk of non-convergence of the solver that can lead to computational failures.

There is an other way of dealing with the mass-mission loop, which consists in releasing it from the design process by adding two design variables and two structural constraints. In practice, it increases the time required for the convergence but may lead to less computational failures. The two additional design variables are:

- the Maximum zero fuel weight (MZFW), in kg,
- the maxium take-off weight (MTOW), in kg.

The two additional constraints that ensure the convergence of the aircraft, i.e. the structural load and the mission range requirements are:

- the step mission take-off weight margin that has to be > 0 kg (DesignMTOW $\geq$ Operationnal MTOW),
- the MZFW margin that has to be > 0 kg (DesignMZFW $\geq$ Operationnal MZFW).

3.1.3 Evolution of the aircraft design optimization

The first step of this thesis was to merge models of aircraft airframe, engine and mission. These models have been presented in Chapter 1. The next step is to introduce degrees of freedom of these three parts within the same optimization process. We lead this approach step by step, i.e. adding degrees of freedom progressively. The main reasons of this step-by-step approach are the following ones.

- We want to keep an eye on the validity of the models behavior.
- We want to ensure the validation the optimization process by following the evolution of the results.
- We want to study the impact on the aircraft performances of each additional group of degrees of freedom.

Note that the more degrees of freedom are added, the more the chance that some points of the design space failed increases. This often happens because of incompatible extreme values of the design space variables. To deal with this, the optimization algorithm has to be robust, this is also a reason why we tested various algorithms, from the gradient based to the heuristics as presented in the Chapter 2.

To follow this step-by-step approach, we consider groups of additional degrees of freedom. The usual values of the first four additional variables are written in Table 3.1. From the **basic design group**, the wing area, the SLSThrust, the DesignMTOW and the DesignMZFW, we select the following additional groups:

i) the **more detailed design group**: the wing Aspect Ratio (WingAR) and the engine By-Pass Ratio (BPR), which are classical parameters that control the overall aircraft configuration,

ii) the **overall trajectory group**: the top of climb altitude (ZpRef) and the cruise Mach, which are the main parameters of the trajectory,

iii) the **detailed trajectory group**: the four following speeds of the step-by-step mission:

- the initial speed, denoted StepMisVcas0, usually equal to 250 kt,
- the first step speed, denoted StepMisVcas1, usually equal to 250 kt,
- the second step speed, denoted StepMisVcas2, usually equal to 250 kt,
- the first step descent speed, denoted StepMisVcas3, usually equal to 270 kt,
- the second step descent speed, denoted StepMisVcas4, usually equal to 250 kt.

This last group of parameters allow to finely tune the efficiency of the climb and descent phases.

Note that when they are not considered as optimization variables, they are set to their usual value.

We also select the classical cash operating cost (COC) criterion as a second objective of the optimization process. Its unit is in \$/trip. It is an interesting value for the airlines, as their business model is based on the minimization of this cost. We will present the numerical results in tables where are compared the design and the performances of the different optimized aircraft.

In parallel, a contribution of this thesis was to include the environmental aspects during the preliminary aircraft design phase. Therefore we propose to add the following additional objective to the optimization process: a climatic impact measure, the *absolute pulsed global warming potential* (APGWP), in $W/m^2/km/year$.

3.1.4 The hybrid aircraft optimization approach

We present in Chapter 1, Section 1.3.4 a new concept of aircraft, with an hybrid propulsion system with electricity and fuel. Among the new design parameters brought by the hybridization of the aircraft, we select three of them as additional degrees of freedom of the optimization process. They are the main drivers of the electric system:

- the electric fan power,
- the electric fan diameter,
- the generator electric ratio, which is the ratio of mechanical energy produced by the thermal engine which is used to generate electricity.

As mentioned in Chapter 1, Section 1.3.4, we add some prediction models of the three following technologies values associated with the hybridization of the propulsion system, as a function of the year:

- the power density of electrical engine and the power density of electrical generator (EPD), which is the amount of power per unit mass (in W/kg),
- the energy density of accumulators (EED), which is the amount of energy stored in a given system per unit mass (in Wh/kg).

We recall in Figure 3.1 the functions that model the predicted evolution of these technologies values.

For the deterministic studies of this chapter, we decide to fix the year that is driving the technologies maturity. We will refer the reader to the conclusion of the study found in [141]: the hybrid configuration should be equivalent to the conventional configuration with a 0.95 probability in year 2025. So we fix the year to 2025.

We propose to apply the step-by-step methodology detailed in the previous section to the optimization of this hybrid aircraft. Moreover, as presented in Chapter 1, Section 1.3.4, we try to improve this configuration by taking the maximum of benefits from the hybridization. We can the recall the three improvements that we propose to the basic hybrid aircraft:

a) remove the thrust reverser from the thermal engines, and use the electric engine instead. The thrust reverser increases the ability of the aircraft to slow down, and it is a relatively heavy system. The electric fan allow to consider its use as a thrust reverser

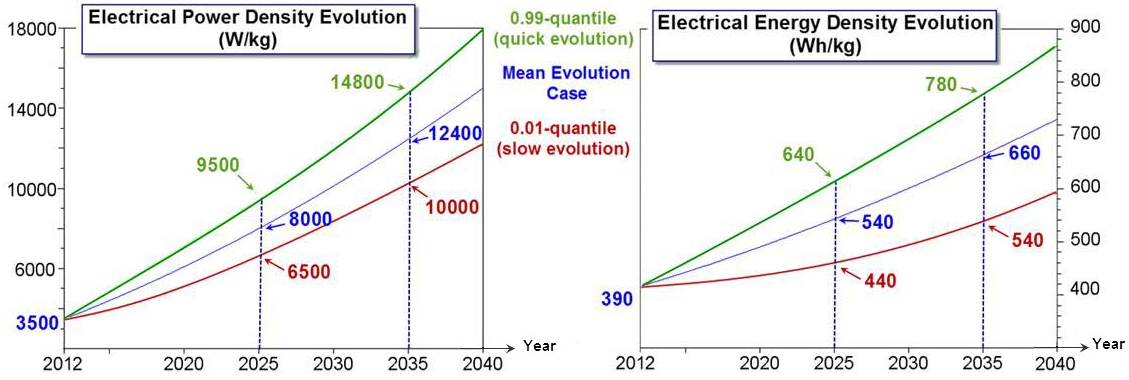

Figure 3.1: Prediction functions of electrical technologies evolution.

by equipping it with variable pitch blades. This synergy comes with the following additional constraint. The electric fan take-off nominal thrust has to be higher than 1000 daN, to allow the use of the electric fan as a thrust reverser,

b) remove the Auxiliary Power Unit (APU) and use the electric engine battery to which we add 100 kg additional one,

c) use boundary layer ingestion (BLI) technology with the electric engine to improve the global specific fuel consumption (SFC) of the power system by 5%. This is possible by putting the fan at the rear of the fuselage as presented in Figure 3.2.

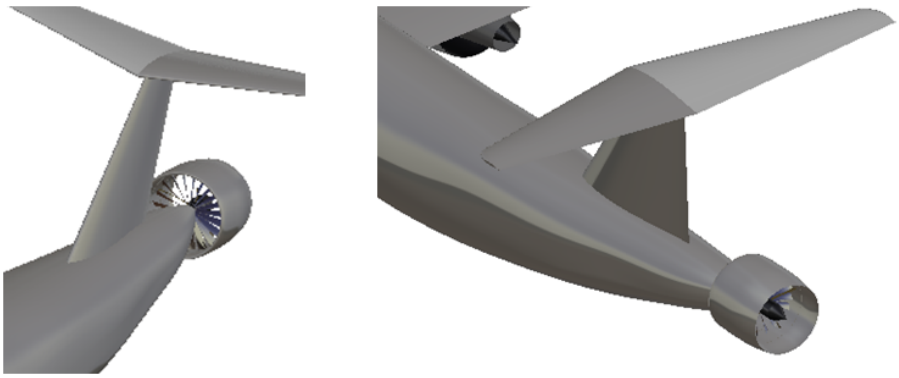

Figure 3.2: Electric fan placed such that it can ingest the boundary layer of the fuselage, in order to reduce the global SFC of the aircraft.

We then propose to also follow a step-by-step approach in order to validate these additional synergies and to weight their different impact on the aircraft performances. Therefore, we optimize each hybrid configuration, from the basic one without any of the synergies, adding one by one the synergies. This yields a matrix of aircraft to optimize, as represented in Figure 3.3. The abscissa axes represent the increasing number of the optimization degrees of freedom, the ordinate represents the increasing number of synergies included in the configuration to optimize. By doing this, we are able to compare the

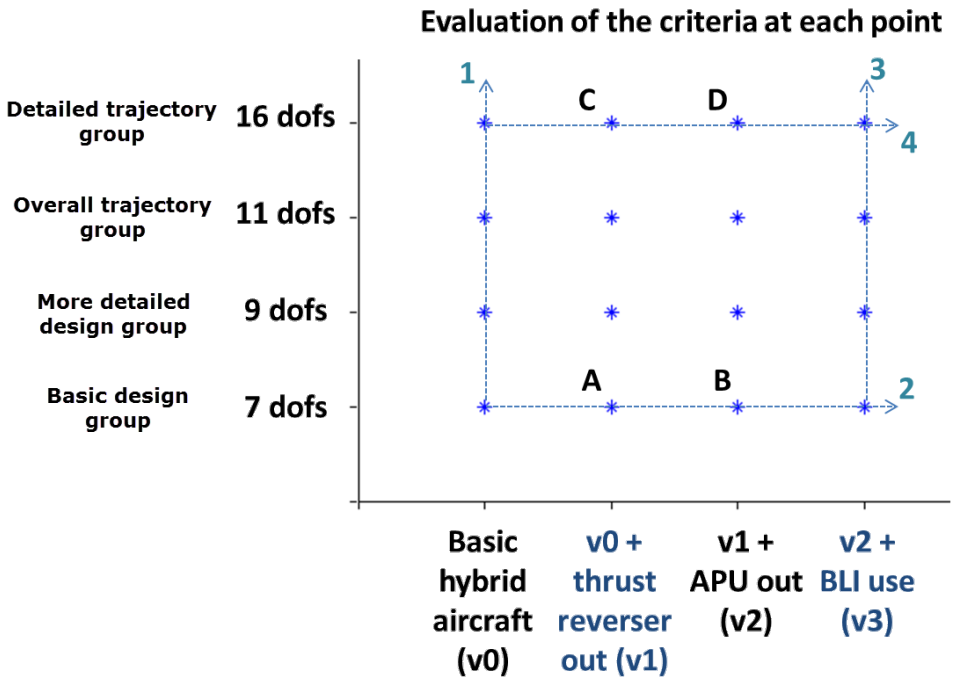

Figure 3.3: Matrix representing the panoply of hybrid aircraft to optimize, with variable number of degrees of freedom (dof) and variable use of the synergies.

criterion evolution from both directions. It is then possible to observe the coupling between the additional synergies and the increasing number of degrees of freedom. For instance, if we compare in a first time the criterion value between point A and point B (from Figure 3.3), and in a second time between point C and point D, we can observe if 16 degrees of freedom allow to take more benefit of the synergies than 7 degrees of freedom, or not.

We also present tables of numerical results in the following sections. The idea is to put in the same table the evolution of the optimized aircraft following the path represented by the arrows in Figure 3.3. Beginning with the basic aircraft, with 7 degrees of freedom, we will first present a table that shows the evolution of the optimized configuration according to the increasing number of degrees of freedom (arrow number 1), followed by a table with the evolution according to the additional synergies with the 16 degrees of freedom (arrow number 4). Secondly, we will present the other path, from the basic aircraft to the all-synergies aircraft with 7 degrees of freedom (arrow number 2) in a first table, and then the effect of the increasing degrees of freedom on this all-synergies aircraft (arrow number 3).

Finally as for the conventional configuration, we present a table with the different optimized aircraft according to the three criteria.

3.1.5 To sum up

First we list in Table 3.3 all the design variables that can be used for the optimization process, both for the conventional and the hybrid aircraft. We also present their bounds, and the dimension n of the problem in the conventional and the hybrid case. Table 3.4

lists all the constraints.

Table 3.3: Optimization Variables for conventional aircraft, with the additional ones brought by the hybrid aircraft configuration.

	n (conv.)	n (hyb.)	**Name**	**Bounds**	**Unit**
Conventional	1	1	Wing Area	$[100, 250]$	m^2
	2	2	Sea Level Static Thrust	$[6000, 15000]$	daN
	3	3	MZFW	$[60000, 80000]$	kg
	4	4	MTOW	$[65000, 85000]$	kg
	5	8	Wing Aspect Ratio	$[8, 16]$	no dim.
	6	9	Thermal engine BPR	$[8, 12]$	no dim.
	7	10	Top of climb altitude	$[25000, 45000]$	ft
	8	11	Cruise Mach	$[0.6, 0.85]$	Mach
	9	12	Step Mission Vcas 0	$[200, 250]$	knots
	10	13	Step Mission Vcas 1	$[200, 300]$	knots
	11	14	Step Mission Vcas 2	$[200, 300]$	knots
	12	15	Step Mission Vcas 3	$[200, 300]$	knots
	13	16	Step Mission Vcas 4	$[200, 300]$	knots
Hybrid		5	Electric Fan Size	$[1, 2]$	m
		6	Generator Electric Ratio	$[0.01, 0.1]$	no dim.
		7	Electric Fan Power	$[1.5, 4]$	MW

Table 3.4: List of the optimization available constraints.

		Name	**Value**
Conventional	1	Approach Speed (LdSpeed)	< 120 kt
	2	Climb Vz Ceiling (ClbVz)	> 300 ft/min
	3	Cruise Vz Ceiling (CrzVz)	> 100 ft/min
	4	Take-Off Field Length 1	< 2000 m
	5	Second segment limitation 1	< 2000 m
	6	Time-To-Climb	< 25 min
	7	StepMisMTOW margin	> 0 kg
	8	MZFW margin	> 0 kg
Hybrid (v1, v2, v3)	9	Take-Off Nominal Thrust	> 1000 daN

We now have all the tools to solve all the conventional and hybrid aircraft optimizations. Let Ω^n denote the design variables admissible space, which is the Cartesian product of the intervals defined by the bounds on each variable in Table 3.3. Let $f : \Omega \to \mathbb{R}$ denote the black box type function computing the selected objective, and $g_i : \Omega \to \mathbb{R}$, for $i = 1, \ldots, m$ the black box type functions computing the constraint i from Table 3.4. We only have to deal with inequality constraints. For a sake of clarity and without any loss of information, we denote the function g_i as follows:

Table 3.5: List of the selected optimization objectives.

Name	Unit
Maximum Take-Off Weight (MTOW)	kg
Cash Operating Cost (COC)	\$/trip
Absolute Pulsed Global Warming Potential (APGWP)	$W/m^2/km/year$

- if the constraint is of the type $g_i(\boldsymbol{x}) \leq G_i^{sup}$, $g_i(\boldsymbol{x}) = g_i(\boldsymbol{x}) - G_i^{sup}$,
- if the constraint is of the type $g_i(\boldsymbol{x}) \geq G_i^{inf}$, $g_i(\boldsymbol{x}) = G_i^{inf} - g_i(\boldsymbol{x})$.

Finally, for each aircraft design case, we consider the non-linear, non-convex and constrained following deterministic optimization problem:

$$\left| \begin{array}{ll} \min\limits_{\boldsymbol{x}\in\Omega^n} & f(\boldsymbol{x}) \\ \text{s.t.} & g_i(\boldsymbol{x}) \leq 0,\ i = 1, \ldots, m. \end{array} \right. \tag{3.3}$$

The optimization algorithms used to obtain the optimized aircraft, are one of the following ones (see Chapter 2, Section 2.3):

- the DOT optimization tool,
- the MADS optimization tool,
- the modified Nelder-Mead optimization tool.

Since models are black-boxes, we do not have any proof of convergence. Therefore, we run several optimization algorithms from several initial points and when no more improvements are observed in the criterion, we select the solution.

3.2 Conventional Aircraft design optimization results

This section focuses on the deterministic optimization of the conventional aircraft design: first we optimize the aircraft configuration by increasing the number of design variables of the optimization. Secondly, we optimize the aircraft with respect to various criteria.

3.2.1 Impact of the increasing number of design variables

This optimization is done by using the step-by-step trajectory modeling presented in Chapter 1, Section 1.3.2. We run four optimizations of the conventional aircraft configuration, with the MTOW objective and with the increasing number of design variables. We obtain the results presented in the tables of Figure 3.4. We also represent the most important parameters evolution with respect to the increasing number of degrees of freedom (dofs) in Figure 3.5.

We propose to analyze these results between each optimization:

- The first step is the introduction of the additional overall aircraft design dofs (the BPR and the WingAR). As expected, the BPR is set to its upper bound. The

	Unit	Number of degrees of freedom			
		4	6	8	13
WingArea	m2	168,6	163,6	132,6	131,6
SLSThrust	daN	10 434	10 457	8 861	8 859
WingAR	no_dim	9	11,3	12,7	12,9
BPR	no_dim	9	*12*	*12*	*12*
ZpRef	ft	35 000	35 000	***25 000***	***25 000***
CruiseMach	mach	0,76	0,76	0,65	0,65
StepMisVcas0	kt	250	250	250	***250***
StepMisVcas1	kt	250	250	250	262
StepMisVcas2	kt	250	250	250	258
StepMisVcas3	kt	270	270	270	***200***
StepMisVcas4	kt	250	250	250	***200***
OWE	kg	43 807	43 868	39 881	39 807
DesignMTOW	kg	74 453	72 229	67 393	67 148
StepMisFuelBlock	kg	9 401	7 560	7 096	6 933
CashOpCost	$/trip	7 534	7 242	7 553	7 559
APGWP	1e-6.W/m2/km/year	0,280	0,258	0,241	0,236
Tofl1	m	1 674	1 620	2 000	2 000
ExtTofl1	m	718	659	878	877
LdSpeed1	kt	120	120	120	120
ClbVz1	ft/min	412	491	966	990
CrzVz1	ft/min	100	169	614	640
TimeToClimb	min	21,3	19,6	23,2	22,2

Figure 3.4: Conventional aircraft optimization results with increasing number of dofs, with respect to the MTOW.

WingAR is not set to its maximum value. This is due to the balance between the two following effects: on one hand, when the WingAR increases, the drag is decreasing, and so less fuel is consumed. On the other hand, the WingAR increase also yields a heavier structure that leads to a higher fuel consumption. However, if some technology improvements could lead to lighter wings, with the same structural strength, the optimal WingAR would be higher. In this case, we can also be limited by the airport infrastructure, that can not afford aircraft with high wingspan. Then folding wings could be of interest.

The MTOW criterion decreases by 3%: this is mainly due to the decrease of the fuel consumption (StepMisFuelBlock). This was expected, since the BPR and the WingAR directly influence the fuel consumption.

In the two cases (4 and 6 dofs), the landing speed (LdSpeed1) constraint is active, which directly prevents the size of the wing area to decrease. The cruise vertical speed (CrzVz1) constraint is no longer active in the second case and is probably replaced by the BPR set on its upper bound.

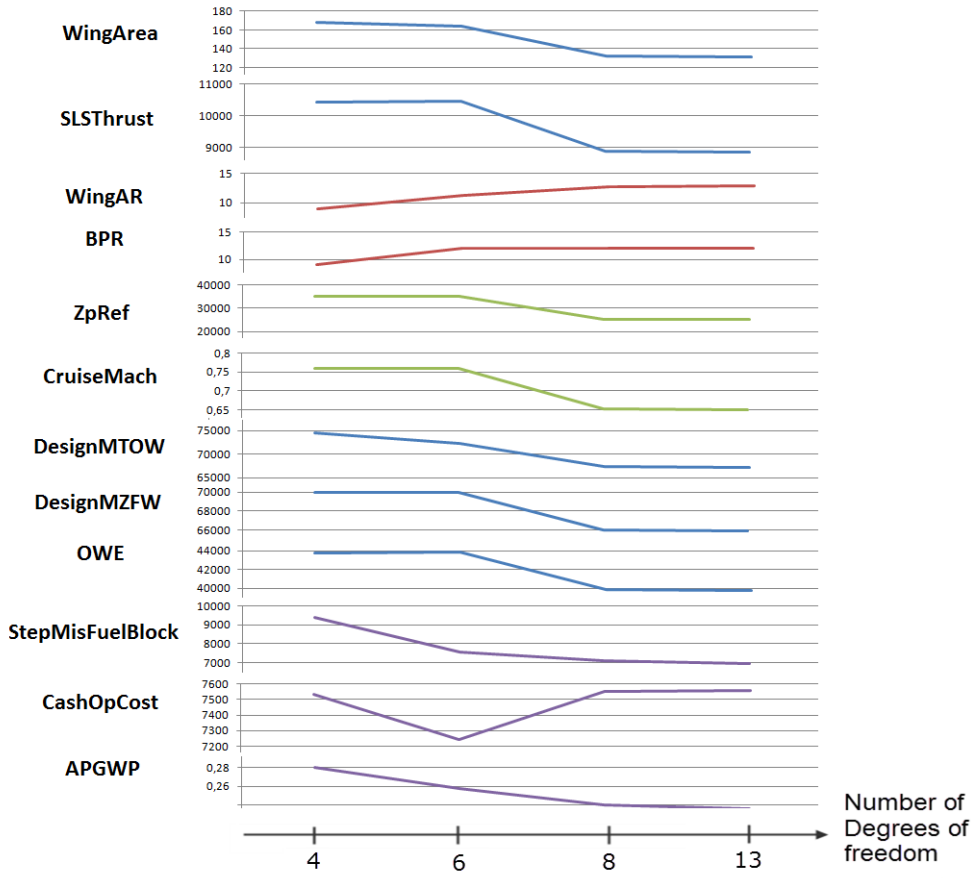

Figure 3.5: Conventional aircraft optimization graphs with increasing number of dofs, with respect to the MTOW.

The APGWP is decreasing, mainly due to the fuel consumption decrease.

- The second step is the introduction of the mission parameters. The top of climb altitude (ZpRef) is set to its lower bound, and the Mach is set to the value of 0.65. This is mostly due to the apparition of an additional drag, namely the compressibility drag, that appears when the Mach is higher than 0.65. In addition, this drag increases as the Mach increases.

  This step is the one with the highest effect on the criterion with a decrease by 6.7%. This is mainly due to the thrust decrease. The take-off field length (Tofl1) becomes an active constraint. It is a low speed constraints, whereas the CrzVz1 was a top of climb constraint. The wing area decreases, since the aircraft is lighter, but the decrease remains limited by the active landing speed constraint.

  The COC increases by 4.3%, due to the Mach decrease, which yields an increase of the flight duration and so to higher crew costs.

  The APGWP is decreasing, mainly due to the decreasing altitude.

- Finally, the last step is the introduction of the climb and descent speeds (Vcas0 to

Vcas1). This has not much influence on the results, comparing to the first two steps. However, a decrease of 245 kg of the MTOW is not negligible from an operational point of view. This leads to

$$245 \text{ kg} \times 2 \text{ trip per day} \times 365 \text{ days} \approx 180 \text{ t}, \tag{3.4}$$

of fuel savings in a year. This is significant for the airline.

3.2.2 Comparison of MTOW - Cost - Climatic Impact criteria

In this section, we run optimization with the 13 dofs, and for the three different objectives. The results are presented in the table of Figure 3.6, and in the spider chart of Figure 3.7.

The first observation is that the optimization with respect to the COC sets the design

	Unit	Objective		
		MTOW	COC	APGWP
WingArea	m2	131,6	158,4	135,3
SLSThrust	daN	8 859	10 390	8 662
WingAR	no_dim	12,9	***16***	13,7
BPR	no_dim	***12***	***12***	***12***
ZpRef	ft	***25 000***	41 156	***25 000***
CruiseMach	mach	0,65	0,74	0,65
StepMisVcas0	kt	***250***	241	***250***
StepMisVcas1	kt	262	268	278
StepMisVcas2	kt	258	283	276
StepMisVcas3	kt	***200***	232	***200***
StepMisVcas4	kt	***200***	247	***200***
OWE	kg	39 807	44 852	40 237
DesignMTOW	kg	**67 148**	72 181	67 388
StepMisFuelBlock	kg	6 933	6 530	6 778
CashOpCost	$/trip	7 559	**7 128**	7 565
APGWP	1e-6.W/m2/km/year	0,236	0,255	**0,233**
Tofl1	m	2 000	1 661	2 000
ExtTofl1	m	877	631	856
LdSpeed1	kt	120	120	118
ClbVz1	ft/min	990	326	937
CrzVz1	ft/min	640	100	590
TimeToClimb	min	22,2	17,6	22,7

Figure 3.6: Conventional aircraft optimization results with all dofs, with respect to the MTOW, the COC and the AGPWP.

parameters to their maximum values (see the spider chart from the left in Figure 3.7). This is mainly due to the influence of the flight duration on the cost. The high value of

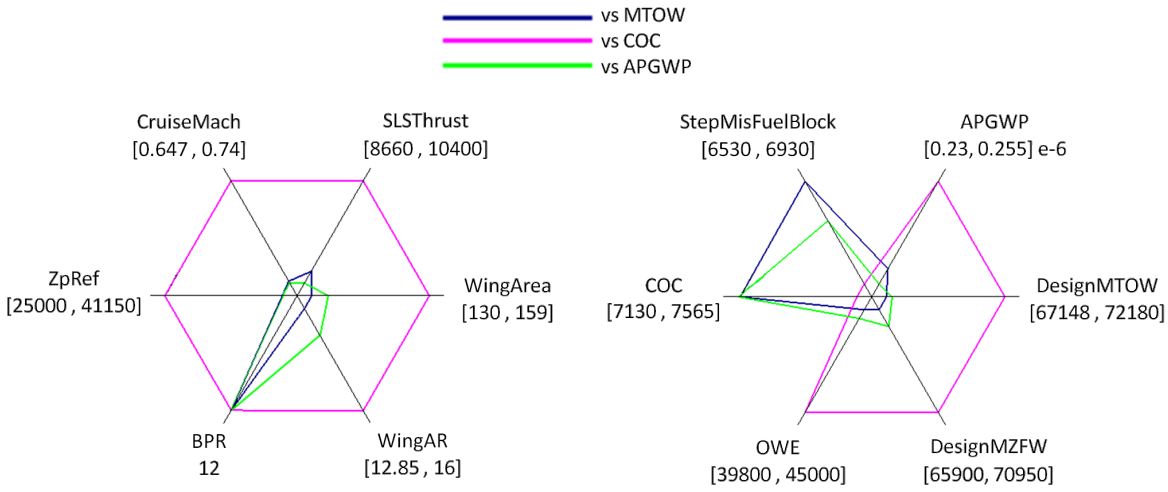

Figure 3.7: Spider chart for the conventional aircraft optimization results with all dofs, with respect to the MTOW, the COC and the AGPWP.

the cruise Mach leads to really high values of the APGWP and the MTOW, comparing to the two other aircraft. The high Mach yields high flight altitude. The mission block fuel is less than for the optimized aircraft with respect to the MTOW: the instantaneous consumption is higher since the Mach is higher, but the flight is performed in less time. Globally, flying fast and high is better for the mission block fuel than flying slow and low. The WingAR is set to its upper bound, it yields heavy wings but it is compensated by the high engine thrust.

The aircraft optimized with respect to the MTOW and the APGWP are quite similar. For both the aircraft, the Mach is set to 0.65 and the altitude to 25000 kft. However, the optimal aircraft with respect to the APGWP leads to an equilibrium slightly different to the one optimized with respect to the MTOW, with a higher wing area but lower SLSThrust.

The results of this section are interesting since they illustrate why the current aircraft are flying high and fast: the COC is the predominant objective. And even if the MTOW is a main contribution of the COC, this is not enough to counterbalance the effect of the flight duration on the cost.

3.3 Hybrid Aircraft design optimization results

This section is dedicated to the deterministic optimization of the hybrid aircraft design. First, we increase the number of design variables and then the number of synergies. Secondly, we start by increasing the number of synergies and then the number of design variables. Thirdly, we compare the results of the optimization for various criteria. Finally, we present a multi-objective optimization of the conventional and of the hybrid aircraft with respect to the MTOW and the COC criteria.

3.3.1 Increased design space and then the number of synergies

We start the optimization of the hybrid aircraft by using no synergy and by increasing the degrees of freedom, similarly to the optimization of the conventional aircraft in Section 3.2.1. Note that the basic optimization of the hybrid aircraft is made with 7 dofs, since the electric ratio, the fan power and the fan size are added to the basic dofs of the conventional aircraft optimization. The second section is dedicated to the hybrid aircraft optimization taking into account step by step each additional synergy.

3.3.1.1 Impact of the increasing number of design variables on the 0-synergies optimized aircraft

The results are presented in Figures 3.8 and 3.9. We observe the same trends as for the

	Unit	Number of degrees of freedom			
		7	9	11	16
WingArea	m2	172,1	168,3	136,3	133,4
SLSThrust	daN	9 341	9 341	9 339	8 855
WingAR	no_dim	9	9,5	15,5	14,1
BPR	no_dim	9	11,9	***12***	***12***
ZpRef	ft	35 000	35 000	34 702	***25 000***
CruiseMach	mach	0,76	0,76	0,64	0,63
StepMisVcas0	kt	250	250	250	***250***
StepMisVcas1	kt	250	250	250	249
StepMisVcas2	kt	250	250	250	250
StepMisVcas3	kt	270	270	270	***200***
StepMisVcas4	kt	250	250	250	***200***
ElecRatio	no_dim	***0,01***	***0,01***	0,03	0,04
eFanPower	MW	2	2	2	2
eFanSize	m	***1***	***1***	***1***	***1***
OWE	kg	44 807	44 464	42 733	41 659
DesignMTOW	kg	75 198	73 341	70 479	69 051
StepMisFuelBlock	kg	9 149	8 014	7 089	6 959
CashOpCost	$/trip	7 588	7 347	7 598	7 672
APGWP	1e-6.W/m2/km/year	0,228	0,204	0,205	0,191
Tofl1	m	1 749	1 698	1 929	2 000
ExtTofl1	m	737	702	755	823
LdSpeed1	kt	120	120	120	120
ClbVz1	ft/min	433	402	949	1 284
CrzVz1	ft/min	149	111	728	961
TimeToClimb	min	22,4	22,6	15,6	17,6

Figure 3.8: Design variables and performances of the optimized hybrid aircraft with zero synergy, with the increasing number of dofs, with respect to the MTOW.

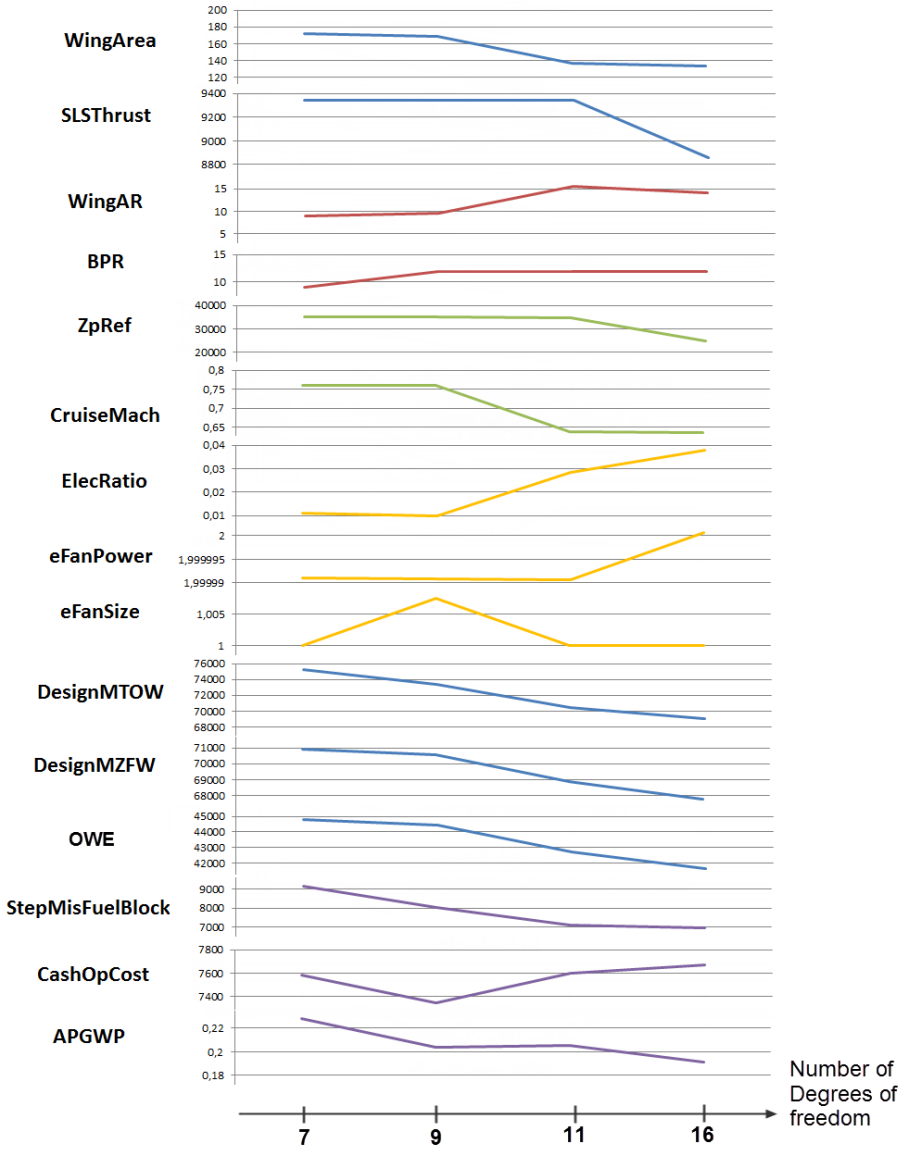

Figure 3.9: Hybrid aircraft optimization graphs 0-synergies, with increasing number of dofs, with respect to the MTOW.

conventional aircraft optimization, but we pay the price of the additional weights brought by the hybrid propulsion system on board. The introduction of the three dofs of the hybrid aircraft does not allow to reach the optimal MTOW of the conventional aircraft (with the maximum dofs, it is 2.8% higher). Moreover, the introduction of all the dofs allows to gain around 6 tonnes (8.2 %), whereas it was 7 tonnes (9.8%) for the conventional aircraft.

We also see that it goes to the lower bound of the electric fan size, but the eFanPower is not set to one of its bounds. The electric ratio increases which seems to indicate that the additional dofs lead to a more hybrid aircraft.

In all cases the landing speed constraint is active, which bounds below the wing area. We observe that the wing area of the last aircraft is quite similar to the one of the last aircraft of the conventional aircraft. We observe that only the last aircraft has an active

TOFL1 constraint, which is correlated to the slow and low aircraft flight.

Globally, the hybrid aircraft has a huge handicap with the weights of the on board additional systems. The introduction of the additional dofs drives the aircraft to a configuration very similar to the optimized conventional aircraft, but with a highest COC (1.5%) and a highest MTOW (2.8%). Nevertheless, the climatic impact (APGWP) is clearly reduced in all the cases (19% less comparing the last aircraft).

3.3.1.2 Impact of the synergies on the 16 design variables optimized aircraft

As previously seen, the introduction of the hybridization by an additional 100%-electric thrust and by a significant amount of electric energy stored on board (by the battery). This hybridization does not only take part in the thrust and the fuel consumption, but also brings some synergies used hereafter, and described in Section 3.2.1. The results of optimization with an increasing number of synergies, are presented in Figure 3.10 and 3.11.

The first step (from 0 synergy to 1 synergy) corresponds to the suppression of the thrust reverser. It leads to a decrease of the MTOW (by 1.3%), with a direct effect of reducing the COC (by 2.3%) and the APGWP (by 4.7%). It also allows the Mach to be higher. This has the interesting direct result of making the COC just below the equivalent one of the conventional aircraft (optimized with respect to the MTOW with all the dofs). However, we do not reach the optimal MTOW of the conventional aircraft.

The second step (from 1 to 2 synergies) is the suppression of the APU, with an additional 1000 kg of battery. In that case, the optimal MTOW becomes close to the one of the optimized conventional aircraft.

Finally, by taking benefit of the BLI, we obtain a lighter MTOW than the one of the optimized conventional aircraft (by 1%). Moreover, the APGWP is slightly higher than the lowest value but really lower than the conventional value (by 21%).

	Unit	Number of synergies			
		0	1	2	3
WingArea	m2	133,4	138,8	133,8	130,8
SLSThrust	daN	8 855	8 170	8 096	8 198
WingAR	no_dim	14,1	***16***	12,7	15
BPR	no_dim	***12***	***12***	***12***	***12***
ZpRef	ft	***25 000***	***25 000***	25 040	25 095
CruiseMach	mach	0,63	0,68	0,66	0,65
StepMisVcas0	kt	***250***	***250***	***250***	***250***
StepMisVcas1	kt	249	268	269	264
StepMisVcas2	kt	250	270	265	240
StepMisVcas3	kt	***200***	***200***	***200***	***200***
StepMisVcas4	kt	***200***	***200***	***200***	***200***
ElecRatio	no_dim	0,04	***0,01***	***0,01***	***0,01***
eFanPower	MW	2,00	1,51	1,53	1,54
eFanSize	m	1,00	1,51	1,48	1,45
OWE	kg	41 659	41 490	39 816	40 102
DesignMTOW	kg	69 051	68 125	67 143	66 610
StepMisFuelBlock	kg	6 959	6 317	6 944	6 248
CashOpCost	$/trip	7 672	7 493	7 543	7 492
APGWP	1e-6.W/m2/km/year	0,191	0,182	0,183	0,187
Tofl1	m	2 000	2 000	2 000	2 000
ExtTofl1	m	823	773	853	808
LdSpeed1	kt	120	120	120	120
ClbVz1	ft/min	1 284	901	920	1 100
CrzVz1	ft/min	961	530	570	758
TimeToClimb	min	17,6	22,2	23,3	18,6
eTONthrust	daN		1 000	1 000	1 000

Figure 3.10: Design variables and performances of the optimized hybrid aircraft for the 16 dofs optimization, with the increasing number of synergies, with respect to the MTOW.

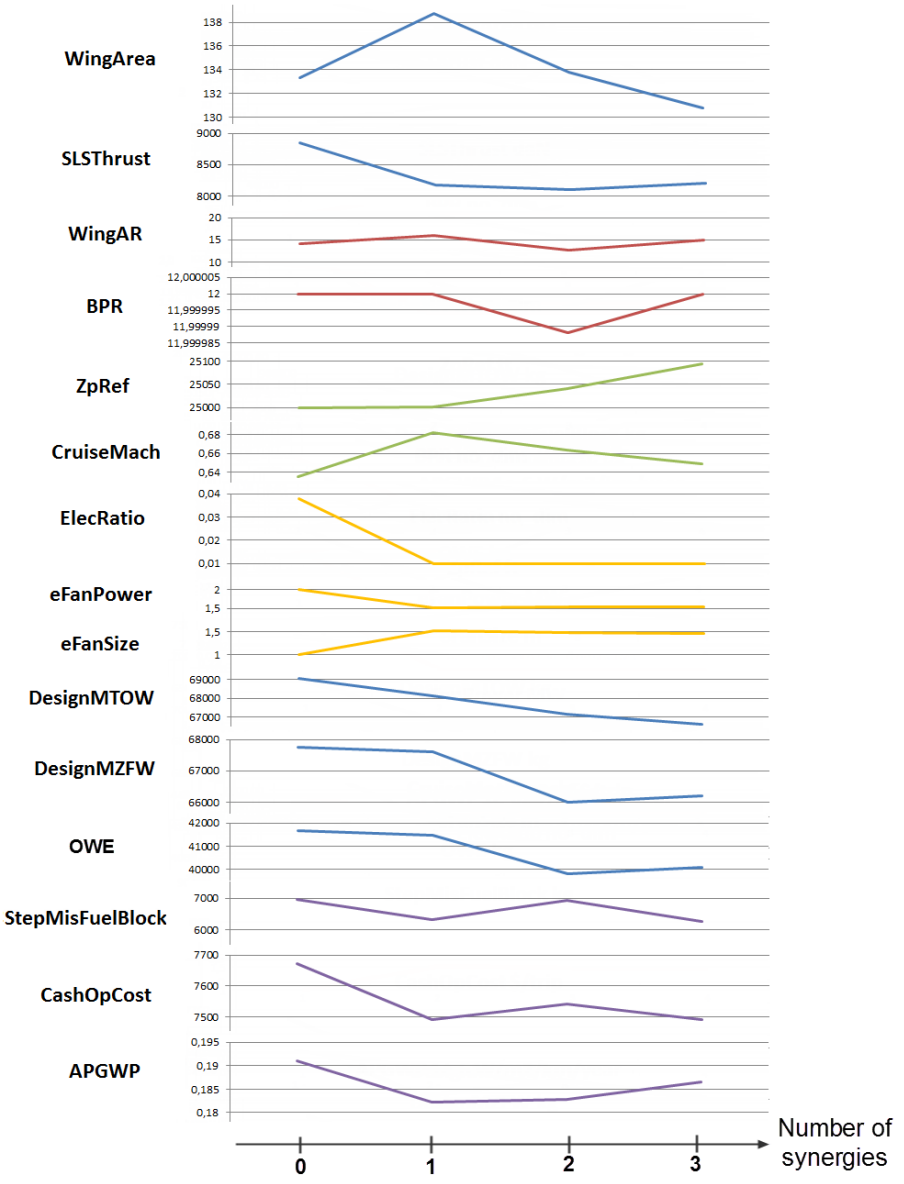

Figure 3.11: Hybrid aircraft optimization graphs with increasing number of synergies, for the 16 dofs optimization, with respect to the MTOW.

3.3.2 Increased the number of synergies and then the design space

In this section, we present the following additional approach: the first step is to observe the impact of additional synergies on the optimization of the basic hybrid aircraft (with the first 7 dofs). The second step is to observe the impact of an increasing number of dofs on the hybrid aircraft with all the synergies. Detailed results (tables and graphs) are presented in Appendix B.

We propose to present here the evolution of the main parameters - the wing area and the SLSThrust - and the performances - the MTOW, the APGWP and the COC - for all the optimized aircraft presented in Figure 3.3. We compare the evolution of each point with respect to the value of its neighboors, in percentage.

In Figure 3.12, we present the evolution of the SLSThrust, and in Figure 3.13, the evolution of the wing area.

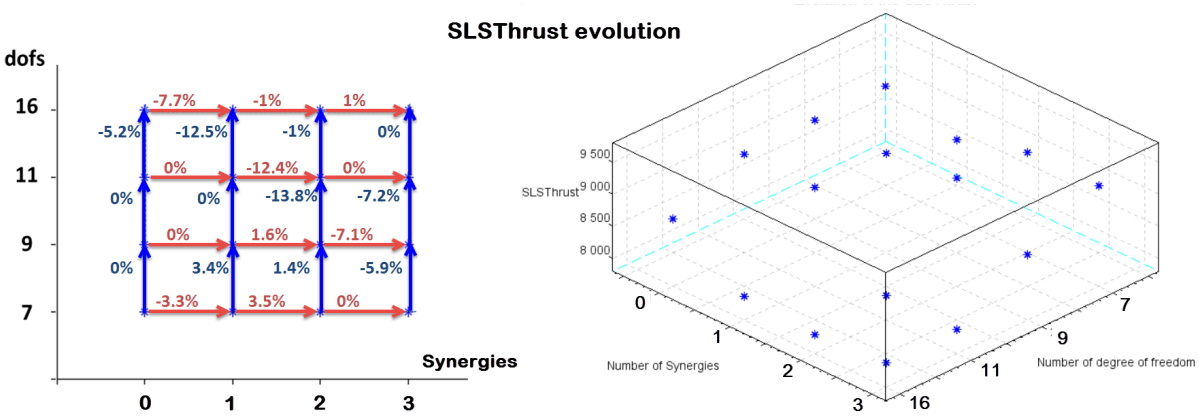

Figure 3.12: SLSThrust of the optimized hybrid aircraft with respect to the number of dofs and the number of synergies.

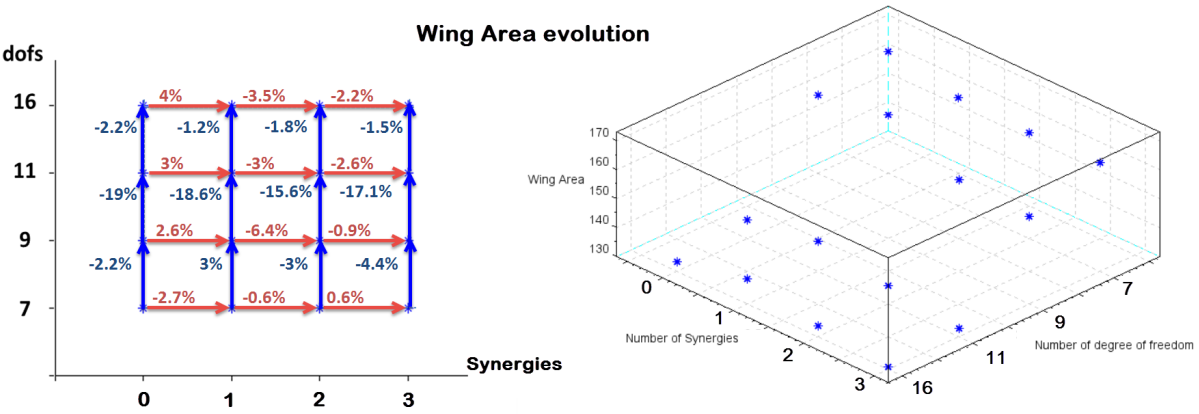

Figure 3.13: Wing area of the optimized hybrid aircraft with respect to the number of dofs and the number of synergies.

The global tendency of the SLSThrust is to decrease while adding synergies and degrees

of freedom. The wing area follows the same tendency, with a noticeable decrease when we add the overall mission parameters ZpRef and CruiseMach (9 to 11). The addition of the step-by-step trajectory parameters (11 to 16) does not really influence the wing area.

In Figure 3.14, we present the evolution of the APGWP and in Figure 3.15, the evolution of the COC.

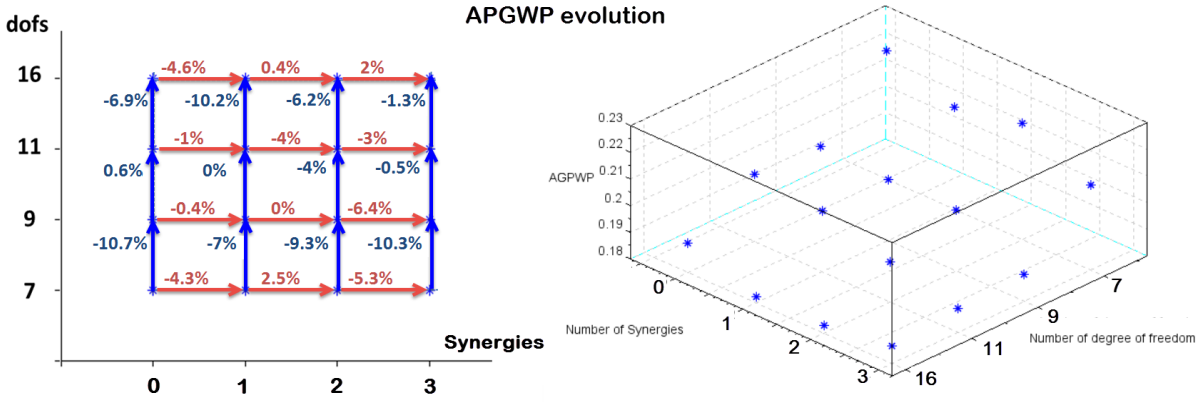

Figure 3.14: APGWP of the optimized hybrid aircraft with respect to the number of dofs and the number of synergies.

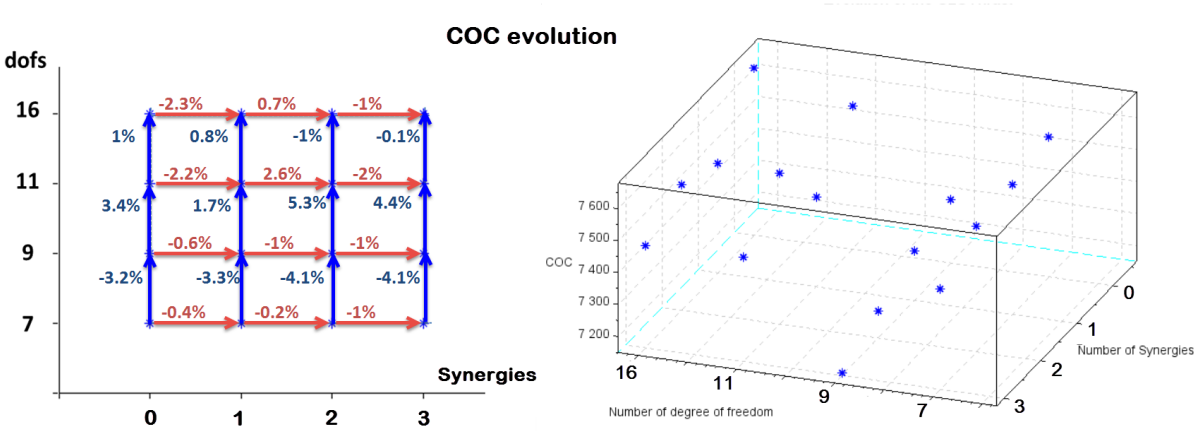

Figure 3.15: COC of the optimized hybrid aircraft with respect to the number of dofs and the number of synergies.

We observe that the APGWP is really reduced by the introduction of the WingAR and the BPR (7 to 9) and by the introduction of the step-by-step trajectory parameters (11 to 16). The influence of the synergies on the APGWP does not bring any other information. We observe that the COC is mainly reduced by the WingAR and BPR introduction (7 to 9), but it increases when the ZpRef and the CruiseMach are added (9 to 11). This is due to the decrease of the cruise Mach to 0.65 which leads to an increase of the flight duration and then to higher crew costs.

Finally, Figure 3.16 shows the evolution of the optimization criterion, the MTOW. We observe that the main decrease in the MTOW is when we add the ZpRef and the

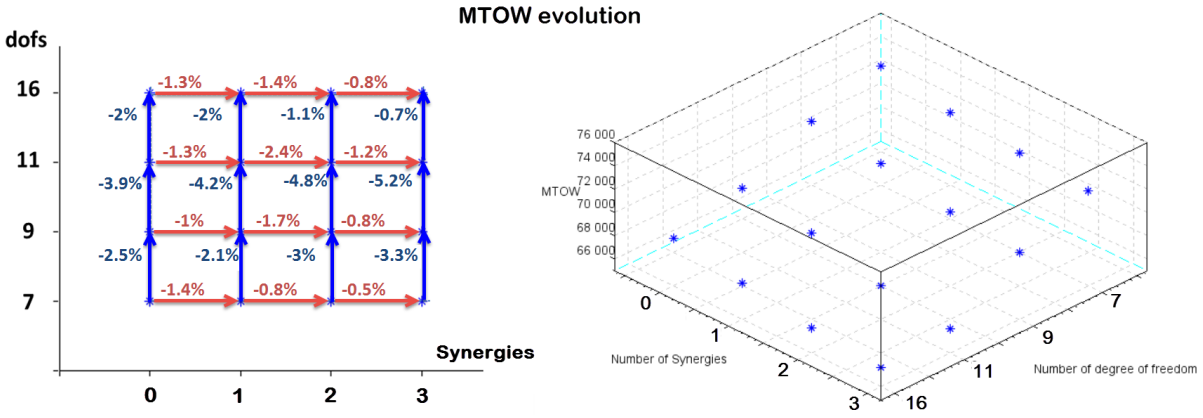

Figure 3.16: MTOW (criterion) of the optimized hybrid aircraft with respect to the number of dofs and the number of synergies.

CruiseMach (9 to 11), and when we add the second synergy (the APU suppression). In other cases, the effects have more or less a similar range.

3.3.3 Comparison of MTOW - Cost - Climatic Impact criteria

In this section, we run the hybrid aircraft optimization with all synergies, with the 16 dofs, and for the three different objectives. The results are presented in Figure 3.17, and in the spider chart of Figure 3.18.

We observe the same behavior as for the conventional aircraft: the aircraft optimized with respect to the COC has even higher cruise Mach and altitude ZpRef. It yields a COC value lower than 1.8% from the minimal COC of the conventional aircraft. The optimal MTOW is 1% lower than the optimal one of the conventional aircraft and the APGWP is 23.6% lower than the optimal one of the conventional aircraft. Nevertheless, we note that these interesting results are only possible since we took advantage of the opportunities brought by the hybridization, except for the APGWP which is in all cases better for the hybrid aircraft.

	Unit	Objective		
		MTOW	COC	APGWP
WingArea	m2	130,8	163,7	133,3
SLSThrust	daN	8 198	9 295	8 180
BPR	no_dim	***12***	***12***	***12***
WingAR	no_dim	15	***16***	13,5
ZpRef	ft	***25 000***	43 113	***25 000***
CruiseMach	mach	0,65	0,76	0,65
StepMisVcas0	kt	***250***	248	***250***
StepMisVcas1	kt	264	268	265
StepMisVcas2	kt	240	246	265
StepMisVcas3	kt	***200***	211	209
StepMisVcas4	kt	***200***	204	209
ElecRatio	no_dim	***0,01***	***0,01***	0,024
eFanPower	MW	1,54	2	1,54
eFanSize	m	1,45	1,20	1,45
OWE	kg	40 102	45 220	39 929
DesignMTOW	kg	**66 610**	71 901	66 889
StepMisFuelBlock	kg	6 248	5 985	6 613
CashOpCost	$/trip	7 492	**6 998**	7 539
APGWP	1e-6.W/m2/km/year	0,187	0,186	**0,178**
Tofl1	m	**2 000**	1 682	**2 000**
ExtTofl1	m	808	623	837
LdSpeed1	kt	**120**	**120**	**120**
ClbVz1	ft/min	1 100	**300**	1 008
CrzVz1	ft/min	758	**100**	673
TimeToClimb	min	18,6	17,8	20,3
eTONthrust	daN	**1 000**	1 158	**1 000**

Figure 3.17: Variables and performances of the optimized hybrid aircraft for the 16 dofs optimization, with respect to the MTOW, the COC and the AGPWP.

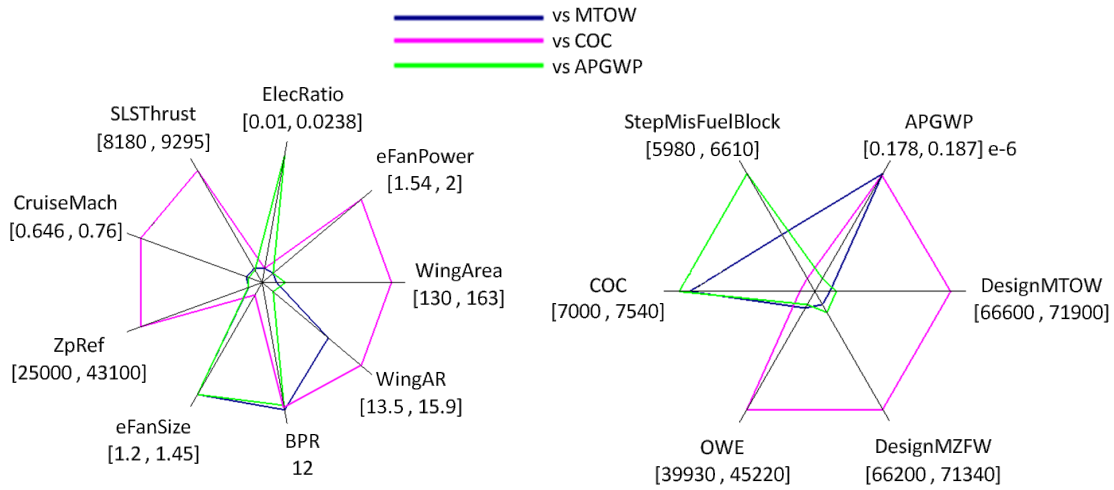

Figure 3.18: Spider chart for the hybrid aircraft optimization results with all dofs and all synergies, with respect to the MTOW, the COC and the AGPWP.

3.3.4 Hybrid and conventional aircraft COC with respect to MTOW Pareto front

Finally, to end this study we propose to solve multi-objective optimization of both the hybrid and the conventional aircraft. We started by computing the 3 dimensional Pareto front with the following objectives: the MTOW, the COC and the APGWP. However, the resulting Pareto front was not useful, since the MTOW driven aircraft has a low APGWP, and vice versa. Then a bi-objective Pareto front appears to be enough. We select then the MTOW and the COC objectives, and we draw the Pareto front for each aircraft using genetic algorithms method. They are presented in Figure 3.19.

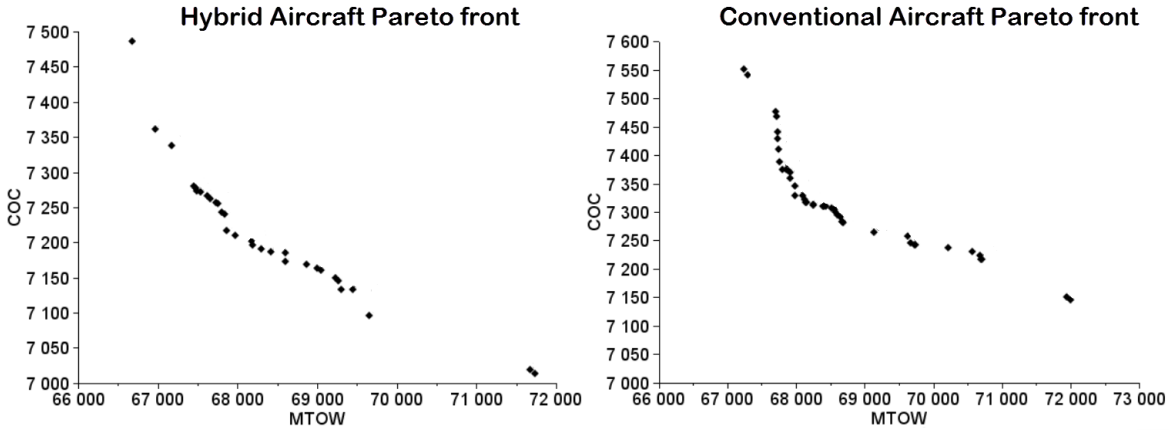

Figure 3.19: COC versus MTOW Pareto front, for the hybrid and the conventional aircraft.

We can observe from Figure 3.19 the trading cost between the COC and the MTOW for the two aircraft. For both the aircraft, two linear tendencies can be seen. For the conventional one, from a MTOW of 72t to a MTOW of around 69.5t, we have the following cost: 100kg less has a cost of around 4.5$. In the lower MTOW, 100kg less costs around 13.5$. For the hybrid aircraft, between 72t and 68t of MTOW, a decrease of 100kg has a cost of 5$, whereas for the lower MTOW, a decrease of 100kg has a cost of around 20$. The higher trading values for the hybrid aircraft can be explained by its ability to reach lower value of both the criteria than the conventional aircraft. It shows that every additional gain in one objective is most expensive in the minimal values of the other.

3.4 Conclusion

In this chapter we describe the optimized hybrid aircraft configuration with respect to the MTOW. A three-view drawing is given in Figure 3.20. The main characteristics (geometry, weights, performances, mission data) of this configuration are given in the tables of Figures 3.21, 3.22 and 3.23.

A Catia model of the hybrid aircraft has been realized and sent to a 3D printing. The 3D-printed aircraft is shown in the pictures of Figure 3.24. Note that this aircraft has forward-swept wings. This is our very last proposition for improving the hybrid configuration. Indeed, since we obtain low Mach of operations, this modification leads to an even

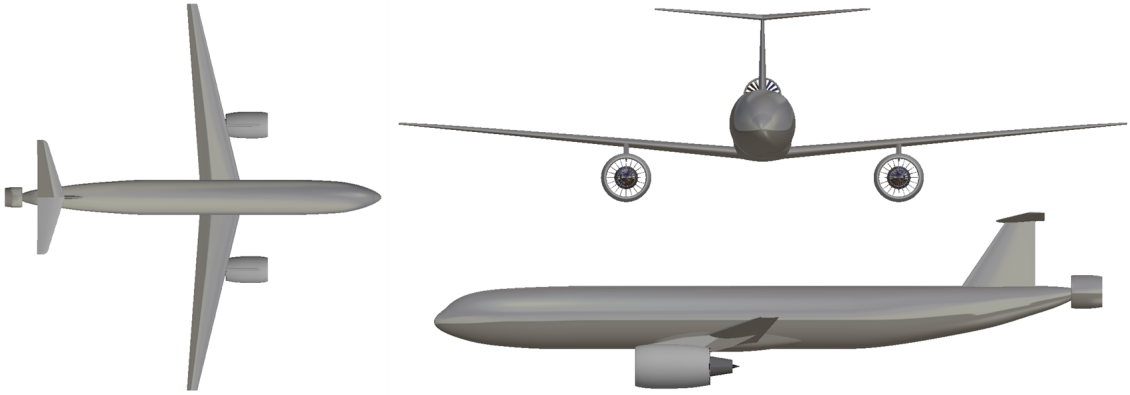

Figure 3.20: A three–views drawing of the optimized hybrid aircraft.

lower MTOW criterion. The interest is coming from the laminarity of such a wing, which generates less drag, especially with low Mach number.

Description	Label	Unit	Value
Total number of passengers	TotalNpax	int	180
Total fuselage length	FusLength	m	42
Fuselage section height	FusHeight	m	4,16
Fuselage section width	FusWidth	m	3,88
Wing reference area	WingArea	m2	131
Wing span	WingSpan	m	44
Wing aspect ratio	WingAR	no_dim	15
Wing taper ratio	WingTR	no_dim	0,25
Wing sweep angle at 25% chord	WingSweep	deg	14
Horizontal tail plane area	HtpArea	m2	23
Vertical tail plane area	VtpArea	m2	25
Number of engine	nEngine	int	2
Number of installed reversers	nReverser	int	2
Engine by pass ratio	BPR	no_dim	12
Engine overall pressure ratio	OPR	no_dim	27
Fan or propeller diameter	FanSize	m	2,68
Number of electrical engine	nEmotor	int	1
eFan diameter	eFanSize	m	1,45
eNacelle width	eNacWidth	m	1,60
eNacelle length	eNacLength	m	1,82
Target range for nominal mission	DesignRange	NM	2000
Target MTOW for structural reinforcement	DesignMTOW	kg	66610
Target MZFW for structural reinforcement	DesignMZFW	kg	66210
Fuselage equipped structural mass	FusMass	kg	10127
Wing equipped structural mass	WingMass	kg	9482
Strut mass	StrutMass	kg	0
Horizontal tail equipped structural mass	HtpMass	kg	508
Vertical tail equipped structural mass	VtpMass	kg	719
Landing gear mass	LdgMass	kg	2495
Reverser mass	ReverserMass	kg	0
Engine mass including reversers	EngineMass	kg	3303
Engine pylons equipped structural mass	PylonMass	kg	557
eEngine pylons equipped structural mass	ePylonMass	kg	123
eEngine mass	eEngineMass	kg	572
Power electronic mass	PowerElecMass	kg	140
APU mass	ApuMass	kg	0
System mass including APU	SystemMass	kg	3698
Furnishings	FurnMass	kg	3798
Operator item mass	OpItemMass	kg	3467
Containers and Pallets mass	ContPallMass	kg	708
Accumulator mass	AccuMass	kg	405
Evaluation MWE	MWE	kg	35522
Evaluation Operational empty weight	OWE	kg	40102
Maximum zero fuel weight	MZFW	kg	66210
Maximum fuel weight	MFW	kg	25131
Maximum landing weight	MLW	kg	66610
Maximum take off weight	MTOW	kg	66610

Figure 3.21: Optimized with respect to MTOW hybrid aircraft data table (1/3).

Initial cruise altitude	ZpRef	ft	25095
Cruise mach number	CruiseMach	mach	0,65
Lift factor for maximum LoD	LoDmaxCz	no_dim	0,92
Maximum lift to drag ratio	LoDmax	no_dim	24

Sea level static thrust	SLSThrust	daN	8198
Ratio of fan shaft power diverted to generator	ElecRatio	no_dim	0,01
e-Fan power	eFanPower	MW	1,54
Reference year for technology projection	ReferenceYear	year	2025
Accumulator energy density	EnergyDensity	Wh/kg	240
Motor & generator power density	PowerDensity	W/kg	6500

Normal take off total thrust	TONthrust	daN	6475
eFan take off thrust	eTONthrust	daN	1000
Required electrical power at take off	eTONelecPower	kW	1536
Generated electrical power at take off	eTONgenePower	kW	82
Maxi continuous total thrust	MCNthrust	daN	2936
eFan maxi continuous thrust	eMCNthrust	daN	21
Required electrical power in MCN rating	eMCNelecPower	kW	39
Generated electrical power in MCN rating	eMCNgenePower	kW	39
Maxi climb total thrust	MCLthrust	daN	2221
eFan maxi climb thrust	eMCLthrust	daN	514
Required electrical power in MCL rating	eMCLelecPower	kW	1536
Generated electrical power in MCL rating	eMCLgenePower	kW	49
Maxi cruise total thrust	MCRthrust	daN	2010
eFan maxi cruise thrust	eMCRthrust	daN	514
Required electrical power in MCR rating	eMCRelecPower	kW	1536
Generated electrical power in MCR rating	eMCRgenePower	kW	44
Field length for take off case 1	Tofl1	m	1999
Field 2nd segment for take off case 1	ExtTofl1	m	808
Approach speed for landing case 1	LdSpeed1	kt	120
Required vertical speed for climb case 1	ClbVz1	ft/min	1100
Required vertical speed for cruise case 1	CrzVz1	ft/min	758
Range of cost mission	CostMisRange	NM	500
Take off weight of cost mission	CostMisTOW	kg	62077
Payload of cost mission	CostMisPayload	kg	18360
Block fuel of cost mission	CostMisBlockFuel	kg	1936
Block time of cost mission	CostMisBlockTime	h	1,40

Fuel cost	FuelCost	$/trip	1274
Frame maintenance cost	FrameMC	$/trip	665
Engine maintenance cost	EngineMC	$/trip	368
Cockpit crew	CockpitCrew	$/trip	1130
Landing fees	LDGfees	$/trip	577
Navigation fees	NAVfees	$/trip	329
Standard operating cost	StdOpCost	$/trip	4343
Cabin crew	CabinCrew	$/trip	670
Catering	Catering	$/trip	553
Pax handling	PaxHandling	$/trip	360
Ramp handling	RampHandling	$/trip	1566
Cash operating cost	CashOpCost	$/trip	7492
Cash operating cost	SpecificCOC	$/NM/pax	0,08

Figure 3.22: Optimized with respect to MTOW hybrid aircraft data table (2/3).

Range of detailed mission	StepMisRange	NM	2000
Take off weight of detailed mission	StepMisTOW	kg	66610
Initial speed of detailed mission	StepMisVcas0	kt	250
First step altitude of detailed mission	StepMisZp1	ft	10000
First step speed of detailed mission	StepMisVcas1	kt	264
Second step altitude of detailed mission	StepMisZp2	ft	20000
Second step speed of detailed mission	StepMisVcas2	kt	240
Minimum climb speed in MCL rating	StepMisVzMinClb	ft/min	300
Minimum climb speed in MCR rating	StepMisVzMinCrz	ft/min	100
First step decent speed of detailed mission	StepMisVcas3	kt	200
First step descent altitude of detailed mission	StepMisZp3	ft	10000
Second step descent speed of detailed mission	StepMisVcas4	kt	200
Landing weight of detailed mission	StepMisLDW	kg	60362
Climb fuel of detailed mission	StepMisFuelClimb	kg	678
Cruise fuel of detailed mission	StepMisFuelCruise	kg	5208
Descent fuel of detailed mission	StepMisFuelDescent	kg	65
Block fuel of detailed mission	StepMisFuelBlock	kg	6248
Block time of detailed mission	StepMisTimeBlock	h	6,03

Reference year for LEEA calculation	EmissionYear	year	2014
Absolute Pulse Global Warming Potential	APGWP	1e-6.W/m2/km/year	0,19
Absolute Sustained Global Warming Potential	ASGWP	1e-6.W/m2/km/year	14,23
Absolute Pulse Global Temperature Potential	APGTP	1e-6.K/m2/km/year	0,000622
Absolute Sustained Global Temperature Potential	ASGTP	1e-6.K/m2/km/year	0,14

Figure 3.23: Optimized with respect to MTOW hybrid aircraft data table (3/3).

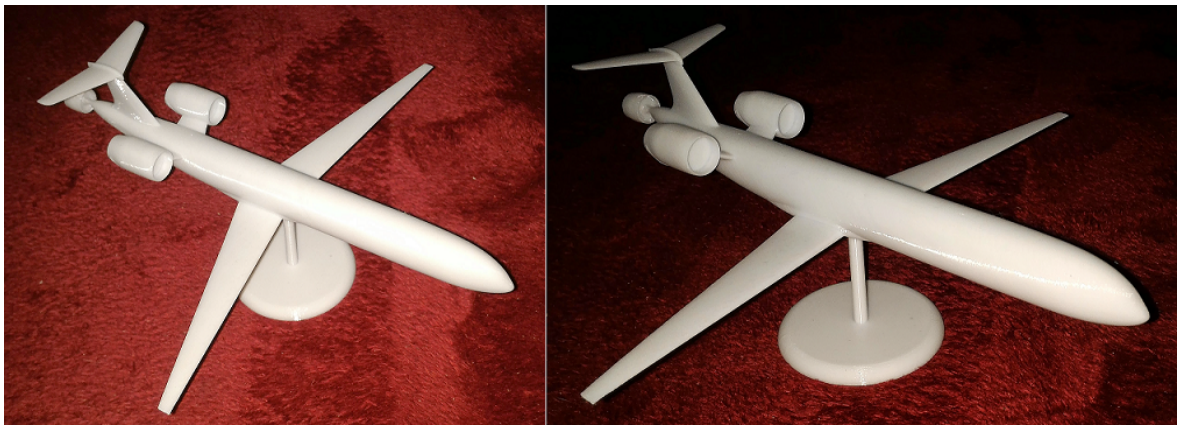

Figure 3.24: 3D-printed hybrid aircraft.

Chapter 4

Uncertainty Analysis

Contents

All along our studies of aircraft preliminary design, we are dealing with numerical model, coming from physical laws but also from empirical modeling. These models are presented in Chapter 1. When coming from physical laws, these models are sometimes based on a simplistic views of the involved physics. When coming from empirical modeling, they are often the results of regression through databases of existing aircraft. All the models are then constructed such that they are surrounded by errors, that can be also named uncertainties. Until now, studies are yet all deterministic. This uncertainty is managed by engineers know-how, using a posteriori margins on the results, which can sometimes not be really accurate.

This chapter is dedicated to the methods that can be used in uncertainty analysis. The main objective of this chapter is to bring an overview of methods to manage uncertainties through the models that have an interest in design engineering. The first section introduces the main definitions used in the field of uncertainty management, around the notion of random variables. General information, properties and examples are given. The second section presents how uncertainties can be quantified and characterized, with the introduction of a new family of distribution, named Beta-Mystic. The last section is dedicated to the methods that can be used to propagate uncertainties through function. Various methods are described: Monte-Carlo propagation method, Taylor expansion methods, quadrature and reduced quadrature methods, polynomial chaos expansion methods. A particular attention is paid to the conditions of use of the method, with each time the link between the uncertain input available information and the required accuracy on the uncertain output. The cost, the accuracy and the limitations of the methods are also presented. At the end of the last section, some numerical experiments are introduced, to illustrate the methods. Finally, the conclusion brings out the main characteristics of the methods and propose some guidelines to select the method according to a non-exhaustive list of criteria.

4.1 Definitions and general information about uncertainties

This section is dedicated to recall some important definitions and principles that will useful all along this chapter.

4.1.1 Uncertainties

A relevant definition of *uncertainties* can be found in [121]: "*The first meaning of uncertainty has its roots in probability and statistics: the estimated amount or percentage by which an observed or calculated value may differ from the true value... The second meaning of uncertainty relates to lack of knowledge about physical systems*". According to this definition, uncertainties can be classified into two kinds:

- Aleatory uncertainty, which describes physical variations caused by intrinsic randomness in a system and its environment. It is most commonly represented mathematically by a probability distribution, and is also referred in the literature as irreducible uncertainty, variability or inherent uncertainty [153].

- Epistemic uncertainty, which is caused either by a lack of knowledge about the system or its environment nor by the approximations made during process modeling. That kind of uncertainty can be reduced by a more accurate knowledge of the system, e.g.

by a refinement of a model. It is also referred in literature as reducible uncertainty or subjective uncertainty [153].

As mentioned above, the first kind of uncertainty is intrinsic to the system and then cannot be reduced. It appears to be often negligible compared to the epistemic uncertainty as it is the case in the future project studies. The latter uncertainty is coming from modeling the aircraft preliminary design environment.

As mentioned in Chapter 1, preliminary aircraft design requires models that allow quick evaluations of new aircraft configurations. It yields that the used toolbox is built with low level semi-empirical models. The latter are coming either from physical equations, either from databases of existing aircraft from which interpolations are made, based on engineer know-how. Then, in most of the cases, model uncertainties can be obtained from a sampling of the interpolation error distribution. The study of innovative aircraft configurations such as the hybrid aircraft from Chapter 5 is also bringing new uncertainties as assumptions are made around hybridization technologies.

4.1.2 About random variables

Definition 4.1. *Given Ω a sample space, $\mathcal{F}$ a set of events, a (real)* ***random variable*** *X is a function from Ω to $\mathbb{R}$ such that:*

$$\forall B \text{ interval of } \mathbb{R},\ X^{-1}(B) \in \mathcal{F}. \tag{4.1}$$

The set of values taken by X is denoted by: $X(\Omega) = \{X(\omega) \in \mathbb{R} : \omega \in \Omega\}$.

There are two types of random variables.

Definition 4.2. *A random variable that takes a finite or countable number of values, is called* ***discrete random variable****.*

Definition 4.3. *A random variable that can take any value in an interval, is called a* ***continuous random variable****.*

We will focus in this chapter on continuous random variables.

Definition 4.4. *Given X a random variable defined on a probability space $(\Omega, \mathcal{F}, \mathbb{P})$, where Ω is the sample space, $\mathcal{F}$ is a set of events, and $\mathbb{P}$ is a probability measure associated to $\mathcal{F}$. A* ***probability law*** *of X, denoted $\mathbb{P}_X$ is the function that associates to all part B of $\mathbb{R}$ the value:*

$$\mathbb{P}_X(B) = \mathbb{P}\left(X^{-1}(B)\right) = \mathbb{P}\left(\{\omega \in \Omega : X(\omega) \in B\}\right). \tag{4.2}$$

A probability law can be characterized by its cumulative distribution function or its probability density function.

Definition 4.5. *The* ***cumulative distribution function*** *(cdf) is defined for every real value x by*

$$F_X(x) = \mathbb{P}(X \leq x). \tag{4.3}$$

It has the following properties:

- $\forall x \in \mathbb{R}$, $0 \leq F_X(x) \leq 1$,
- the function F_X converges to 0 in $-\infty$ and to 1 in $+\infty$,
- the function F_X is increasing,
- the function F_X is continuous right.

Two random variables with the same cumulative distribution function, are following the same probability law.

Definition 4.6. *Given X a random variable with a cumulative distribution function F_X strictly increasing from $I \subset \mathbb{R}$ in $]0,1[$. The q-**quantile**, $q \in [0,1]$, of X is the number $x_q \in I$, such that $F_X(x_q) = q$, i.e.:*

$$\mathbb{P}(X \leq x_q) = q. \tag{4.4}$$

Definition 4.7. *Given X a continuous random variable, the **probability density function** (pdf) of X is the positive function f_X such that for any two numbers a and b, with $a < b$, we have:*

$$\mathbb{P}(a < X \leq b) = \int_a^b f_X(x)dx. \tag{4.5}$$

That value is the probability that the random variable X takes on a value in the interval $[a, b]$. Observe that since $\lim_{x \to +\infty} F_X(x) = 1$, then

$$\int_{\mathbb{R}} f_X(x)dx = 1. \tag{4.6}$$

If F_X is the cumulative distribution function of X, we have:

$$F_X(x) = \int_{-\infty}^{x} f_X(z)dz. \tag{4.7}$$

The result is that the probability density function is the derivative of the cumulative distribution function. As the cumulative distribution function, the probability density function characterizes the probability law, in the sense that two random variables with the same probability density function are following the same probability law. An example of Probability Density Function of a continuous variable following a normal law is given in Figure 4.1.

Random continuous variables have characteristics that will be useful for our studies.

Definition 4.8. *The **mode** of a continuous probability distribution is the value x at which its probability density function reaches its maximum value.*

The example of Figure 4.1 is an unimodal distribution: it admits an unique mode.

Definition 4.9. *Given a random continuous variable X with a pdf f_X, the **expectation** (or mean) of X is defined by:*

$$\mathrm{E}[X] = \int_{\mathbb{R}} x f_X(x)dx. \tag{4.8}$$

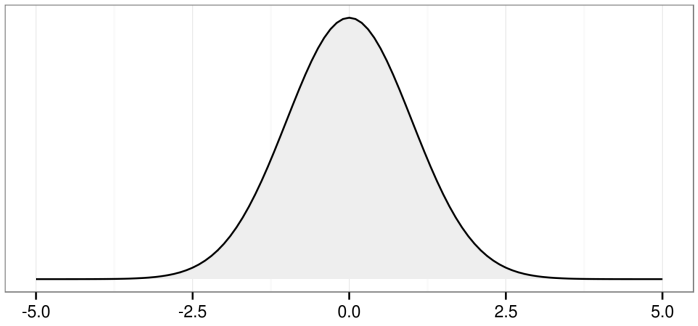

Figure 4.1: Probability Density Function of a continuous variable.

The mean of X is often denoted μ_X and has the following properties:

- Linearity: $\forall (a,b) \in \mathbb{R}^2$, we have $\mathrm{E}[a+bX] = a + b\,\mathrm{E}[X]$.
- Positivity: if $X \geq Y$ then $\mathrm{E}[X] \geq \mathrm{E}[Y]$.

Definition 4.10. *Given a random variable X, if g is a function from $\mathbb{R}$ to $\mathbb{R}$ then $g(X)$ is a random variable. If X is a random continuous variable with a pdf f_X, the expectation of $g(X)$ is defined by:*

$$\mathrm{E}[g(X)] = \int_{\mathbb{R}} g(x) f_X(x) dx. \tag{4.9}$$

If g is the identity function then $\mathrm{E}[g(X)] = \mathrm{E}[X]$.

Definition 4.11. *The **variance** of a random variable X, denoted by $\mathrm{var}(X)$, is given by:*

$$\mathrm{var}(X) = \mathrm{E}\left[(X - \mathrm{E}[X])^2\right] = \mathrm{E}\left[X^2\right] - \mathrm{E}[X]^2. \tag{4.10}$$

It is a measure of how far a variable is spread out and it has the following property:

$$\forall (a,b) \in \mathbb{R}^2,\ \mathrm{var}(aX+b) = a^2\,\mathrm{var}(X). \tag{4.11}$$

Definition 4.12. *The square root of the variance, denoted by σ_X, is called the **standard deviation** of X.*

$$\mathrm{var}(X) = \sigma_X^2. \tag{4.12}$$

It has the same dimension as the data and is then comparable to deviations from the mean.

4.1.3 Moments of a random variable

Let us denote $X : \Omega \to \mathbb{R}$ a random continuous variable and f_X its joint probability density function. The definition of the classical moments of order p of X is:

$$m_{p,X} = \mathrm{E}[X^p] = \int_{\mathbb{R}} x^p f_X(x) dx. \tag{4.13}$$

The first order moment corresponds to the previously defined mean, denoted by μ_X. For all $p \geq 2$, centered moments are defined by:

$$\mu_{p,X} = \mathrm{E}\left[(X - \mathrm{E}\left[X\right])^p\right]. \tag{4.14}$$

They can be expressed as functions of classical moments via the following formulas:

$$\begin{aligned} \mu_{1,X} &= m_{1,X}, \\ \mu_{2,X} &= m_{2,X} - m_{1,X}^2, \\ \mu_{3,X} &= m_{3,X} - 3m_{2,X}m_{2,X} + 2m_{1,X}^3, \\ \mu_{4,X} &= m_{4,X} - 4m_{3,X}m_{1,X} + 6m_{2,X}m_{1,X}^2 - 3m_{1,X}^4, \end{aligned} \tag{4.15}$$

The first four centered reduced moments of X, also called standardized moments, are denoted by $(\mu_X, \sigma_X^2, \gamma_X, \Gamma_X)$. They are respectively called the mean, the variance, the skewness and the kurtosis, and can be expressed by relations (4.16) to (4.19):

$$\mu_X = E\left[X\right] = \mu_{1,X}, \tag{4.16}$$

$$\sigma_X^2 = E\left[(X - \mu_X)^2\right] = \mu_{2,X}, \tag{4.17}$$

$$\gamma_X = \frac{E\left[(X - \mu_X)^3\right]}{\sigma_X^3} = \frac{\mu_{3,X}}{\sigma_X^3}, \tag{4.18}$$

$$\Gamma_X = \frac{E\left[(X - \mu_X)^4\right]}{\sigma_X^4} - 3 = \frac{\mu_{4,X}}{\sigma_X^4} - 3. \tag{4.19}$$

Skewness and kurtosis give two important characterizations of a distribution. The skewness characterizes the degree of asymmetry of a distribution around its mean. The kurtosis measures the relative peakedness or flatness of a distribution, relative to a normal distribution. A representation of the link between the sign of these two parameter values and the corresponding shape of the distribution is given in Figure 4.2. It is important to note that

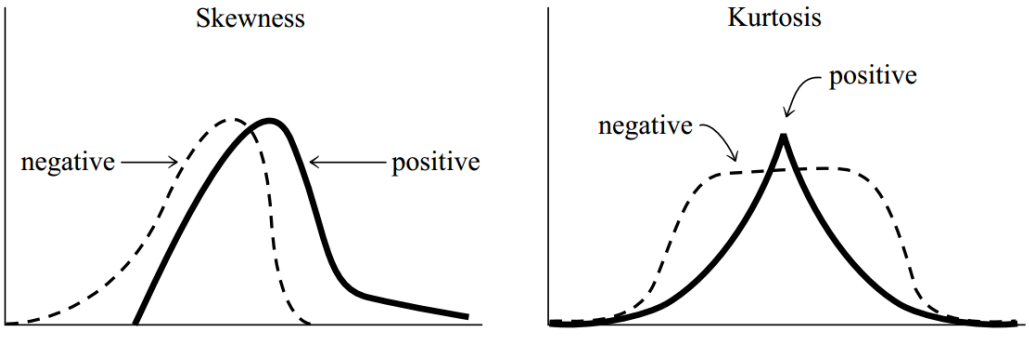

Figure 4.2: Skewness and Kurtosis role in the distribution shape.

while the mean and variance are dimensional quantities, the skewness and the kurtosis are conventionally defined in such a way as to make them adimensional.

4.1.4 Multidimensional random variables

Definition 4.13. *A (real)* ***random vector*** *of dimension n is a vector of $\mathbb{R}^n$ whose coordinates are real random variables. It is written $\boldsymbol{X} = (X_1, \ldots, X_n)$, where each variable X_i is a real random variable.*

Definition 4.14. *The distribution of a random vector is characterized by its* ***joint probability density function****. It is a generalization of the concept of probability density function. The joint pdf is defined such that:*

$$\mathbb{P}(\boldsymbol{X} \in [a_1, b_1] \times \ldots \times [a_n, b_n]) = \int_{a_1}^{b_1} \ldots \int_{a_n}^{b_n} f_{\boldsymbol{X}}(x_1, \ldots, x_n) dx_1 \ldots dx_n. \tag{4.20}$$

Definition 4.15. *Two random variables are said to be* ***independent*** *if the realization of one does not affect the probability distribution of the other. Two random variables X and Y, with probability densities f_X and f_Y, are independent if and only if the combined random vector (X, Y) has the following joint cumulative distribution function:*

$$f_{X,Y}(x, y) = f_X(x) f_Y(y). \tag{4.21}$$

Proposition 4.1. *Two random variables X and Y are independent if and only if for any functions g and h in $\mathbb{R}$:*

$$\mathrm{E}\left[g(X) \times h(Y)\right] = \mathrm{E}\left[g(X)\right] \mathrm{E}\left[h(Y)\right]. \tag{4.22}$$

Definition 4.16. *Given (X, Y) a couple of random variables such that their variances exist, the* ***covariance*** *of the couple (X, Y) is defined by:*

$$\mathrm{cov}(X, Y) = \mathrm{E}\left[(X - \mathrm{E}\left[X\right])(Y - \mathrm{E}\left[Y\right])\right] = \mathrm{E}\left[XY\right] - \mathrm{E}\left[X\right] \mathrm{E}\left[Y\right]. \tag{4.23}$$

It is a measure of how much they are changing together.

Definition 4.17. *From the covariance of two random variables X and Y, we define the Pearson's correlation coefficient by:*

$$\rho(X, Y) = \frac{\mathrm{cov}(X, Y)}{\sigma_X \sigma_Y}. \tag{4.24}$$

Proposition 4.2. *If X and Y are independent and if their variances exist, then:*

$$\mathrm{cov}(X, Y) = 0, \text{ and } \mathrm{var}\left(X + Y\right) = \mathrm{var}\left(X\right) + \mathrm{var}\left(Y\right). \tag{4.25}$$

The converse of this proposition is not true. Note that two random variables are said to be uncorrelated if their covariance is zero. Then, the properties are equivalent to say that if two variables are independent then they are uncorrelated but the inverse is not true. The properties of independence of random variables will be used in the further studies.

Definition 4.18. *We defined the* ***conditional density*** *of X given Y by:*

$$f_{X|Y}(x|y) = \frac{f_{X,Y}(x, y)}{f_Y(y)}. \tag{4.26}$$

Then we have

$$\mathbb{P}(a \leq X \leq b | Y = y) = \int_a^b f_{X,Y}(x|y) dx. \tag{4.27}$$

Definition 4.19. *We then defined the* ***conditional expectation*** *of X given $Y = y$ by:*

$$\mathrm{E}\left[X | Y = y\right] = \int_{-\infty}^{\infty} x f_{X|Y}(x|y) dx. \tag{4.28}$$

4.1.5 Examples of well-known random variables

4.1.5.1 The Normal Distribution

The Normal or Gaussian distribution is certainly the most common occurring continuous probability distribution. The normal distribution is depending on two parameters: the mean μ and the variance σ^2. A random variable X is said to follow a normal law of mean μ and variance σ^2, denoted by:

$$X \sim \mathcal{N}(\mu, \sigma^2), \tag{4.29}$$

if its support is $\mathbb{R}$ and its pdf is given by:

$$f(x; \mu, \sigma) = \frac{1}{\sigma\sqrt{2\pi}} e^{-\frac{(x-\mu)^2}{2\sigma^2}}. \tag{4.30}$$

Various normal distributions are shown in Figure 4.3.

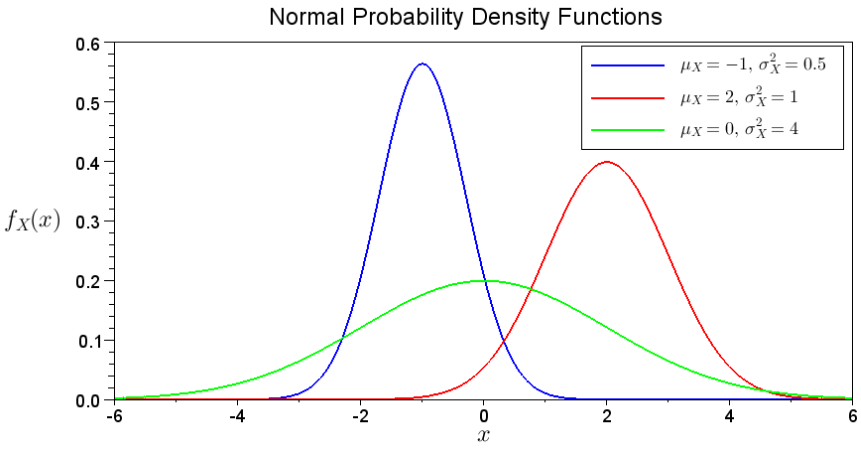

Figure 4.3: Probability density function for different normal distributions.

4.1.5.2 The Beta Distribution

The Beta distribution is a family of continuous probability distributions whose support is $[0, 1]$. A random variable X is said to follow a Beta law of parameters $\alpha > 0$ and $\beta > 0$ and denoted by $X \sim \text{Beta}(\alpha, \beta)$, if its pdf is:

$$f(x, \alpha, \beta) = \frac{\Gamma(\alpha + \beta)}{\Gamma(\alpha)\Gamma(\beta)} x^{1-\alpha}(1-x)^{\beta-1}, \tag{4.31}$$

where: $\Gamma : t \mapsto \int_0^\infty z^{t-1}e^{-t}dt$ is the well-known Gamma function. Various Beta distributions are shown in Figure 4.4.

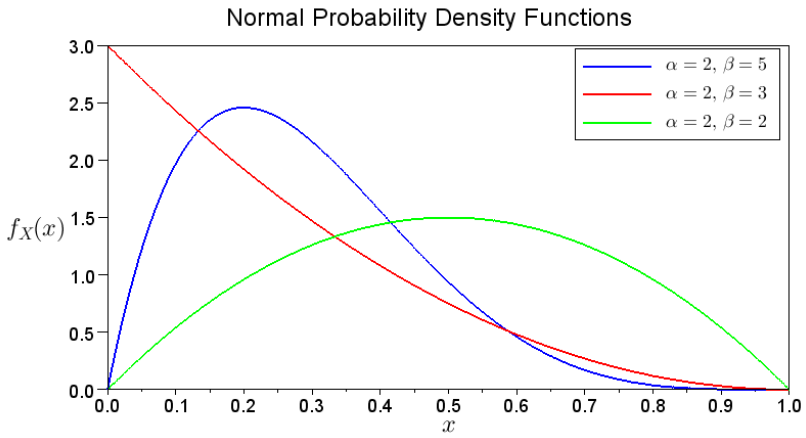

Figure 4.4: Probability density function for different beta distributions.

4.1.5.3 The Triangular Distribution

The Triangular distribution is a continuous probability distribution defined by three parameters: its lower limit a, its upper limit b and its mode c, where $a < b$ and $a \leq c \leq b$. A random variable is said to follow a triangular law of parameters a, b and c, if its pdf is:

$$f(x, a, b, c) = \begin{cases} 0 & \text{if } x < a, \\ \dfrac{2(x-a)}{(b-a)(c-a)} & \text{if } a \leq x < c, \\ \dfrac{2}{b-a} & \text{if } x = c, \\ \dfrac{2(b-x)}{(b-a)(b-c)} & \text{if } c < x \leq b, \\ 0 & \text{if } b < x. \end{cases} \tag{4.32}$$

An example of triangular distribution is given in Figure 4.5.

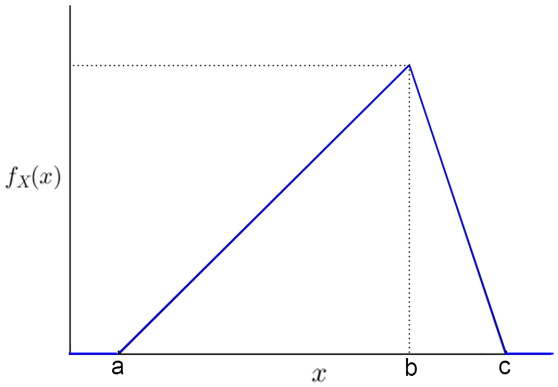

Figure 4.5: Probability density function of a triangular distribution.

4.1.5.4 The Uniform Distribution

The Uniform distribution is a continuous probability distribution defined by two parameters: its lower limit a and its upper limit b, where $a < b$. All intervals with the same length on the support $[a, b]$ are equiprobable. A random variable X is said to follow a uniform law of parameters a and b and denoted by $X \sim \mathrm{U}(a, b)$, if its pdf is:

$$f(x) = \begin{cases} \dfrac{1}{b-a} & \text{if } a \leq x \leq b, \\ 0 & \text{for } x < a \text{ if } x > b. \end{cases} \tag{4.33}$$

An example of uniform distribution is given in Figure 4.6.

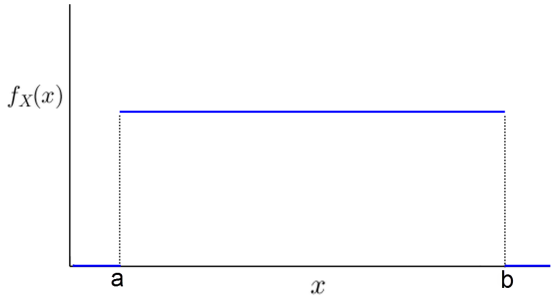

Figure 4.6: Probability density function of an uniform distribution.

4.2 Modeling uncertainty

This section addresses methods that aim at quantifying and characterizing uncertainties. Uncertainty quantification is defined as the science of quantitative characterization and reduction of uncertainties in applications. A part of the work from [22] dedicated to the uncertainty quantification is presented in Sections 4.2.1 and 4.2.2. Section 4.2.3 presents a new family of a generic probability distribution law. The objective is to propose a probability law that well models our uncertainties and that can be used by engineers not necessarily expert in mathematics. A part of this work has been done in collaboration with [22].

4.2.1 Uncertainty quantification

In engineering design, modeling a process consists in building models that compute some parameters as function of some others. Sometimes models are coming from the physics, when they are available and computationally affordable. If it is not the case, these models can come from experimentations. In our case, in order to build simple models for aircraft design process, these experimentations are databases of existing aircraft. We can find all the masses of the aircraft and of its different parts, its performances, its geometry, etc.

To illustrate this, assume that we want to model the mass of the fuselage without computing finite elements or any computationally expensive method. Then we use databases

of existing aircraft. Let

$$\begin{aligned} f : \mathbb{R}^n &\to \mathbb{R}, \\ \boldsymbol{x} &\mapsto f(\boldsymbol{x}), \end{aligned} \tag{4.34}$$

be the fuselage mass, i.e. f is the representation of a fuselage mass model. The selection of the input parameters $\boldsymbol{x}$ can be done by one or mixing the two following approaches:

- according to engineers know-how,
- with some statistics tools that allow to select the most influential parameters of a model.

For example, engineers may assume the fuselage mass can be expressed, with a "good" accuracy, as a function of the fuselage length, height and width. Once this is done, a function of this input vector is chosen. For instance, if $\boldsymbol{x} \in \mathbb{R}^2$, and if we want to approximate the model by a polynomial of the second degree, we state:

$$f(x_1, x_2) = ax_1^2 + bx_2^2 + cx_1x_2 + dx_1 + ex_2, \tag{4.35}$$

where a, b, c, d and e have to be tuned such that f is the best representation of the model. In our case we use some regression technique and the coefficients are tuned via a least square optimization using the available databases.

Finally we obtain an analytic model $f(\boldsymbol{x})$, based on an experimental model and with a "good" accuracy. The objective of uncertainty quantification is to estimate this accuracy. This can be done by modeling it with a probability distribution. Assuming that we have a sampling $(\tilde{y}_1, \ldots, \tilde{y}_N)$ from the databases, e.g. the values of the fuselage mass at the corresponding input vectors $(\boldsymbol{x}_1, \ldots, \boldsymbol{x}_N)$, we obtain the uncertainty sampling $(\xi_1, \ldots, \xi_N)$ such that:

$$\xi_i = f(\boldsymbol{x}_i) - \tilde{y}_i. \tag{4.36}$$

An illustration is given in Figure 4.7. The red line has the equation $y = x$. The blue points are the points $(f(\boldsymbol{x}_i), \tilde{y}_i)$. The closest these points are to the red line, the more accurate the analytical model is. The histogram of the model uncertainty is represented in the right graphic in Figure 4.7.

4.2.2 Uncertainty characterization

Once the uncertainty sampling ξ is obtained, as presented in the previous section, several choices can be made, depending on the way uncertainty is going to be used. This is the objective of the uncertainty characterization. The assumption is made that uncertainties can be well represented by a probability distribution law. Then either we can compute moments of the distribution, using formulas presented in the later Section 4.1.3, either we can draw a probability distribution matching the uncertainty histogram (see Figure 4.7), fitting a known distribution type. The uncertainty characterization depends on what the uncertainty will be used for.

As presented in Section 4.3, in the case where we want to propagate uncertainty, the choice of the propagation method is highly coupled to the input uncertainty accuracy. Information about the input uncertainty can be ranked from the low to the more accurate:

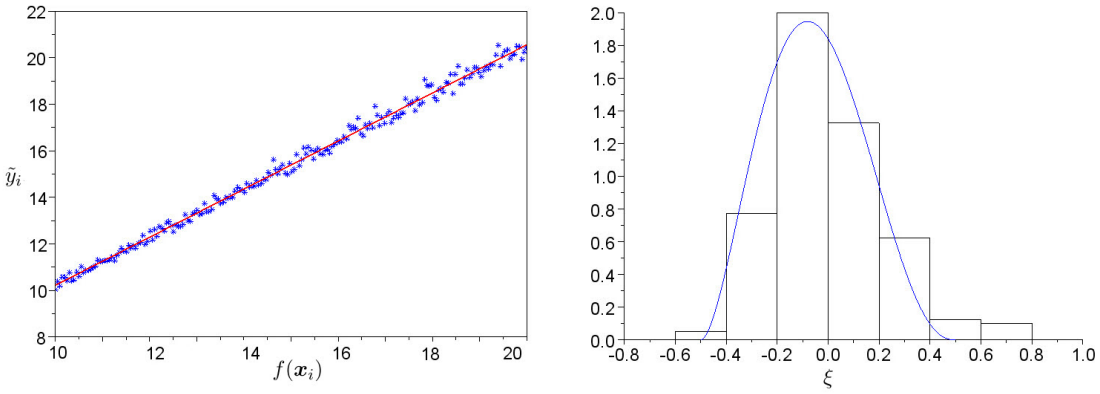

Figure 4.7: Uncertainty quantification: experimental sampling versus analytical model.

- the mean and the variance of the distribution;
- the mean, the variance and some properties of the distribution (for example unimodality, symmetry or finite support);
- the mean, the variance, and some of the higher moments of the distribution;
- the exact nature of the distribution and the corresponding parameters (for example Normal, Beta, Uniform distribution, or else).

When building the exact nature of a distribution from a data sampling, attention has to be payed to the underlying consequences. This attention is illustrated in Figure 7.6: considering a given sampling, we introduced two different sampling intervals and we observe that two different distributions can approximate the same sampling. It is also important to recall here that a probability distribution is uniquely defined by its infinite number of moments. Therefore the knowledge of the first four moments does not allow to compute an unique distribution, but only a family of distributions. In particular, fitting uncertainty by a given distribution family (e.g. Beta, Normal, etc), even well-adapted, implies underlying assumptions on the sampling: this can either overestimate or underestimate some probability measures associated to the distribution. This has to be manipulated carefully. However, it has the benefit of manipulating analytic expressions instead of sampling.

4.2.3 The Beta-Mystic distribution

In this section, we present a distribution that can mimic several most known probability distribution laws and that is used on later studies. The objective is to find a probability density function, easy to manipulate, that covers a wide range of distribution shapes and fulfills the following requirements:

- Compact support,
- Unimodal,
- Continuous.

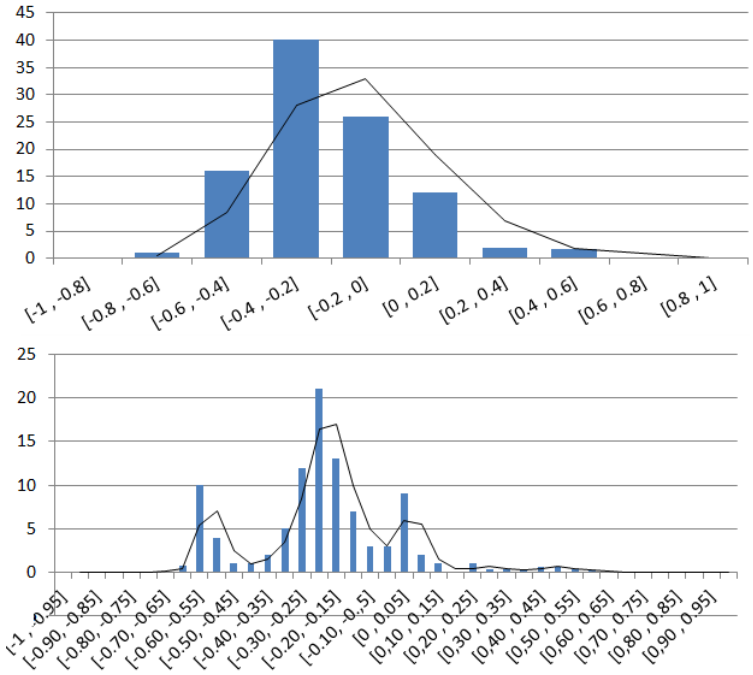

Figure 4.8: Example of approximations of the same sampling by two different distributions. The two graphs have just a different intervals length.

The Beta distribution meets all these requirements and so was retained in a first approach. However, its drawback was the lack of intuitiveness between the parameters α and β of the law and the behavior of the distribution shape. This is illustrated in Figure 4.9: the link between each parameter and the shape is not obvious. For a fixed parameter α or β, the variation of the other is changing at the same time the symmetry and the peakedness of the distribution. In our mind it was essential to improve the dissociation of the latter

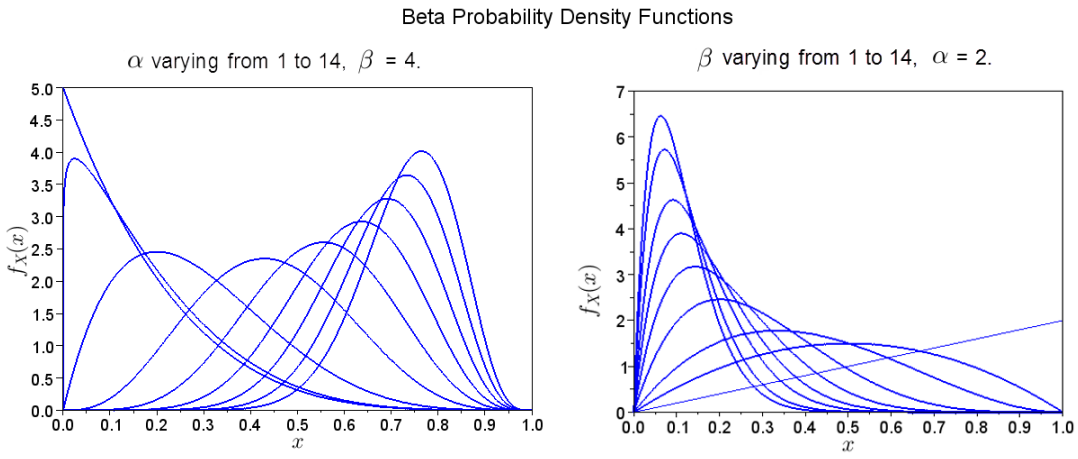

Figure 4.9: Examples of Beta distributions for different values of α and β.

two characteristics and to be able to simply control the shape of the distribution by tuning its parameters.

4.2.3.1 Definition of the Beta-Mystic distribution

Therefore, we introduce a new family, namely the *Beta-Mystic* distribution.

A random variable X is said to follow a Beta-Mystic distribution, denoted by $X \sim BetaMyst(a, b, Z, P)$, where $-1 \leq Z \leq 1$ and $0 \leq P$, if its pdf is:

$$f_X(x; a, b, Z, P) = \begin{cases} \dfrac{(b-x)^{q_1-1} \cdot (x-a)^{p_1-1}}{\beta\,(p_1, q_1) \cdot (b-a)^{p_1+q_1-1}} & \text{, if } a \leq x \leq b, \\ 0 & \text{, if } x < a \text{ or } b < x, \end{cases} \tag{4.37}$$

where:

$$\begin{aligned} & W = \max\Big(\varepsilon - 1, \min(Z, 1-\varepsilon)\Big), \\ & K = \frac{3.3 \times \max(\varepsilon, P)}{b-a}, \\ & M = \frac{1}{2} \times \left(a\,(1-W) + b\,(1+W)\right), \\ & p_1 = 1 + K \cdot (M-a)\,, \\ & q_1 = 1 + K \cdot (b-M)\,, \\ & \beta(p_1, q_1) = \frac{\Gamma(p_1)\Gamma(q_1)}{\Gamma(p_1+q_1)}, \\ & \Gamma \text{ is the Gamma function: } \Gamma(t) = \textstyle\int_0^\infty x^{t-1}e^{-x}dx, \\ & \varepsilon > 0. \end{aligned}$$

In practice, the parameter ε is chosen equal to the computer computation accuracy. Introducing such a ε avoids computational problems when the P and Z parameters reach their respective bounds. The introduction of this new Beta-based probability density law allows the following intuitive control of the distribution shape:

- a and b respectively represent the lower and upper bound of the support,
- Z controls the symmetry of the distribution, $Z \in [-1, 1]$,
- P controls the spreading.

The graphs from Figure 4.10 illustrate the evolution of the shape of the distribution law when P varies between 0 and 10 and Z equals to 0. It shows the wide range of distributions with different spreading that covers the law. The graphs from Figure 7.7 illustrate the evolution of the shapes for P varying between 0.5 and 4 and Z varying between -1 and 0. The behavior is symmetric when $0 < Z < 1$. Graphs from Figure 4.12 illustrate the ability of the law to mimic most known probability distributions (Normal, Uniform or Triangular).

Note that the normal law $\mathcal{N}(0, \sigma^2)$ can be approximated by $BetaMyst(-6\sigma, 6\sigma, 0, 10)$ and the Uniform $U(a, b)$ is equivalent to the $BetaMyst(a, b, 0, 0)$.

The Beta-Mystic distribution has already been used for some future project studies: the first experiments have shown that it can be a very powerful tool to replace current engineers know-how based margins and to manage models uncertainties.

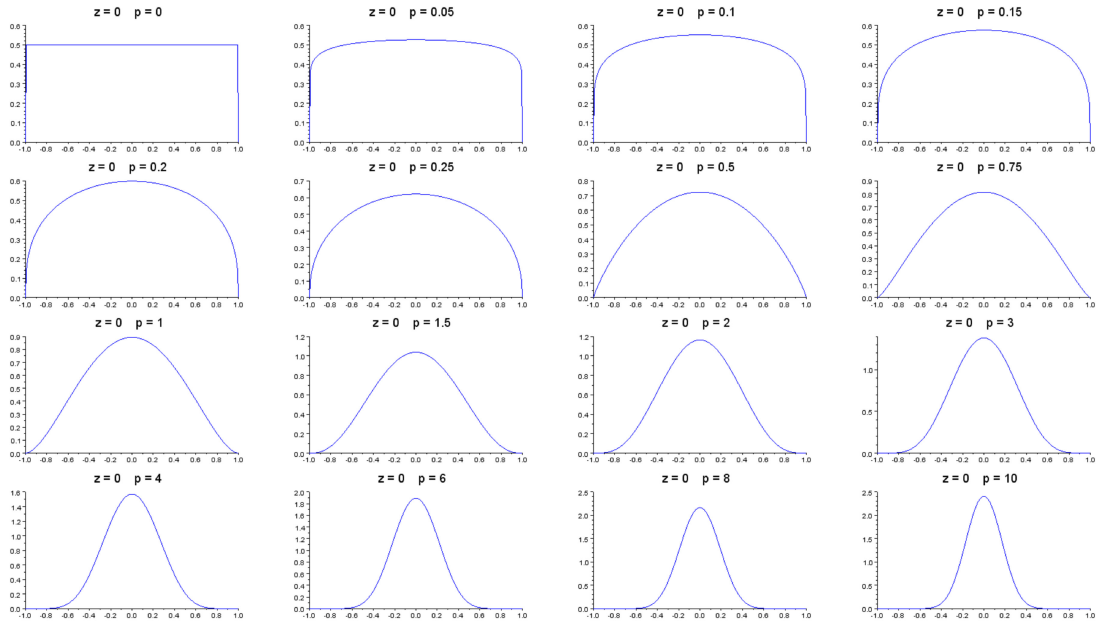

Figure 4.10: Evolution of the shape of the distribution law ($0 \leq P \leq 10$ and $Z = 0$).

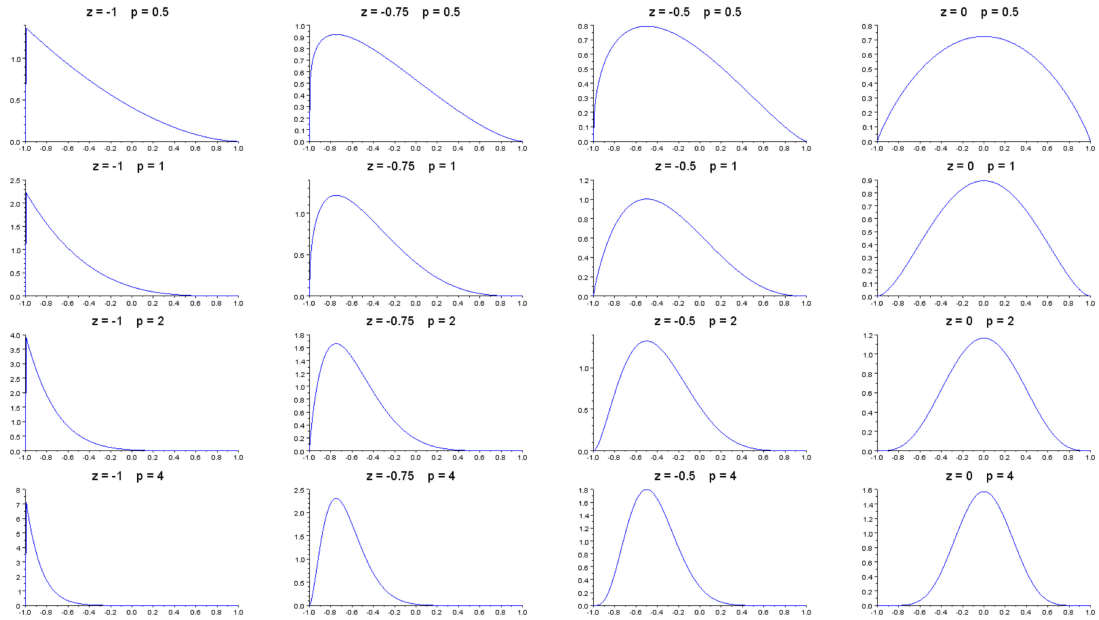

Figure 4.11: Evolution of the shape of the distribution law ($0.5 \leq P \leq 4$ and $-1 \leq Z \leq 0$).

4.2.3.2 Characterization of the Beta-Mystic law by its moments

The Beta-Mystic distribution is a four parameters probability distribution law. We here choose to compute its first four moments. The expression of the mean μ, the variance σ^2, the skewness γ and the kurtosis Γ of a Beta-Mystic distribution of parameters (a, b, Z, P)

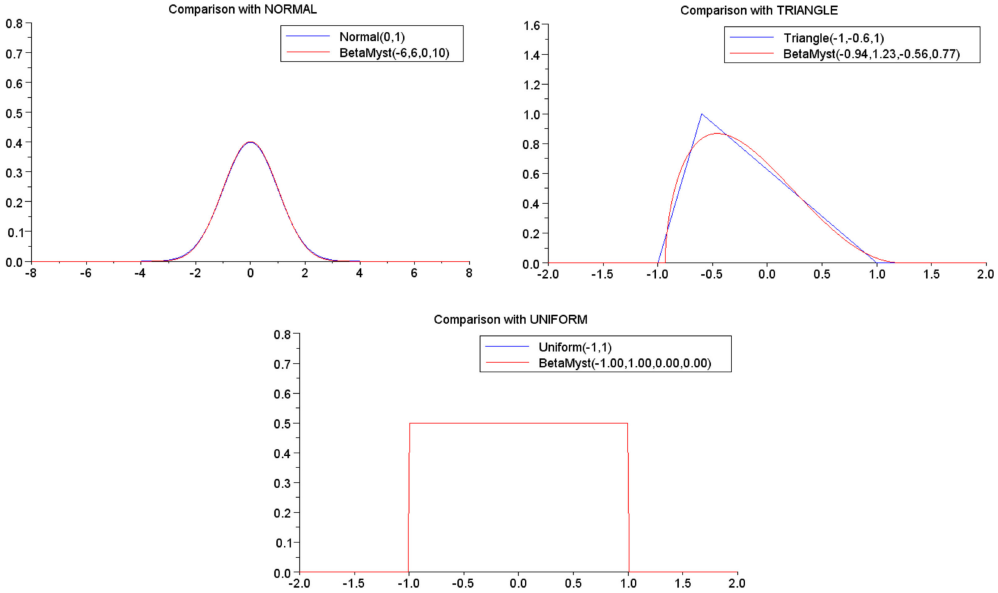

Figure 4.12: Illustration of the flexibility of the Beta-Mystic law.

are simple to obtain as shown by equations (4.38) to (4.41):

$$\mu = \frac{p_1 \cdot b + q_1 \cdot a}{p_1 + q_1}, \tag{4.38}$$

$$\sigma^2 = \frac{p_1 \cdot q_1 \cdot (b-a)^2}{(p_1 + q_1 + 1) \cdot (p_1 + q_1)^2}, \tag{4.39}$$

$$\gamma = \frac{2 \cdot (q_1 - p_1) \cdot \sqrt{p_1 + q_1 + 1}}{(p_1 + q_1 + 2) \cdot \sqrt{p_1 \cdot q_1}}, \tag{4.40}$$

$$\Gamma = 6 \cdot \frac{(p_1 + q_1 + 1) \cdot (q_1 - p_1)^2 - p_1 \cdot q_1 \cdot (p_1 + q_1 + 2)}{p_1 \cdot q_1 \cdot (p_1 + q_1 + 2) \cdot (p_1 + q_1 + 3)}, \tag{4.41}$$

where:

$$\tilde{Z} = \max\left(-1 + \varepsilon, \min\left(Z, 1 - \varepsilon\right)\right), \tag{4.42}$$

$$m = \frac{a(1 - \tilde{Z}) + b(1 + \tilde{Z})}{2}, \tag{4.43}$$

$$r = \frac{3.3 \times P}{b - a}, \tag{4.44}$$

$$p_1 = 1 + r(m - a), \tag{4.45}$$

$$q_1 = 1 + r(b - m). \tag{4.46}$$

Moreover, for the Beta-Mystic law, these expressions can be inversed in a certain domain of skewness and kurtosis, shown in Figure 4.13. We then obtain the parameters (a, b, Z, P) with respect to $(\mu, \sigma^2, \gamma, \Gamma)$:

$$a = \mu - p_1 \cdot fac, \tag{4.47}$$

$$b = \mu + q_1 \cdot fac, \tag{4.48}$$
$$Z = \frac{2 \cdot \mu + q_1 \cdot fac}{b - a}, \tag{4.49}$$
$$P = \frac{p_1 + q_1 - 2}{3.3}, \tag{4.50}$$

where:

$$\left| \begin{array}{rcl} sum & = & \dfrac{6 \cdot (\gamma^2 - \Gamma - 2)}{2 \cdot \Gamma - 3 \cdot \gamma^2}, \\ prod & = & \dfrac{6 \cdot (sum + 1) \cdot sum^2}{\Gamma \cdot (sum + 2) \cdot (sum + 3) + 30 \cdot sum + 36}, \\ det & = & sum^2 - 4 \cdot prod, \\ sign & = & \dfrac{\gamma}{|\gamma|}, \\ p_1 & = & \dfrac{sum - sign\sqrt{det}}{2}, \\ q_1 & = & \dfrac{sum + sign\sqrt{det}}{2}, \\ fac & = & \sqrt{\sigma^2 \cdot \dfrac{p_1 + q_1 + 1}{p_1 \cdot q_1}}. \end{array} \right. \tag{4.51}$$

4.2.3.3 Limitations of the Beta-Mystic

Some couples of kurtosis and skewness appear to have no antecedent in the domain of the parameters of the Beta-Mystic law, as represented in Figure 4.13. After some experimen-

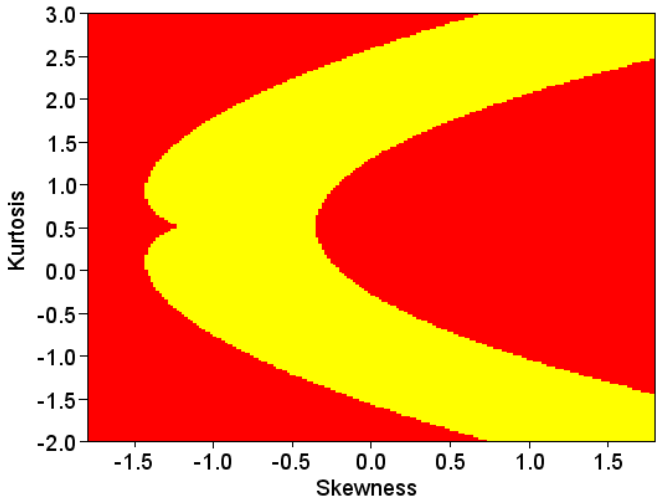

Figure 4.13: Couples of skewness and kurtosis from which a Beta-Mystic law cannot be computed (the red part).

tations and calculations, we notice that we can approximate some of the non-invertible couples by a Beta-Mystic law without to many loss of information. We propose to replace

the corresponding values in relations (4.51) by those given by relations (4.52) to (4.55). By doing so, we set a maximum value reachable by P and a maximum value of kurtosis that can be reached with the current skewness. Further analysis is required to better manage this limitation of the Beta-Mystic law. More details can be found in [22].

$$P_{max} = 99, \tag{4.52}$$

$$K_{limit} = \min\left(\Gamma, \frac{(9.9 \cdot P_{max} + 12) \cdot \gamma^2 - 12}{6.6 \cdot P_{max} + 10}\right), \tag{4.53}$$

$$sum = \frac{6 \cdot (\gamma^2 - K_{limit} - 2)}{2 \cdot K_{limit} - 3 \cdot \gamma^2}, \tag{4.54}$$

$$prod = \frac{6 \cdot (sum + 1) \cdot sum^2}{K_{limit} \cdot (sum + 2) \cdot (sum + 3) + 30 \cdot sum + 36}, \tag{4.55}$$

Pearson distributions presented in [10, 80, 7, 130], are used in a similar way to represent four moments distributions by a Pearson type distribution under some assumptions. The same problem appears with non-reversible couples of skewness and kurtosis.

The quantification and characterization of uncertainties, whether with Beta-Mystic law, whether with moments and some properties of the distributions, can now be realized.

4.3 Review of uncertainty propagation methods

In design engineering, the challenge is to obtain the "best" design according to well selected input design variables and matching a given number of requirements and performances.

The deterministic approach leads to a design with no clue about its reliability, about its feasibility and about the accuracy of its performances. Once uncertainties have been characterized, the objective is to take them into account when assessing the performances. In practical that means that these performances become in their turn uncertain. The finality of uncertainty propagation is to assess accurately and rigorously these output uncertainties.

Design process generally relies on one or several optimizations in order to minimize, or maximize, a criterion. Therefore, uncertainty propagation plays an important role in the resolution of optimization problems under uncertainty.

The community of simulation-based design is increasingly interested in this field [118, 67, 80, 177, 19]. When solving a design optimization problem under uncertainty, the formulation of the objective and constraint functions, is crucial: they are generally functions of the output uncertainties as presented in Chapter 5, Section 5.1. Uncertainty propagation methods are a key tool that provides these output uncertainties. The choice and the accuracy of the propagation method depend on three main entities: the information on input uncertainty, the process design functions properties (for instance linear process, or in the worst case, black-box process) and any additional information on output uncertainty.

Input uncertainty information, as already mentioned in Section 4.2, can be of the two following kinds:

- Error distributions are entirely available,
- Only moments of input distributions are available.

It is important to note here that as reasonably expected, the accuracy of the output strictly depends on the accuracy of the input. Figure 4.14 proposes a representation of the

available output uncertainty information as a function of the available information on input uncertainty. Abscissa axis represents the input information, from the smallest (i.e. only the mean of the uncertainty is known), to the most complete (i.e. the entire distribution). Ordinate axis is likewise but for the output information.

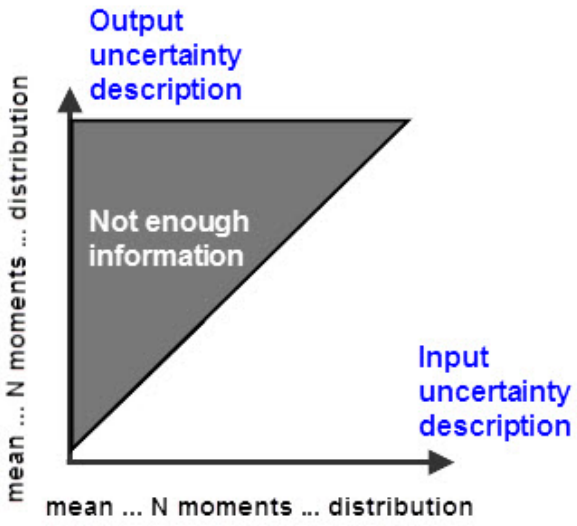

Figure 4.14: Available uncertain output versus available uncertain input [127].

For instance, if only the mean of the uncertain input is known, it would not really have a sense to try to compute the complete distribution of an uncertain output. To obtain it, more information about the input uncertainty are needed. Ideally, when input distribution uncertainties are known, some methods allow to compute the output uncertainty distribution. They will be presented in next Sections.

Moreover, since the beginning of design under uncertainty, engineers and operational researchers have often worked with objectives and constraints functions represented by a weighted sum of mean and variance [80, 67]. We can also find multi-objective formulations in which the objectives are the mean and the variance.

It has been known for a while that such a framework may be inadequate when dealing with generic (e.g. asymmetric or multi-modal) output distributions [152, 154]. One of the possible options is to increase the number of output moments to be considered, e.g. by including skewness and kurtosis [126, 103]. For example Padulo and Liou [129] have shown that four moments can be readily included in an optimization approach by a straightforward numerical procedure, named Bivariate Reduction Quadrature and described in Section 4.3.4.6.

An open question is to determine the "best" way to obtain numerically such higher statistics, when the considered function is not known analytically, which is generally the case in engineering design. We try to answer this question by comparing several uncertainty propagation methods, and ranking them, when it is possible, in terms of accuracy, computational cost, required input information and easiness of implementation.

In the first section, we recall the definition of the problem. Then Monte-Carlo propagation methods are presented. Taylor-based method of moments propagation, stochastic quadrature techniques and multidimensional extension of the Gauss-like quadrature, in-

cluding full tensorial and reduced quadrature schemes [146, 182, 129] are described in the next sections. The last presented method brings some proposal for constructing adaptive non-intrusive methods, in particular by using various of the quadrature techniques. We finally apply the selected methods to different numerical test cases. This allows to highlight benefits and drawbacks of the different methods: for each method, we bring out the required input information as function as the computable output information.

4.3.1 Definition of the problem

Formally we consider a process that encompass models. As shown in Figure 4.15, this process admits deterministic inputs $\boldsymbol{x}$ and uncertainties $\boldsymbol{\Xi}$ seen as random variables. The latter also can be seen as inputs, once they have been characterized. An output function f of this process is a function of $\boldsymbol{x}$ and $\boldsymbol{\Xi}$, and for any given point $\boldsymbol{x} \in \mathbb{R}^m$, the quantity $f(\boldsymbol{x}, \boldsymbol{\xi})$ is uncertain. The characteristics of this uncertainty highly depend on the characteristics

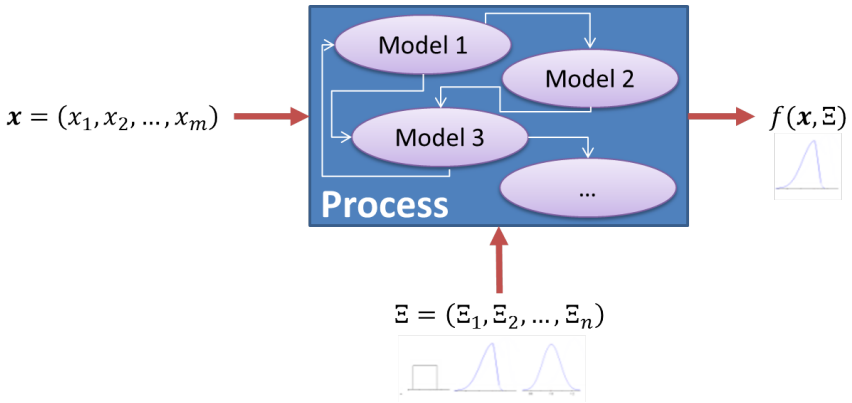

Figure 4.15: Process variables and uncertainties modeling.

of the input uncertainty $\boldsymbol{\Xi}$. For the sake of simplicity, assume that the certain input $\boldsymbol{x}$ is fixed. Let:

$$\begin{aligned} F : \mathbb{R}^n &\to \mathbb{R}, \\ \boldsymbol{\xi} &\mapsto F(\boldsymbol{\xi}) = f(\boldsymbol{x}, \boldsymbol{\xi}). \end{aligned} \tag{4.56}$$

The variable $\boldsymbol{\xi}$ will denote the realizations of the random variable $\boldsymbol{\Xi}$.

The following methods aim at finding the characteristics or the representation of the output uncertainty $F(\boldsymbol{\Xi})$. The next section is dedicated to the most well known Monte-Carlo method applied to uncertainty propagation and moments estimation.

4.3.2 Monte-Carlo Methods

Monte-Carlo methods cover a wide class of computational algorithms that rely on running a high number of function evaluations for a random sampling input. Typically, processes or functions are simulated for a given sample of random uncertain inputs in order to obtain a sample of the output. More details about such methods can be found among many others in [108, 70, 162].

Monte-Carlo sampling is a reference in terms of propagation method: it can be used in order to precisely obtain the output distribution in the case where input uncertainty

distribution is available. Given an input sampling vector $(\boldsymbol{\xi}_i)_{i=1,\dots,N}$, relations (4.57) to (4.60) from [46] give an estimation of the first four standardized moments $(\mu_F, \sigma_F^2, \gamma_F, \Gamma_F)$ of the random variable $F(\boldsymbol{\Xi})$.

$$\hat{\mu}_F = \frac{1}{N}\sum_{i=1}^{N} F(\boldsymbol{\xi}_i), \tag{4.57}$$

$$\hat{\sigma}_F^2 = \frac{1}{N}\sum_{i=1}^{N} (F(\boldsymbol{\xi}_i) - \hat{\mu}_F)^2, \tag{4.58}$$

$$\hat{\gamma}_F = \frac{N}{(N-1)(N-2)}\sum_{i=1}^{N} \left(\frac{F(\boldsymbol{\xi}_i) - \hat{\mu}_F}{\hat{\sigma}_F}\right)^3, \tag{4.59}$$

$$\hat{\Gamma}_F = \frac{N(N+1)}{(N-1)(N-2)(N-3)} \cdot \sum_{i=1}^{N} \left(\frac{F(\boldsymbol{\xi}_i) - \hat{\mu}_F}{\hat{\sigma}_F}\right)^4 - 3\frac{(N-1)^2}{(N-2)(N-3)}. \tag{4.60}$$

These formulas will be used as a baseline to compare the following moment propagation methods. Observe that we have to know exactly the input distribution in order to generate a Monte-Carlo sampling.

The Monte-Carlo estimation error is roughly proportional to $1/\sqrt{N}$ for a large N. Monte-Carlo can be considered as the simplest method to handle, but in general any other applicable method is better than Monte-Carlo. However, Monte Carlo remains very practical and powerful when the dimension of the inputs becomes too large: it may be as accurate as any quadrature technique using too many points along each dimension coordinate.

To illustrate the convergence of the estimation error of moments by the Monte-Carlo method, we test it on a simple numerical example:

$$F : \xi \mapsto cos\left(\frac{\pi}{4}\xi\right), \text{ with } \Xi \sim Beta(2,5). \tag{4.61}$$

The Monte-Carlo estimates are shown on Figure 4.16. We can see how the ranges of the mean, the variance, the skewness and the kurtosis estimates are decreasing when the number of sampling is increasing. The variance of the estimator of the kth-order moment is estimated in [106]: it depends on the moment of k^2th order. For all variance estimators, the lead term is in $O(1/N)$.

In the case where the input distribution is not entirely known, Monte-Carlo method becomes unusable. How to generate a sample of an unknown distribution? This issue can be partially solved by using a family of distributions like Pearson, Beta or even Beta-Mystic distributions as follows.

As presented in section 4.2.3.2, it is possible to approximate an uncertain sampling by a Beta-Mystic distribution using the first four moments of the distribution, thanks to relations (4.57) to (4.60). However this approach raises the following two limitations:

- The first one is the impact of the Monte-Carlo moments estimation error on the distribution approximation. The Monte-Carlo sampling size N will affect the moments approximation and consequently the distribution approximation. When the evaluation of an individual is computationally expensive, the cost of a more accurate Monte-Carlo approximation is not affordable.

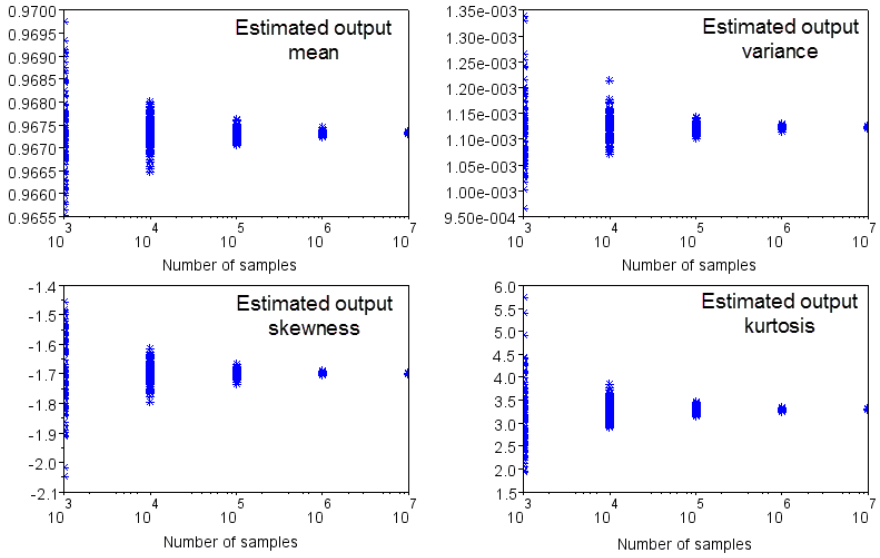

Figure 4.16: Convergence of mean, variance, skewness and kurtosis estimate for random sampling using Monte-Carlo method.

- The second one is that the method approximates a finite number of moments of a distribution by a given distribution. A finite number of moments only defines a family of distribution and not an unique one. In the case where the uncertainties are used to compute risk measures, for instance in robust design optimization, this can lead to underestimate the risk measure and then to decrease the level of reliability of the solution. It can also overestimate the measure and then lead to no solutions. This approximation has to be done conscientiously, depending on the use of the output distributions.

In all cases, when the objective is for instance to compute probability measures (e.g. a quantile), the impact of these approximations on the measure should be carefully considered. To my best knowledge no specific rule exists to quantify the impact of the latter approximations.

As in practical other methods have some benefits comparing to Monte-Carlo methods, in term of accuracy, computational cost and flexibility, following sections are dedicated to a non exhaustive review of alternative propagation methods.

4.3.3 Taylor Expansion methods

Let us consider the function F defined in Section 4.3.1 and denote $\mu_{\boldsymbol{\xi}} = (\mu_1, \ldots, \mu_n)$ the input mean vector of $\boldsymbol{\Xi} = (\Xi_1, \ldots, \Xi_n)$. We assume that $F \in C^5(\mathbb{R}^n, \mathbb{R})$ admits a Taylor expansion in some neighborhood of $\mu_{\boldsymbol{\xi}}$ and that F, F^2, F^3 and F^4 are integrable on this neighborhood. Then as shown in [128, 125], F can be approximated by its Taylor series expansion at the point $\boldsymbol{\mu_\xi} = (\mu_1, \ldots, \mu_n)$, truncated to the fifth order:

$$F(\boldsymbol{\xi}) = F\left(\boldsymbol{\mu_\xi}\right) + \sum_{i=1}^{n} \left(\frac{\partial F}{\partial \xi_i}\left(\boldsymbol{\mu_\xi}\right) \right) \Delta\xi_i + \frac{1}{2} \sum_{i=1}^{n} \sum_{j=1}^{n} \left(\frac{\partial^2 F}{\partial \xi_i \partial \xi_j}\left(\boldsymbol{\mu_\xi}\right) \right) \Delta\xi_i \Delta\xi_j \tag{4.62}$$

$$
\begin{aligned}
&+ \frac{1}{6}\sum_{i=1}^{n}\sum_{j=1}^{n}\sum_{k=1}^{n}\left(\frac{\partial^3 F}{\partial\xi_i\partial\xi_j\partial\xi_k}\left(\boldsymbol{\mu_\xi}\right)\right)\Delta\xi_i\Delta\xi_j\Delta\xi_k \\
&+ \frac{1}{24}\sum_{i=1}^{n}\sum_{j=1}^{n}\sum_{k=1}^{n}\sum_{l=1}^{n}\left(\frac{\partial^4 F}{\partial\xi_i\partial\xi_j\partial\xi_k\partial\xi_l}\left(\boldsymbol{\mu_\xi}\right)\right)\Delta\xi_i\Delta\xi_j\Delta\xi_k\Delta\xi_l \\
&+ \frac{1}{120}\sum_{i=1}^{n}\sum_{j=1}^{n}\sum_{k=1}^{n}\sum_{l=1}^{n}\left(\frac{\partial^5 F}{\partial\xi_i\partial\xi_j\partial\xi_k\partial\xi_l\partial\xi_m}\left(\boldsymbol{\mu_\xi}\right)\right)\Delta\xi_i\Delta\xi_j\Delta\xi_k\Delta\xi_l\Delta\xi_m \\
&+ o\left(\|\left(\Delta\xi_1,...,\Delta\xi_n\right)\|^5\right),
\end{aligned}
$$

where $\Delta\xi_i = \xi_i - \mu_i$, $\forall i = 1,...,n$. Now we assume that the first four moments of each uncertain input variable ξ_i, $i = 1,\ldots,n$ of F are known. Let us denote μ_i, σ_i^2, γ_i and Γ_i the respective mean, variance, skewness and kurtosis of ξ_i. Let us introduce the first four moments of F, denoted by μ_F, σ_F^2, γ_F and Γ_F, and defined by:

$$\mu_F = E\left[F(\boldsymbol{\Xi})\right], \tag{4.63}$$

$$\sigma_F^2 = E\left[\left(F(\boldsymbol{\Xi}) - \mu_F\right)^2\right], \tag{4.64}$$

$$\gamma_F = \frac{E\left[\left(F(\boldsymbol{\Xi}) - \mu_F\right)^3\right]}{\sigma_F^3} = \frac{\mu_{3,F}}{\sigma_F^3}, \tag{4.65}$$

$$\Gamma_F = \frac{E\left[\left(F(\boldsymbol{\Xi}) - \mu_F\right)^4\right]}{\sigma_F^4} - 3 = \frac{\mu_{4,F}}{\sigma_F^4} - 3. \tag{4.66}$$

Using the Taylor expansion (4.62) and the definitions of the moments (4.63) to (4.65), Evans [62] gives relations (4.67) to (4.70) to compute the mean μ_F, the variance σ_F^2, the centered 3rd-order moment $\mu_{3,F}$ and the centered 4th-order moment $\mu_{4,F}$, in the case of independent random input variables. Skewness γ_F and kurtosis Γ_F can then be determined thanks to relations (4.63) to (4.66). Note that in the case of dependent random input variables, it is possible to refer to the independent case by the use of techniques such as spectral decomposition or Cholesky decomposition [91, 124]. In the formulas, the derivatives $\partial^k F/\partial\xi^k$ are computed at point $\boldsymbol{\mu_\xi}$, which is omitted to lighten the notations.

$$
\begin{aligned}
\mu_F = &\overbrace{F\left(\boldsymbol{\mu_\xi}\right)}^{M_1} + \overbrace{\frac{1}{2}\sum_{i=1}^{n}\left(\frac{\partial^2 F}{\partial\xi_i^2}\right)\sigma_i^2}^{M_2} + \overbrace{\frac{1}{6}\sum_{i=1}^{n}\left(\frac{\partial^3 F}{\partial\xi_i^3}\right)\gamma_i\sigma_i^3}^{M_3} + \overbrace{\frac{1}{24}\sum_{i=1}^{n}\left(\frac{\partial^4 F}{\partial\xi_i^4}\right)\Gamma_i\sigma_i^4}^{M_4} \\
&+ \overbrace{\frac{1}{8}\sum_{i=1}^{n}\sum_{\substack{j=1\\ j\neq i}}^{n}\left(\frac{\partial^4 F}{\partial\xi_i^2\partial\xi_j^2}\right)\sigma_i^2\sigma_j^2}^{M_5} + \overbrace{\frac{1}{120}\sum_{i=1}^{n}\left(\frac{\partial^4 F}{\partial\xi_i^4}\right)G_i\sigma_i^5}^{M_6} \\
&+ \overbrace{\frac{1}{12}\sum_{i=1}^{n}\sum_{\substack{j=1\\ j\neq i}}^{n}\left(\frac{\partial^5 F}{\partial\xi_i^3\partial\xi_j^2}\right)\gamma_i\sigma_i^3\sigma_j^2}^{M_7} + o\left(\|\left(\sigma_1,...,\sigma_n\right)\|^5\right),
\end{aligned} \tag{4.67}
$$

$$
\sigma_F^2 = \overbrace{\sum_{i=1}^{n}\left(\frac{\partial F}{\partial\xi_i}\right)^2\sigma_i^2}^{V_1} + \overbrace{\sum_{i=1}^{n}\left(\frac{\partial^2 F}{\partial\xi_i^2}\right)\left(\frac{\partial F}{\partial\xi_i}\right)\gamma_i\sigma_i^3}^{V_2} + \overbrace{\frac{1}{3}\sum_{i=1}^{n}\left(\frac{\partial^3 F}{\partial\xi_i^3}\right)\left(\frac{\partial F}{\partial\xi_i}\right)\Gamma_i\sigma_i^4}^{V_3} \tag{4.68}
$$

$$
\begin{aligned}
&+\overbrace{\frac{1}{2}\sum_{i=1}^{n}\sum_{\substack{j=1\\ j\neq i}}^{n}\left(\frac{\partial^3 F}{\partial\xi_i^2\partial\xi_j}\frac{\partial F}{\partial\xi_j}+\left(\frac{\partial^2 F}{\partial\xi_i\partial\xi_j}\right)^2+\frac{\partial^3 F}{\partial\xi_j^2\partial\xi_i}\frac{\partial F}{\partial\xi_i}\right)\sigma_i^2\sigma_j^2}^{V_4}\\
&+\overbrace{\frac{1}{4}\sum_{i=1}^{n}\left(\frac{\partial^2 F}{\partial\xi_i^2}\right)^2(\Gamma_i-1)\,\sigma_i^4}^{V_5}+\overbrace{\frac{1}{12}\sum_{i=1}^{n}\left(\frac{\partial^4 F}{\partial\xi_i^4}\right)\left(\frac{\partial F}{\partial\xi_i}\right)G_i\sigma_i^5}^{V_6}\\
&+\overbrace{\sum_{i=1}^{n}\sum_{\substack{j=1\\ j\neq i}}^{n}\left(\frac{1}{2}\frac{\partial F}{\partial\xi_i}\frac{\partial^4 F}{\partial\xi_i^2\partial\xi_j^2}+\frac{1}{2}\frac{\partial^2 F}{\partial\xi_i^2}\frac{\partial^3 F}{\partial\xi_i\partial\xi_j^2}+\frac{\partial^2 F}{\partial\xi_i\partial\xi_j}\frac{\partial^3 F}{\partial\xi_i^2\partial\xi_j}+\frac{1}{3}\frac{\partial^4 F}{\partial\xi_i^3\partial\xi_j}\frac{\partial F}{\partial\xi_j}\right)\gamma_i\sigma_i^3\sigma_j^2}^{V_7}\\
&+\overbrace{\frac{1}{6}\sum_{i=1}^{n}\left(\frac{\partial^2 F}{\partial\xi_i^2}\right)\left(\frac{\partial^3 F}{\partial\xi_i^3}\right)(G_i-\gamma_i)\,\sigma_i^5}^{V_8}+o\left(\|\,(\sigma_1,...,\sigma_n)\,\|^5\right),
\end{aligned}
$$

$$
\begin{aligned}
\mu_{3,F}=&\overbrace{\sum_{i=1}^{n}\left(\frac{\partial F}{\partial\xi_i}\right)^3\gamma_i\sigma_i^3}^{S_1}+\overbrace{\frac{3}{2}\sum_{i=1}^{n}\left(\frac{\partial^2 F}{\partial\xi_i^2}\right)\left(\frac{\partial F}{\partial\xi_i}\right)^2(\Gamma_i-1)\,\sigma_i^4}^{S_2}\\
&+3\overbrace{\sum_{i=1}^{n}\sum_{\substack{j=1\\ j\neq i}}^{n}\left(\frac{\partial F}{\partial\xi_i}\right)\left(\frac{\partial F}{\partial\xi_j}\right)\left(\frac{\partial^2 F}{\partial\xi_i\partial\xi_j}\right)\sigma_i^2\sigma_j^2}^{S_3}+\overbrace{\frac{1}{2}\sum_{i=1}^{n}\left(\frac{\partial F}{\partial\xi_i}\right)^2\left(\frac{\partial^3 F}{\partial\xi_i^3}\right)(G_i-\gamma_i)\,\sigma_i^5}^{S_4}\\
&+\overbrace{3\sum_{i=1}^{n}\sum_{\substack{j=1\\ j>i}}^{n}\left(\frac{1}{2}\left(\frac{\partial F}{\partial\xi_i}\right)^2\frac{\partial^3 F}{\partial\xi_i\partial\xi_j^2}+\frac{\partial F}{\partial\xi_i}\left(\frac{\partial^2 F}{\partial\xi_i\partial\xi_j}\right)^2+\frac{\partial^2 F}{\partial\xi_i^2}\frac{\partial^2 F}{\partial\xi_i\partial\xi_j}\frac{\partial F}{\partial\xi_j}+\frac{\partial^3 F}{\partial\xi_i^2\partial\xi_j}\frac{\partial F}{\partial\xi_j}\frac{\partial F}{\partial\xi_i}\right)\gamma_i\sigma_i^3\sigma_j^2}^{S_5}\\
&+\overbrace{\frac{3}{4}\sum_{i=1}^{n}\left(\frac{\partial F}{\partial\xi_i}\right)\left(\frac{\partial^2 F}{\partial\xi_i^2}\right)^2(G_i-2\gamma_i)\,\sigma_i^5}^{S_6}+o\left(\|\,(\sigma_1,...,\sigma_n)\,\|^5\right),
\end{aligned}
\tag{4.69}
$$

$$
\begin{aligned}
\mu_{4,F}=&\overbrace{\sum_{i=1}^{n}\left(\frac{\partial F}{\partial\xi_i}\right)^4(\Gamma_i-3)\,\sigma_i^4}^{K_1}+\overbrace{2\sum_{i=1}^{n}\left(\frac{\partial^3 F}{\partial\xi_i^3}\right)\left(\frac{\partial^2 F}{\partial\xi_i^2}\right)(G_i-4\gamma_i)\,\sigma_i^5}^{K_2}\\
&+\overbrace{12\sum_{i=1}^{n}\sum_{\substack{j=1\\ j\neq i}}^{n}\left(\frac{\partial F}{\partial\xi_i}\right)^2\left(\frac{\partial F}{\partial\xi_j}\right)\left(\frac{\partial^2 F}{\partial\xi_i\partial\xi_j}\right)\gamma_i\sigma_i^3\sigma_j^2}^{K_3}+o\left(\|\,(\sigma_1,...,\sigma_n)\,\|^5\right)+3\sigma_F^4.
\end{aligned}
\tag{4.70}
$$

We observe in these equations the existence of the term G_i, which denotes the 5th-order moment of ξ_i. This illustrates the need for information about the uncertain input variables

in order to be able to compute accurate approximation of moments of F. It also shows the limit of the Taylor expansion method: a more accurate approximation of higher order moments of F does not only require the higher order derivative of F but also the higher order moments of ξ_i. Moreover, to my best knowledge, moments of order 5 are not used in practice. Hence a first truncation of the equations can be done by keeping only the terms for which the exponent k of σ_i^k is strictly lower than the one of the first term where G_i appears.

Since in practice the derivatives of f can be expensive to compute, we focus on first order and second order methods, which only require the calculation of the gradient and/or the Hessian of the function F. Assuming that the first four moments $(\mu_i, \sigma_i^2, \gamma_i, \Gamma_i)$ of input variables are known, we then have:

- First-Order Moments method, applied to aircraft design in [141], for which we only need: $F \in C^1(\mathbb{R}^n, \mathbb{R})$. Based on relations (4.67) to (4.68) and on the first order truncation, we obtain the following estimation error ε, considering a generic distribution:

$$\begin{aligned}
\varepsilon_{\mu_F} &= o(\sigma_\xi), \\
\varepsilon_{\sigma_F^2} &= o(\sigma_\xi^2), \\
\varepsilon_{\mu_{F,3}} &= o(\sigma_\xi^3), \\
\varepsilon_{\mu_{F,4}} &= o(\sigma_\xi^4).
\end{aligned}$$

- The Second-Order Moments method, for which we only need $F \in C^2(\mathbb{R}^n, \mathbb{R})$. Considering a generic distribution, the error is the following one:

$$\begin{aligned}
\varepsilon_{\mu_F} &= o(\sigma_\xi^2), \\
\varepsilon_{\sigma_F^2} &= o(\sigma_\xi^3), \\
\varepsilon_{\mu_{F,3}} &= o(\sigma_\xi^4), \\
\varepsilon_{\mu_{F,4}} &= o(\sigma_\xi^4).
\end{aligned}$$

The main advantage of these techniques is the computational efficiency when gradient and Hessian are available. Limitations appear with the terms of higher order, or with the terms of input moments of order 5.

Another approach to compute F moments is to use directly the moment definitions by integrals, from relations (4.16) to (4.19).

4.3.4 Quadrature Propagation Methods

This section presents some of the main used techniques to compute higher order moments by integrative quadrature rules. Quadrature numerical integration methods aim at computing an approximation of the integral of a function over a space domain. These methods can be used to compute the first four moments of F by using the following definitions:

$$\mu_F = E\left[F(\boldsymbol{\Xi})\right] = \int_{\mathbb{R}^n} F(\boldsymbol{\xi}) f_{\boldsymbol{\Xi}}(\boldsymbol{\xi}) d\boldsymbol{\xi}, \tag{4.71}$$

$$\sigma_F^2 = E\left[\left(F(\boldsymbol{\Xi}) - \mu_F\right)^2\right] = \int_{\mathbb{R}^n} \left(F(\boldsymbol{\xi}) - \mu_F\right)^2 f_{\boldsymbol{\Xi}}(\boldsymbol{\xi}) d\boldsymbol{\xi}, \tag{4.72}$$

$$\gamma_F = \frac{E\left[(F(\boldsymbol{\Xi}) - \mu_F)^3\right]}{\sigma_F^3} = \frac{1}{\sigma_F^3} \int_{\mathbb{R}^n} (F(\boldsymbol{\xi}) - \mu_F)^3 f_{\boldsymbol{\Xi}}(\boldsymbol{\xi}) d\boldsymbol{\xi}, \tag{4.73}$$

$$\Gamma_F = \frac{E\left[(F(\boldsymbol{\Xi}) - \mu_F)^4\right]}{\sigma_F^4} - 3 = \frac{1}{\sigma_F^4} \int_{\mathbb{R}^n} (F(\boldsymbol{\xi}) - \mu_F)^4 f_{\boldsymbol{\Xi}}(\boldsymbol{\xi}) d\boldsymbol{\xi} - 3. \tag{4.74}$$

The next section recalls principle of these methods. The second and third sections are dedicated to the basic quadrature rules in one and higher dimensions. The fourth section is dedicated to sparse grid quadrature methods that were developed to improve the computational efficiency. The last two sections present reduced-order quadrature method, that have the advantage to be easy to implement. They have been provided by the generalized dimension-reduction methods from [182]. The method involves an additive decomposition of an N-dimensional function F into at most S-dimensional functions, where $S \ll N$. Among these methods, a Univariate Reduced Quadrature (URQ) from [146] provides good results in [128, 125], with an interesting balance between cost and accuracy.

4.3.4.1 General principle

Let us denote $\Omega \subset \mathbb{R}^n$ the integration domain and g the function to be integrated, with $g \in L^1(\mathbb{R}^n)$. A quadrature rule consists in building an approximation of the integral of g over Ω. This approximation is a weighted sum of the function values at specified points within the integration domain:

$$\int_\Omega g(\boldsymbol{x}) d\boldsymbol{x} \approx \sum_{i=1}^{N} \omega_i g(\boldsymbol{x}^{(i)}). \tag{4.75}$$

The first step of the quadrature rule is to choose a sample of points $\boldsymbol{x}^{(i)} \in \Omega$, $i = 1, ..., N$ at which the function will be evaluated. The second step is to compute the weights of each evaluation, according to the selected quadrature rule.

In practice, when the dimension of $\boldsymbol{x}$ is 1, these methods are widely used since the number of required evaluations of g in order to obtain a "satisfying" approximation, is small enough. It becomes problematic when the dimension of $\boldsymbol{x}$ increases.

Conventional methods detailed in [95], are the following ones: Newton-Cotes formulas, Monte-Carlo methods, Gauss quadrature and Clenshaw-Curtis quadrature. The last two are the most suitable for probability integrals and will be described in the next section. Their main advantage is the efficient choices of both the nodes and weights compared to the first two methods. Note that the accuracy criterion of the quadrature is generally the exactness of the approximation when g is a low order polynomial.

4.3.4.2 One dimensional quadrature rule

Let us describe quadrature rule in an one-dimensional setting. We consider here the basic problem of numerically computing the integral of a function $g(x)$ over a finite interval $\Omega = [a, b]$.

Univariate quadrature can be used to approximate the mathematical expectation of the random variable $g(X)$ as follows:

$$E\left[F(\Xi)\right] = \int_a^b F(\xi) f_\Xi(\xi) d\xi \approx \sum_{i=1}^{N} \omega_i F(\xi^{(i)}). \tag{4.76}$$

In this expression, $\xi^{(i)}$ are the quadrature nodes and ω_i are the quadrature weights. They both respond to specific rules detailed hereafter.

One of the most accurate and most used quadrature rule in the probability case, is the Gaussian quadrature [95]. It was originally built such that a n-point Gaussian quadrature rule yields an exact result for polynomials of degree $2n-1$ or less. Gaussian quadrature proposes an approximation such that:

$$\int_a^b F(\xi)w(\xi)d\xi \approx \sum_{i=1}^{N} \omega_i F(\xi^{(i)}), \tag{4.77}$$

where $w(\xi)$ is called a weighting function. Common weighting functions include the following ones:

- Chebyshev-Gauss quadrature, with $w(\xi) = (1-\xi^2)^{1/2}$, and $[a,b] = [-1,1]$.
- Gauss-Legendre quadrature, with $w(\xi) = 1$, and $[a,b] = [-1,1]$.
- Gauss-Jacobi quadrature, with $w(\xi) = (1-\xi)^{\alpha}(1+\xi)^{\beta}$, $\alpha, \beta > -1$, and $[a,b] = [-1,1]$.
- Gauss-Laguerre quadrature, with $w(\xi) = \xi^{\alpha}e^{-\xi}$, $\alpha > -1$, and $[a,b] = [0,\infty]$.
- Gauss-Hermite quadrature, with $w(\xi) = e^{-\xi^2}$, and $[a,b] = [-\infty,\infty]$.

By using the latter weighting functions, the nodes of the quadrature are the roots of the polynomials having the same name. The choice of the quadrature rule depends on the form of the integrated function, and on the integration space. Once a rule is selected, the next step is to set the nodes and weights from the rules table [2] or to use an appropriate algorithm to calculate them as done in [95] for instance. Note that it is often necessary to use a change of variables in order to apply the method to any integration interval.

Hence, to compute $E[F(\Xi)]$, an appropriate rule has to be selected according to the probability distribution f_{Ξ}, when it is known. For example the Gauss-Hermite quadrature rule is more appropriated when the distribution follows a Normal law (4.30): its support is $[-\infty,\infty]$ and $E[F(\Xi)]$ can be expressed by a simple change of variables as the product of a new function and the weight function of the Gauss-Hermite quadrature.

The Gaussian quadrature has been extended by the $(2n+1)$-point Gauss-Kronrod rules [65], which yields to an exact value of the integral whenever the integrand is a polynomial of degree less than or equal to $3n+1$. It has also the advantage to be a nested quadrature, which means that the node set of each formula, is a subset of the nodes set of its successors. In other words, when the number of quadrature nodes increases from N to N', the node of the N-quadrature are also the nodes of the N'-quadrature. It offers really important computational benefits when applying adaptive quadrature.

Another nested quadrature rule is the Clenshaw-Curtis [40] which in theory, evaluates the integrand at $N+1$ points and exactly integrates polynomials only up to degree N. However, it appears in practice that this method can have similar accuracy comparable to that of Gaussian quadrature. In fact, in the case where a function is analytic in a large neighborhood of $[-1,1]$, Gauss quadrature outperforms Clenshaw-Curtis [167]. In the case of non-analytic functions, this latter becomes sometimes better. More details on these techniques can be found in [64, 30]. For practical applications, nodes and weights values can be found in [2]. The next section explains how to deal with dimensions higher than 1 to compute integration.

4.3.4.3 Multivariate quadrature rule

In higher dimensions, a natural approach for multivariate integration consists in product rules, where N points are selected along each dimension. The quadrature points in the domain Ω are then selected thanks to the Cartesian product of all the unidimensional set of points. More precisely, we assume that $\Omega = \Omega_1 \times \ldots \times \Omega_n$, where $\times$ represents the Cartesian product and $\Omega_i \subset \mathbb{R}$, $\forall i = 1, ..., n$.

Finally, applying the same one-dimensional integration rule with N nodes per dimension and given weights ω_i to each mono-dimensional domain Ω_i, the integral of g can be approximated as follows:

$$\int_{\Omega} g(\boldsymbol{\xi}) d\boldsymbol{\xi} \approx \sum_{i_1=1}^{N} \omega_{i_1} \left(\sum_{i_2=1}^{N} \omega_{i_1} \left(... \sum_{i_n=1}^{N} \omega_{i_n} g\left(\xi_{i_1}, ..., \xi_{i_n}\right) \right) \right) \tag{4.78}$$

In a generic approach, three-nodes formulas ($N = 3$) are often adopted to obtain a good agreement between accuracy and computational cost. However, even with only 3 nodes per dimension, methods adopting full Cartesian product rules have limited application in computational robust design. In that case, the number of required function evaluations is 3^n. We are confronted to the curse of dimensionality.

4.3.4.4 Sparse grids Quadrature

To overcome the curse of dimensionality, some techniques have been developed, such as sparse grid and multi-variate quadratures [72]. The following sections are dedicated to three of them. We start by mentioning sparse grid methods, more particularly Smolyak quadrature, that highly reduces the number of function evaluations with a controllable accuracy. Sparse grid quadrature methods are constructed using combinations of tensors products of one-dimensional quadrature rules over domains $\Omega \in \mathbb{R}^n$. The main benefit of these methods is to overcome the curse of dimensionality to a certain extent.

One of the most known sparse grid method is the Smolyak quadrature rule from [43, 160, 120]. It provides a competitive alternative, with an error bound of $O\left(N^{-r} log(N)^{(d-1)(r+1)}\right)$, where d is the dimension, r estimates the regularity of the integrated function and N is the number of nodes. Smolyak rule outperforms its competitors in the domain of smooth integrands. An example of construction is given hereafter.

We consider the case $\Omega = [0, 1]$, but the results can be generalized to other domains, see [86]. For an univariate function $g : [0, 1] \mapsto \mathbb{R}$ and a sequence of non-decreasing integers m_k, $k \in \mathbb{N}$, we denote $U_{m_k} g$ a sequence of univariate quadrature rules by:

$$U_{m_k} g = \sum_{i=1}^{m_k} \omega_{i,k} g(x_{i,k}), \tag{4.79}$$

where $\omega_{i,k}$ are the weights and $x_{i,k}$ the nodes of the quadrature. Assuming $m_1 = 1$, $U_{m_1} g = g(1/2)$ and $U_{m_0} := 0$, we define the difference quadrature formula such that:

$$\Delta_k = U_{m_k} - U_{m_{k-1}}, \text{ for } k \geq 1. \tag{4.80}$$

If we now consider $g : [0, 1]^n \mapsto \mathbb{R}$ a multivariate function, then the Smolyak method [86] approximates the integral of g over Ω^n such that:

$$\int_{\Omega^n} g(\boldsymbol{x}) d\boldsymbol{x} \approx \sum_{|\boldsymbol{k}|_1 \leq l+n-1} \Delta_{\boldsymbol{k}} g, \text{ where } l \text{ is the level of the quadrature.} \tag{4.81}$$

In the last expression, $\boldsymbol{k} \in \mathbb{N}^n$ denotes a multi-index with $|\boldsymbol{k}|_1 = \sum_{j=1}^{n} k_j$, and such that:

$$\Delta_{\boldsymbol{k}} g = (\Delta_{k_1} \otimes \ldots \otimes \Delta_{k_n})\, g, \text{ with } k_j > 0. \tag{4.82}$$

An example of sparse grid is presented in Figure 4.17, in dimension $n = 2$ with a level $l = 3$. The sparse grid contains much fewer nodes than the corresponding full tensor product grid.

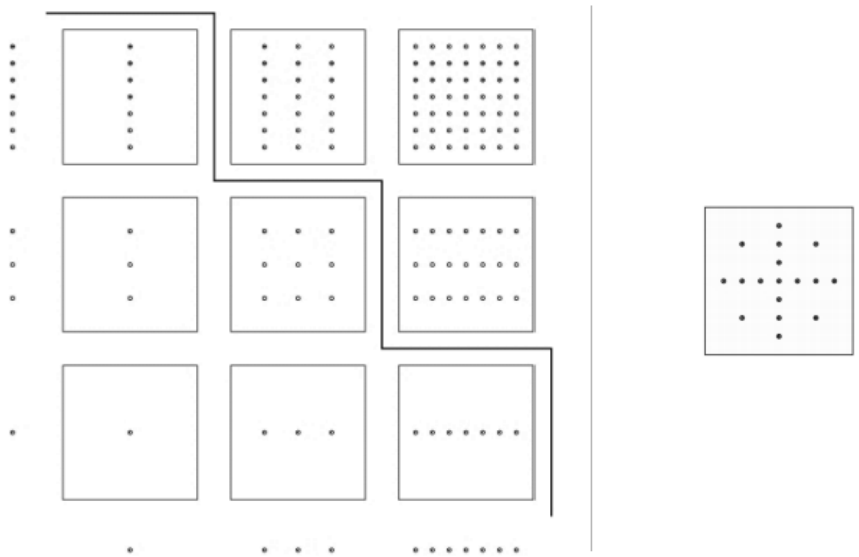

Figure 4.17: Example of sparse grid construction with level $l = 3$ and dimension $n = 2$ [71]. On the left, product grids $\Delta_{(k_1,k_2)}$, for $1 \leq k_j \leq 3$, $j = 1, 2$, based on an univariate rule with $m_1 = 1$, $m_2 = 3$ and $m_3 = 7$ points. On the right the corresponding sparse grid.

Another example of sparse grid methods are Monte-Carlo (MC) and Quasi Monte-Carlo (QMC) quadrature rules from [117]. By applying Monte Carlo integration with N random nodes, the absolute value of the error has the average order of magnitude $O\left(N^{-1/2}\right)$. These methods have been improved by the so-called quasi-Monte Carlo method [114]. The main principle yields the construction of pseudo-random sets of nodes that perform significantly better than the average of MC. This one gives the improved approximation error bound of $O\left(N^{-1}(log(N)^s\right)$. An example of MC, QMC and sparse grid is illustrated in Figure 4.18.

One of the benefit of the Smolyak rule is to have strong theoretical foundations. This is a deterministic method that does not call costly functions randomly and its rate of convergence overcomes both MC and QMC techniques in problems with sufficiently high smoothness. The Smolyak quadrature rule also retains the polynomial exactness of the unidimensional quadrature rule, a property for which neither MC nor QMC accounts. However, in term of computational cost, the number of nodes in high dimensions can still be too important.

4.3.4.5 Univariate Reduced Quadrature

Univariate quadrature approximates $\mathrm{E}[F(\boldsymbol{\Xi})]$ by a weighted sum of 1-dimensional functions. It is based on Gauss-type quadrature integration method. Details can be found in

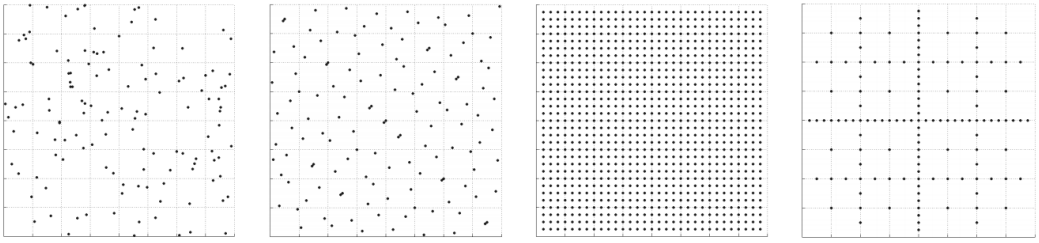

(a) Monte Carlo (b) Quasi-MC (c) Product grid (d) Sparse grid

Figure 4.18: Example of four different classes of sparse grid methods for multivariate integration [86].

[145, 62, 126]. A generalization of these techniques is also presented in [146].

The goal of this reduced quadrature is to compute the higher order moments of $F(\boldsymbol{\Xi})$ as a weighted sum of the function values in suitable chosen nodes. The originality of this approach is to use moment-based quadrature rules. Let us recall the definition of the p^{th} statistical moment of $F(\boldsymbol{\Xi})$:

$$m_p = E\left[F(\boldsymbol{\Xi})^p\right] = \int_{\mathbb{R}^n} F(\boldsymbol{\xi})^p f_{\boldsymbol{\Xi}}(\boldsymbol{\xi}) d\boldsymbol{\xi}. \tag{4.83}$$

The generalization of univariate quadrature gives:

$$m_p = \sum_{i=0}^{p} \binom{i}{p} \cdot S_n^i \cdot \left(-(n-1)\, F\left(\mu_1, ..., \mu_n\right) \right)^{p-i}, \tag{4.84}$$

where the coefficients S_n^i can be calculated using the recursive formula:

$$S_j^i = \sum_{k=0}^{i} \binom{i}{k} \cdot S_{j-1}^k \cdot E\left[F\left(\mu_1, ..., \mu_{j-1}, \Xi_j, \mu_{j+1}, \mu_n\right)^{i-k}\right]. \tag{4.85}$$

Rahman et al. in [146] introduce a new moment based quadrature method in order to compute the expectancy appearing in the relation (4.85). The advantage of this kind of quadrature is to be independent of the input distribution laws. It can then be used with any arbitrary distribution. Let N be the number of nodes per dimension. The moment based quadrature rule gives the following approximation:

$$E\left[F\left(\mu_1, ..., \mu_{j-1}, \Xi_j, \mu_{j+1}, \mu_n\right)^l\right] \cong \sum_{i=1}^{N} \omega_j^{(i)} F\left(\mu_1, ..., \mu_{j-1}, \tilde{\xi}_j^{(i)}, \mu_{j+1}, \mu_n\right)^l, \tag{4.86}$$

where $\tilde{\xi}_j^{(i)}$, $i = 1, \ldots, N$ are the interpolation points of dimension j, and $\omega_j^{(i)}$ are the weights. Both are calculated according to the moments of the input variables. It is important to note that in this case the number of interpolation points is strictly linked to the available number of inputs moments. For example mean, variance and skewness are required to compute a 2-nodes per dimension quadrature. To my best knowledge, no error estimation has been found in the general case.

A particular case is the Univariate Reduced Quadrature from [128, 125], which is an interesting moment based quadrature. It is based on matching moments quadratures formulas to the one of Evans formulas (4.67) to (4.70), in order to compute weights. By considering two nodes by dimension denoted by $\boldsymbol{\xi}_+^{(i)}$ and $\boldsymbol{\xi}_-^{(i)}$, $\forall i = 1, ..., n$, to which is added a central point corresponding to the mean $\boldsymbol{\mu}_\xi$, we obtain the following expressions:

$$\mu_F = W_0 F\left(\boldsymbol{\mu}_\xi\right) + \sum_{i=1}^{n} \omega_i \left(\frac{F(\boldsymbol{\xi}_+^{(i)})}{h_i^+} - \frac{F(\boldsymbol{\xi}_-^{(i)})}{h_i^-} \right), \tag{4.87}$$

$$\begin{aligned} \sigma_F^2 = \sum_{i=1}^{n} \Big[& \omega_i^+ \left(\frac{F(\boldsymbol{\xi}_+^{(i)}) - F(\boldsymbol{\mu}_\xi)}{h_i^+} \right)^2 + \omega_i^- \left(\frac{F(\boldsymbol{\xi}_-^{(i)}) - F(\boldsymbol{\mu}_\xi)}{h_i^-} \right)^2 \\ & + \omega_i^{\pm} \frac{\left(F(\boldsymbol{\xi}_+^{(i)}) - F(\boldsymbol{\mu}_\xi)\right)\left(F(\boldsymbol{\xi}_-^{(i)}) - F(\boldsymbol{\mu}_\xi)\right)}{h_i^+ h_i^-} \Big], \end{aligned} \tag{4.88}$$

$$\mu_{F,3} = \sum_{i=1}^{n} \gamma_i \sigma_i^3 \left(\frac{F(\boldsymbol{\xi}_+^{(i)}) - F(\boldsymbol{\xi}_-^{(i)})}{h_i^+ - h_i^-} \right)^3, \tag{4.89}$$

$$\mu_{F,4} = \sum_{i=1}^{n} \Gamma_i \sigma_i^4 \left(\frac{F(\boldsymbol{\xi}_+^{(i)}) - F(\boldsymbol{\xi}_-^{(i)})}{h_i^+ - h_i^-} \right)^4, \tag{4.90}$$

where:

$$\begin{aligned} & \boldsymbol{\xi}_\pm^{(i)} = \boldsymbol{\mu}_\xi + h_i^\pm \sigma_i \boldsymbol{e}_i \ ; \ h_i^\pm = \frac{\gamma_i}{2} \pm \sqrt{\Gamma_i - \frac{3\gamma_i^2}{4}}, \\ & W_0 = 1 + \sum_{i=1}^{n} \frac{1}{h_i^+ h_i^-} \ ; \ \omega_i = \frac{1}{h_i^+ - h_i^-}, \\ & \omega_i^+ = \frac{(h_i^+)^2 - h_i^+ h_i^- - 1}{(h_i^+ - h_i^-)^2} \ ; \ \omega_i^- = \frac{(h_i^-)^2 - h_i^+ h_i^- - 1}{(h_i^+ - h_i^-)^2}, \\ & \omega_i^\pm = \frac{2}{(h_i^+ - h_i^-)^2}. \end{aligned} \tag{4.91}$$

This method has a reduced cost of $(2n+1)$ function evaluations, where n is the dimension of the input vector, and is easy to implement. Assuming that the univariate terms of the function F are accurately approximated, an error can be computed taking into account the first non univariate terms of Evans relations (4.67) to (4.70). It yields the following error:

$$\varepsilon_{\mu_F} = M_5 + o(\sigma_\xi^4) \tag{4.92}$$

$$\varepsilon_{\sigma_F^2} = V_4 + o(\sigma_\xi^4) \tag{4.93}$$

$$\varepsilon_{\mu_{3,F}} = S_3 + o(\sigma_\xi^4) \tag{4.94}$$

$$\varepsilon_{\mu_{4,F}} = o(\sigma_\xi^4) \tag{4.95}$$

We highlight the terms M_5, V_4 and S_3 since they include crossed partial derivatives. Thus if the interactions between variables are reduced, these terms become negligible. The error on μ_F, σ_F^2 and $\mu_{3,F}$ then becomes of order σ_ξ^4.

4.3.4.6 Generalized Dimension Reduction and Bivariate Quadrature (BRQ) methods

Following the same approach than in the previous section, we now present a Bivariate Reduced Quadrature (BRQ) from [129].

Bivariate quadrature and generalized dimension-reduction method for integration in stochastic domain, are well explained in [62, 182]. We want to use here a S-variate dimension reduction technique, which aims at only considering the interactions of order lower than S between the input variables. For instance the univariate case corresponds to first order interactions (S=1). Then, quite similarly to the univariate case, the p^{th} moment of F can be approximated by:

$$m_p = \sum_{i=0}^{S} (-1)^i \binom{n-S+i-p}{i} \sum_{k_1<\ldots<k_{S-i}} E\left[F\left(\mu_1, \ldots, \mu_{k_1-1}, \Xi_{k_1}, \mu_{k_1+1}, \ldots, \Xi_{k_{S-i}}, \ldots, \mu_n\right)^p\right]. \tag{4.96}$$

By definition of the expectation, we have:

$$\begin{aligned} &E\left[F\left(0, ..., 0, \Xi_{k_1}, 0, ..., 0, \Xi_{k_{S-i}}, 0, ..., 0\right)^p\right] \\ &= \int_{\mathbb{R}^{S-i}} F\left(0, ..., 0, \xi_{k_1}, 0, ..., 0, \xi_{k_{S-i}}, 0, ..., 0\right)^p f_{\tilde{\boldsymbol{\Xi}}}(\tilde{\boldsymbol{\xi}}) d\tilde{\boldsymbol{\xi}} \end{aligned} \tag{4.97}$$

where $\tilde{\boldsymbol{\xi}} = (\xi_{k_1}, ..., \xi_{k_{S-i}}) \in \mathbb{R}^{S-i}$ and $f_{\tilde{\boldsymbol{\Xi}}}$ is the joint probability density of $\tilde{\boldsymbol{\Xi}}$. To compute this $(S-i)$-dimensional integral, standard Gaussian quadrature rules can be used according to the distribution of $\tilde{\boldsymbol{\Xi}}$.

An interesting and easy to implement example of bivariate reduced quadrature is the BRQ method from [129]. This method has a cost of $(2n^2+1)$ function evaluations. As for URQ technique, it is based on matching the moments quadrature formulas of F with Evans formulas (4.67) to (4.70). BRQ method is based on a bivariate Gauss-type quadrature method, by considering the central point corresponding to the mean $\boldsymbol{\mu}_\xi$ as the first node and two nodes for each dimension, denoted by $\boldsymbol{\xi}_+^{(i)}$ and $\boldsymbol{\xi}_-^{(i)}$, $\forall i = 1, ..., n$, to which are added $\xi_{i^\pm j^\pm}$, $\forall i, j = 1, ..., n$. Evans in [62] gives the following quadrature formulas to compute $E\left[\left(F(\boldsymbol{\Xi}) - F(\boldsymbol{\mu}_\xi)\right)^p\right]$, $p = 1, ..., 4$:

$$\begin{aligned} E\left[F(\boldsymbol{\Xi}) - F(\boldsymbol{\mu}_\xi)\right] = \sum_{i=1}^{n} \Big[\omega_i \Big(&\frac{F(\boldsymbol{\xi}_+^{(i)}) - F(\boldsymbol{\mu}_\xi)}{h_i^+} - \frac{F(\boldsymbol{\xi}_-^{(i)}) - F(\boldsymbol{\mu}_\xi)}{h_i^-} \Big) \\ + \sum_{j=i+1}^{n} \omega_{ij} \Big(&\frac{F(\boldsymbol{\xi}^{(i^+ j^+)}) - F(\boldsymbol{\mu}_\xi)}{h_i^+ h_j^+} + \frac{F(\boldsymbol{\xi}^{(i^- j^-)}) - F(\boldsymbol{\mu}_\xi)}{h_i^- h_j^-} \\ &- \frac{F(\boldsymbol{\xi}^{(i^+ j^-)}) - F(\boldsymbol{\mu}_\xi)}{h_i^+ h_j^-} - \frac{F(\boldsymbol{\xi}^{(i^- j^+)}) - F(\boldsymbol{\mu}_\xi)}{h_i^- h_j^+} \Big) \Big], \end{aligned} \tag{4.98}$$

$$\begin{aligned} E\left[\left(F(\boldsymbol{\Xi}) - F(\boldsymbol{\mu}_\xi)\right)^2\right] = \sum_{i=1}^{n} \Big[\omega_i \Big(&\frac{\left(F(\boldsymbol{\xi}_+^{(i)}) - F(\boldsymbol{\mu}_\xi)\right)^2}{h_i^+} - \frac{\left(F(\boldsymbol{\xi}_-^{(i)}) - F(\boldsymbol{\mu}_\xi)\right)^2}{h_i^-} \Big) \\ + \sum_{j=i+1}^{n} \omega_{ij} \Big(&\frac{\left(F(\boldsymbol{\xi}^{(i^+ j^+)}) - F(\boldsymbol{\mu}_\xi)\right)^2}{h_i^+ h_j^+} + \frac{\left(F(\boldsymbol{\xi}^{(i^- j^-)}) - F(\boldsymbol{\mu}_\xi)\right)^2}{h_i^- h_j^-} \end{aligned} \tag{4.99}$$

$$- \frac{\Big(F(\boldsymbol{\xi}^{(i^+j^-)}) - F(\boldsymbol{\mu}_\xi)\Big)^2}{h_i^+ h_j^-} - \frac{\Big(F(\boldsymbol{\xi}^{(i^-j^+)}) - F(\boldsymbol{\mu}_\xi)\Big)^2}{h_i^- h_j^+}\Big)\Big],$$

$$E\left[\Big(F(\boldsymbol{\Xi}) - F(\boldsymbol{\mu}_\xi)\Big)^3\right] = \sum_{i=1}^{n}\Big[\omega_i\Big(\frac{\Big(F(\boldsymbol{\xi}_+^{(i)}) - F(\boldsymbol{\mu}_\xi)\Big)^3}{h_i^+} - \frac{\Big(F(\boldsymbol{\xi}_-^{(i)}) - F(\boldsymbol{\mu}_\xi)\Big)^3}{h_i^-}\Big) \tag{4.100}$$
$$+ \sum_{j=i+1}^{n}\omega_{ij}\Big(\frac{\Big(F(\boldsymbol{\xi}^{(i^+j^+)}) - F(\boldsymbol{\mu}_\xi)\Big)^3}{h_i^+ h_j^+} + \frac{\Big(F(\boldsymbol{\xi}^{(i^-j^-)}) - F(\boldsymbol{\mu}_\xi)\Big)^3}{h_i^- h_j^-}$$
$$- \frac{\Big(F(\boldsymbol{\xi}^{(i^+j^-)}) - F(\boldsymbol{\mu}_\xi)\Big)^3}{h_i^+ h_j^-} - \frac{\Big(F(\boldsymbol{\xi}^{(i^-j^+)}) - F(\boldsymbol{\mu}_\xi)\Big)^3}{h_i^- h_j^+}\Big)\Big],,$$

$$E\left[\Big(F(\boldsymbol{\Xi}) - F(\boldsymbol{\mu}_\xi)\Big)^4\right] = \sum_{i=1}^{n}\Big[\omega_i\Big(\frac{\Big(F(\boldsymbol{\xi}_+^{(i)}) - F(\boldsymbol{\mu}_\xi)\Big)^4}{h_i^+} - \frac{\Big(F(\boldsymbol{\xi}_-^{(i)}) - F(\boldsymbol{\mu}_\xi)\Big)^4}{h_i^-}\Big) \tag{4.101}$$
$$+ \sum_{j=i+1}^{n}\omega_{ij}\Big(\frac{\Big(F(\boldsymbol{\xi}^{(i^+j^+)}) - F(\boldsymbol{\mu}_\xi)\Big)^4}{h_i^+ h_j^+} + \frac{\Big(F(\boldsymbol{\xi}^{(i^-j^-)}) - F(\boldsymbol{\mu}_\xi)\Big)^4}{h_i^- h_j^-}$$
$$- \frac{\Big(F(\boldsymbol{\xi}^{(i^+j^-)}) - F(\boldsymbol{\mu}_\xi)\Big)^4}{h_i^+ h_j^-} - \frac{\Big(F(\boldsymbol{\xi}^{(i^-j^+)}) - F(\boldsymbol{\mu}_\xi)\Big)^4}{h_i^- h_j^+}\Big)\Big],$$

where:

$$\begin{aligned}
&\boldsymbol{\xi}_\pm^{(i)} = \boldsymbol{\mu}_\xi + h_i^\pm \sigma_i \boldsymbol{e}_i, \qquad (4.102)\\
&\boldsymbol{\xi}^{(i^\pm j^\pm)} = \boldsymbol{\mu}_\xi + h_i^\pm \sigma_i \boldsymbol{e}_i + h_j^\pm \sigma_j \boldsymbol{e}_j,\\
&h_i^\pm = \frac{\gamma_i}{2} \pm \sqrt{\Gamma_i - \frac{3\gamma_i^2}{4}},\\
&\omega_i = \frac{1 + \left(\sum_{p=1}^{n} \frac{1}{h_k^+ h_k^-}\right) - \frac{1}{h_i^+ h_i^-}}{(h_i^+ - h_i^-)},\\
&\omega_{ij} = \frac{1}{(h_i^+ - h_i^-)(h_j^+ - h_j^-)}.
\end{aligned}$$

Finally we can deduce the moments $m_{1,F}$, $m_{2,F}$, $m_{3,F}$ and $m_{4,F}$ such that:

$$m_{1,F} = E\left[\Big(F(\boldsymbol{\Xi}) - F(\boldsymbol{\mu}_\xi)\Big)\right] - F(\boldsymbol{\mu}_\xi), \tag{4.103}$$

$$m_{2,F} = E\left[\Big(F(\boldsymbol{\Xi}) - F(\boldsymbol{\mu}_\xi)\Big)^2\right] + 2m_{1,F}F(\boldsymbol{\mu}_\xi) - F(\boldsymbol{\mu}_\xi)^2, \tag{4.104}$$

$$m_{3,F} = E\left[\Big(F(\boldsymbol{\Xi}) - F(\boldsymbol{\mu}_\xi)\Big)^3\right] + 3m_{2,F}F(\boldsymbol{\mu}_\xi) - 3m_{1,F}F(\boldsymbol{\mu}_\xi)^2 + F(\boldsymbol{\mu}_\xi)^3, \tag{4.105}$$

$$m_{4,F} = E\left[\Big(F(\boldsymbol{\Xi}) - F(\boldsymbol{\mu}_\xi)\Big)^4\right] + 4m_{3,F}F(\boldsymbol{\mu}_\xi) - 6m_{2,F}F(\boldsymbol{\mu}_\xi)^2 + 4m_{1,F}F(\boldsymbol{\mu}_\xi)^3 - F(\boldsymbol{\mu}_\xi)^4, \tag{4.106}$$

And then using Formulas (4.15) we can calculate the first four centered moments of F. Concerning the error, we have the following estimation, using Evans formulas (4.67) to (4.70):

$$\varepsilon_{\mu_F} = o(\sigma_\xi^4), \tag{4.107}$$
$$\varepsilon_{\sigma_F^2} = o(\sigma_\xi^4), \tag{4.108}$$
$$\varepsilon_{\mu_{3,F}} = o(\sigma_\xi^4), \tag{4.109}$$
$$\varepsilon_{\mu_{4,F}} = o(\sigma_\xi^4). \tag{4.110}$$

In practice these methods offer a very good compromise between cost and accuracy, and their implementation is very easy.

4.3.5 Polynomial Chaos Expansion (PCE) and Stochastic Collocation methods

This section is dedicated to techniques of uncertainty propagation based on a polynomial representation of stochastic processes. These techniques rely on expanding F in a series of random variables. They propose to model stochastic processes of random variables and are most used in the field of uncertainty quantification and propagation [88, 1, 180, 60, 59, 52]. Polynomial chaos have been first introduced in [179] in 1938 as a part of the set of homogeneous chaos in the integration theory.

Let us define a polynomial basis $(\psi_k)_{k\in\mathbb{N}}$, a stochastic process $g(\boldsymbol{\Xi})$, where $\boldsymbol{\Xi} = (\Xi_1, ..., \Xi_N)$ is a set of independent random variables. The polynomial chaos expansion of the stochastic process is defined by:

$$g(\boldsymbol{\xi}) = \sum_{k=0}^{\infty} \beta_k \psi_k(\boldsymbol{\xi}), \tag{4.111}$$

Any stochastic process can be modeled by a polynomial chaos expansion by choosing a suitable orthogonal basis of polynomials [181]. Table 4.1 presents the preferred choice of the basis according to the to-be-modeled distribution. Then, knowing the input uncertainty distribution, it is possible to accurately build the output uncertainty distribution. Once the basis has been selected, the knowledge of the coefficients β_k in (4.111) fully characterizes the uncertain process $g(\boldsymbol{\Xi})$. The next sections present how to numerically compute these coefficients.

Table 4.1: Correspondence between the orthogonal polynomials and the continuous random variables.

Random variables type	Orthogonal polynomials	Distribution support
Gaussian	Hermite	$[-\infty, \infty]$
Gamma	Laguerre	$[0, \infty]$
Beta	Jacobi	$[a, b]$
Uniform	Legendre	$[a, b]$

PCE techniques can be separated into two kinds: intrusive and non-intrusive ones. Intrusive methods become really complex when there are changes in the process equations.

Moreover it must be adapted again whenever the process is not the same. Therefore we choose to focus on non-intrusive methods.

As previously mentioned, PCE is mainly used to compute a distribution process, but it is important to know that analytic formulas exist to compute the first order moments of $F(\boldsymbol{\Xi})$ [1]. The above decomposition (4.111) can be used and we obtain the following relations:

$$\mu_F = \beta_0, \tag{4.112}$$

$$\sigma_F^2 = \sum_{k=1}^{\infty} \beta_k^2 \|\psi_k(\boldsymbol{\xi})\|, \tag{4.113}$$

$$\gamma_F = \sum_{k=1}^{\infty} \beta_k^3 \|\psi_k(\boldsymbol{\xi})\|^{3/2} + 3\sum_{i=1}^{\infty} \beta_i^2 \sum_{\substack{j=1 \\ j\neq i}}^{\infty} \beta_j \langle \psi_i^2(\boldsymbol{\xi}), \psi_j(\boldsymbol{\xi})\rangle + ... \tag{4.114}$$

$$... + 6\sum_{i=1}^{\infty}\sum_{j=i+1}^{\infty}\sum_{k=j+1}^{\infty} \beta_i\beta_j\beta_k \langle \psi_i(\boldsymbol{\xi}), \psi_j(\boldsymbol{\xi})\psi_k(\boldsymbol{\xi})\rangle,$$

$$\Gamma_F = \sum_{k=1}^{\infty} \beta_k^4 \|\psi_k(\boldsymbol{\xi})\|^2 + 4\sum_{i=1}^{\infty} \beta_i^3 \sum_{\substack{j=1 \\ j\neq i}}^{\infty} \beta_j \langle \psi_i^3(\boldsymbol{\xi}), \psi_j(\boldsymbol{\xi})\rangle + ... \tag{4.115}$$

$$... + 6\sum_{i=1}^{\infty} \beta_i^2 \sum_{j=i+1}^{\infty} \beta_j^2 \langle \psi_i^2(\boldsymbol{\xi}), \psi_j^2(\boldsymbol{\xi})\rangle + ...$$

$$... + 12\sum_{i=1}^{\infty} \beta_i^2 \sum_{\substack{j=1 \\ j\neq i}}^{\infty} \beta_j \sum_{\substack{k=j+1 \\ k\neq i}}^{\infty} \beta_k \langle \psi_i^2(\boldsymbol{\xi}), \psi_j(\boldsymbol{\xi})\psi_k(\boldsymbol{\xi})\rangle + ...$$

$$... + 24\sum_{i=1}^{\infty}\sum_{j=i+1}^{\infty}\sum_{k=j+1}^{\infty}\sum_{l=k+1}^{\infty} \beta_i\beta_j\beta_k\beta_l \langle \psi_i(\boldsymbol{\xi})\psi_j(\boldsymbol{\xi}), \psi_k(\boldsymbol{\xi})\psi_l(\boldsymbol{\xi})\rangle.$$

However, as demonstrated in [103], the computation of the moments of $F(\boldsymbol{\Xi})$ using the latter relations, is not better than previous quadrature techniques. Computing β_k gives the information of the entire distribution, so at a same cost level it is more interesting than reducing it to its first four moments.

In the following, we first introduce polynomial chaos expansion truncation, which is the main numerical application of PCE. Then, an example of stochastic collocation is described. The third section is dedicated to the work from [122] which is used to study the accuracy on the computation of $F(\boldsymbol{\Xi})$ depending on input information accuracy.

4.3.5.1 Expansion truncation

Chaos polynomial expansion is an infinite series. Expansion truncation consists in considering only a finite number M of terms, i.e. a truncated expansion of the expression (4.111):

$$F(\boldsymbol{\xi}) \approx \sum_{k=0}^{M} \beta_k \psi_k(\boldsymbol{\xi}). \tag{4.116}$$

The number M of terms in the expansion depends on the total number of input parameters n and on the order d of the expansion, according to the formula [122]:

$$M = \frac{(n+d)!}{n!d!}, \tag{4.117}$$

If $\boldsymbol{\xi} \in \mathbb{R}$, the univariate polynomials ψ_k are selected according to Table 4.1. In the case where $n > 1$, assuming that the input parameters $\boldsymbol{\Xi} = (\Xi_1, ..., \Xi_n)$ are independent random variables, the multidimensional basis can be built as a simple product of the univariate polynomials P_j, $j = 1, \ldots, n$, selected according to Table 4.1:

$$\psi_k(\xi_1, ..., \xi_n) = \prod_{j=1}^{n} P_j^{(\alpha_j^k)}(\xi_1, \ldots, \xi_n). \tag{4.118}$$

In the previous expression, α_j^k is the degree of the polynomial of index i in dimension j. Since the polynomial basis is orthogonal, the coefficients β_k can be computed as:

$$\beta_k = \frac{\langle F(\boldsymbol{\xi}), \psi_k(\boldsymbol{\xi}) \rangle}{\langle \psi_k(\boldsymbol{\xi}), \psi_k(\boldsymbol{\xi}) \rangle}, \; k = 1, ..., n, \tag{4.119}$$

where the inner product is defined by:

$$\langle F(\boldsymbol{\xi}), G(\boldsymbol{\xi}) \rangle = \int_{\Omega} F(\boldsymbol{\xi}) G(\boldsymbol{\xi}) f_{\boldsymbol{\Xi}}(\boldsymbol{\xi}) d\boldsymbol{\xi}. \tag{4.120}$$

Knowing the polynomials ψ_k, the denominator part of β_k coefficients can be calculated analytically. However, the numerator has to be computed by a well adapted numerical integration technique. The latter can for instance be chosen among the quadrature integration methods from Section 4.3.4. The choice of the quadrature depends on the input uncertainty $\boldsymbol{\Xi}$ via the choice of the polynomial basis, see Table 4.1.

Drawbacks of the quadrature methods appear at this step. Full tensorial grids suffer of the curse of dimensionality. Therefore, univariate or bivariate techniques can be of great interest.

A particular attention should also be paid when computing $\langle F(\boldsymbol{\xi}), \psi_k(\boldsymbol{\xi}) \rangle$. Indeed, the total degree of the function to be integrated is the sum of the degrees of F and ψ_k. Then for a given F, since the degree of the polynomials ψ_k is becoming high, the number of quadrature points has to increase in order to maintain the same level of accuracy on the result. Therefore, adaptive methods could be of interest, since we could increase the number of points along the dimensions where the polynomials degree is the highest. Unfortunately, these dimensions are generally not known. An interesting alternative approach relies on computing the error between two successive integrations with an increasing number of points. The user can then define a threshold ε and stop to increase the number of points when the error is smaller than ε.

4.3.5.2 An example of stochastic collocation method

In the case where input distribution of $\boldsymbol{\Xi}$ is not known accurately, it is not possible to build the output uncertain distribution with a good accuracy. Then, it is possible to use PCE in order to compute moments of F with a method quite easy to implement. We present in this section an example of stochastic collocation method to compute these moments. We focus on non-intrusive Stochastic Collocation methods. Details can be found in [25].

Based on univariate polynomial interpolation and a suitable set of nodes $\{\boldsymbol{\xi}^{(q)}, q = 1, \ldots, N\}$, we can define the following stochastic expansion of $F(\boldsymbol{\Xi})$ according to the random variable $\boldsymbol{\Xi}$ by:

$$F(\boldsymbol{\xi}) \approx \sum_{q=1}^{N} P_q(\boldsymbol{\xi}) F(\boldsymbol{\xi}^{(q)}), \tag{4.121}$$

where $P_q(\boldsymbol{\xi})$ is the application of a tensor product rule to the one-dimensional polynomial interpolation. If n is the dimension of $\boldsymbol{\xi} = (\xi_1, \ldots, \xi_n)$, we obtain the expression of F thanks to relation (4.122).

$$F(\boldsymbol{\xi}) \approx \sum_{q_1=1}^{N_1} \cdots \sum_{q_n=1}^{N_n} P_{q_1}(\xi_1) \ldots P_{q_n}(\xi_n) F(\xi_1^{(q_1)}, \ldots, \xi_n^{(q_n)}), \tag{4.122}$$

where the nodes are denoted $\{\boldsymbol{\xi}^{(q)} = (\xi_1^{(q)}, \ldots, \xi_n^{(q)}),\ q = 1, ..., N_i,\ i = 1, \ldots, n\}$, and $N = N_1 + ... + N_n$. Following Table 4.1, the choice of the collocation points $\boldsymbol{\xi}^{(q)}$ is associated to the Gauss points, which are the roots of the corresponding orthogonal polynomials. Following the last expression of F, the expectation of F can be approximated as follows:

$$E[F(\boldsymbol{\Xi})] \approx \sum_{q=1}^{N} F(\boldsymbol{\xi}^{(q)}) E\left[P_q(\boldsymbol{\xi})\right], \tag{4.123}$$

where $E[P_q(\boldsymbol{\xi})]$ is thus the associated quadrature weight, defined by:

$$E[P_q(\boldsymbol{\Xi})] = \int_{D_\xi} P_q(\boldsymbol{\xi}) F_{\boldsymbol{\Xi}}(\boldsymbol{\xi}) d\boldsymbol{\xi}. \tag{4.124}$$

The same way, an estimation of the moments of higher order can be calculated. It relies on interpolating the function F^k rather than F, and then on computing the expectation of the resulting interpolation. It yields the following expression:

$$E\left[(F(\boldsymbol{\Xi}))^k\right] \approx \sum_{q=1}^{N} \left(F(\boldsymbol{\xi}^{(q)})\right)^k E[P_q(\boldsymbol{\Xi})] \tag{4.125}$$

In that case, the accuracy of the moment estimate directly depends on the interpolation error of the function F^k. This error tends to increase with the kth-order moment, since the degree of F^k accordingly increases. More interpolation points should then be employed. Centered moments can be retrieved using relations (4.15).

In this case, the integration method relies on a Gaussian-type quadrature with a tensor product rule, thus the computation cost depends on the chosen quadrature as mentioned in Section 4.3.4. As this method relies on univariate interpolation, one advantage is that it is simple to apply adaptive rules to compute the integration.

Next section presents a recent example of PCE method that is based on arbitrary choice of polynomial chaos basis. It can be very useful in case no information is known about the distribution type. This approach is used to study the impact of input uncertainty information on the accuracy of the output.

4.3.5.3 An example of arbitrary PCE method

The idea of the arbitrary PCE method [122] is to construct an orthonormal polynomial basis for arbitrary distributions exploiting only the moments of the input uncertainty. It also shows that finite-order expansion only requires a finite number of these moments. Polynomials $\psi_k(\xi)$ of degree k, where $\xi \in \Omega \subset \mathbb{R}$, are defined by:

$$\psi_k(\xi) = \sum_{i=0}^{k} p_i^{(k)} \xi^i, \tag{4.126}$$

where $p_i^{(k)}$ are the coefficients in $\psi_k(\xi)$ and $k \in [0, d]$, d being the truncation order of the polynomial basis. Denoting by m_i the i^{th} moment of the random variable ξ, [122] shows that we can express coefficients $p_i^{(k)}$ by solving the inverse problem:

$$\begin{bmatrix} m_0 & m_1 & \dots & m_k \\ m_1 & m_2 & \dots & m_{k+1} \\ \dots & \dots & \dots & \dots \\ m_{k-1} & m_k & \dots & m_{2k-1} \\ 0 & 0 & \dots & 1 \end{bmatrix} \begin{bmatrix} p_0^{(k)} \\ p_1^{(k)} \\ \dots \\ p_{k-1}^{(k)} \\ p_k^{(k)} \end{bmatrix} = \begin{bmatrix} 0 \\ 0 \\ \dots \\ 0 \\ 1 \end{bmatrix}. \tag{4.127}$$

This system implies that any difference between distributions becoming visible only in moments of order higher than $(2d-1)$, will be invisible to any order d polynomial expansion technique. Therefore the existence of the moments m_0 to m_{2d} is a necessary and sufficient condition for constructing an orthonormal basis $\{\psi_k\}_{k=1,\dots,d}$ up to degree d. In [122], the author also presents an explicit form of these polynomial chaos. Using this technique we obtain the coefficient of the polynomial basis as presented in Table 4.2. We give also the

Table 4.2: Arbitrary PCE method: coefficients of $\psi^{(k)}$ polynomials [122].

0 degree	$p_0^{(0)} = 1$
1^{st} degree	$p_0^{(1)} = -m_1$, $p_1^{(1)} = 1$
2^{nd} degree	$p_0^{(2)} = -m_2 - \dfrac{m_1(m_1 m_2 - m_3)}{m_2 - m_1^2}$, $p_1^{(2)} = \dfrac{m_1 m_2 - m_3}{m_2 - m_1^2}$, $p_2^{(2)} = 1$

expression of the coefficients of $\psi^{(k)}$ polynomials as a function of the normalized moments μ, σ^2 and γ in Table 4.3. The expression of the corresponding coefficients can be found in

Table 4.3: Arbitrary PCE method: coefficients of $\psi^{(k)}$ polynomials as a function of the normalized input moments.

0 degree	$p_0^{(0)} = 1$
1^{st} degree	$p_0^{(1)} = -\mu$, $p_1^{(1)} = 1$
2^{nd} degree	$p_0^{(2)} = -\sigma^2 + \mu^2 + \mu\gamma\sigma$, $p_1^{(2)} = -\gamma\sigma - 2\mu$, $p_2^{(2)} = 1$

[122] and from relation 4.127 it can be shown that the 5th-order moments of the input are required to build the 3^{rd} degree polynomials.

The following numerical example aims at underlying the way of convergence of the output distribution according to the input distribution informations.

Considering the input uncertainty $\xi \in \mathbb{R}$, we want to approximate the uncertain output $y = F(\xi)$ by a polynomial chaos expansion of order 2:

$$y_{PC} = c_0\psi_0(\xi) + c_1\psi_1(\xi) + c_2\psi_2(\xi), \tag{4.128}$$

where, according to Table 4.2, we can compute the polynomials as:

$$\psi_0(\xi) = p_0^{(0)} = 1, \tag{4.129}$$
$$\psi_1(\xi) = p_0^{(1)} + p_1^{(1)}\xi = -m_1 + \xi, \tag{4.130}$$
$$\psi_2(\xi) = p_0^{(2)} + p_1^{(2)}\xi + p_2^{(2)}\xi^2. \tag{4.131}$$

Since the polynomial basis is orthogonal, the coefficients c_i are then defined by:

$$c_i = \frac{\int_\Omega F(\xi)\psi_i(\xi)f_\Xi(\xi)d\xi}{\int_\Omega \psi_i^2(\xi)f_\Xi(\xi)d\xi}. \tag{4.132}$$

It yields:

$$c_0 = \frac{1}{\int_\Omega \psi_0^2(\xi)f_\Xi(\xi)d\xi}\int_\Omega F(\xi)f_\Xi(\xi)d\xi, \tag{4.133}$$
$$c_1 = \frac{1}{\int_\Omega \psi_1^2(\xi)f_\Xi(\xi)d\xi}\left(-m_1c_0 + \int_\Omega F(\xi)\xi f_\Xi(\xi)d\xi\right), \tag{4.134}$$
$$c_2 = \frac{1}{\int_\Omega \psi_2^2(\xi)f_\Xi(\xi)d\xi}\left(p_0^{(2)} + p_1^{(2)}\int_\Omega F(\xi)\xi f_\Xi(\xi)d\xi + \int_\Omega F(\xi)\xi^2 f_\Xi(\xi)d\xi\right). \tag{4.135}$$

In order to compute c_0, c_1 and c_2, we observe that we only have to compute:

$$E\left[F(\Xi)\right] = \int_\Omega F(\xi)f_\Xi(\xi)d\xi, \tag{4.136}$$
$$E\left[\Xi F(\Xi)\right] = \int_\Omega F(\xi)\xi f_\Xi(\xi)d\xi, \tag{4.137}$$
$$E\left[\Xi^2 F(\Xi)\right] = \int_\Omega F(\xi)\xi^2 f_\Xi(\xi)d\xi, \tag{4.138}$$

and:

$$E\left[\psi_i(\Xi)^2\right] = \int_\Omega \psi_i^2(\xi)f_\Xi(\xi)d\xi,\ i = 0, \ldots, 2. \tag{4.139}$$

Observe that with a polynomial expansion of order 2, the computation of relation (4.139) requires input moments of order 4 since a term in ξ^4 appears under the integrand. The expression of the norm of the polynomial ψ_k as a function of the normalized input moments is given in Table 4.4. In the general case, moments until the order $2d$ are required to apply the method at any order d of expansion. Two examples are presented in Section 4.3.7.2 in order illustrate the convergence of the method with respect to the order of expansion of the polynomial basis.

Table 4.4: Arbitrary PCE method: coefficients of $\psi^{(k)}$ polynomials as a function of the normalized input moments μ, σ^2, γ and Γ.

k	$\int \left(\sum_{i=0}^{k} c_i^{(k)} \xi^i\right)^2 f_\Xi(\xi) d\xi$
$k=0$	1
$k=1$	σ_ξ^2
$k=2$	$\sigma^4 \left(\Gamma - \gamma^2 - 1\right)$

The computation of Equation (4.136) to Equation (4.138) require integration methods. In the mono-dimensional case, an univariate quadrature is sufficient. However, if $\boldsymbol{\xi} \in \mathbb{R}^n$, with $n \geq 2$, an idea is to use a quadrature according to the available input information. For instance in the case where the first four moments are available, we already know that polynomial basis of order 2 is sufficient. This means that integrals from Equations (4.136) would include interactions of order 2. Hence a bivariate quadrature, such as the one of Section 4.3.4.6, is well adapted and allows to take benefit from all the available information.

4.3.6 Towards adaptive rules

This section introduces adaptive techniques. The main objective is to adapt the number of nodes according to specific criteria and to provide additional computational relief, for example if the problem is spatially oriented. Details of such techniques can be found in [26, 79, 73]. They often use Gaussian unimodal quadrature rules with an intuitive management of the number of points. In our mind, the idea is to have an error estimate when:

- we have to select the number points by dimensions. It would in this case trigger higher order quadrature if needed for example.
- we have to choose the dimension reduction order. It would for example trigger higher than unidimensional or bi-dimensional integrations, if needed.

These adaptive rules can be applied to the general framework with Equations (4.84) and (4.86), as it requires the integration of dimension reduced functions with the use of nested quadrature rules. For example, applied to the univariate case, the use of Gauss-Kronrod quadrature rule from [66] could be used instead of rules from URQ. It has a cost of $4n+1$ function evaluations, with a highest results accuracy.

The first idea to compute an error between two integrations: a first one with a given method and a second one with a more accurate method. Therefore when the difference is higher than a given threshold ε, we keep looking for a better integration rule. Once the error is small enough according to the user's requirements, the gain in term of accuracy is too small compared to the cost in function evaluations. Numerical examples of such methods are given in the last section of the chapter. However, the implementation of these adaptive techniques requires deeper studies in order to limit the number of function evaluations. One important improvement should consist in finding how to compute two integrations using for the accurate one the nodes of the first one.

4.3.7 Numerical examples

4.3.7.1 Moment methods comparison

We choose four test functions in order to compare the different methods presented in Section 4.3:

1. $f_1(\xi_1) = 4(\xi_1 - 0.2)^3$,
2. $f_2(\xi_1, \xi_2) = \xi_1^3 + 2\xi_2^2 - 0.5\xi_1\xi_2^3$,
3. $f_3(\xi_1, \xi_2) = \xi_1 \cos(\xi_2)$,
4. $f_4(\xi_1, \xi_2, \xi_3) = \dfrac{\exp(\xi_1) + 4\xi_3\xi_2^4}{\cos(\xi_3)^2 + 2}$.

Without loss of generality, the uncertain input variable are chosen as random variables following independent Normal laws, with a mean equal to 1 and a standard deviation equal to 0.01 (case 1), 0.1 (case 2) and 0.3 (case 3). Since the functions are not linear, the output distributions will not follow Normal law. Note that in this case that the input skewness and kurtosis are null, but this does not mean that the output skewness and kurtosis will be null.

Let n be the dimension of $\boldsymbol{\xi}$. The output centered-reduced moments μ_f, σ_f^2, γ_f and Γ_f are computed thanks to the following methods:

- Monte-Carlo methods (Section 4.3.2), with $N = 2 \cdot 10^7$,
- Univariate Reduced Quadrature (URQ) method (Section 4.3.4.5), with a computational cost of $2n + 1$ function evaluations,
- Bivariate Reduced Quadrature (BRQ) method (Section 4.3.4.6), with a computational cost of $2n^2 + 1$ function evaluations,
- First order moments (FOM) method (Section 4.3.3), with a minimal computational cost of $n + 1$ function evaluations to compute the 1^{st} order derivatives„
- Second order moments (SOM) method (Section 4.3.3), with a minimal computational cost of $1 + n + n^2/2$ function evaluations the 2^{nd} order derivatives,
- Stochastic Collocation (SC) method (Section 4.3.5.2), with a computational cost of 3^n function evaluations,

Note that MC mean estimation has the following approximated 95% confidence interval:

$$\left[\mu - 1.96\frac{\sigma}{\sqrt{N}}, \mu + 1.96\frac{\sigma}{\sqrt{N}}\right], \tag{4.140}$$

where N is the sampling size. Another moment estimator confidence intervals can be found in [106], with a lead term in $O(1/N)$.

The four following tables 4.5, 4.6, 4.7 and 4.8 respectively present the mean, the variance, the skewness and the kurtosis estimations, with respect to the method (in columns), for the four test functions f_1 to f_4 (in lines), and with the three different input variances (in lines).

Table 4.5: Mean Estimation for normal input distribution $\mathcal{N}(1, \sigma^2)$.

Function	σ	MC	URQ	BRQ	FOM	SOM	SC
f_1	0.01	2.1439	2.144	2.144	2.048	2.144	2.144
	0.1	3.008	3.008	3.008	2.048	3.008	3.008
	0.3	4.928	4.928	4.928	2.048	4.928	4.928
f_2	0.01	2.535	2.52	2.535	2.5	2.535	2.535
	0.1	2.85	2.73	2.85	2.5	2.85	2.85
	0.3	3.55	3.2	3.55	2.5	3.55	3.55
f_3	0.01	0.5376	0.5385	0.5376	0.54	0.5376	0.5376
	0.1	0.514	0.523	0.514	0.54	0.513	0.514
	0.3	0.465	0.49	0.465	0.54	0.459	0.465
f_4	0.01	3.0487	2.97	3.0487	2.93	3.0481	3.0487
	0.1	4.156	3.33	4.151	2.93	4.1	4.156
	0.3	6.895	4.20	6.81	2.93	6.44	6.93

First let us have a comment on the mean estimation from Table 4.5. As expected that the FOM method is the less accurate method (and also the less costly) and the SC method is the more accurate (and also the more costly). It is however interesting to compare the three other methods. For low input variances, the URQ method produces an output mean almost as accurate as the SOM method, with a really lower cost. The BRQ method offers a really good compromise between cost and accuracy, with results close to the one of the SC method.

Table 4.6: Variance Estimation for normal input distribution $\mathcal{N}(1, \sigma^2)$.

Function	σ	MC	URQ	BRQ	FOM	SOM	SC
f_1	0.01	9.82	9.72	9.72	5.9	7.74	9.82
	0.1	0.627	0.627	0.627	0.59	0.61	0.627
	0.3	57.4	54.8	54.8	17.7	34.3	57.3
f_2	0.01	0.127	0.128	0.127	0.125	0.127	0.127
	0.1	1.48	1.52	1.47	1.25	1.46	1.48
	0.3	6.22	6.39	6.2	3.75	5.62	6.215
f_3	0.01	0.01	0.01	0.01	0.01	0.01	0.01
	0.1	0.0984	0.0946	0.0983	0.1	0.108	0.0985
	0.3	0.285	0.255	0.282	0.3	0.377	0.285
f_4	0.01	0.6596	0.636	0.6592	0.586	0.618	0.6598
	0.1	15.42	11.49	14.71	5.86	9.02	15.41
	0.3	151	81	121	17.6	46	152

For the variance estimation from Table 4.6, the same remarks can be done. We can observe that the FOM and SOM method are really more impacted by the increasing input variance than other methods. We can also observe that the BRQ method has really good

performances even for the function f_4 which produces important output uncertainties.

Table 4.7: Skewness Estimation, with normal input distribution $\mathcal{N}(1, \sigma^2)$.

Function	σ	MC	URQ	BRQ	FOM	SOM	SC
f_1	0.01	2.15	0	1.96	0	1.58	2.12
	0.1	0.74	0	0.71	0	0.72	0.74
	0.3	3.24	0	1.74	0	1.52	3.03
f_2	0.01	0.179	0	0.17	0	0.166	0.179
	0.1	0.8	0	0.55	0	0.43	0.79
	0.3	1.94	0	0.98	0	0.51	1.83
f_3	0.01	0.111	0	0.11	0	0.113	0.111
	0.1	0.272	0	0.226	0	0.32	0.274
	0.3	0.276	0	0.032	0	0.447	0.326
f_4	0.01	0.9795	0	0.9217	0	0.8851	0.9773
	0.1	3.41	0	2.26	0	1.59	3.19
	0.3	5.95	0	2.756	0	1.24	4.73

Concerning the skewness estimation from Table 4.7, we can observe as expected that the URQ and the FOM methods take into account only the first term of the Taylor development of f (Equation (4.69) for FOM and Equation (4.89) for URQ) which is equal to zero here. We also observe that the BRQ method is having troubles when the variance increases, whatever the function is.

Table 4.8: Kurtosis Estimation, with normal input distribution $\mathcal{N}(1, \sigma^2)$, $N = 2 \cdot 10^7$ for the Monte-Carlo (MC) propagation.

Function	σ	MC	URQ	BRQ	FOM	SOM	SC
f_1	0.01	0.86	0	0.17	0	0	0.83
	0.1	7.42	0	0.87	0	0	5.6
	0.3	17	0	1.13	0	0	9.95
f_2	0.01	0.086	0	-0.07	0	0	0.082
	0.1	1.84	0	-0.44	0	0	1.3
	0.3	8.5	0	-0.37	0	0	4.88
f_3	0.01	0.0165	0	0.0165	0	0	0.0156
	0.1	0.165	0	0.146	0	0	0.181
	0.3	0.472	0	0.4	0	0	0.616
f_4	0.01	1.6614	0	0.7703	0	0	1.5817
	0.1	21.29	0	4.9	0	0	14
	0.3	65	0	7.45	0	0	25.66

Finally about the kurtosis estimation from Table 4.8, we observe that the SC method tends to be in trouble when the input variance increases. This illustrates the limits of the BRQ method in the case where the term that contains the 5th-order moment, denoted

by G_i in Equations (4.70), becomes high in comparison to the other terms, i.e. when the higher derivatives of the function have a bigger impact on its Taylor development. Therefore, we obtain the more accurate results only with the function f_3, for which higher order derivatives are not really impacting its Taylor development.

4.3.7.2 Arbitrary Polynomial Chaos

This section is presenting the arbitrary polynomial chaos expansion. We propose to propagate uncertainties through two different polynomial functions. The first one is of degree 2 and the second one of degree 3. For each function, we propagate an uncertainty that is represented by its moments. The first propagation is done assuming that we only know the mean and the variance of the input uncertainty. Therefore, as mentioned in Section 4.3.5.3, we can only use a polynomial expansion of order 1. The second propagation is done assuming we know the mean, the variance, the skewness and the kurtosis of the uncertain input. Therefore we can use a polynomial expansion of order 2. In the following example we select two polynomial functions for which we compute the coefficients of the polynomials analytically, using Equations (4.133) to (4.135).

The graphs from Figure 4.19 are presenting the propagation of the uncertain input Ξ with mean $\mu_\Xi = 1$, variance $\sigma^2_\Xi = 0.4$, skewness $\gamma_\Xi = 0.1$, and kurtosis $\Gamma_\Xi = 0.2$ through the function $f(\xi) = \xi^2 + \xi - 1$. The propagation with the arbitrary polynomial chaos is represented in blue and a Monte-Carlo propagation is presented in red. As expected, the polynomial of order 2 (in the right graph) completely fit the uncertain output $f(\Xi)$, whereas the polynomial of order 1 does not. The graphs from Figure 4.20 is presenting

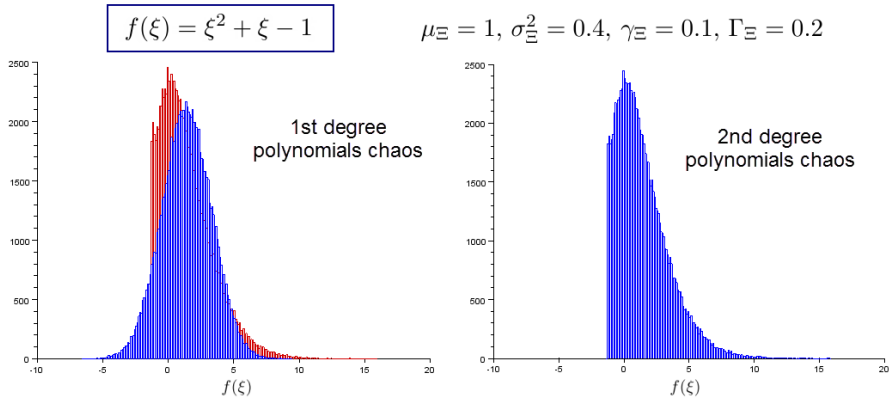

Figure 4.19: Arbitrary polynomials chaos expansion for a polynomial function of degree 2.

the propagation of the uncertain input Ξ with mean $\mu_\Xi = 1$, variance $\sigma^2_\Xi = 0.4$, skewness $\gamma_\Xi = 0.1$, and kurtosis $\Gamma_\Xi = 0.2$ through the function $f(\xi) = 2\xi^3 - \xi^2 + \xi - 1$. It is interesting to observe how the two expansion behave. Once again the first order polynomial does not give account for the skewed output uncertainty, whereas the second order polynomial does. It is interesting to observe the impact of the knowledge of the input uncertainty on the distribution, especially if the objective is to use the distribution to compute some probability or quantile measures (see Chapter 5). Indeed, the computation of a quantile measure from the red sample or from the blue sample can lead to completely different

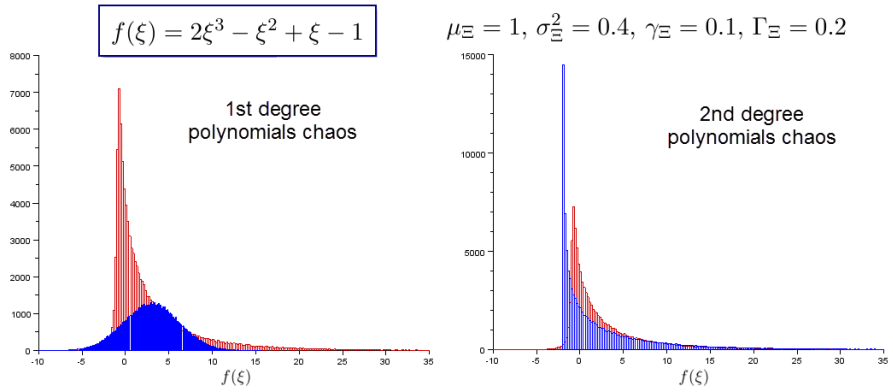

Figure 4.20: Arbitrary polynomials chaos expansion for a polynomial function of degree 3.

values, especially when the available information are only the mean and the variance of the input (left graph from Figure 4.20). In that case it could be interesting not to compute the distribution which would clearly be false, but to compute instead some bounds on the desired risk measure. These techniques are described in Chapter 5.

4.4 Conclusion and choice of the method

We have presented in this chapter various techniques of uncertainty propagation. The focus has been made on non-intrusive methods, for the sake of simplicity and adaptability of the methods to any engineering process. The principal advantage of the presented methods, is to directly produce output uncertainty as functions of input uncertainty and function evaluations. The main objective is to underline for each method what is necessary to compute the output uncertainty in term of knowledge: on the uncertain input, on the process functions, on the required computation time, and on the required accuracy.

Several issues have been raised along the chapter. First of all, one has to identify the available information on the uncertain input so that one can know what kind of uncertain output he will be able to compute. To sum up it can be one of the following, from the lowest to the highest information accuracy:

- the mean and the variance of the distribution;
- the mean, the variance, and higher moments of the distribution;
- the exact nature of the distribution and the corresponding parameters (for example Normal, Beta, Uniform distribution, Beta-Mystic, or else).

According to this available input, the same input can be computed. This chapter also presents the available methods to compute the output uncertainty, according to the available information on the input, but also according to the need of information for the output with the objective of the lowest computational cost. The graph from Figure 4.21 presents the methods that can be used according to the input information and the available output. The abscissa represents the available information on the input, and the ordinates the reachable information on the output. Once the input information is known, the decision

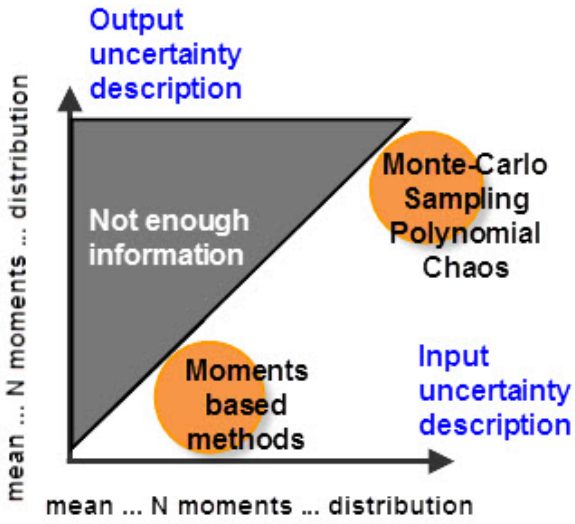

Figure 4.21: Available uncertain output versus available uncertain input: choice of the method [127].

criteria for the choice of the method is a trade between the affordable cost and the required accuracy. It is important to underline here that the error on uncertainty computation is a key for a correct use of the uncertainty afterwards. For instance, for the moments based methods, if we have the first four moments of the input, but we are only interesting in the mean and the variance of the output, the URQ method, or even the SOM method can be sufficient in term of computational cost. It is clear that if higher order moments are required we have to select a more expensive, but more accurate, method (for instance the BRQ or the SC method). The choice of the method is also based on the information on the function, the more regular the function is, the more a low computational cost method can be used. This has been illustrated in the examples of Section 4.3.7.1, where the function type has an important impact on the higher order moments computation. In fact, what can be retained from both the Taylor based approximation of moments, the BRQ and URQ methods, and also the arbitrary polynomial chaos is that computing the uncertain output with only the first four input moments takes into account only the derivatives of order two of the Taylor development of the output function. It follows that a careful attention has to be paid when the higher order derivatives of the output function are significant.

Therefore, limitations of the moments methods come from the available information about output uncertainty. For instance if any information about the order 5 moment of the input uncertainty, Equations (4.67) to (4.70) could be used to compute output moments with a better accuracy, involving order three derivatives. The curse of dimensionality is also one of the main limit of quadrature methods. The required number of function evaluations is significantly increasing as the uncertain input space size is. Then, dimension reduction methods (the URQ and BRQ methods) used to obtain higher order moment from non-linear functions offer very good compromise between cost, accuracy and adaptability according to input available information.

Finally, the example from Section 4.3.7.2 well reflects the attention that has to be paid to the use of the output distribution. As it will be presented in Chapter 5, the output

uncertainty can be used to compute a risk measure in order to solve robust optimization problem, for instance a quantile or a probability. The impact of the input available knowledge on such a risk measure can therefore become considerable (Figure 4.20). The corresponding risk measure will have then to take into account this lack of knowledge on the input uncertainty, some methods are presented in Chapter 5.

To sum up, the choice of the uncertainty propagation method is a question of compromise and carefulness. All the problem parameters have to be delicately taken into account: available information on the uncertain input, available information of the model functions, required accuracy on the uncertain output, cost of the method (number of function evaluations), further use of the uncertain output. This chapter enables the identification of these guidelines that might be helpful particularly for practitioners in the field of optimization under uncertainty.

Chapter 5

Hybrid aircraft Chance Constrained Optimization

Contents

The purpose of this chapter is to present a Chance Constrained Optimization of an unconventional configuration of hybrid-powered-aircraft. Chance-constrained programming is a part of the stochastic programming. A general definition coming from the Stochastic Programming Society is the following one:

Stochastic programming is a framework for modeling optimization problems that involve uncertainty.

It is often opposite to deterministic optimization problem that are formulated with certain parameters. To study the aircraft design uncertain problem, the two following approaches can be of interest:

- uncertainty intervals, or bounds of uncertainty: these approach are managed with robust optimization methods. An introduction of these techniques is presented in Chapter 6, in which we present a robust optimization of an aircraft design according to the models uncertainties. In that case we find a solution of the problem that is feasible whatever the uncertainty.

- the other approach is called stochastic programming. It aims at dealing with uncertainty distributions and allows more freedom when solving the problem. The solution will be feasible in most of the cases, or according to a given probability.

These approaches helped enhancing decision making under uncertainty in many areas. To my best knowledge, stochastic programming first publications appeared around the middle of the 20th century with [49]. An alternative approach namely chance constrained programming, which is presented in this section, appears quite early with [38].

Since then, an important amount of work can be find on stochastic programming, detailing structural properties of such problems (functions log-concavity as in [138, 140], derivative properties [168], Gaussian distribution properties [83], ...), numerical approaches to compute solutions [116, 137], stability and sensitivity of solutions [85], or applications to various areas [97, 57, 68]. A non exhaustive list of publication until 2007, that already counts more than 4000 references about stochastic programming, can be find in [171]. Books from Prékopa [139], Marti [111] or Birge [21] give references on the subject. Recent works from members of the Stochastic Programming society can be found on their website (`http://stoprog.org/resources.php`) and give a large scope of techniques, approaches and examples of the diversity, but also challenges in stochastic programming.

The robustness requirements can be different between the chance constrained programming approach and the robust design approach. It can be probabilities, variability, or both at the same time. The first section is dedicated to the robust design optimization in a general matter, with the description of the main principles and a presentation of some risk measures. The second section presents the chance constrained programming approach, which is the one we select to solve our aircraft design problem. A formulation with bounds on the probability measures from [128, 129] is described. The third section is dedicated to a numerical approach for solving chance constrained optimization problem, namely the Sequential Optimization Reliability Assessment (SORA) method. Some numerical tests are proposed to explain our choice of this method. Finally, the fourth section is presenting the application of these tools to the hybrid aircraft design optimization. The hybrid configuration is compared to a conventional one, both being designed according to the same set of requirements. Results are commented at the end. Some conclusions and perspectives are finally proposed.

5.1 Robust design optimization

It is important to be careful with the terminology as robust design optimization is not necessary equivalent to robust optimization. Even if the notion of robustness is considered in both case, the definition of robust design optimization allows a reliability level as for chance constrained optimization. On the other side, robust optimization often requires a feasible solution whatever the uncertainty is.

The term *Robust Design* was introduced by Taguchi [161] around 1960 with a specific objective: greatly improve engineering productivity by considering what he called "noise factors" of an engineering process (environmental variation, manufacturing variation or some components deterioration). In other terms, he wanted to reduce variability to increase quality and robustness from the first design stage. His method was first based on conventional statistical tools, particularly on design of experiments techniques. Robust design is complementary to the chance constrained approach, and sometimes they share the objective of reducing the sensitivity of the solution with respect to environment fluctuations. Robust design optimization can be divide into two groups:

- Reliability based optimization: the objective is to minimize the failure probability of the solution. This one is close to the chance constrained optimization approach.
- Variance based optimization: the objective is to minimize the variance of the solution.

We could also cite the mean based optimization which consists in minimizing the mean of a function, with a mean constraint satisfaction, but the interest of this approach is null when robustness is concerned. An interesting review of robust design optimization techniques can be found in [19].

The objective of such techniques is illustrated in Figure 5.1. Consider a function with uncertain inputs (ξ_1, ξ_2). The deterministic solution is denoted by a red point and the robust solution by a blue point. The two points are associated with their uncertainty, represented around the point by a disk and with the projection on the x and y axis. The disk represent the set of uncertainty around the point, which means that with a given probability, the red and the blue solutions can take any value in their related disk. We can see that the deterministic solution point (red) lies on the constraint boundary, and that a big part of its uncertainty disk lies in the infeasible domain. It is clearly a non robust solution. The robust solution (blue) satisfies the constraints satisfaction whatever the uncertainty on (ξ_1, ξ_2) is: all the point of its uncertain disk are in the feasible domain. Moreover in this example, the variability of the robust solution is smaller than the one on the deterministic solution.

Let us first define the classic deterministic optimization problem:

$$\left| \begin{array}{ll} \min\limits_{\boldsymbol{x}\in\mathbb{R}^n} & f(\boldsymbol{x}), \\ \text{s.t.} & g_i(\boldsymbol{x}) \leq 0, \quad i = 1, 2, ..., M. \end{array} \right. \tag{5.1}$$

Let $\boldsymbol{\xi}$ be the uncertain input of the model. The corresponding optimization problem under uncertainty is:

$$\left| \begin{array}{ll} \min\limits_{\boldsymbol{x}\in\mathbb{R}^n} & F[f(\boldsymbol{x}, \boldsymbol{\Xi})], \\ \text{s.t.} & G\left[g_i(\boldsymbol{x}, \boldsymbol{\Xi}) \leq 0\right] \geq \alpha_i \quad i = 1, 2, ..., M, \end{array} \right. \tag{5.2}$$

where G and F are measures of robustness, and $(\alpha_i)_{i=1,...,M}$ traduce the robustness requirement. One of the main objective of the robust optimization problem is to define them.

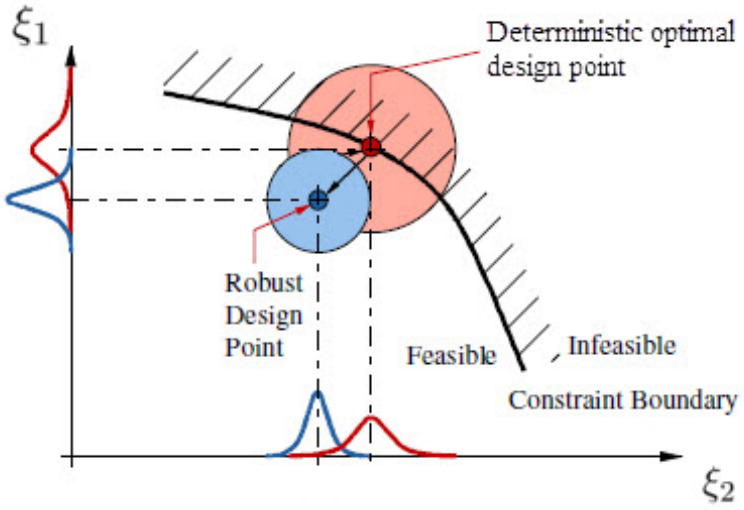

Figure 5.1: Illustration of a deterministic non robust optimum and a robust one.

As an example, let us select the expectation as a robustness measure of the constraints satisfaction, i.e. $G(\cdot) := \mathrm{E}(\cdot)$. This is clearly not a reliable measure: it would mean that the probability of satisfying the constraint is equal to the probability of the constraint not to be satisfied. Nevertheless, sometimes some constraints may have less importance than others and so you can affect a different probability of satisfaction to it. In practice, the function G can be a given probability measure. The function F is classically the expectation $\mathrm{E}\left[f(\boldsymbol{x}, \boldsymbol{\Xi})\right] = \mu_f$ of f or the variance σ_f^2. Since both can be of great interest, a natural way is to introduce a multi-objective optimization [20] with these two objectives. It would then be interesting for instance to draw the related Pareto front. It brings additional freedom when it comes to selecting the optimum, and gives information on the trading cost between two solutions. This choice of the "required robustness" really depends on the user requirement. The inconvenient is that multi-objective optimization could be hard to handle. Hence, another frequently used approach consists in using a combination of μ_f and σ_f^2, such that:

$$F[f] = \mu_f + k\sigma_f^2, \tag{5.3}$$

where the coefficient k varies according to the most important objective, the mean or the variance.

The function G is the risk measure, as it defines the acceptable risk for each constraint. One of the first introduced measure is the mean-variance. It was used in finance [109], but conceptual difficulties have then been raised (see e.g. [37]). These limitations lead to more intuitive risk measures based on distribution quantiles [169]. Among the most used, we find the value at risk, and the conditional value at risk, presented hereafter.

The α-quantile associated with the random variable Ξ is defined by:

$$q_\alpha(\Xi) := \inf\left\{\xi | \mathbb{P}(\Xi \leq \xi) \geq \alpha\right\}, \text{ where } \alpha \in [0, 1]. \tag{5.4}$$

This measure is used in chance constrained programming methods. In this case, the value α represents the chance constrained probability of satisfying a constraint.

The value at risk (VaR) is equivalent to the α-quantile. It was first introduced to reduce financial risk in portfolio management [94], in order to reduce the losses. It is defined by:

$$\mathrm{VaR}_\alpha(\Xi) := \inf\{\xi | \mathbb{P}(\Xi \geq \xi) \leq 1 - \alpha\}, \text{ where } \alpha \in [0, 1]. \tag{5.5}$$

An illustration of the VaR is given in Figure 5.2. In this case, α is the probability that Ξ

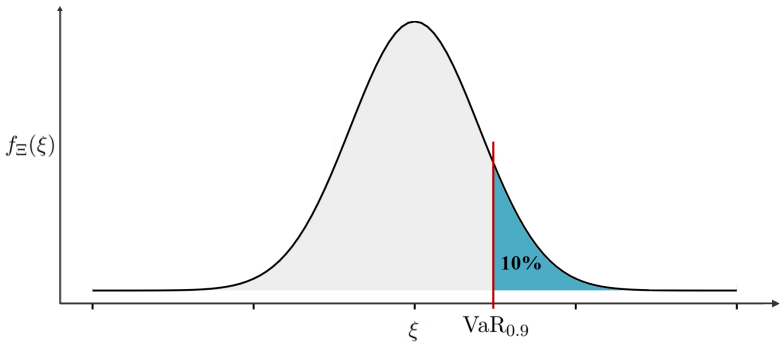

Figure 5.2: Value at risk.

does not overcome the VaR. Some computational and also conceptual limits of VaR are discussed in [9], with a special focus on the accuracy of the behavior of the distribution tail.

This introduces another interesting risk measure: the conditional VaR. It not only presents superior mathematical properties compared to the classic VaR [170], but also offers a different point of view of the robustness principle. The conditional VaR, also named expected shortfall, mean excess loss or tail VaR was introduced in [148] and a review of its benefits can be found in [18]. It has already been used in robust design optimization, e.g. in [128]. The definition of CVaR is:

$$\mathrm{CVaR}_{1-\alpha}(\Xi) := \mathrm{E}\left[\Xi | \Xi \geq \mathrm{VaR}_\alpha(\Xi)\right], \tag{5.6}$$

where $\mathrm{E}\left[\Xi | \Xi \geq \mathrm{VaR}_\alpha(\Xi)\right]$ is a conditional expectation, defined in Chapter 4, Section 4.1.4. An illustration of the CVaR is given in Figure 5.3. The blue part of the distribution area represents the last 10% of Ξ realizations. The CVaR is the value of ξ which corresponds to the expectation of this 10%.

All these risk metrics are of interest and depend on the robustness requirement of the user. However, other risk measures exist [149]. Here we focus only to those presented above, namely the VaR and CVaR. In the case where the solution has to be robust whatever the risk, all the measures can be of interest. The objective of the optimization problem can then be to minimize the maximum value of all the risk measures. Some examples of such applications can be found in [129].

5.2 Chance constrained programming

Among stochastic programming techniques, chance constrained approaches have already proved their efficiency. Applications can be found in finance [35], electrical engineering [105], chemical process studies [84], trajectories modeling [24], etc. This section presents a

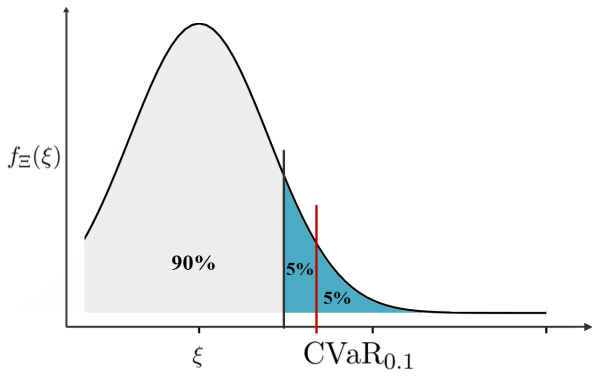

Figure 5.3: Conditionnal Value at risk.

chance constrained programming approach that will be applied to aircraft uncertain design in Section 5.4.

Chance constrained programming consists in solving an optimization problem with a random objective or/and random constraint functions and to replace classical deterministic constraints by probabilities of these constraints to reach a given value. This can be separated in two cases:

- the individual chance constraints case, where different probabilities are affected to each constraint satisfaction. Problem (5.2) can then be expressed as:

$$\left| \begin{array}{ll} \min\limits_{\boldsymbol{x}\in\mathbb{R}^n} & \mathrm{E}[f(\boldsymbol{x},\boldsymbol{\Xi})] \\ \text{s.t.} & \mathbb{P}\big[g_i(\boldsymbol{x},\boldsymbol{\Xi}) \leq 0\big] > \alpha_i, \text{ where } \alpha_i \in [0,1],\ \forall i = 1,\ldots,M. \end{array} \right. \tag{5.7}$$

- The joint constraints case: the only constraint is the probability that all deterministic constraints are satisfied. Problem (5.2) then becomes:

$$\left| \begin{array}{ll} \min\limits_{\boldsymbol{x}\in\mathbb{R}^n} & \mathrm{E}[f(\boldsymbol{x},\boldsymbol{\Xi})] \\ \text{s.t.} & \mathbb{P}\big[g_i(\boldsymbol{x},\boldsymbol{\Xi}) \leq 0,\ \forall i = 1,\ldots,M\big] > \alpha, \text{ where } \alpha \in [0,1]. \end{array} \right. \tag{5.8}$$

In the above expressions, we assume that:

- $f, g_i : \mathbb{R}^n \times \Omega \to \mathbb{R}$ are at least differentiable with respect to $\boldsymbol{x} \in \mathbb{R}^n$,
- $\boldsymbol{x} \in \mathbb{R}^n$ is the deterministic (certain) optimization variable,
- $\boldsymbol{\Xi} \in \Omega \subset \mathbb{R}^p$ is a vector of random variables,
- $\mathbb{P}(.)$ defines the probability operator,
- $\mathrm{E}[.]$ defines the expectation operator,
- $\alpha, (\alpha_i)_{i=1,\ldots,M}$ define reliability levels, in practice equal to 0.95 or 0.99.

An illustration of an individual chance constraints problem is given in Figure 5.4. The constraint g_i is evaluated at various design points, x_1, x_2 and x_3, according to some uncertainties ξ_1 and ξ_2. The constraints are uncertain. Given a requirement $g_i^{\max}$ (which

is the deterministic constraint bound, i.e. zero in the case of Problem 5.7), we can see in the output part of Figure 5.4 that each design point leads in an uncertain output y_j. We can then calculate the probability of satisfying the constraint $g_i(\boldsymbol{x}, \boldsymbol{\xi}) \leq g_i^{max}$ and the probability requirement α_i to satisfy the constraint will then replace the deterministic constraint.

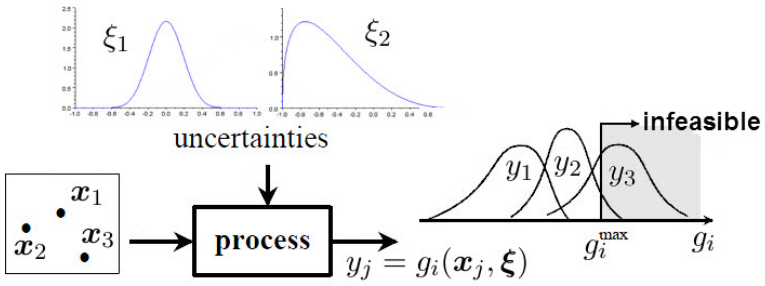

Figure 5.4: Uncertain process: feasibility of an uncertain constraint.

Focus will not be made here on structural properties of such problems, as in practice functions f and g_i are black boxes that can eventually be provided with their gradient. The joint constraints approach, which is not used in our studies, generally offers a better robustness than the individual constraints approach [81], but it can be more difficult to handle since the related output distributions are multidimensional ones. We can also notice the crucial role of the distributions properties in several approaches [83, 4]. For example when the distributions are Gaussian ones, the problem structure can become easier to manage.

However in our case, problem structure is not well defined and distributions, if they are known, are not necessary Gaussian. Techniques to solve problems without regularity assumptions are often only heuristics with no proofs of optimality.

In our case, we have information on the input distributions $\boldsymbol{\Xi}$ but not on the distribution of $g_i(\boldsymbol{x}, \cdot)$. This has then to be determined using some uncertainty propagation methods (see Chapter 4). Once the output uncertainty distribution is assessed, the probability of satisfying the constraint $\mathbb{P}(g_i(\boldsymbol{x}, \boldsymbol{\xi}) \leq 0)$ can be retrieved from the cumulative distribution function. Finally the optimization algorithm can be selected among those presented in Chapter 2. When input uncertainties are not entirely known, e.g. when one has only first moments of the distribution $\boldsymbol{\Xi}$, some techniques of robust design optimization still allow to find robust solutions. The main idea is to consider a family of distributions that have the properties brought by the available information. Then the goal is to compute a worst case from all the considered distributions. This has to be done according to the studied risk measure, after a reformulation of the problem.

5.2.1 Reformulation of a chance constrained optimization problem

Assume that the objective of the optimization is to minimize the expectation of f with respect to risk measure constraints, selected among the above two. It can be written:

$$\left|\begin{array}{ll} \min\limits_{\boldsymbol{x}\in\mathbb{R}^n} & \mathrm{E}[f(\boldsymbol{x}, \boldsymbol{\Xi})] \\ \text{s.t.} & \text{or } \mathbb{P}(g_i(\boldsymbol{x}, \boldsymbol{\Xi}) \leq 0) > \alpha_i,\ i = 1, \ldots, M. \\ & \text{or } \mathrm{E}\left[g_i\left(\boldsymbol{x}, \boldsymbol{\Xi}\right) | g_i\left(\boldsymbol{x}, \boldsymbol{\Xi}\right) \geq \mathrm{VaR}_{\alpha_i}\left[g_i\left(\boldsymbol{x}, \boldsymbol{\Xi}\right)\right]\right] \leq 0,\ i = 1, \ldots, M. \end{array}\right. \tag{5.9}$$

And we have the following equivalences:

$$\begin{aligned} \mathbb{P}(g(\boldsymbol{x}, \boldsymbol{\Xi}) \leq 0) > \alpha \quad & \Leftrightarrow q_\alpha \left(g\left(\boldsymbol{x}, \boldsymbol{\Xi}\right)\right) < 0 \\ & \Leftrightarrow \mathrm{VaR}_\alpha \left(g\left(\boldsymbol{x}, \boldsymbol{\Xi}\right)\right) < 0. \end{aligned} \tag{5.10}$$

In the case where uncertainties are not exactly known, a methodology exists that take into account some available informations, according to the risk measure we want to minimize. The following section describes this methodology, which is based on a reformulation of the risk constraints.

5.2.2 Bounds on the risk measures

Normality is one of the property that comes to mind when talking about distributions. In design optimization the assumption of normality for input distributions is current. Some transformations can also be made in order to obtain this normality (e.g. Box-Cox transformation from [29]). Then, in the simple case where functions of the process are linear, output uncertainties $g_i(\boldsymbol{x}, \boldsymbol{\Xi})$, are going to be normal. However, when processes are not linear, there is no reason for obtaining normal distributions. The normality assumptions about the output can even have an impact on the solution, e.g. by underestimating the robustness constraint [129].

Here, we want to compute either a value at risk (equivalent to a quantile), either a conditional VaR, both with a given level of reliability $\alpha \in [0, 1]$. The goal is to compute these measures. When the distributions are known, these measures can be analytically computed by using their definitions that can be found in Chapter 4. However, when the distributions are not fully known, we have to find their best approximation, or to find bounds on their value, according to the available information.

Here, we assume we can obtain the following information on the output distribution constraint $g(\boldsymbol{\Xi})$, by using one of the uncertainty propagation methods presented in Chapter 4:

- the first two moments μ_g and σ_g are known, or
- the first four moments μ_g, σ_g, γ_g and Γ_g are known.

In the case where the first two moments are known, Cantelli inequality [133] states that:

$$\mathbb{P}\left[g(\boldsymbol{\Xi}) - \mu_g \geq k\sigma_g\right] \quad \leq \frac{1}{1 + k^2}, \tag{5.11}$$

where k is a real number depending on the required probability level α. It can be rewritten as:

$$\begin{aligned} & \mathbb{P}\left[g(\boldsymbol{\Xi}) \geq \mu_g + k\sigma_g\right] \quad \leq 1 - \alpha, \\ \Leftrightarrow \quad & \mathbb{P}\left[g(\boldsymbol{\Xi}) \leq \mu_g + k\sigma_g\right] \quad \geq \alpha, \end{aligned} \tag{5.12}$$

where: $\alpha = \frac{1}{1+k}$, or equivalently $k = \sqrt{\frac{\alpha}{1-\alpha}}$. Then the probability constraint $\mathbb{P}\big(g_i(\boldsymbol{x}, \boldsymbol{\Xi}) \leq 0\big) > \alpha_i$ can be replaced in a conservative way by:

$$\mu_{g_i}(\boldsymbol{x}) + k(\alpha_i)\sigma_{g_i}(\boldsymbol{x}) \leq 0, \tag{5.13}$$

as Inequality (5.13) implies Inequality (5.12). However this approach can be too conservative [124], and then not well adapted to accurate robust design. For instance when some

properties of the distribution are known (normality, unimodalilty, ...), using the above approximation (5.13) leads to overestimate the constraint. Hence, applying the extensions of the Cantelli inequality [156], it is possible to use the known properties of the distribution to reduce the conservatism of this approximation. These properties can be select among the following ones:

- bounded support, or
- symmetry, or
- unimodality, or
- symmetry and unimodality, or
- normality.

The work from [129], that merges researches from [135, 36, 63], uses some generalizations of the Cantelli inequality to assess the best probability bound according to the above properties of the distribution, assuming the mean and the variance are known. Note that this work also includes the probability bound when the probability measure is the CVaR. Results are presented in Table 5.1.

In the case where the first four moments are available, with no particular distributional assumptions [90], Table 5.2 present the value of k with respect to the required probability measure.

To sum up, this section gives a way for computing bounds on risk measures according to the available information on the input distributions. This approach ensures robustness of the solution in a conservative manner.

This allows to replace the probability constraints:

$$G\big(g_i(\boldsymbol{x}, \boldsymbol{\Xi}) \leq 0\big) \leq \alpha_i, \tag{5.14}$$

by the deterministic constraint:

$$\mu_{g_i}(\boldsymbol{x}) + k(\alpha_i)\sigma_{g_i}(\boldsymbol{x}) \leq 0. \tag{5.15}$$

Coefficient $k(\alpha_i)$ is defined according to the desired risk measure G, the desired level of reliability α_i and the information on the distribution properties, according to Tables 5.1 and 5.2. The adaptability of this approach is of great interest for the formulations of robust design constraints.

Once the problem is reformulated with the constraint (5.15), a classical approach is to apply well-suited deterministic optimization algorithms, see Section 2.3. However the computational time of this approach depends not only on the number of iterations of the optimization algorithm, but also on the computation of the expectation, variance, skewness and kurtosis, when required, of each constraint at each iteration. In the case where the latter computation has a too important cost, some other methods should be applied.

5.3 S.O.R.A. method

In this section, we present a methodology for robust design optimization, which consists in solving a sequence of deterministic optimization problems, without computing the uncertainty at each iteration. An adaption of this method with the risk measure bounds presented above is developed.

Table 5.1: Value of k for VaR and CVaR upper bounds with known μ_g and σ_g.

Validity	VaR	CVaR
No distributional assumption $0 \leq \alpha \leq 1$	$k = \sqrt{\frac{\alpha}{(1-\alpha)}}$	
Bounded support: $y \in [a, b]$ $0 \leq \alpha \leq \frac{1}{1+k_a^2}$ $\frac{1}{1+k_a^2} \leq \alpha \leq \frac{k_b^2}{1+k_b^2}$ $\frac{k_b^2}{1+k_b^2} \leq \alpha$	$k = \frac{k_a(k_a+k_b)\alpha}{(k_a+k_b)(1-\alpha)-k_a}$ $k = \sqrt{\frac{\alpha}{(1-\alpha)}}$ $k = k_b$ with: $k_a = \frac{\mu_g - a}{\sigma_g}$ and $k_b = \frac{b-\mu_g}{\sigma_g}$ and $k_a k_b \geq 1$	$k = \frac{k_a \alpha}{(1-\alpha)}$
Symmetry $0 \leq \alpha \leq \frac{1}{2}$ $\frac{1}{2} \leq \alpha < 1$	$k = 0$ $k = \frac{1}{\sqrt{2(1-\alpha)}}$	$k = \frac{\sqrt{\alpha}}{\sqrt{2}(1-\alpha)}$
Unimodality $0 \leq \alpha \leq \frac{5}{6}$ $\frac{5}{6} \leq \alpha < 1$	$k = \sqrt{\frac{3\alpha}{3\alpha-2}}$ $k = \sqrt{\frac{9\alpha-5}{9(1-\alpha)}}$	NA NA
Symmetry and Unimodality $0 \leq \alpha \leq \frac{1}{3}$ $\frac{1}{3} \leq \alpha \leq \frac{1}{2}$ $\frac{1}{2} \leq \alpha \leq \frac{2}{3}$ $\frac{2}{3} \leq \alpha < 1$	$k = 0$ $k = \sqrt{\frac{2}{9(1-\alpha)}}$	$k = \frac{2\sqrt{\alpha}}{3(1-\alpha)}$ $k = \sqrt{3}\alpha$ $k = \frac{2}{3\sqrt{1-\alpha}}$
Normality (exact value) $0 \leq \alpha \leq 1$	$k = \Phi^{-1}(\alpha)$	$k = \frac{\phi(\Phi^{-1}(\alpha))}{1-\alpha}$
	where Φ is the PDF of the standard Gaussian variable and ϕ its CDF.	

The S.O.R.A. method, for Sequential Optimization and Reliability Assessment, was introduced by Du and Chen [56], and improved in [183]. It was developed in order to uncouple the reliability analysis required for a robust optimization, from the optimization. It has the particularity to only solve a sequence of simple deterministic optimization problems while taking into account a given requirement of reliability. Since chance constrained optimization is sometimes hard to solve, because of the lack of regularity of the risk measures, or because of the computational time required for uncertainty computation, the sequential

Table 5.2: Value of k for VaR and CVaR upper bounds with known μ_g, σ_g, γ_g and Γ_g.

Validity	VaR	CVaR
$0 \leq \alpha < \frac{1}{2}\left(1 + \frac{\gamma_g}{\sqrt{\gamma_g^2+4}}\right)$	$W\left(V\left(k_y\right)\right) = \alpha$	$k_y = -\frac{\alpha}{1-\alpha} V\left(k_y\right)$
$\frac{1}{2}\left(1 + \frac{\gamma_g}{\sqrt{\gamma_g^2+4}}\right) < \alpha < 1$	$W\left(k_y\right) = 1-\alpha,$ with: $R(u) = \gamma_g Q(u) + \Delta u$, $S(u) = Q(u) + \Delta u$, $Q(u) = 1 + \gamma_g u - u^2$, $\Delta = \Gamma_g - \gamma_g^2 - 1$, $W(u) = \frac{\Delta}{Q^2(u) + \Delta(1+u^2)}$, $V(u) = \frac{R(u) - \sqrt{R^2(u) + 4Q(u)S(u)}}{2Q(u)}$.	

method approach allows to manage these drawbacks.

The principle of the method is described in Figure 5.5. We want to solve the following chance constrained optimization problem (we choose here the VaR risk measure but the methodology can be applied with any measure with computable bounds):

$$\left| \begin{array}{ll} \min\limits_{\boldsymbol{x} \in \mathbb{R}^n} & f(\boldsymbol{x}, \mu_{\boldsymbol{\Xi}}) \\ \text{s.t.} & \mathbb{P}\left[g_i(\boldsymbol{x}, \boldsymbol{\Xi}) \leq 0\right] > \alpha_i,\ i = 1, \ldots, M. \end{array} \right. \tag{5.16}$$

Here, we assume without a loss of generality that the minimization of $f(\boldsymbol{x}, \mu_{\boldsymbol{\Xi}})$ is equivalent to the minimization of $\mathrm{E}\left[f(\boldsymbol{x}, \boldsymbol{\Xi})\right]$. Let us first introduce the thresholds s_i, $i = 1, \ldots, M$. They will ensure the robustness of the solution by a smart modification of the inequality constraints g_i, $i = 1, \ldots, M$. The principle of the method is the following one:

- **Step 1**: set the thresholds s_i equal to zero, and set the vector of uncertain input $\boldsymbol{\Xi}$ equal to its mean $\mu_{\boldsymbol{\Xi}}$. Then do step 2 to 5 while the solution does not satisfy the required robustness level evaluated at step 4.
- **Step 2**: run a first deterministic optimization, a solution $\boldsymbol{x}_{sol}$ is obtained.
- **Step 3**: compute the output uncertainties $g_i(\boldsymbol{x}_{sol}, \boldsymbol{\Xi})$ using a propagation technique (see Chapter 4). From these uncertainties, evaluate the probability constraint $\mathbb{P}\left[g_i(\boldsymbol{x}_{sol}, \boldsymbol{\Xi}) \leq 0\right]$.
- **Step 4**: if this value is satisfying the robustness criteria, i.e. if: $\mathbb{P}\left[g_i(\boldsymbol{x}_{sol}, \boldsymbol{\Xi}) \leq 0\right] \geq \alpha_i$, then it means that the solution is robust for the considered constraint. if it is not, compute λ_i according to the required level of robustness α_i of the constraint g_i, so that the threshold $s_i = s_i - \lambda_i$. This is usually computed assuming g_i is following a Gaussian distribution, by:
$$\lambda_i = \Phi^{-1}(\alpha_i)\sigma_{g_i}, \tag{5.17}$$
where Φ is the PDF of the standard Gaussian law.
- **Step 5**: go to step 2 with the new s_i.

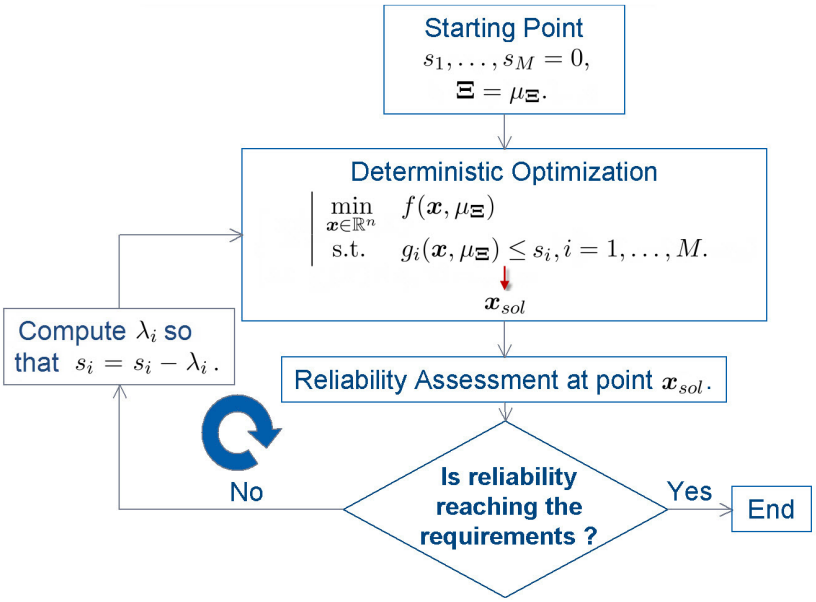

Figure 5.5: S.O.R.A method principle

5.3.1 Improvement with the risk measure bounds

Classically the reliability assessment is computed using the Most-Probable Point (MPP) approach presented in [55]. The concept of the MPP is to find the point that contributes the most to the integral for probability estimation and to evaluate the probability of the called limit state function $g_i(\boldsymbol{x}_{sol}, \boldsymbol{\Xi})$ to be less or equal to zero. The concept of MPP raises limitations as mentioned in [8], with some non-sense examples of application.

Here, we choose to apply a reliability assessment based on what is done in [92]. However it is a good method but only when uncertainties are supposed to follow normal distributions. We propose then the following extension when uncertainties are not necessary known or when we only have information on their properties, or their first moments. Following the results from Section 5.2.2, we compute λ_i (see Figure 5.5) such that:

$$\lambda_i = k(\alpha_i)\sigma_{g_i}, \tag{5.18}$$

where $k(\alpha_i)$ depends on the properties of the distribution, on the required risk measure and on the required robustness level α_i, according to Tables 5.1 and 5.2. Doing so, the conservative property of the bounds is kept and it avoids to underestimate the reliability of the solution. Moreover, this approach allows to have an accurate reliability assessment according to the level of information on the distributions.

5.3.2 Numerical example

This section presents an example application of S.O.R.A. method compared to classical methods of chance constrained optimization. The Rosenbrock function is a non-convex function defined from $\mathbb{R}^2$ to $\mathbb{R}$ by:

$$f(x_1, x_2) = (1 - x_1)^2 + 100(x_2 - x_1^2)^2. \tag{5.19}$$

It has a global minimum at $(x_1, x_2) = (1, 1)$, where $f(x_1, x_2) = 0$. We add the following arbitrary constraints:

$$\left| \begin{array}{l} g_1(x_1, x_2) \leq 0, \\ g_2(x_1, x_2) \leq 0, \end{array} \right. \tag{5.20}$$

where:

$$\left| \begin{array}{l} g_1(x_1, x_2) = (x_1 + 1)^2 + (x_2 - 0.3)^2 - 1, \\ g_2(x_1, x_2) = -0.05 - 2x_1 - 0.8x_2 - 0.01 f(x_1, x_2). \end{array} \right. \tag{5.21}$$

We denote $\boldsymbol{x} = (x_1, x_2)$. The deterministic constrained optimization problem is defined by:

$$\min_{\boldsymbol{x} \in \mathbb{R}^2} f(\boldsymbol{x}) \text{ s.t. } \left| \begin{array}{l} g_1(\boldsymbol{x}) \leq 0, \\ g_2(\boldsymbol{x}) \leq 0. \end{array} \right. \tag{5.22}$$

We select a Sequential-Quadratic-Programming method (see Chapter 2) to solve this problem. We then introduce the uncertainty $\boldsymbol{\Xi} = [\Xi_1, \Xi_2, \Xi_3, \Xi_4]$ on the objective and the constraint functions, which become:

$$\left| \begin{array}{l} f(\boldsymbol{x}, \boldsymbol{\xi}) = (\xi_1 - x_1)^2 + 100(x_2 - x_1^2)^2 \xi_2, \\ g_1(\boldsymbol{x}, \boldsymbol{\xi}) = (x_1 + \xi_3)^2 + (x_2 - 0.3\xi_3)^2 - 1, \\ g_2(\boldsymbol{x}, \boldsymbol{\xi}) = -0.05 - 2x_1 - 0.8x_2 \xi_4 - 0.01 f(x_1, x_2) \xi_4. \end{array} \right. \tag{5.23}$$

And so we have the following chance constrained optimization problem:

$$\min_{\boldsymbol{x} \in \mathbb{R}^2} \mathrm{E}\left[f(\boldsymbol{x}, \boldsymbol{\Xi})\right] \text{ s.t. } \left| \begin{array}{l} \mathbb{P}\left[g_1(\boldsymbol{x}, \boldsymbol{\Xi}) \leq 0\right] > 0.95, \\ \mathbb{P}\left[g_2(\boldsymbol{x}, \boldsymbol{\Xi}) \leq 0\right] > 0.95. \end{array} \right. \tag{5.24}$$

We assume all the uncertain input are independent and we only know their first four moments. We select the same moments for all the uncertain input:

$$\begin{aligned} &\mu = 1, \\ &\sigma^2 = 0.0002778, \\ &\gamma = 0.8, \\ &\Gamma = 1. \end{aligned}$$

We propose to solve Problem (5.24) by using a classical method, such as the one presented in Section 5.2.2. In this case, the probabilistic constraints are replaced by their corresponding bounds (see Table 5.2). The optimizer used is the same as for the deterministic case. Note that in this case, at each iteration of the optimization process the uncertainty on the constraints is computed. We compare this method to the S.O.R.A. approach for which the uncertainty analysis is uncoupled from the optimization.

Results are presented in Table 5.3.

We observe that the two robust optimum are very close to each other. The deterministic optimum and the robust one are drawn on Figure 5.6, with the deterministic constraints. In order to validate the results, we put in Table 5.3 the probability that the constraints are satisfied at each solution. To do that, we select a family of distributions, here the Beta-Mystic, and we draw a Beta-Mystic distribution that has the four input moments. We obtain the one presented in Figure 5.7. Then we also draw an Beta-Mystic distribution with the first four propagated moments of each constraint at the solution points. We obtain the distribution presented in Figure 5.8.

Table 5.3: Results of a chance constrained optimization of the Rosenbrock function using a classical method and the S.O.R.A. method.

	Deterministic Optimization	**Chance Constrained with FSQP**	**Chance Constrained with SORA**
$x1_{opt}$	-0.416	-0.4590	-0.4587
$x2_{opt}$	-1.112	-1.123	-1.123
$\mathrm{E}\left[f(\boldsymbol{x}, \boldsymbol{\Xi})\right]$	167	179.98	179.92
$\mathbb{P}\left[g_1(\boldsymbol{x}, \boldsymbol{\Xi}) \leq 0\right]$	0.55	0.992	0.992
$\mathbb{P}\left[g_2(\boldsymbol{x}, \boldsymbol{\Xi}) \leq 0\right]$	0.44	0.999	0.999
Number of function calls	138	2089	491

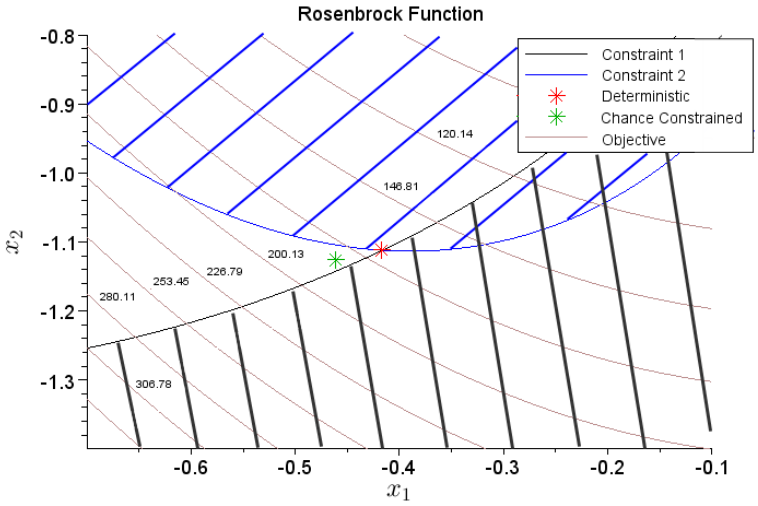

Figure 5.6: The Rosenbrock constrained function optimization: Comparison of deterministic & Chance constrained Optima.

As expected, the deterministic solution is not robust, as it is satisfied with a probability lower than the required value of 0.95. This illustrates the importance of taking into account the uncertainty when a robust optimum is required. The table also present the "cost" of this robustness, which is the highest value of the objective function.

Another interesting observation is the difference of call to the functions. As we could expect, the deterministic optimization is clearly less computationally expensive than the two chance constrained optimization. We also notice that the cost of the S.O.R.A. method is lower than the the classical method, with a same solution accuracy. The improvement of S.O.R.A. with the probability bounds then shows in this illustration that it gives the same results as for a classical method, but with a more affordable computational cost.

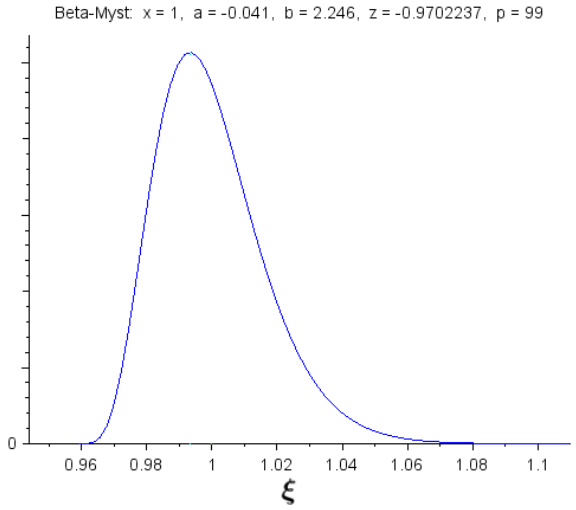

Figure 5.7: Uncertain input distribution, using a Beta-Mystic and the first four moments.

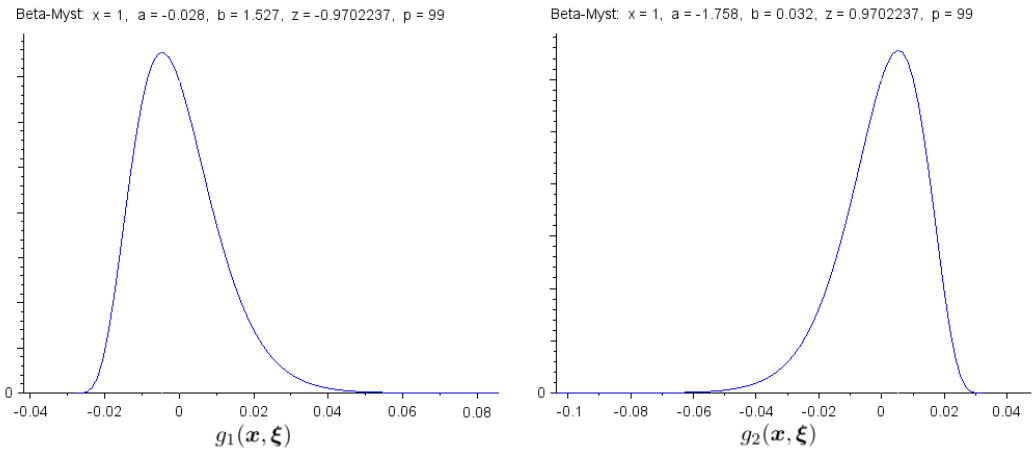

Figure 5.8: Uncertain constraints distributions at the robust solution point, using a Beta-Mystic and the first four moments.

5.4 Hybrid aircraft chance constrained optimization

This section presents an application of the improved S.O.R.A. method to a chance constrained optimization of an hybrid aircraft design.

The first objective is to compare the performances of the hybrid aircraft versus the ones of a conventional aircraft, given a same set of requirements and specifications. The first work around the chance constrained optimization of the hybrid aircraft [141], shows that current technologies values on the performances of the electric part of the propulsion system are not good enough to obtain an hybrid aircraft at least competitive versus the conventional one. Since research activities on the electric propulsion systems, are in constant progress, we decide to compare the performances of the hybrid aircraft versus the

conventional aircraft in the next years. We also have in mind that the technologies of the conventional will progress and get its performances better. Since the hybrid configuration basis is a conventional aircraft to which we add the electric fan, the battery, and the electric generator, we assume that any improvement on the conventional aircraft will also apply to the hybrid one.

The second objective of the study is to take into account the uncertainties linked to the evolution of the technologies used to hybridize the aircraft, such that the optimum hybrid aircraft is robust versus the constraints with respect to a given high probability.

The hybrid and conventional aircraft configuration and design process are described in the first section. The second section is dedicated to the uncertainties coming from the technologies evolution. We proposed in the third section a formulation of a chance constrained optimization problem to find when the hybrid aircraft will be competitive versus the conventional one, with a probability of 0.95.

5.4.1 Conventional and hybrid aircraft configuration

We first select the baseline aircraft for both the conventional and the hybrid configuration. It is described by the parameters of Table 5.4.

Table 5.4: Description of the baseline aircraft specifications.

Name	**Value**
Number of Passengers (Npax)	180
Design Range	3000 NM
Cost Mission Range	500 NM
Number of Turbofan Engine	2

Then we set the specifications, that mainly are the operational constraints, and are described in Table 5.5.

Table 5.5: Description of the aircraft design specifications for the conventional and the hybrid configuration.

		Name	**Value**
Conventional	1	Approach Speed (LdSpeed)	< 130 kt
	1	Climb Vz Ceiling (ClbVz)	> 500 ft/min
	2	Cruise Vz Ceiling (CrzVz)	> 300 ft/min
	3	Take-Off Field Length 1	< 1800 m
	4	Take-Off Field Length 2 (in high and hot conditions)	< 2500 m

The hybrid aircraft concept is the one presented in Chapter 1, Section 1.3.4. The main characteristics of this concept are recalled:

- it has two conventional thermal engines and an electric fan in its rear fuselage, as illustrated in Figure 5.9. The electric fan size is set to 1.5m.

- It has an accurate use of the additional energy brought by the electric fan and some accumulators during the different flight phases (see Chapter 1, Section 1.3.4).

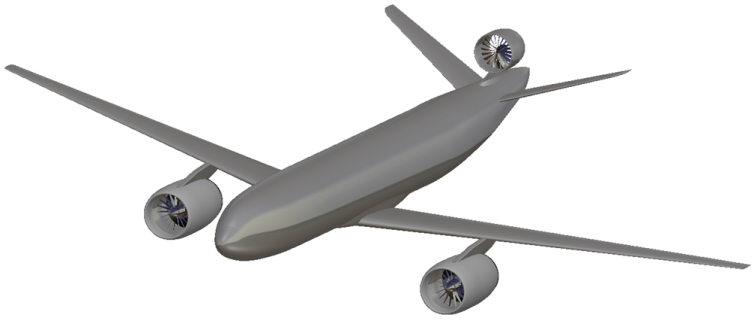

Figure 5.9: Hybrid Aircraft Configuration for the chance constrained optimization study.

We select the design variables presented in Table 5.6 to run the chance constrained optimization.

Table 5.6: Optimization Variables for conventional aircraft configuration, with the additional ones for the hybrid aircraft configuration.

	n (conv.)	n (hyb.)	**Name**	**Bounds**	**Unit**
	1	1	Wing Area	$[100, 250]$	m^2
	2	2	Sea Level Static Thrust	$[6000, 15000]$	daN
	5	8	Wing Aspect Ratio	$[8, 18]$	no dim.
	6	9	Thermal engine BPR	$[8, 14]$	no dim.
	7	10	Top of climb altitude	$[25000, 45000]$	ft
	8	11	Cruise Mach	$[0.6, 0.85]$	Mach
Conventional		6	Generator Electric Ratio	$[0.01, 0.1]$	no dim.
Hybrid		7	Electric Fan Power	$[1, 4]$	MW

5.4.2 Preliminary uncertainty analysis

The models developed for the aircraft design process are presented in Chapter 1. They are semi-empirical models. We can assume, according to expert know-how, that the uncertainties coming from the masses, the geometry, the thermal engines, and the mission models are of the same magnitude for the hybrid and the conventional aircraft. After some sensitivity studies, we observe that the most impacting uncertainties are the one coming from the prediction models of the hybridization technologies. They are the power density of electrical engine and the power density of electrical generator (EPD), and the energy density of accumulators (EED). Thanks to several assumptions found in literature [158, 48], we model the evolution of these values as a function of the year. This is presented in Figure 5.10). The assumptions proposes a best and a worst evolution cases. From this, we

quantify the uncertainties coming with the prediction models, which is increased with the year. We proposed to represent this uncertainty by a Normal distribution. For instance, in 2025 we have the distributions represented in Figure 5.11. We also represent in FIgure 5.10 the 0.99-quantile and the 0.01-quantile measure as function of the year.

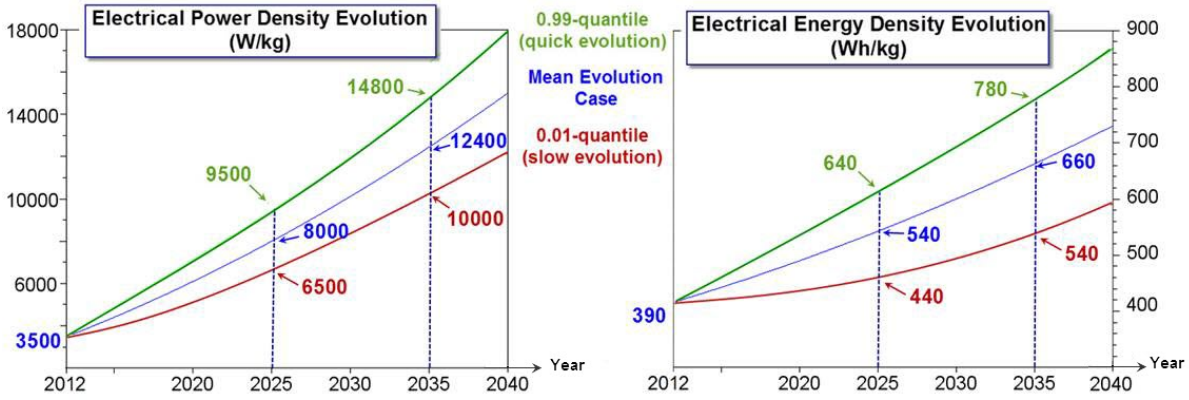

Figure 5.10: Prediction functions for the electrical power density evolution and the electrical energy density evolution, with their uncertainties.

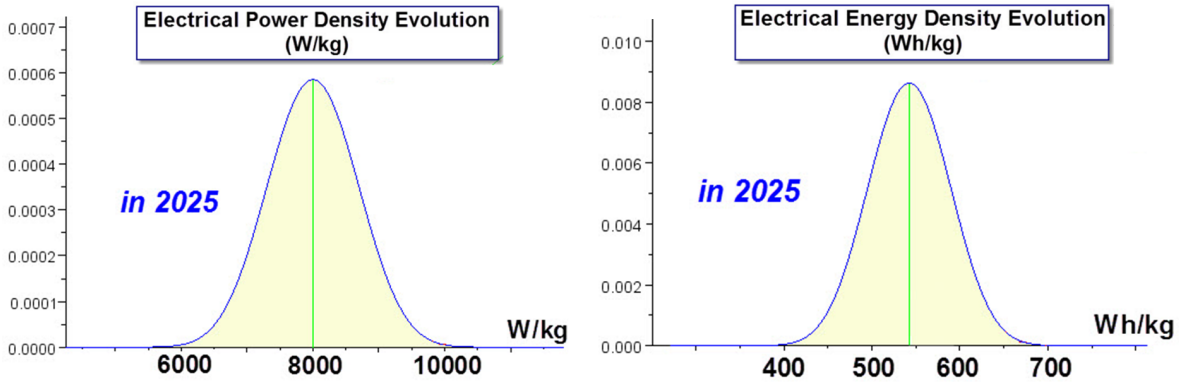

Figure 5.11: Prediction functions for the electrical power density evolution and the electrical energy density evolution, with their uncertainties.

5.4.3 Formulation of the aircraft design problem

Now that the uncertainties are defined and the models described, we propose the following approach to run the chance constrained optimization of the hybrid aircraft. The goal is to find the closest year from now when the hybrid aircraft will have the same performances than the conventional one with a 0.95 probability, with respect to the uncertainties on the technologies evolution. Moreover, we also want to ensure that the same set of requirements (defined in Table 5.5) with a 0.95 probability, with respect to the same uncertainties. The performances are compared according to the criteria defined in Table 5.7.

Table 5.7: List of the performances criterion.

Name	Unit
Mission Block Fuel	kg
Cash Operating Cost (COC)	\$/trip
Absolute Pulsed Global Warming Potential (APGWP)	$W/m^2/km/year$

Since we want to compare the optimal criterion of the hybrid aircraft design to the one of the conventional aircraft, the first step is to obtain the optimal value of the selected criterion, that can be reached by the conventional aircraft. Since we only take into account in this study the uncertainties from the hybridization technologies evolution, we decide to solve a deterministic optimization of the design of the conventional aircraft. The problem is:

$$\left| \begin{array}{ll} \min\limits_{\boldsymbol{x}\in\Omega^n} & f(\boldsymbol{x}) \\ \text{s.t.} & g_i(\boldsymbol{x}) \leq 0,\ i = 1, \ldots, M, \end{array} \right. \tag{5.25}$$

where f is representing one of the objective of Table 5.7, $\boldsymbol{x}$ is the vector of the variables from Table 5.6 (the conventional case), Ω^n is the Cartesian product of the intervals of definition of each variables, and g_i are the constraints from Table 5.5 (also for the conventional case).

Once Problem (5.25) is solved, we have the optimal criteria value of the conventional aircraft, namely f^*_{conv}. We propose to solve the following chance constrained optimization of the hybrid aircraft design:

$$\left| \begin{array}{ll} \min\limits_{\boldsymbol{x}\in\Omega^{n+1}} & Y(\boldsymbol{x}) = \text{Year} \\ \text{s.t.} & \mathbb{P}\left[g_i(\boldsymbol{x}, \boldsymbol{\Xi}) \leq 0\right] \geq 0.95,\ i = 1, \ldots, M, \\ & \mathbb{P}\left[f(\boldsymbol{x}, \boldsymbol{\Xi}) \leq f^*_{conv}\right] \geq 0.95, \end{array} \right. \tag{5.26}$$

where Y is representing the year, which is driving the technologies maturity as presented in Figure 5.10, f is representing one of the objective of Table 5.7, $\boldsymbol{x}$ is the vector of the variables from Table 5.6 (the hybrid case), g_i are constraints from Table 5.5 (also for the hybrid case), and $\Omega^{n+1} = \Omega^n \times [2015, +\infty]$. The additional input variable is the year.

The whole process is summarized in Figure 5.12. We select a surrogate based optimization algorithm, based on Kriging surrogate and the FSQP optimization method, to run the optimizations.

5.4.4 Chance constrained optimization results

We propose to run the optimization process for the three following objective functions f of Table 5.7, the Block Fuel, the COC, and the APGWP. We present the results in Figure 5.13. The first step is the deterministic optimization of the conventional aircraft configuration (Problem (5.25)), which is presented in the first column for each different criteria. The second step of the process is the chance constrained optimization of the hybrid aircraft configuration (Problem (5.26)). Active constraints are indicated in each case. Note that the active constraints in the chance constrained case are the constraints for which the probability constraint is active. The minimal year is presented in red. Note that the criteria figures for the hybrid aircraft are the 0.95-quantile values. This is why the value indicated for each criterion is equal to the value of the deterministic optimization of

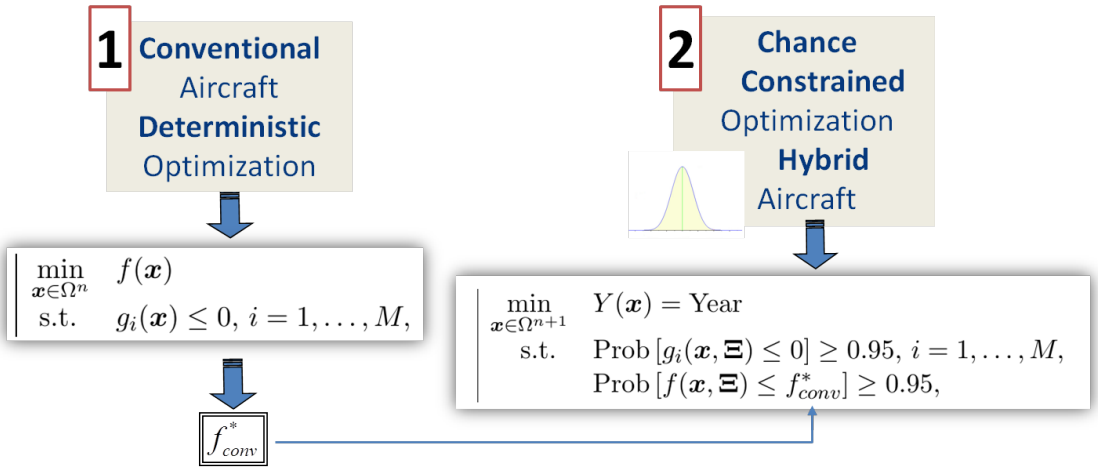

Figure 5.12: Definition of the hybrid aircraft chance constrained optimization problem.

the conventional aircraft. We can observe that the probability constraints on the criterion value is active for all optimizations.

Optimize versus	Cost Mission Block Fuel		Cash Operating Cost (COC)		Climate Impact (APGWP)	
	Conventional	Hybrid	Conv.	Hyb.	Conv.	Hyb.
Equilibrium Year		2026		2025		2020
SLSThrust (daN)	11620	11160	12260	11760	10950	11120
WingArea (m^2)	152	152	150	154	175	175
Wing Aspect Ratio	17	17	15	16	10	*8*
Cruise Mach	0,63	0,61	0,75	0,66	0,66	0,61
Cruise Altitude (ft)	35 000	35 000	35000	35000	31400	30000
BPR	*8*	*8*	*8*	*8*	12,9	12,2
eFan Power (MW)		1,1		*1*		1,7
Electric Ratio		*0,01*		*0,01*		0,012
Active Constraints	TOFL1	TOFL1	TOFL1 - LdSpeed	TOFL1 - LdSpeed	TOFL1 - ClbVz	TOFL1
Cost Mis. Fuel	**1650**	**1650**	1780	1780	2100	2300
COC	4400	4470	**4200**	**4200**	4600	4920
APGWP	$3{,}1\text{x}10^{-5}$	$3{,}06\text{x}10^{-5}$	$3{,}25\text{x}10^{-5}$	$3{,}2\text{x}10^{-5}$	**$2{,}77\text{x}10^{-5}$**	**$2{,}77\text{x}10^{-5}$**

Figure 5.13: Hybrid Configuration Chance-constrained Optimization results

The main observation is that the hybrid aircraft most important interest is for the climatic impact reduction, since its impact becomes with a 0.95 probability equivalent to the one of the conventional aircraft in 2020. The results also show that under model uncertainties we would be able to reach an economically viable hybrid-powered-aircraft with a probability of 0.95 between 2025 and 2026. This is possible thanks to an amount of work on the implementation of the electricity in aircraft propulsion. Moreover, we find

the equilibrium, so all steps that are coming next will obviously improve the results.

5.5 Conclusion and perspectives

The presented modified SORA method, with the uncertainty propagation using the first four moments appears to be very powerful for robust optimization. The method is validated via the chance constrained optimization test case using the Rosenbrock function. The results show a significant improvement in term of number of calls to the function in comparison with a classical chance constrained method without degrading the accuracy.

The application to an industrial problem is presented: the chance-constrained optimization of an unconventional hybrid aircraft configuration. The results seem to be consistent. As a matter of fact, the hybrid aircraft configuration chance-constrained optimization suggests that the technologies evolution needed to reach the equilibrium with current conventional aircraft will occur in around 5 or 10 years, according to the criterion. Moreover, through these results, it is important to stress the impact of a good adequateness between the technologies, the way to operate it and how it is implemented within the general arrangement. In other terms, an important work of integration needs to be done to take the maximum benefit of a new technology.

The next steps of the study is to use more of the synergies proposed by the hybrid aircraft configuration: we propose for instance to remove the thrust reverser from the thermal engines, and use the electric engine instead, and to remove the Auxiliary Power Unit (APU) and use the electric engine battery to which we add 100 kg additional one. We have seen in Chapter 3 that the introduction of these synergies are really bringing benefit to the configuration performances. Then we could expect to have an hybrid aircraft competitive with respect to the conventional one, with a 0.95 probability, sooner than the presented results.

Chapter 6

A first step towards a Robust Optimization for Aircraft Design

Contents

This chapter is an article recently submitted.

6.1 Introduction

Accounting for uncertainties during the preliminary design phases of an aircraft design is of crucial importance. The objective is to avoid the mistakes appearing during the test phase of the aircraft, which can have a huge impact on the performances. For example when the final mass of the aircraft is assessed, it is important to know the uncertainty that comes with it. Research in this field started around the end of 20^{th} century, with a big amount of work on uncertainty quantification [33, 61, 113, 58, 119], and on reliable optimization techniques [69, 82, 178, 19]. It is a particular concern at Airbus as attested by the publications [12, 39, 22].

Uncertainties on computed solutions must be known precisely and at the very beginning phases of the design in order to have a better knowledge of the solution reliability and thus to control it. However, it raises several problems. Methods have recently been developed in order to obtain more reliable and accurate designs, in reasonable computational time. Among them we can find the following ones: robust design methods [161], chance constrained optimization methods using min-max objectives and constraints [129, 126, 125], sequential methods with reliability assessment [92], or surrogate based chance constrained optimization methods [93]. The main issues are the way of accounting for the uncertainties and the choice of the optimization algorithms. Solving chance constrained programming problem relies on a probability of constraint satisfaction. Robust optimization methods [19] have a wide range of applications, with for instance the minimization of the failure probability of a solution or the minimization of the variance of a solution. Here we propose to ensure the robustness of the solution whatever the uncertainty, which means that the constraints must be satisfied. This is why we resort to robust optimization [16, 17].

The aircraft preliminary design optimization problem can be written in the following form:

$$\min_{X\in\mathbb{R}^n} f(X) \quad \text{s.t.} \quad \left| \begin{array}{l} g_i(X) \leq 0,\ \forall i = 1,\dots,l \\ X_{min} \leq X \leq X_{max}. \end{array} \right. \tag{6.1}$$

In our study, the cost function f can be the fuel consumption over a given mission or the global cost of the aircraft. The optimization variables X can be selected from the following non-exhaustive list: the wing area and the sea-level static thrust for the 2D case, the wing aspect-ratio, the engine By-Pass ratio, the cruise Mach or the reference cruise altitude for the multidimensional case. The constraint functions g_i represent operational constraints, such as the take-off field length, cruise and climb speed ceiling, landing speed, which are known to be convex functions. All these functions and their gradients are provided as black-boxes by SiMCAD, a toolbox developed by Airbus in Scilab. This toolbox is based on low granularity models for geometry, aerodynamics, propulsion, trajectory and masses. More details can be found in [22].

The contribution of this paper is to give a complete methodology for the robust optimization of the aircraft preliminary design. Indeed, all existing studies are mainly deterministic. Until now, uncertainties around the models are taken into account by margins chosen according to engineers know-how, which can sometimes lead to unexpected disappointing performances. Taking uncertainties into account could be done in two ways: chance constrained optimization as done in [141], and robust optimization. In this paper we investigate the robust optimization approach. Due to the particular structure of involved functions,

our approach first consists in approximating the initial aircraft preliminary design problem (6.1) by a linear program and then to apply dedicated robust optimization techniques, namely the ones described in [16].

The outline of the paper is as follows. Section 6.2 is dedicated to the modeling of the uncertain optimization problem in three steps: first we build an affine approximation of Problem (6.1); then we define uncertainties related to the modeling and present the way we deal with them; lastly we use the techniques developed by [16, Chapter 1] to obtain an equivalent tractable formulation. Finally, in Section 3, after a short description of the Airbus toolbox SiMCAD, two cases of robust optimization of aircraft design are solved and numerical results are presented.

6.2 Modeling the uncertain linear optimization problem

Engineers knowledge and first computations concur in assuming that objective functions such as cost or fuel consumption, are almost affine in the design variables, and that the constraint set could be approximated by a polyhedral set, i.e. by a finite set of affine constraints. This will enable us in Section 6.2.1 to replace Problem (6.1) by a linear programming problem of the form:

$$\left| \begin{array}{ll} \min\limits_{X\in\mathbb{R}^n} & c^\top X + d, \\ \text{s.t.} & A\cdot X \leq b,\ X_{min} \leq X \leq X_{max} \end{array} \right. \tag{6.2}$$

where $\mathbf{A} \in \mathbb{R}^{m\times n}$, $\mathbf{b} \in \mathbb{R}^m$, $\mathbf{c} \in \mathbb{R}^n$ and $d \in \mathbb{R}$. The number of constraints is $m + n$.

The next step will be in Section 6.2.2 to deal with uncertainties naturally arising in the aircraft modeling. The latter will be expressed as uncertainties on the coefficients A, b, c and d. Lastly we formulate in Section 6.2.3 the uncertain linear optimization problem and its robust counterpart, and show that it could be rewritten as a deterministic linear programming problem.

Note that all functions used along the design process are black-box type functions for which gradients are available.

6.2.1 Polyhedral approximation

Assuming that the objective function f is affine, we can replace f by its first order approximation at X_0:

$$f(X) = f(X_0) + \nabla f(X_0)^\top (X - X_0),$$

where X_0 denotes, e.g., the mean point of the bounded domain $\{X \in \mathbb{R}^n : X_{min} \leq X \leq X_{max}\}$. We state:

$$c = \nabla f(X_0),\ d = f(X_0) - \nabla f(X_0)^\top (X - X_0).$$

Let us now focus on building a polyhedral approximation of the constraint set $\{X \in \mathbb{R}^n : g(X) \leq 0\}$. For each constraint $g_j(X) \leq 0$, the idea is first to compute a family of points $(X_i^j)_{i=1,\dots,m_j}$ on the level set $L_0(g_j) = \{X \in \mathbb{R}^n : g_j(X) = 0\}$ and then to build a piecewise linear approximation $\underline{g}_j$ of g_j:

$$\underline{g}_j(X) = \max\left\{ a_i^{j\top}(X - X_i^j) : i = 1, \dots, m_j \right\}.$$

For a given family of points $(X_i^j)_{i=1,...,m_j}$ on the level set $\mathcal{L}_0(g_j)$, we propose two ways for choosing $a_i^j \in \mathbb{R}^n$:

- **Approximation by tangent hyperplanes.** We state:

$$a_i^j = \nabla g_j(X_i^j),\ \forall i = 1, ..., m_j,$$

so that $\left\{a_i^{j\top}(X - X_i^j), i = 1, ..., m_j\right\}$ is a family of hyperplanes tangent to the constraint set $\{X \in \mathbb{R}^n : g_j(X) \leq 0\}$.

- **Approximation by secant hyperplanes.** Assume: $m_j \geq n$. For each n-uplet $(\widetilde{X}_1^j, \ldots, \widetilde{X}_n^j)$ of points selected among the points $X_1^j, \ldots, X_{m_j}^j$, the equation of the hyperplane passing through the points $\widetilde{X}_1^j, \ldots, \widetilde{X}_n^j$ is of the form:

$$a^{j\top}(X - \widetilde{X}_1^j) = 0.$$

Since the coefficients $a^j = (a_i^j)_{i=1,...,n}$ are defined up to a multiplicative constant, we arbitrary impose: $a^{j\top}\widetilde{X}_1^j = 1$, so that a^j is solution of the following system: $a^{j\top}\widetilde{X}_i^j = 1$, $i = 1, \ldots, n$, i.e.:

$$\left[\widetilde{X}_1^j | \ldots | \widetilde{X}_n^j\right]^\top a^j = 1$$

In both cases, the constraint $g_j(X) \leq 0$ is then replaced by $\underline{g_j}(X) \leq 0$. The latter is equivalent to: $a_i^{j\top}(X - X_i^j) \leq 0$ for all $i = 1, \ldots, m_j$ and can be rewritten as:

$$A_j X \leq b_j, \tag{6.3}$$

where $A_j = \left[a_1^j | \ldots | a_{m_j}^j\right]^\top \in \mathbb{R}^{m_j \times n}$ and $b_j = A_j X_i^j \in \mathbb{R}^{m_j}$. Lastly the constraints $g_j(X) \leq 0$, $j = 1, \ldots, l$, are now replaced by the affine constraint:

$$AX \leq b,$$

where: $A = \left[A_1^\top | \ldots | A_l^\top\right]^\top \in \mathbb{R}^{m \times n}$, $b = \left[b_1^\top | \ldots | b_l^\top\right]^\top$ and $m = \sum_{j=1}^{l} m_j$.

In the case where constraints are affine, the tangent hyperplane approximation can be used and is easiest to compute. When the constraint functions g_j, $j \in \{1, \ldots, l\}$, are not affine but convex, we have to select carefully the points X_i^j used in the secant hyperplanes computation: more precisely, we have to choose points on the boundary of the domain $[X_{min}, X_{max}]$ to obtain a conservative approximation of $\{X | g(X) \leq 0\}$. In that case, we get: $g_j(X) \leq \underline{g}_j(X)$ for all X and all $j = 1, \ldots, l$, hence:

$$\{X | g(X) \leq 0\} \subset \left\{X | \underline{g}(X) \leq 0\right\}.$$

Let us now describe the construction of the points $(X_i^j)_{i=1,...,m_j}$ for each level set $\mathcal{L}_0(g_j)$, $j = 1, ..., m$. For the sake of clarity we omit the subscript j in the following explanation. For a given inequality constraint $g(X) \leq 0$, we want to find a family of points $(X_i)_{i=1,...,m}$ such that $g(X_i) = 0$. This problem is then decomposed into two steps: first computing one point X_1 in a reasonable computational time, and then from this first point, to compute $X_2, \ldots, X_m$ such that the family $(X_i)_{i=1,...,m}$ is *well-distributed* on the level set $\mathcal{L}_0(g)$.

6.2.1.1 Computing points on the level set $L_0(g)$

In this section we want to compute at least one point $X_1 \in \mathbb{R}^n$ satisfying: $g(X_1) = 0$. From an analytical point of view, this problem can be formulated as:

$$\min_{X \in \mathbb{R}^n} g(X)^2. \tag{6.4}$$

To solve this problem we propose to use a gradient-type algorithm [27]: let us consider an arbitrary point $\tilde{X_0} \in \mathbb{R}^n$. By definition of the iso-level curve of g, we have: $\tilde{X_0} \in \mathcal{L}_{g(\tilde{X_0})}(g)$. The gradient descent algorithm generates a sequence of iterates $(\tilde{X_k})$ such that:

$$\tilde{X}_{k+1} = \tilde{X}_k - 2s_k g(\tilde{X}_k)\nabla g(\tilde{X}_k), \tag{6.5}$$

where $s_k > 0$ denotes the step length. In this approach we choose the step s_k such that in case of an affine constraint function g, Algorithm (6.5) converges in one single iteration: assuming g is affine, we want to compute s_k such that: $g(X_{k+1}) = 0$ where g can be expressed as:

$$g(X) \quad = \quad g(\tilde{X}_k) + \nabla g(\tilde{X}_k)(X - \tilde{X}_k).$$

This yields:

$$s_k = \frac{1}{2\|\nabla g(\tilde{X}_k)\|^2}. \tag{6.6}$$

Finally we obtain the following iteration for the gradient descent method:

$$\tilde{X}_{k+1} = \tilde{X}_k - \frac{g(\tilde{X}_k)}{\|\nabla g(\tilde{X}_k)\|^2}\nabla g(\tilde{X}_k).$$

The stopping criterion of the algorithm can be defined by either of the following conditions:

1. $|g(\tilde{X}_k)| < \varepsilon_1$,
2. $|s_{k+1} - s_k| < \varepsilon_2$ and $|g(\tilde{X}_{k+1}) - g(\tilde{X}_k))| < \varepsilon_3$.

In the numerical experiments, we choose e.g.: $\varepsilon_1 = \varepsilon_2 = \varepsilon_3 = 10^{-3}$.

6.2.1.2 Find the family $(X_i)_{i=1,\dots,m}$

Once an initial point X_1 has been found, the idea is to run through the tangent hyperplane (H_1): $\nabla g(X_1)^\top (X - X_1) = 0$ using orthogonal directions. In dimension 2 and 3 a small enough step along these directions (according to a subdivision of the minimum and maximum bounds) is defined. Along each direction a new point is computed from which we start the previous search algorithm. Once the current point goes beyond the bounds of the domain, the direction is no longer used. A *well-distributed* family of $(X_i)_{i=1,\dots,m}$ that approximates the level curve $\mathcal{L}_0(g)$ is obtained. This technique is heuristic and then improvements are required to develop a better method. Numerical examples in dimensions 2 and 3 works well. In higher dimension it becomes more difficult. A heuristic way could be to first compute a family of points close to the level curve $\mathcal{L}_0(g)$ with a low cost, and then to run the previous algorithm from all these points. For example surrogate modeling from the real functions could be used to compute the latter family.

However, a general methodology needs to be developed for a better approximation of the level curve.

6.2.2 Modeling Uncertainties

In the following, uncertainties on coefficients A, b, c and d are supposed to be known. In practice, they can be provided by engineers, or obtained by uncertainty propagation methods. We can then define the linear programming problem taking into account the uncertain coefficients A, b, c, d. We have the following family of optimization problems:

$$\begin{array}{ll} \min\limits_{X \in \mathbb{R}^n} & c^\top X + d, \\ \text{s.t.} & A \cdot X \leq b,\ X_{min} \leq X \leq X_{max} \end{array} \tag{6.7}$$

where $(A, b, c, d) \in \mathcal{U}$ and $\mathcal{U} \subset \mathbb{R}^{m \times n} \times \mathbb{R}^m \times \mathbb{R}^n \times \mathbb{R}$ is the uncertain set. Let us state:

$$D = \begin{bmatrix} c^\top & d \\ A & b \end{bmatrix},\ D \in \mathbb{R}^{(1+m)\times(n+1)}. \tag{6.8}$$

In order to remain consistent with the analysis of A. Ben-Tal, L. El Ghaoui and A. Nemirovski in [16], we assume that $\mathcal{U}$ admits an affine parametrization such that:

$$\mathcal{U} = \left\{ D = \begin{bmatrix} c^\top & d \\ A & b \end{bmatrix} \in \mathbb{R}^{(1+m)\times(n+1)} \middle| \, D = D^0 + \sum_{k=1}^{L} \zeta_k D^k, \text{ with } \zeta \in \mathcal{Z} \subset \mathbb{R}^L \right\}, \tag{6.9}$$

where $\mathcal{Z} \subset \mathbb{R}^L$ denotes the perturbation set, D^0 is the nominal value, and D^k is the variation.

In a first approach we consider the worst case situation in which: $L = (m+1)(n+1)$ and the variations D^k are defined such that:

$$D^k_{i,j} = \begin{cases} 1 & \text{if } l = (n+1)(i-1) + j, \\ 0 & \text{otherwise.} \end{cases} \tag{6.10}$$

The perturbation set $\mathcal{Z}$ is then of the form:

$$\mathcal{Z} = \bigotimes_{k=1}^{L} \left[\zeta_k^{inf}, \zeta_k^{sup} \right]. \tag{6.11}$$

The definition of $\mathcal{Z}$ from (6.11) is a worst case approximation of the uncertainty set in the sense that we probably overestimate the uncertain set. This overestimation must be dealt with cautiously so that it does not induce infeasibility of the problem.

Note that the definition of the uncertainty set $\mathcal{U}$ can be simplified by introducing the affine transformation ρ_k:

$$\rho_k : [-1, 1] \rightarrow \left[\zeta_k^{inf}, \zeta_k^{sup} \right] \tag{6.12}$$

$$\xi \mapsto \frac{\zeta_k^{sup} - \zeta_k^{inf}}{2} \xi + \frac{\zeta_k^{sup} + \zeta_k^{inf}}{2}. \tag{6.13}$$

The uncertainty set $\mathcal{U}$ can be rewritten as:

$$\mathcal{U} = \left\{ D = \left(D^0 + \sum_{k=1}^{L} \frac{\zeta_k^{sup} + \zeta_k^{inf}}{2} D^k \right) + \sum_{k=1}^{L} \frac{\zeta_k^{sup} - \zeta_k^{inf}}{2} \xi_k D^k \middle| \, \xi \in [-1, 1]^L \right\} \tag{6.14}$$

$$= \left\{ D = \hat{D}^0 + \sum_{k=1}^{L} \xi_k \hat{D}^k \middle| \xi \in [-1,1]^L \right\}, \tag{6.15}$$

in which

$$\hat{D}^0 = D^0 + \sum_{k=1}^{L} \frac{\zeta_k^{sup} + \zeta_k^{inf}}{2} D^k, \quad \hat{D}^k = \frac{\zeta_k^{sup} - \zeta_k^{inf}}{2} D^k. \tag{6.16}$$

6.2.3 The uncertain linear optimization problem and its robust counterpart

Following [16], the Problem (6.7) is equivalently reformulated in such a way that uncertainties only appear in the constraints:

$$\min_{(X,t) \in \mathbb{R}^{n+1}} t \ \text{ s.t. } \left| \begin{array}{l} AX \leq b, \\ \\ c^\top X + d \leq t, \ X_{min} \leq X \leq X_{max}, \end{array} \right. \tag{6.17}$$

for any $(A, b, c, d) \in \mathcal{U}$. By definition, a robust solution of (6.17) is an optimal solution of its robust counterpart and the robust counterpart of the Problem (6.17) is defined by:

$$\min_{(X,t) \in \mathbb{R}^{n+1}} \left(\sup_{(A,b,c,d) \in \mathcal{U}} t \right) \ \text{ s.t. } \left| \begin{array}{l} AX \leq b, \ c^\top X - t \leq -d, \\ \\ X_{min} \leq X \leq X_{max}, \\ \forall\, (c, d, A, b) \in \mathcal{U}, \end{array} \right.$$

which is equivalent to:

$$\min_{(X,t) \in \mathbb{R}^{n+1}} t \ \text{ s.t. } \left| \begin{array}{l} AX \leq b, \ c^\top X - t \leq -d, \\ \\ X_{min} \leq X \leq X_{max}, \\ \forall\, (c, d, A, b) \in \mathcal{U}. \end{array} \right. \tag{6.18}$$

Let $A := \left[a_1^\top, ..., a_m^\top\right]^\top$. The robust counterpart (6.18) can be rewritten as:

$$\min_{(X,t) \in \mathbb{R}^{n+1}} t \ \text{ s.t. } \left| \begin{array}{l} a_i^\top X \leq b_i, \ i = 1, \ldots, m \\ \\ c^\top X - t \leq -d, \\ X_{min} \leq X \leq X_{max}, \\ \forall\, (c, d, A, b) \in \mathcal{U}. \end{array} \right. \tag{6.19}$$

By means of the techniques of [16], the latter can be rewritten into the following deterministic linear optimization problem (see appendix A for technical details):

$$\min_{\tilde{X} \in \mathbb{R}^{2n+1}} C'^\top \tilde{X} \ \text{ s.t. } \left| \begin{array}{l} A\tilde{X} \leq b, \\ \\ X_{min} \leq X \leq X_{max}, \end{array} \right. \tag{6.20}$$

where the optimization variables are: $\tilde{\mathbf{X}} = \left(X^\top, t, \mathbf{u}^\top\right)^\top$ and:

$$\mathbf{C}' = (0, \ldots, 0, 1, 0, \ldots, 0)^\top \in \mathbb{R}^{2n+1},$$

$$\mathbf{A} = \begin{pmatrix} I_n & 0_n & -I_n \\ -I_n & 0_n & I_n \\ \hat{A^{(0)}} & 0_m & P^{(a)} \\ \hat{\mathbf{C^{(0)}}}^\top & -1 & \mathbf{P^{(c)}} \end{pmatrix} \in \mathbb{R}^{(2n+m+1)\times(2n+1)}, \tag{6.21}$$

$$\mathbf{b} = \left(0_{1\times 2n}, \hat{\mathbf{b}}^{(\mathbf{0})} - \mathbf{P^{(b)}}, -P^{(d)} - \hat{d}^{(0)}\right)^\top \in \mathbb{R}^{(2n+m+1)}. \tag{6.22}$$

The scalars, vectors and matrices $\hat{A^{(0)}}$, $\hat{\mathbf{C^{(0)}}}$, $P^{(a)}$, $\mathbf{P^{(c)}}$, $P^{(b)}$ and $P^{(d)}$ are defined in appendix A. Finally we are dealing with a linear program with $(2n+1)$ unknowns and $(2n+m+1)$ constraints, where m is the number of initial constraints. For example, in the 2-dimensional case-study, we will have $X \in \mathbb{R}^2$, $\mathbf{u} \in \mathbb{R}^2$ and $t \in \mathbb{R}$.

6.3 Application: Aircraft Preliminary Design Robust Optimization

Preliminary aircraft design is the first step in the passenger transport aircraft design process [12]. The goal is to choose, among several concepts, the one which would be relevant according to a well defined objective (cost, fuel consumption or environmental impact). For each concept, the main aircraft parameters have to be assessed consistently according to a common set of requirements.

In this section we first briefly present the aircraft preliminary design process and define the related uncertain optimization problem. We then describe the way to propagate uncertainties through the models, and finally apply the whole methodology to two real cases of aircraft design.

6.3.1 The Aircraft Preliminary Design Process

The design process is multidisciplinary since several physics such as geometry, aerodynamics, mass, propulsion, performance and cost analysis are involved.

We use an aircraft toolbox called SiMCAD (Simple Models for Conceptual Aircraft Design), developed in Scilab [155] and dedicated to research activity in the domain of Overall Aircraft Design. It is a toolbox of models that allows to run simple, but realistic, pre-design processes involving all main physics of an aircraft. It offers the possibility to test multi-disciplinary, multi-level, multi-objective and robust optimization strategies without having to manage huge amount of data and huge computation time. A complete description of these models can be found in [22].

More precisely, we use semi-empirical models for the aerodynamics and the masses, and simplified physical models of operational performances. To sum up, all combined models count around 180 parameters and 50 functions. They have been validated on existing aircraft. We now have to choose some optimization parameters that will allow to define an aircraft configuration. Engineers practice and know-how lead us to choose the Wing Area that controls the dimension of the wing and the Sea Level Static Thrust (SLSThrust) that controls the engine size.

Now, the aircraft configuration has to be optimized according to a given objective. We here choose the Cash Operating Cost (COC) which takes into account the fuel, the masses, the engine and airframe maintenance, the crew cost and some navigation charges. We also need to fix some requirements as the range of the aircraft, that correspond to the

customer demands (see Table 6.1). Operational needs for safety and operations define a set of inequality constraints described in Table 6.2.

Table 6.1: Description of the baseline aircraft requirements.

Name	**Value**
Number of Passengers (Npax)	180
Design Range	2000 NM
Cruise Mach number	0.65
Wing Aspect Ratio	12
Number of Turbofan Engine	2
Engine By Pass Ratio	10
Top of Climb altitude	35000 ft
Engine Overall Pressure Ratio	40

Table 6.2: Objective and Constraints

Objective	f	Cash Operating Cost (COC)	$\$/trip$	
Constraints	g_1	Take-off field length 1 (at Sea Level) (TOFL1)	$\leq$	2000 m
	g_2	Take-off field length 2 (in High & Hot conditions) (TOFL2)	$\leq$	2500 m
	g_3	Climb vertical speed ceiling (CLBVZ)	$\geq$	500 ft/min
	g_4	Cruise vertical speed ceiling (CRZVZ)	$\geq$	300 ft/min
	g_5	Landing Speed (LDSPEED)	$\leq$	130 kt

Models and functions that drive the aircraft configuration computation, are sequential. The whole process can be represented from a global point of view by the diagram presented in Figure 6.1: it shows the way the different physics interact, how an aircraft is computed from requirements and input variables and how objectives and constraints are computed.

Moreover, the design process is significantly improved when the uncertainty associated to each criteria is provided. Therefore robust optimization has a high added value compared to a classic deterministic one. As mentioned before, uncertainty quantification has already been assessed and the most important impact of uncertainty is coming from the computation of aerodynamic efficiency, specific fuel consumption and structural weight. Taking these uncertainties into account, we present in this section a two-dimensional and a three-dimensional application cases. The different steps of our approach are summarized hereafter:

- Build an affine approximation for the objective and a polyhedral approximation for the constraints set.
- Quantify and propagate uncertainties with a first order approximation method in order to obtain L^∞ boxes on all ζ's.
- Build corresponding A, b, c and d in order to obtain the Problem (6.20)

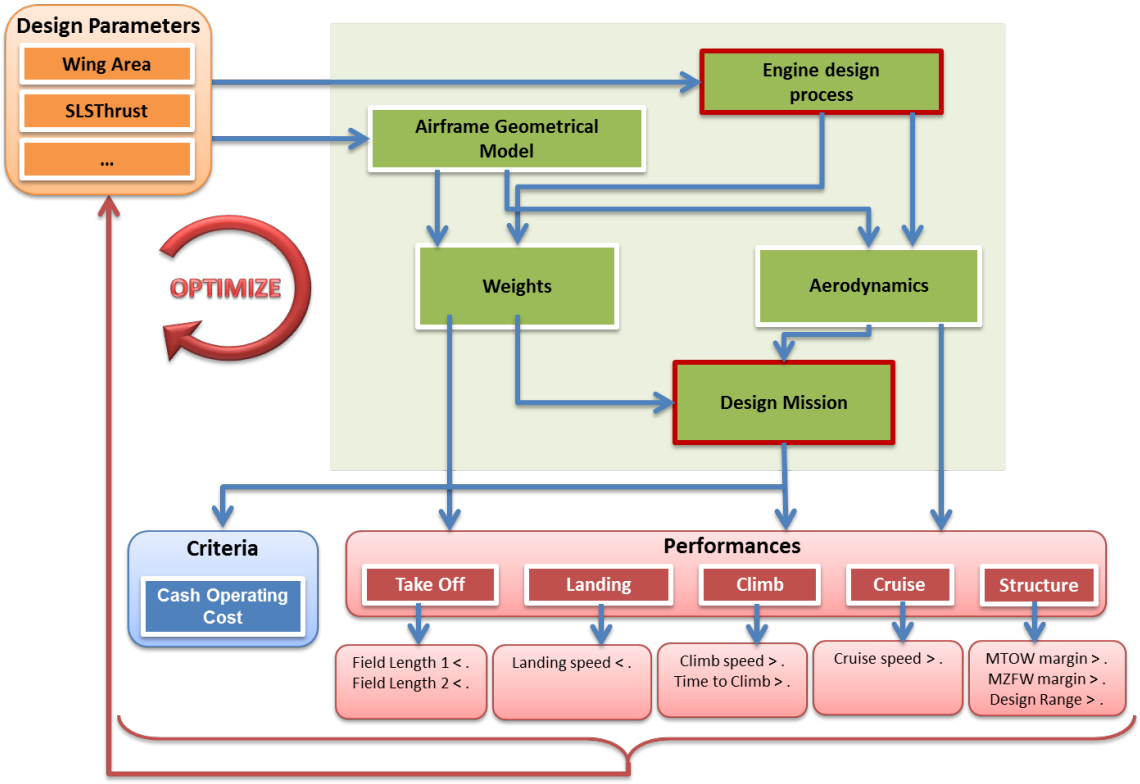

Figure 6.1: Aircraft Simple Design Process Diagram.

- Solve the linear constrained programming problem (6.20) using the simplex algorithm [98]. Here we use the *linpro* function from Scilab.

In each test case, the robust solution, i.e. the solution of (6.20), is compared to the (non robust) solution of the initial deterministic optimization problem (6.1). The latter is solved using a Feasible Sequential Quadratic Programming algorithm [184], here the *fsqp* Scilab function.

6.3.2 Uncertainty propagation method

The processes involved in the preliminary aircraft design, are bringing uncertainties. They are based on semi-empirical models in which some equations are replaced by regressions from databases. Recently, these uncertainties have been quantified [22]. It is now the time to take them into account in the design process.

To evaluate uncertainties on the coefficients A, b, c, d of the Problem (6.2), several propagating methods can be used [129, 126, 125, 141]. The Monte-Carlo sampling is the more accurate one but also the one with the highest computational cost. Moreover we have to take into account the following important information: the evaluation of the constraints and the objective functions is computationally expensive and the constraints and the objective functions are almost affine.

This is why we choose to use a moment based propagation method with a first order Taylor approximation of the uncertain function: it is a non intrusive method which offers in our case a good compromise between accuracy and computational cost. The main steps

of the propagation method are the following:

- Get or compute the first moments of the model input uncertainty distributions,
- Propagate moments through computation process and get the moments of the output uncertain values using a first order moment method [104, 163],
- Use these moments to determine the uncertainty set on coefficients A, b, c and d. This is done by following Moments Methods from [131], that allows to reconstruct a distribution from its moments. Based on this approach, [22] shows that we can compute distributions parameters as a function of the moments and thus determine the distribution support. The bounds of the supports are then the interval of output uncertainty.

An other example of use of the moment propagation method can be found in [141].

6.3.3 Robust Aircraft Design Optimization

We choose the baseline short range aircraft presented in Section 6.3.1. We start with the following robust optimization problem:

$$\min_{X\in\mathbb{R}^n} f(X) \text{ s.t. } \left| \begin{array}{ll} g_i(X) \leq 0, & i = 1,\ldots,5, \\ X_{min} \leq X \leq X_{max}, & \end{array} \right. \tag{6.23}$$

where the objective and the constraints are defined in Table 6.2. All constraints are written under the standard form: $g_i(X) \leq 0$, and the optimization variables are defined in Table 7.1. They have to satisfy box constraints. In the case $n = 2$ the cruise Mach is set to 0.65.

Table 6.3: Optimization variables (x_1, x_2) when $n = 2$ and (x_1, x_2, x_3) when $n = 3$.

	Name	Unit	Lower and Upper bounds
x_1	Wing Area	m^2	$[100, 170]$
x_2	Sea-Level Static Thrust	daN	$[9000, 13000]$
x_3	Cruise Mach	Mach	$[0.65, 0.76]$

In what follows, the objective function f denotes the Cash Operating Cost (COC) computed with respect to the Wing Area x_1, the Sea-Level Static Thrust x_2 and the Cruise Mach x_3. This function is almost affine in (x_1, x_2, x_3) while the constraint functions g_i are convex.

6.3.3.1 Case n=2

In two dimensions, the formulation of the problem is the following one:

$$\min_{(x_1,x_2)\in\mathbb{R}^2} f(x_1, x_2, 0.65) \text{ s.t. } \left| \begin{array}{ll} g_i(x_1, x_2) \leq 0, & i = 1,\ldots,5, \\ 100 \leq x_1 \leq 170, & \\ 9000 \leq x_2 \leq 13000. & \end{array} \right. \tag{6.24}$$

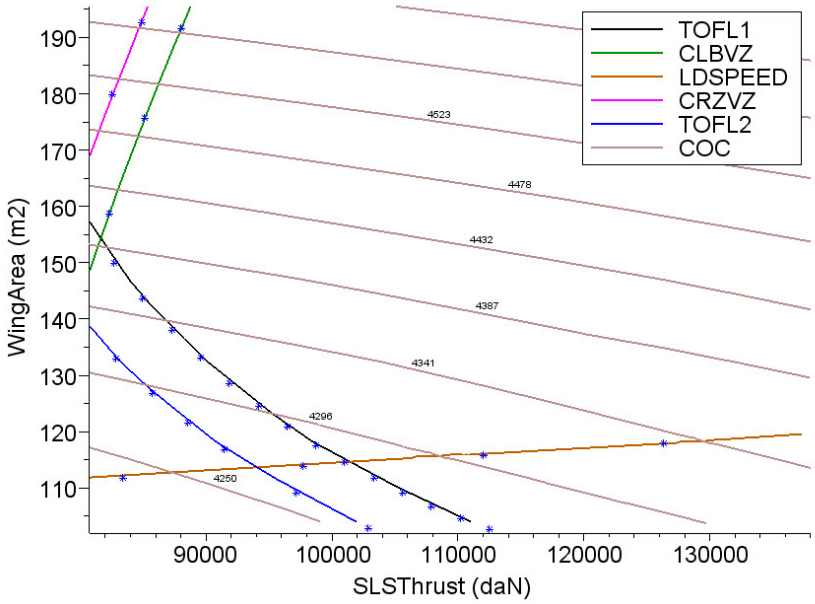

Figure 6.2: Aircraft 2D Design Problem, with constraints and objective level curves.

For a better understanding of the proposed approach, Figure 6.2 shows a 2D map with constraints and some level curves of the objective function.

The first step of our approach is to compute the affine approximation of f at the mean point of the domain of definition, and the piecewise affine approximation of the g_i at points X_j^i, $j = 1, ..., m_j$. For this we apply the method to find points on each constraint level curve. These points are the crosses from Figure 6.2. They will also be represented in the next figures. Then, as constraints are convex functions, we choose to build secant hyperplanes. Observe that the more non-affine the constraint, the higher the number of approximating hyperplanes. Figure 6.3 shows the polyhedral approximation of the constraints set and some level curves of the linearized objective. The corresponding hyperplanes equations are of the form:

$$a_1^{(i)} x_1 + a_2^{(i)} x_2 = 1,\ i = 1, ..., m. \tag{6.25}$$

Once we have the equations of the constraints and of the objective, the next step is the propagation of uncertainty. We consider the following sources of uncertainty:

- from aerodynamic models: Lift over Drag coefficient (LoD) is calculated with an error of $\pm 1\%$ around its nominal value,
- from mass models: Maximum Overall Empty Weight (MWE) is calculated with an error of $\pm 1\%$ around its nominal value,
- from propulsion models: Specific Fuel Consumption (SFC) is calculated with an error of $\pm 1\%$ around its nominal value.

The first order Taylor based propagation method gives as a result the uncertain interval on $\left(a_1^{(i)}, a_2^{(i)}\right)$, $i = 1, ..., m$. The uncertainty interval is also computed for the affine objective function coefficients.

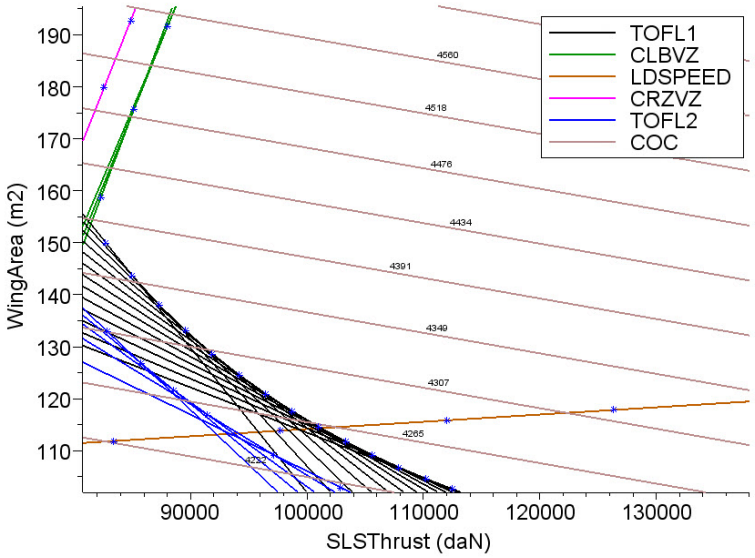

Figure 6.3: Approximation of Aircraft 2D Design Problem, with piecewise affine constraints and affine objective.

Finally the original problem is reformulated as a linear programming problem such as (6.20). We obtain in this case with an initial number of approximating hyperplanes $m = 25$, a linear programming problem in dimension 5 with a total of 30 constraints. Using a classical linear programming solver (linpro from scilab) based on the simplex method we obtain the solution presented in Figure 6.4. Constraints at the solution point are also represented on this figure. And we have the following solution:

$$X_{sol} = \left(10292 \text{ daN}, 115.6 \text{ m}^2\right) \text{ , with the objective value: } COC = 4285 \text{ \$/pax.}$$

The robust solution X_{sol} is then compared to the non robust solution X_{sol}^{det} of the initial deterministic optimization problem (6.1):

$$X_{sol}^{det} = \left(10121 \text{ daN}, 114.3 \text{ m}^2\right) \text{ , with the objective value: } COC^{det} = 4279 \text{ \$/pax.}$$

As expected, the price of robustness is a small increase of cash operating cost (COC) value.

The last step is to verify the robustness of the solution X_{sol}. For that we run from the obtained solution point X_{sol} a reliability assessment with the original constraint functions. Using the previously mentioned propagation method we compute the interval of error on each constraint (written in the form $g(X) \leq 0$). For a constraint $g(X_{sol})$ we obtain the uncertain interval $\left[g^{min}(X_{sol}), g^{max}(X_{sol})\right]$. Then the solution is robust, meaning that constraints are always satisfied, if and only if $g^{max}(X_{sol}) \leq 0$. Results are in Table 6.4. Relative upper bound represents the upper bound divided by the required value of Table 6.2 for each constraint. We observe that active constraints (Take-off field length 1 and Landing Speed) have the lowest relative reliability margin as expected.

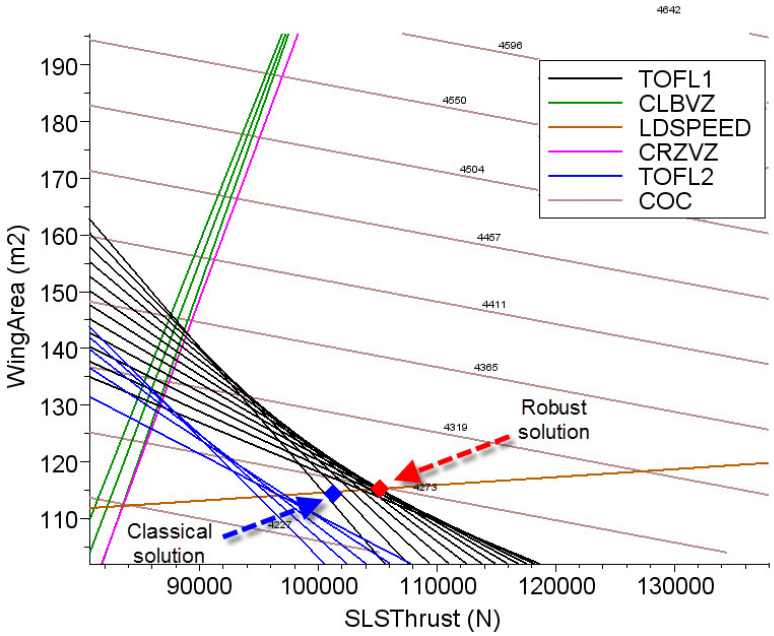

Figure 6.4: Robust Approximation of Aircraft 2D Design Problem and its solution.

Table 6.4: Constraints reliability assessment at point X_{sol} (case $n = 2$).

Constraint	Upper Bound ($g^{max}(X_{sol})$)	Relative Upper Bound
Take-off field length 1	- 5.8	-0.003
Take-off field length 2	- 176	-0.07
Climb vertical speed ceiling	- 3	-1.2
Cruise vertical speed ceiling	- 3.1	-2.0
Landing Speed	- 0.02	-0.0003

6.3.3.2 Case n=3

In this case, the cruise Mach number is added to the optimization variables. The formulation of the problem is the following one:

$$\min_{(x_1,x_2,x_3)\in\mathbb{R}^3} f(x_1,x_2,x_3) \text{ s.t. } \begin{array}{l} g_i(x_1,x_2,x_3) \leq 0, \qquad i = 1,\ldots,5, \\ 100 \leq x_1 \leq 170, \\ 9000 \leq x_2 \leq 13000, \\ 0.65 \leq x_3 \leq 0.76. \end{array} \tag{6.26}$$

We follow the same steps as for the case $n = 2$. We first compute an affine approximation of f at the mean point of the definition domain, and then a piecewise affine approximation of the g_i at points X_j^i, $j = 1, ..., m_j$. For that we apply the method to find points on each constraint level curve. Since the constraint functions are known to be convex, we choose to build secant hyperplanes. Then we consider the same sources of uncertainties from aerodynamic, mass and propulsion models. Finally we reformulate the problem in order

to obtain a linear programming formulation such as in Equation (6.20). We obtain in this case with an initial number of approximating hyperplanes $m = 43$, a linear programming problem in dimension 7 with a total of 50 constraints. Using the *linpro* linear programming solver from Scilab we obtain the solution:

$$X_{sol} = \left(9764 \text{ daN}, 141.2 \text{ m}^2, \text{Mach } 0.76\right), \text{ with: } COC = 4080 \text{ \$/pax.}$$

The robust solution X_{sol} is then compared to the non robust solution X_{sol}^{det} of the initial deterministic optimization problem (6.1):

$$X_{sol}^{det} = \left(9306 \text{ daN}, 137 \text{ m}^2, \text{Mach } 0.76\right), \text{ with: } COC^{det} = 4070 \text{ \$/pax.}$$

We also run the reliability assessment at the solution. We obtain the Table 6.5 for each constraint. Reliability is satisfied. Let us finally have an insight into the computational

Table 6.5: Constraints reliability assessment at point X_{sol} (case $n = 3$).

Constraint	Upper Bound	Relative Upper Bound
Take-off field length 1	- 95	-0.05
Take-off field length 2	- 267	-0.11
Climb vertical speed ceiling	- 1.1	-0.44
Cruise vertical speed ceiling	- 1.2	-0.8
Landing Speed	- 0.41	-0.006

cost of the robust design approach: Table 6.6 presents the number of calls to the process in the deterministic case and in the robust case. Note that the computational effort spent using the robust approach, comes only from the linearization process.

Table 6.6: Number of calls to the aircraft design process.

	Deterministic Optimization with SQP	Robust Optimization
2D case	25	160
3D case	55	389

6.4 Conclusion and perspectives

This paper proposes a methodology to apply techniques of robust linear programming to the aircraft preliminary design problem. Under the assumptions of an affine objective and convex constraints, the problem is first approximated in a conservative manner by an uncertain linear program. In the case where the uncertainty set on the output is unknown, a propagation method can be used. The uncertain linear optimization problem is obtained and its robust counterpart is formulated. Results are presented for a two and a three dimensional test cases. In both cases, the obtained solutions are robust.

However this approach raises several limitations. The first issue appears during the approximation of constraint level curves. The way of building the secant hyperplanes from

a family of points from the level curve is heuristic. In dimension two and three, a heuristic method that consists in merging closest points to build hyperplanes and then browse the level curve going through all directions, allows to construct a good approximation. It may be more difficult in higher dimension. A further step in the study would be to find a general methodology to build a piecewise affine approximation of a level curve whatever the design space dimension is. The second issue is in the case where one only has uncertainties about model inputs. The choice of the propagation method to build the uncertain set on output is important. The need of being conservative makes fundamental the accuracy of the output error interval. An underestimation of this interval could lead to non-robust solutions.

Conclusion

The first objective of this thesis was to state, investigate, and solve the highly multidisciplinary and multi-objective problem of aircraft design and operation. This objective was reached by using a step-by-step approach. The first contribution was to incorporate thoroughly and progressively new models of the engine, of the mission profile and of the climate impact, into the usual basic models. We validated each model increment by comparing the simulation results with existing aircraft data.

The second contribution was to incorporate new design variables into the aircraft design optimization process. To the two basic degrees of freedom - the wing area and the sea level static thrust (driving the engine size and power) - , we added the wing aspect ratio from the airframe, the engine by-pass ratio from the propulsion system, the cruise altitude and the Mach number from the overall trajectory parameters, and finally speeds of the climb and descent. We validated the results of the optimization by a step-by-step integration of these new degrees of freedom.

Another objective of this thesis was to solve the problem of the environmentally efficient aircraft design. We then incorporated a climate impact model into the processes. From this model, we selected a representative measure of the climate impact, which was added as a new criterion of the aircraft design optimization. For that environmental purpose, we proposed an unconventional aircraft configuration: a hybrid electric-fuel propelled aircraft. It came with an electric fan on its rear fuselage, electric generators on the thermal engines, and additional battery. The concept was modeled with an accurate way of using the batteries, the fan and the generators along the mission. We then optimized both the conventional and the hybrid aircraft design, with respect to the same specifications. For that purpose, we applied a step-by-step integration of the degrees of freedom. Moreover, we compared the optimization in terms of climate impact, operating costs and a criterion representing the global efficiency of the aircraft, namely the maximum take-off weight. The analysis of the final results highlighted the proportional impact of each group of degrees of freedom on the optimized aircraft. We also observed that the cost and the climate impact are two conflicting criteria. Another interesting result was the environmental efficiency of the hybrid configuration. Finally, we proposed to take advantage of the hybrid configuration by working on the synergies offered by the electric fan and the batteries. We observed that this work on the synergies was necessary to obtain a competitive hybrid aircraft.

The other contributions of the thesis are the following:

1. the integration of an automatic differentiation method into the numerical tools, by overloading all the basic operators and functions of the processes. This allowed to reach a better accuracy than the classical finite difference methods when computing gradients and Hessians. Moreover, it may bring significant improvement of convergence of gradient based methods.

2. The comparison and selection of the optimization methods well-adapted to the aircraft design problem. Gradient based methods were first used with the gradients provided by the automatic differentiation tool. However, some points of the design space appeared to be non computable. This is why we resorted to derivative free optimization techniques. Genetic algorithms (NSGA II) were tested to solve mono-objective and also multi-objective optimization. Differential evolution algorithms were modified to deal with constraints, and applied in some studies. An implementation of the MADS algorithm compiled from C++ also proved to have good convergence properties in our design studies. Finally the increasing number of degrees of freedom motivated the study of surrogate based optimization tools.

3. The use of a new family of probability distributions with four parameters, namely the Beta-Mystic distribution, which covers a wide range of unimodal distributions.

4. A detailed study and comparison of uncertainty propagation methods, with respect to criteria of accuracy, computing cost and knowledge on the models. The comparison is made between Monte-Carlo, Taylor expansion, Polynomial chaos expansion, and quadrature methods. A particular attention is paid to moment based propagation methods, which have powerful practical applications on design under uncertainties problems.

5. An approach of the aircraft design optimization under uncertainty. For that, a chance constrained programming approach was proposed. We brought modifications to a numerical method of robust design optimization, namely the Sequential Optimization Reliability Assessment (SORA) method. By using a technique that computes bounds on probability measures, the SORA method is able to handle a larger variety of distributions.

6. The application of all the previously mentioned tools to an unconventional aircraft design chance constrained optimization. We solved the following problem: find the year from which the hybrid aircraft will perform like the conventional one with a 0.95 probability.

7. The first steps towards another approach of the robust optimization of the aircraft design. The result is an optimal aircraft which satisfies all realizations of the constraints within some uncertainty box. A particular attention was paid to the modeling of such an approach.

Finally, this thesis contributes to sensitize the future project office to uncertainty management by using probability distributions. It also yields the development and the improvement of internal numerical tools, namely SiMCAD and OCCAM, used for solving the aircraft design problem. All the models developed in the frame of this thesis - the climate impact, the hybrid aircraft, the thermodynamic engine and the detailed mission profile - were incorporated into these tools, and validated by the presented studies. In the frame of some internal projects, this thesis participated in sensitivity studies on the hybrid aircraft design parameters, and presented a complete study of this innovative concept. Moreover, this thesis leads to the integration of the uncertainty propagation methods to the numerical design tools. In particular the first order, the second order, the univariate reduced quadrature and the bivariate reduced quadrature methods.

The results obtained in this thesis yield the following perspectives.

The first one is to continue the robust optimization approach leaded of Chapter 6. Indeed, the application of the methodology worked fine for the two and three dimensional cases, and should be generalized to higher dimension.

Another perspective was raised by the robust optimization approach, when it comes to propagate the uncertainties. It could be interesting to study the impact of the accuracy of the uncertain output on the selected risk measure, or even on the risk measure bound. This would allow to be aware of the error that is made when the measure is computed and then to be aware of the real robustness of the problem solution. For instance, in the proposed chance constrained optimization, we use the moments of the output uncertainty to compute the probability measure bounds. The impact of the moment computation error on the bound should be assessed.

Another point could be to automate the study of a solution in the case of the deterministic studies. The neighborhood of the solution is of interest for the various actors of air transportation. The sensitivity of the results to the design variable is of important matter, e.g. the sensitivity to the cruise Mach number and the cruise altitude, which are extremely important quantities for the airlines operations.

Also, the integration of all the tools and methods into internal numerical tools bring the opportunity to study other aircraft concepts, particularly other configurations of hybridization. This already started with an internship on the optimization of a new concept of hybrid aircraft, compared to more conventional ones.

Another perspective which could bring important benefits in robust design optimization is the study of the joint probability case. It could be useful for the practitioners in robust design to build a joint probability with some dimension reduction methods. In the frame of this thesis, we did not have the opportunity to study the copulas, which are an interesting tool to represent multidimensional random variables. This might be a next step.

Finally, very recent methods in the field of robust design could be of interest, particularly when a large number of uncertainty input are involved. These are coupling adaptive uncertainty quantification tools and direct search optimization algorithms [44]. These methods showed very interesting convergence properties, with reasonable computing time.

Chapter 7

Version française raccourcie : Approche novatrice pour la conception et l'exploitation d'avions écologiques

Contents

7.1 Introduction

Depuis les années 1950, le trafic aérien est en constante croissance: actuellement, le nombre de passagers est d'environ 3 milliards par an et, selon les prévisions les plus basses, il devrait doubler sur les quinze prochaines années. Les acteurs du transport aérien - les constructeurs de moteur, les avionneurs, et les compagnies aériennes - sont concentrés chacun sur des enjeux propres à leur secteur d'activité, ce qui peut s'avérer limitant pour atteindre les objectifs ambitieux qui devront répondre à la croissance du trafic. En particulier, avec la place de plus en plus importante de la problématique environnementale, les objectifs règlementaires récemment mis en place afin de réduire l'impact de l'aviation sur le réchauffement climatique vont devoir être pris en compte dès la phase préliminaire de conception d'un nouvel avion.

De façon classique, lors de cette phase, le but de l'avionneur est de comparer les performances de nombreuses configurations afin de déterminer les paramètres de conception qui optimiseront l'avion de demain. L'étude des performances d'un avion est un problème d'optimisation multidisciplinaire déterministe sous contraintes. Les objectifs de cette optimisation sont traditionnellement la consommation de fuel, le cout global d'opération de l'avion ou encore la masse maximale au décollage de l'avion (qui rend compte de l'efficacité globale de l'avion). Les contraintes sont définies par les exigences du cahier des charges. Habituellement, les degrés de liberté de cette optimisation sont fixés: il s'agit de la surface de la voilure et de la taille du moteur. Des études sont souvent menées sur l'avion optimisé, afin d'en étudier la sensibilité à d'autres paramètres de la géométrie, du moteur ou de la mission par exemple. Aussi, les études préliminaires de conception sont lancées à partir de modèles parfois très simplifiés, soit par volonté de réduction du temps de calcul, soit par manque de connaissance sur les concepts technologiques abordés.

Dans cette thèse, réalisée aux Avant-Projets d'Airbus, une nouvelle approche holistique du problème d'optimisation de la conception d'avion est introduite : le but est d'agréger aux modèles classiques de conception, des modèles plus précis de la partie propulsive et de la trajectoire. Une fois ces modèles validés en se basant sur des données d'avions existants, ils ont été intégrés aux outils existants. Afin d'utiliser au mieux cette intégration et de profiter des synergies de cette approche, une des contributions de la thèse a été d'intégrer aux degrés de liberté usuels, des paramètres de conception du moteur et des degrés de liberté de la mission. L'étude des résultats met en évidence les gains apportés par cette nouvelle approche en comparaison avec l'approche classique.

Cette thèse contribue également à répondre à la problématique de l'impact environnemental de l'aviation en ajoutant la minimisation de l'impact climatique aux objectifs classiques de la conception d'avion. Une modélisation de cet impact est intégrée aux modèles existants. Pendant la phase préliminaire de conception d'avion, de nombreuses technologies innovantes sont étudiées afin de minimiser les critères précédemment cités. Nous sélectionnons certaines de ces innovations pouvant s'intégrer au système propulsif de l'avion, à son système aérodynamique, à sa géométrie ou encore à sa mission afin de tirer de la configuration le maximum de bénéfices en termes de performances. Nous proposons ainsi d'appliquer l'approche holistique à un concept innovant d'avion à propulsion hybride électrique-fuel. Les modèles construits et utilisés pour optimiser cet avion hybride sont présentés et viennent compléter les modèles existants après validation par des experts dans le domaine. Les résultats de cette optimisation sont comparés à ceux d'un avion conventionnel répondant au même cahier des charges.

Toutes les études menées jusqu'à présent sont déterministes. Des incertitudes autour des modèles utilisés existent et sont traditionnellement prises en compte par des marges basées sur le savoir-faire ingénieur. Cela peut parfois mener à des contre-performances inattendues. Dans cette thèse nous introduisons une nouvelle approche consistant à prendre en compte consciencieusement ces incertitudes. Pour cela, un des chapitres de la thèse est consacré au recensement et à la comparaison des méthodes de gestion des incertitudes qui pourraient s'appliquer à notre problème de conception, selon des critères propres à nos études (temps de calcul, précision, hypothèses sur les modèles, ...). Nous proposons ensuite de résoudre une optimisation sous contrainte en probabilité du concept d'avion hybride, en prenant en compte les incertitudes liées à l'évolution des technologies nécessaires à l'hybridation. Enfin, cette thèse présente une nouvelle approche d'optimisation robuste de la conception d'avion: nous cherchons à concevoir un avion optimal vis-à-vis du cout ou de la consommation en fuel et dont les performances sont satisfaites quelle que soit l'incertitude présente. Cette approche est complémentaire à l'approche sous contraintes en probabilité. L'application de ces méthodes d'optimisation robuste nécessite une modélisation particulière du problème qui est décrite dans le dernier chapitre de cette thèse.

7.2 Modélisation, simulation et validation

7.2.1 Description du processus de conception avion

Le processus de conception avion (OAD pour *Overall Aircraft Design*) est le processus de définition globale d'un avion. La première étape consiste à sélectionner un certain nombre de spécifications telles que le nombre de passagers, le rayon d'action de l'avion et les performances attendues. La conception est généralement optimisée par rapport à un critère donné tel que le cout d'opération de l'avion (COC pour *Cash Operating Cost*), la consommation en fuel ou la masse maximum au décollage (MTOW pour *Maximum Take-Off Weight*) qui est un indicateur de performance de l'avion. Les variables de conception classiques sont la surface de la voilure et la poussée statique au niveau de la mer (SLSthrust pour *Sea Level Static Thrust*) qui conditionne la taille des moteurs. Les outils numériques de l'OAD permettent de calculer la configuration complète d'un avion et ses performances. Le but est de trouver les valeurs des variables de conception permettant à l'avion de satisfaire les spécifications demandées tout en minimisant le critère choisi. Cette optimisation qui englobe le calcul de la configuration de l'avion, est une optimisation mono-objectif déterministe sous contraintes. Le principe de l'OAD classique est résumé sur la Figure 7.1. Ce diagramme montre comment les différentes disciplines interagissent, comment un avion est calculé à partir des spécifications et des variables d'entrée et comment les objectifs et les contraintes sont calculés.

La conception préliminaire avion est le processus multi-disciplinaire décrivant les interactions entre différents domaines de la physique (cela correspond au cadre vert dans le diagramme de la Figure 7.1). Parmi les plus importants, citons la géométrie, l'aérodynamique, les masses, la propulsion, la trajectoire, l'impact environnemental. Chaque discipline est caractérisée par un ou plusieurs paramètres réels ainsi que par des fonctions de ces paramètres. L'outil de conception utilisé au cours de la thèse est un outil interne à Airbus, appelé OCCAM et développé en Scilab, qui est l'aboutissement de dix années de recherche et d'expérimentations au sein du groupe [12, 22]. Une description complète de ces modèles

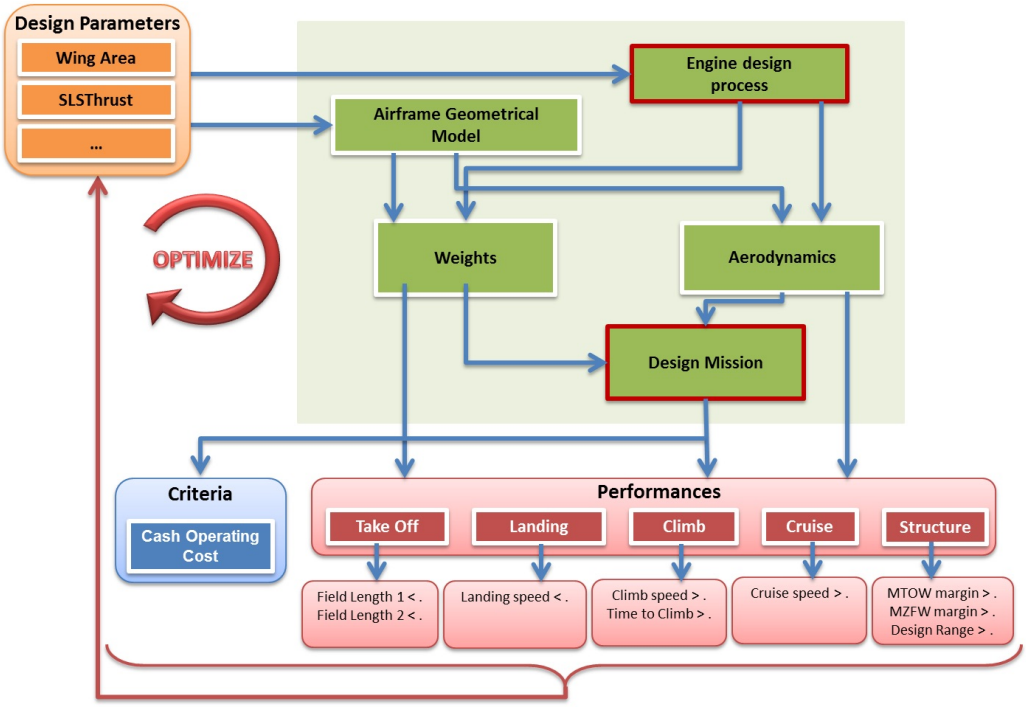

Figure 7.1: Diagramme du processus classique de conception avion.

peut être trouvée dans la thèse de J. Birman [**?**]: il s'agit de modèles semi-empiriques issus soit des lois de la physique, soit de régressions sur une base de données d'une soixantaine d'avions.

Un des objectifs de la thèse était d'intégrer au processus de nouveaux modèles semi-empiriques d'un moteur thermodynamique et de la trajectoire. Le processus de conception avion décrit par la Figure 7.1 a alors été renforcé au cours de la thèse, cf Figure 7.2. Tout d'abord, on élargit l'ensemble des paramètres de conception (et donc de l'optimisation) en prenant en compte à la fois les paramètres de la cellule avion (taille du moteur, surface de la voilure, allongement des ailes), les paramètres du moteur thermodynamique (rapport entre les flux d'air froid et d'air chaud - BPR pour *By-Pass Ratio*) et les paramètres de mission (altitude de croisière, mach de vol, vitesses de montée et de descente de la trajectoire).

Les contraintes opérationnelles peuvent être nombreuses et variées et doivent garantir à la fois la capacité à voler et la sécurité des avions. Schématiquement, un avion doit être capable de décoller des pistes existantes des aéroports actuels, de monter jusqu'à son altitude de croisière en un temps limité, de s'y maintenir et d'atterrir sur les pistes existantes. Ceci se traduit en terme de longueur maximale de pistes au décollage ou à l'atterissage, de masse maximum au décollage, de temps de montée, de vitesse d'approche, etc.

Quant aux critères de l'optimisation, nous nous sommes intéressés à trois critères classiques particuliers: le cout d'opération (COC) de l'avion, la masse maximum au décollage (MTOW) et la consommation en fuel. Nous avons ajouté à ces critères une mesure de l'impact climatique de l'avion APGWP (*Absolute Pulsed Global Warming Potential*). Ce critère reconnu par le protocole de Kyoto, est très difficile à évaluer car très dépendant de différentes disciplines et d'un grand nombre de paramètres. Au niveau des Avant-Projets

d'Airbus, la méthode choisie pour mesurer cet impact climatique est une méthode développée dans le cadre d'un projet européen nommé LEEA (*Low Emission Effect Aircraft*) [89]. L'impact climatique est calculé comme une fonction de plusieurs paramètres réels: la quantité de polluants émise, l'altitude d'émission de ces polluants, la distance parcourue en vol et la consommation en fuel. L'impact environnemental est avant tout lié à la consommation en fuel mais aussi à l'endroit où les polluants sont émis. A noter que la zone entre 35000 et 37000 pieds est le pire endroit où émettre des polluants azotés et que c'est la zone dans laquelle volent les avions actuels.

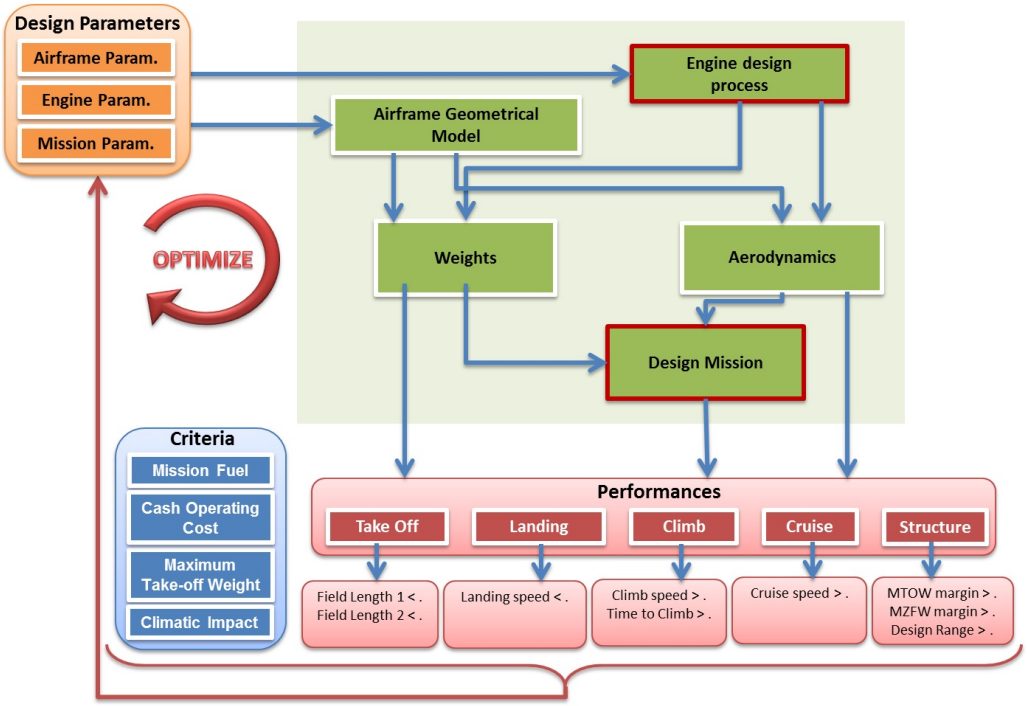

Figure 7.2: Diagramme du processus de conception avion étudié pendant la thèse.

7.2.2 Configuration de l'avion hybride

Répondant au même cahier des charges, nous avons proposé d'appliquer l'approche holistique décrite précédemment à un concept innovant d'avion à propulsion hybride électrique-fuel représenté sur la Figure 7.3. L'idée a été de conserver une configuration classique d'avion et d'ajouter un moteur électrique sur le fuselage arrière de l'avion. Afin d'alimenter ce moteur, des batteries ont été placées au niveau du caisson central de l'avion. Des générateurs électriques ont été montés sur les turboréacteurs de façon à ce qu'ils puissent récupérer une partie de leur énergie et faire fonctionner le moteur électrique ou recharger les batteries. Il a ensuite fallu faire des hypothèses sur le mode de gestion de l'énergie pour cet avion en tirant partie des nouvelles possibilités apportées par l'hybridation. Il faut garder à l'esprit que ces accumulateurs électriques sont des sources d'énergie additionnelles mais temporaires. Ils permettent de réduire le sur-dimensionnement des moteurs thermodynamiques en les soulageant lors des phases critiques de la mission (décollage, fin de montée). La stratégie choisie est résumée sur la Figure 7.4.

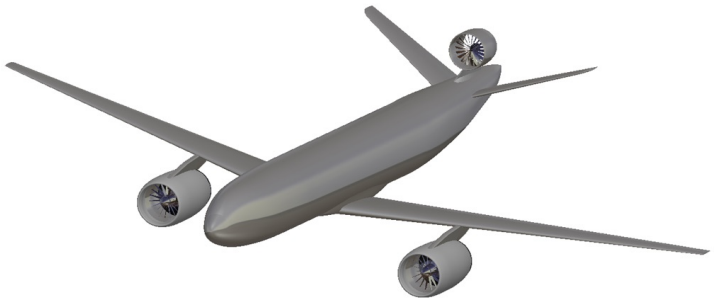

Figure 7.3: Configuration d'avion hybride.

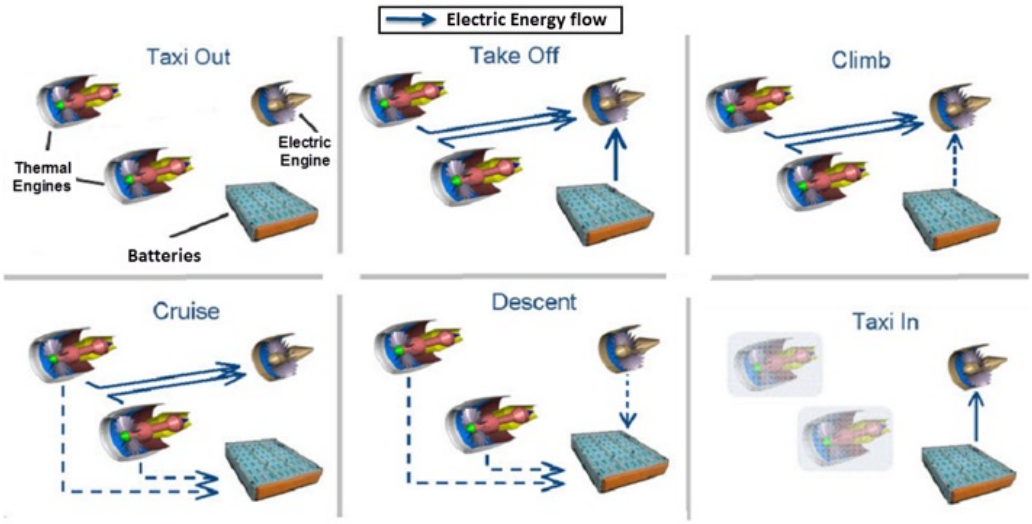

Figure 7.4: Stratégie de gestion des flux d'énergie. Les flèches bleues indiquent les flux d'énergie électrique.

De nouveaux modèles, par exemple de propulsion électrique, ont été construits et viennent compléter les modèles existants après validation par des experts du domaine. On sélectionne alors des variables de conception additionnelles associées à l'hybridation: en plus des variables décrites au paragraphe précédent, on ajoute la taille du moteur électrique, la puissance du moteur électrique, la densité de puissance du moteur électrique et des générateurs électriques et la densité d'énergie des batteries. Quelques améliorations du concept d'avion hybride sont proposées dans la thèse (voir en détails dans le Chapitre 1).

7.3 De l'optimisation déterministe à l'optimisation sous contraintes en probabilité

Une fois le modèle d'avion hybride défini, un des objectifs de la thèse a été de résoudre un problème d'optimisation globale de l'avion, regroupant les paramètres de tous les modèles (cellule avion, moteur, mission et le cas échéant, hybridation) pour un avion conventionnel de référence d'une part et pour l'avion hybride d'autre part, à cahier des charges identique. Les résultats de l'optimisation sont comparés selon les 3 objectifs suivants: cout global

d'opération de l'avion, masse maximale au décollage et impact climatique. L'objet de l'étude a été d'augmenter progressivement le nombre de variables de l'optimisation afin de mesurer l'impact de chacune sur la configuration optimisée de l'avion conventionnel puis de l'avion hybride.

7.3.1 Formulation du problème

Considérons le problème d'optimisation de conception avion sous sa forme générique:

$$\min_{x\in\mathbb{R}^n} f(x) \quad \text{sous:} \quad g_i(x) \leq 0,\ i = 1,\dots,l, \qquad x_{min} \leq x \leq x_{max}. \tag{7.1}$$

Dans cette étude, nous avons travaillé avec 3 fonctions objectifs f différentes: le cout global d'opération de l'avion, la masse maximale au décollage et l'impact climatique. Pour un avion conventionnel court-courrier de référence, nous considérons 13 variables d'optimisation décrivant la cellule avion, les moteurs thermodynamiques et la mission, et 8 contraintes opérationnelles portant essentiellement sur la vitesse d'approche, les vitesses verticales de montée et de croisière, la longueur de piste au décollage, le temps de montée. Quant à l'avion hybride, nous ajoutons 3 variables associées à l'hybridation: la taille du moteur électrique, le taux de prélèvement de puissance des générateurs et la densité de puissance du moteur électrique. Nous obtenons ainsi un problème avec 16 variables de conception et 1 contrainte opérationnelle sur la poussée des moteurs au décollage.

Du point de vue de l'optimisation, le problème (7.9) est un problème non linéaire, non convexe mais différentiable presque partout. Les gradients sont accessibles par différentiation automatique, une méthode implémentée au cours de la thèse, ce qui nous permet d'utiliser des algorithmes d'optimisation numérique différentiable. Les algorithmes utilisés pour résoudre le problème (7.9) sont les suivants: DOT (*Design Optimization Tools*) [172], MADS (*Mesh Adaptive Direct Search*) [11] et un algorithme de Nelder-Mead modifié pour intégrer des contraintes et développé en interne aux Avant-Projets pendant cette thèse.

Les résultats de l'optimisation par exemple par rapport au COC (cout global d'opération de l'avion) montrent que l'avion conventionnel a intérêt à voler "vite" pour minimiser le cout lié à la durée du vol et "haut" pour minimiser le cout lié à la consommation en carburant. Plus précisément, à l'optimum, les variables de l'optimisation sont à saturation. En particulier, la valeur très élevée du Mach de croisière implique des valeurs très élevée de l'impact climatique (APGWP) et de la masse maximum au décollage (MTOW). Les polluants sont émis à la pire altitude possible du point de vue de l'impact environnemental. Quant à l'avion hybride, il est très nettement handicapé par l'excédent de masse du système de propulsion hybride. L'optimisation de l'avion hybride donne une configuration similaire à celle de l'avion conventionnel optimisé avec un cout global d'opération plus élevé de 1.5%, une masse maximale au décollage plus élevée de 2.6%. En revanche l'impact climatique (APGWP) est nettement réduit (environ 19% inférieur) par rapport à celui de l'avion conventionnel.

Ainsi à la question naturelle de savoir si cet avion est compétitif par rapport à un avion conventionnel, la réponse est clairement non compte-tenu des technologies actuelles. L'idée a alors été d'ajouter un modèle de prédiction de l'évolution des technologies nécessaires à l'hybridation en fonction de l'année et prenant en compte l'incertitude sur ces prédictions, cf Figure 7.5. Ceci se traduit en incertitude dans les modèles.

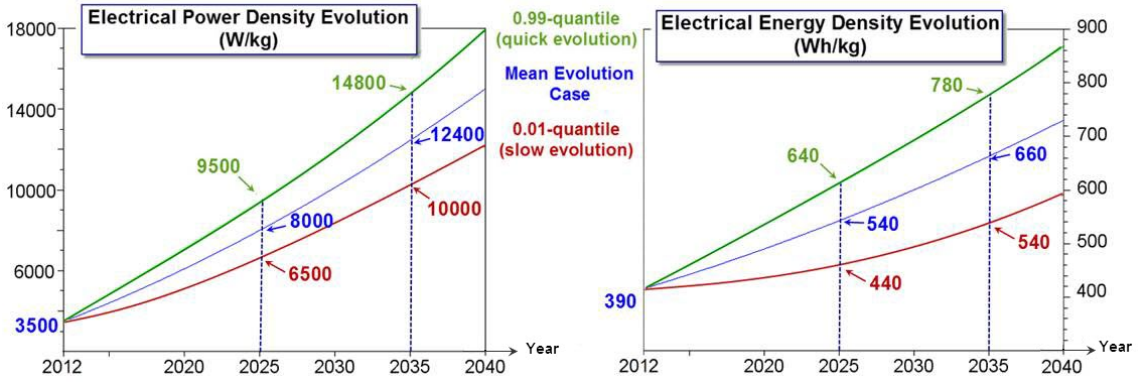

Figure 7.5: Prédiction de l'évolution des technologies électriques liées à l'hybridation avec leurs incertitudes.

Les incertitudes peuvent provenir de deux sources complémentaires: les incertitudes liées à l'évolution des technologies et celles liées au processus de modélisation. En pratique, les incertitudes présentes dans les modèles sont prises en compte au travers de marges basées sur le savoir-faire ingénieur. Cela peut parfois mener à des contre-performances inattendues qui se traduisent en pénalité (en terme de cout) pour les constructeurs d'avion. De plus dans le cas de l'avion hybride, nous ne disposons pas de ce savoir-faire ingénieur: il faut donc s'attaquer au "vrai" problème et non à une représentation moyenne (déterministe) de celui-ci. Dans la thèse, nous avons pris en compte ces incertitudes par des approches d'optimisation robuste. Le problème de conception avion peut alors être considéré comme un problème d'optimisation stochastique pour lequel nous avons proposé deux approches. La première approche consiste à reformuler le problème en un problème d'optimisation sous contraintes en probabilité: notons Ξ le vecteur aléatoire modélisant les incertitudes en entrée. On veut résoudre:

$$\min_{x\in\mathbb{R}^n} \mathbb{E}[f(x,\Xi)] \quad \text{sous:} \quad \mathbb{P}\left[g_i(x,\Xi)\leq 0\right] > p_i,\ i=1,\dots,l, \qquad x_{min}\leq x\leq x_{max}. \tag{7.2}$$

La seconde approche explorée dans la thèse consiste à reformuler le problème de conception avion en un problème d'optimisation robuste selon la terminologie de A. Ben-Tal, L. El Ghaoui et A. Nemirovski [16]: soit $\mathcal{U}$ l'ensemble des incertitudes. Nous considérons le problème:

$$\inf_{x\in\mathbb{R}^n}\left(\sup_{\xi\in\mathcal{U}} f(x,\xi)\right) \quad \text{sous:} \quad g_i(x,\xi)\leq 0,\ \forall i=1,\dots,l,\ \forall\xi\in\mathcal{U}, \qquad x_{min}\leq x\leq x_{max}. \tag{7.3}$$

L'intérêt de cette approche est bien entendu de proposer une solution qui satisfasse toutes les contraintes imposées lorsque la violabilité des contraintes est interdite. Une formulation particulière du problème de conception avion est proposée au paragraphe 7.3.4 et permet d'obtenir algorithmiquement des configurations robustes.

7.3.2 Quantification et propagation d'incertitudes

Avant toute chose, la formulation des problèmes (7.2) et (7.3) met en évidence la nécessité de savoir quantifier et propager l'incertitude dans les modèles. Plusieurs méthodes ont été

introduites en détails dans le Chapitre 4 de la thèse pour caractériser les incertitudes et les propager: un état de l'art conséquent est proposé dans lequel les méthodes de propagation d'incertitudes sont présentées, classées en fonction de leurs spécificités (temps de calcul, précision, hypothèses nécessaires sur les modèles) et comparées sur des exemples numériques académiques. Le but de cette étude est de permettre à l'utilisateur de sélectionner une méthode adaptée à son problème de dimensionnement d'avion sous incertitude.

7.3.2.1 Quantification et caractérisation des incertitudes

En conception technique, modéliser un processus consiste à construire des modèles calculant certaines fonctions d'intérêt en fonction de paramètres d'entrée identifiés au préalable. Ces modèles peuvent provenir soit des lois de la physique quand c'est possible, soit de régression sur des bases de données d'avions existants. Plus précisément, le processus de modélisation se fait en deux temps: tout d'abord, on sélectionne les paramètres d'entrée en se basant soit sur le savoir-faire ingénieur soit sur des études statistiques permettant d'identifier les paramètres les plus influents. Ensuite, on choisit un modèle analytique dont on ajuste les paramètres par des techniques par exemple de régression sur les bases de données existantes. Le but de la quantification d'incertitudes est d'estimer la précision avec laquelle le modèle analytique approche le modèle réel. Plus concrètement, étant donné un échantillon de données $(x_i, y_i)_{i=1,\dots,N}$, on veut estimer l'échantillon:

$$\xi_i = f(x_i) - y_i,$$

appelé échantillon d'incertitudes. Une fois cet échantillon estimé, on cherche la loi de distribution de probabilité qui le représente le mieux. En pratique, on fait l'hypothèse que tout échantillon d'incertitude peut être représenté par une loi de distribution de probabilité. Pour identifier cette loi, on peut soit calculer les moments de la distribution, soit chercher graphiquement une distribution correspondant au mieux au diagramme des incertitudes. Il faut cependant garder à l'esprit que la connaissance d'un nombre fini de moments ne permet pas de définir une unique loi de probabilité et qu'un même échantillon représenté à deux échelles différentes, peut être approché par (au moins) deux lois très différentes, cf Figure 7.6.

Une des contributions de la thèse en collaboration avec J. Birman [22], a été de proposer une nouvelle famille de loi de probabilité, appelée Beta-Mystique, qui englobe plusieurs familles de distributions uni-modales. Plus précisément, le but était de proposer une loi facile à manipuler pour un non-spécialiste, couvrant un large spectre de formes de distributions et vérifiant certaines propriétés: à support compact, uni-modale et continue. La loi Beta aurait pu faire l'affaire mais le choix de ses paramètres est peu intuitif. La loi Beta-Mystique est définie de la façon suivante:

Definition 7.1. *On dit qu'une variable aléatoire X suit une loi Beta-Mystique de paramètres (a, b, Z, P) , avec $-1 \leq Z \leq 1$ et $P \geq 0$, si sa fonction de densité est de la forme:*

$$f_X(x; a, b, Z, P) = \begin{cases} \dfrac{(b-x)^{q_1-1} \cdot (x-a)^{p_1-1}}{\beta\,(p_1, q_1) \cdot (b-a)^{p_1+q_1-1}} & , \textit{ si } a \leq x \leq b, \\ 0 & , \textit{ si } x < a \textit{ ou } b < x, \end{cases} \tag{7.4}$$

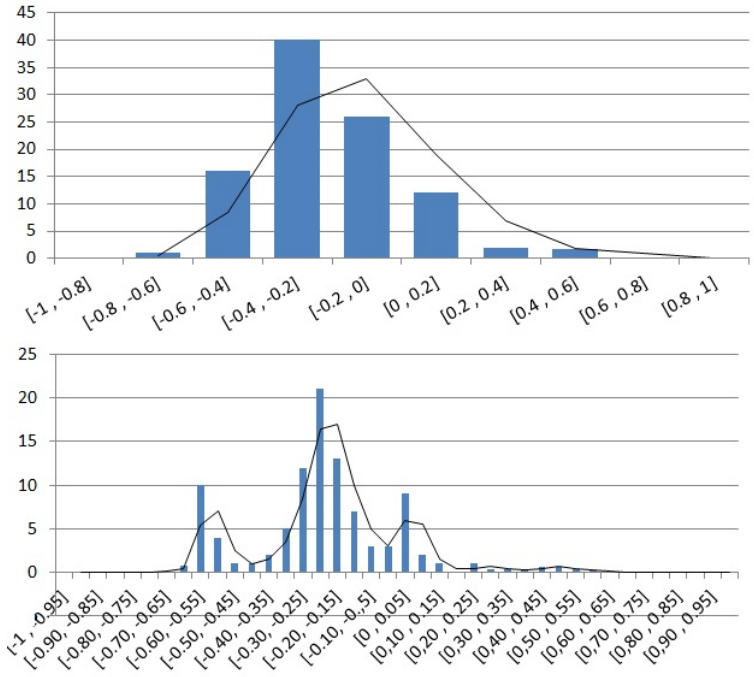

Figure 7.6: Exemple de deux approximations du même échantillon représenté à deux échelles différentes, par deux distributions différentes.

avec:

$$W = \max\Big(\varepsilon - 1, \min(Z, 1-\varepsilon)\Big), \quad K = 3.3\frac{\max(\varepsilon, P)}{b-a}, \quad M = \frac{1}{2}\left(a(1-W) + b(1+W)\right),$$

$$p_1 = 1 + K\left(M - a\right), \quad q_1 = 1 + K\left(b - M\right), \quad \beta(p_1, q_1) = \frac{\Gamma(p_1)\Gamma(q_1)}{\Gamma(p_1+q_1)},$$

$$\varepsilon > 0.$$

où Γ *est la fonction Gamma définie par :* $\Gamma(t) = \int_0^\infty x^{t-1}e^{-x}dx$.

En pratique, le paramètre ε est choisi égal à la précision de calcul des ordinateurs. L'introduction de ce paramètre permet d'éviter les problèmes numériques lorsque les paramètres P et Z atteignent leurs bornes respectives. L'avantage de cette nouvelle loi de probabilité est que l'on peut facilement contrôler la forme de sa distribution: $[a, b]$ est le support de la loi, Z contrôle la symétrie de la distribution, $Z \in [-1, 1]$, et P contrôle l'étalement de la loi. La Figure 7.7 illustre la façon dont les paramètres Z et P contrôlent la forme de la distribution: lorsque Z est fixé, plus P est petit, plus la distribution est large. Si $Z = 0$, la distribution est symétrique. A noter par exemple que la loi normale $\mathcal{N}(0, \sigma^2)$ peut être approchée par la loi Beta-Mystique de paramètres $(-6\sigma, 6\sigma, 0, 10)$ et que la loi uniforme $U(a, b)$ est équivalente à la loi Beta-Mystique de paramètres $(a, b, 0, 0)$.

Un autre avantage de la loi Beta-Mystique est de pouvoir être caractérisée par ses 4 premiers moments: son espérance μ, sa variance σ^2, sa dissymétrie (*skewness*) γ et son aplatissement (*kurtosis*) Γ. Plus précisément, les 4 moments $(\mu, \sigma^2, \gamma, \Gamma)$ ont des expressions analytiques simples en fonction des paramètres (a, b, Z, P) et inversement. Le lecteur

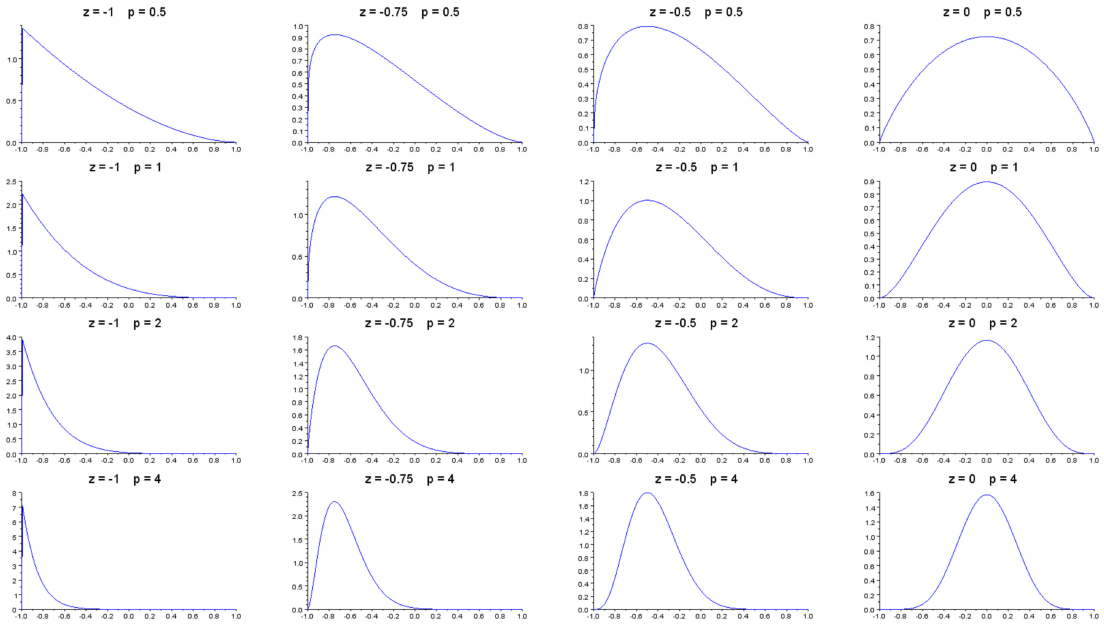

Figure 7.7: Evolution de la forme de la loi Beta-Mystique en fonction de $P \in [0.5, 4]$ et $Z \in [-1, 0]$.

intéressé pourra se référer à [22] ou au Chapitre 4 de cette thèse pour davantage de précisions.

La loi Beta-Mystique distribution a déjà été utilisée pour quantifier les incertitudes au sein du bureau des Avant-Projets d'Airbus: les premières expériences ont montré qu'il s'agissait d'un outil très efficace pour remplacer le savoir-faire ingénieur basé sur des marges et gérer les incertitudes dans les modèles.

7.3.2.2 Propagation des incertitudes

La problématique est la suivante: connaissant certaines informations sur l'incertitude Ξ en entrée, que savons-nous sur l'incertitude en sortie i.e. sur $f(x, \Xi)$ et $g(x, \Xi)$? Autrement dit, étant donné un modèle $F(\xi) = f(x, \xi)$ où ξ est une réalisation de la variable aléatoire Ξ, on cherche à déterminer les caractéristiques ou une représentation de l'incertitude $F(\Xi)$ en sortie. Deux cas se présentent:

1^{er} **cas: Ξ suit une loi de probabilité.** Plusieurs méthodes sont alors envisageables: méthodes de Monte-Carlo, méthodes basées sur le développement de Taylor, méthodes d'expansion stochastiques, méthodes de quadrature. Toutes ces méthodes sont décrites en détails dans le Chapitre 4 de cette thèse, classées en fonction de leurs spécificités (temps de calcul, précision, hypothèses nécessaires sur les modèles) et comparées sur des exemples numériques académiques. Le but de cette étude est de permettre à l'utilisateur de sélectionner une méthode adaptée à son problème de dimensionnement d'avion sous incertitude.

$2^{ème}$ **cas: on connait le support $[a, b]$ de Ξ.** Dans ce cas, on cherche les supports de $f(x, \Xi)$ et $g(x, \Xi)$. Une approche naturelle serait d'utiliser des techniques de propaga-

tion d'intervalles mais celles-ci sont difficile à appliquer à notre problème de configuration avion. L'alternative a été d'appliquer les méthodes de propagation d'incertitudes décrites dans le premier cas à une distribution de probabilité de support $[a, b]$ et de récupérer le support de la distribution en sortie pour avoir celui de $f(x, \Xi)$ et $g(x, \Xi)$.

Dans les deux cas, il faut se demander de quel type d'information on a besoin sur l'incertitude en sortie des modèles: la nature exacte de la distribution de probabilité, les premiers moments, une mesure de risque ? Le choix de la méthode de propagation est fortement couplé à la précision que l'on a sur l'incertitude en entrée, la précision que l'on souhaite sur l'incertitude en sortie et le cout de calcul que l'on peut se permettre. Le guide proposé dans le Chapitre 4 de cette thèse permet de répondre à ces questions et de sélectionner la méthode la plus adaptée au problème considéré.

7.3.3 Optimisation sous contrainte en probabilité de l'avion hybride

Considérons le problème de conception avion sous la forme d'un problème d'optimisation sous contraintes en probabilité (individuelles) de la forme:

$$\min_{x \in \mathbb{R}^n} \mathbb{E}[f(x, \Xi)] \quad \text{sous:} \quad \begin{aligned} &\mathbb{P}\left[g_i(x, \Xi) \leq 0\right] > p_i, \ i = 1, \dots, l, \\ &x_{min} \leq x \leq x_{max}, \end{aligned} \tag{7.5}$$

où x est la variable (certaine) de l'optimisation et Ξ le vecteur aléatoire modélisant les incertitudes d'entrée. Les paramètres $(p_i)_{i=1,\dots,l}$ sont les niveaux de fiabilité, choisis en pratique entre 0.95 et 0.99. Les fonctions $f : \mathbb{R}^n \to \mathbb{R}$ et $g : \mathbb{R}^n \to \mathbb{R}^l$ sont supposées différentiables en tout point $x \in \mathbb{R}^n$. En revanche le problème est *a priori* non linéaire et non convexe.

Une des difficultés dans notre cas est que bien qu'ayant des informations sur l'incertitude en entrée Ξ, on ne sait rien à propos de l'incertitude en sortie. Dans le cas où l'on connait l'incertitude en entrée, les méthodes de propagation décrites dans le Chapitre 4 de cette thèse permettent d'évaluer l'espérance de l'objectif et les contraintes en probabilité et ainsi d'appliquer un algorithme d'optimisation classique. Toutefois cette approche directe étant très couteuse, des recherches ont été menées sur des méthodes d'optimisation séquentielles sous incertitude telles que la méthode S.O.R.A. (*Sequential Optimization and Reliabilty Assessment*) introduite par X. Du et W. Chen dans [56] et améliorée dans [183]. L'idée de ces méthodes est de découpler l'optimisation de l'analyse de fiabilité. Dans un premier temps, on remplace le problème sous contraintes en probabilité (7.5) par une suite de problèmes déterministes:

$$\min_{x \in \mathbb{R}^n} f(x, \mu_\Xi) \quad \text{sous:} \quad \begin{aligned} &g_i(x, \mu_\Xi) \leq s_i, \ i = 1, \dots, l, \\ &x_{min} \leq x \leq x_{max}, \end{aligned} \tag{7.6}$$

L'évaluation de la fiabilité (i.e. des contraintes $\mathbb{P}\left[g_i(x_{sol}, \Xi) \leq 0\right]$) est effectuée dans un second temps. Le principe de la méthode est le suivant:

Initialisation: $s_i = 0$, $i = 1, \dots, l$.

Tant que $\exists i \in \{1, \dots, l\}$, $\mathbb{P}\left[g_i(x_{sol}, \Xi) \leq 0\right] < p_i$,

1. Résoudre le problème déterministe (7.6). On note x_{sol} la solution obtenue.

2. Calculer les incertitudes $g_i(x_{sol}, \xi)$, $i = 1, \ldots, l$, en utilisant une technique de propagation d'incertitudes bien choisie et évaluer les probabilités: $\mathbb{P}\left[g_i(x_{sol}, \Xi) \leq 0\right]$.
3. Pour chaque $i = 1, \ldots, l$, faire
   - Si $\mathbb{P}\left[g_i(x_{sol}, \Xi) \leq 0\right] < p_i$ alors le seuil s_i est mis à jour de la façon suivante:

$$s_i = s_i - k(p_i)\sigma_{g_i}(x_{sol}), \tag{7.7}$$

     où $\sigma_{g_i}(x)$ est la variance de $g_i(x, \Xi)$ à x fixé. Le coefficient $k(p_i)$ est défini en fonction de la mesure de risque désirée (ici une probabilité), du niveau de fiabilité p_i désiré et des informations disponibles sur la distribution de probabilité associée à $g_i(x, \Xi)$ (à x fixé).

Revenons sur la mise à jour (7.7) des seuils s_i dont le but est de décaler les contraintes violées vers le domaine de faisabilité en intégrant les coefficients de seuil s_i dont le calcul est basé sur les informations de fiabilité obtenues à l'itération précédente. Plus précisément, les contraintes en probabilité $\mathbb{P}\left[g_i(x, \Xi) \leq 0\right] \geq p_i$ peuvent être remplacées de façon conservative par la contrainte déterministe:

$$\mu_{g_i}(x) + k(p_i)\sigma_{g_i}(x) \leq 0 \tag{7.8}$$

Plus précisément, si la contrainte (7.8) est satisfaite alors:

$$\mathbb{P}\left[g_i(x, \Xi) \leq 0\right] \geq \mathbb{P}\left[g_i(x, \Xi) \leq \mu_{g_i}(x) + k(p_i)\sigma_{g_i}(x)\right] \geq p_i.$$

Les contraintes violées (ou ayant une fiabilité trop faible) sont décalées vers le domaine de faisabilité en intégrant des coefficients de seuil s_i dont le calcul est basé sur les informations de fiabilité obtenues à l'itération précédente. La mise à jour proposée est une généralisation de celle proposée pour les lois de distribution gaussienne dans [92], au cas où les incertitudes ne sont pas complètement connues (par exemple lorsque l'on ne dispose que des premiers moments de la loi de probabilité) et pas nécessairement gaussiennes.

7.3.3.1 Application à l'optimisation sous contrainte en probabilité de l'avion hybride

La méthodologie précédente, testée sur un exemple académique, a ensuite été appliquée à l'optimisation de l'avion hybride. Nous nous sommes intéressés au problème suivant: compte-tenu de l'évolution (prédite) des technologies nécessaires à l'hybridation, trouver l'année à partir de laquelle l'avion hybride sera aussi performant qu'un avion conventionnel avec une probabilité de 95%, à cahier des charges identique.

La démarche adoptée est la suivante: commençons par résoudre une optimisation déterministe d'un avion conventionnel de référence, i.e. résoudre:

$$\min_{x \in \mathbb{R}^n} f(x) \quad \text{sous:} \quad \begin{array}{l} g_i(x) \leq 0,\ i = 1, \ldots, l, \\ x_{min} \leq x \leq x_{max}. \end{array}$$

Le cout f représente soit la consommation en fuel, soit le cout globale d'opération de l'avion (COC), soit une mesure de l'impact climatique (APGWP). On note f^*_{conv} la valeur de la fonction cout à l'optimum. Nous proposons ensuite de résoudre le problème:

$$\min_{(x,t) \in \mathbb{R}^{n+1}} t \quad \text{sous:} \quad \mathbb{P}\left[g_i(x, \Xi) \leq 0\right] \geq 0.95,\ i = 1, \ldots, l, \tag{7.9}$$

$$\begin{aligned} &\mathbb{P}\left[f(x,\Xi) \leq f^*_{conv}\right] \geq 0.95, \\ &x_{min} \leq x \leq x_{max},\ t \geq 2015. \end{aligned} \tag{7.10}$$

où la variable t représente l'année qui indique le degré de maturité des technologies nécessaires à l'hybridation. Les résultats obtenus sont présentés dans le tableau de la Figure 7.3.3.1.

Optimize versus	Cost Mission Block Fuel		Cash Operating Cost (COC)		Climate Impact (APGWP)	
	Conventional	Hybrid	Conv.	Hyb.	Conv.	Hyb.
Equilibrium Year		2026		2025		2020
SLSThrust (daN)	11620	11160	12260	11760	10950	11120
WingArea (m^2)	152	152	150	154	175	175
Wing Aspect Ratio	17	17	15	16	10	*8*
Cruise Mach	0,63	0,61	0,75	0,66	0,66	0,61
Cruise Altitude (ft)	35 000	35 000	35000	35000	31400	30000
BPR	*8*	*8*	*8*	*8*	12,9	12,2
eFan Power (MW)		1,1		*1*		1,7
Electric Ratio		*0,01*		*0,01*		0,012
Active Constraints	TOFL1	TOFL1	TOFL1 - LdSpeed	TOFL1 - LdSpeed	TOFL1 - ClbVz	TOFL1
Cost Mis. Fuel	**1650**	**1650**	1780	1780	2100	2300
COC	4400	4470	**4200**	**4200**	4600	4920
APGWP	$3{,}1\text{x}10^{-5}$	$3{,}06\text{x}10^{-5}$	$3{,}25\text{x}10^{-5}$	$3{,}2\text{x}10^{-5}$	**$2{,}77\text{x}10^{-5}$**	**$2{,}77\text{x}10^{-5}$**

Plus qu'une réelle révolution, cette optimisation est une très bonne validation des études parallèles menées précédemment quant à la pertinence du modèle et à la sensibilité des variables de conception. On retrouve par exemple le fait que pour réduire l'impact climatique, les avions devraient voler moins haut que les 35000 pieds actuels et moins vite, mais que cela entraine une augmentation significative de la masse maximale au décollage et du cout global d'opération de l'avion. On observe également que d'ici 2025-2026, l'évolution des technologies nécessaires à l'hybridation devraient permettre de proposer un avion hybride qui soit économiquement viable par rapport à l'avion conventionnel avec une probabilité de 95%. Ainsi même s'il reste un gros travail à faire sur la conception de cet avion, nos résultats montrent qu'un avion hybride est une piste de recherche à considérer.

7.3.4 Premiers pas vers l'optimisation robuste

Dans la dernière partie de la thèse, nous nous sommes intéressés à une approche différente, quoique complémentaire, de l'optimisation pour la conception préliminaire d'avions. En se basant sur le savoir-faire des ingénieurs et sur les simulations réalisées au cours de cette thèse, il apparait que pour certaines fonctions objectif telles que le cout ou la consommation en fuel, le problème de conception préliminaire avion décrit au paragraphe 7.3.1, peut être vu comme un problème d'optimisation sous incertitudes dont la fonction objectif est presque affine et les contraintes quasiment convexes. Nous avons alors montré que le problème initial peut être approché de manière conservative par un problème de programmation linéaire incertain auquel nous pourrons appliquer les techniques de programmation linéaire robuste décrites dans [16, Chapitre 1]. Cette méthodologie est ensuite appliquée à deux cas réels

de conception avion dont nous présentons les résultats numériques. Dans ce mémoire, nous nous contenterons d'en donner les grandes étapes et de présenter les résultats numériques obtenus. Le lecteur intéressé par les détails pourra se référer soit au Chapitre 6 de la thèse, soit à l'article [142].

Partons du problème générique de conception d'avion présenté au paragraphe 7.3.1 i.e.:

$$\min_{x\in\mathbb{R}^n} f(x,\xi) \quad \text{sous:} \quad g_i(x,\xi)\leq 0,\ i=1,\dots,l, \qquad x_{min}\leq x\leq x_{max}. \tag{7.11}$$

où ξ est le vecteur des entrées incertaines du modèle. Les grandes idées sont les suivantes: basé sur le savoir-faire des ingénieurs et des simulations numériques qui viennent corroborer ces observations, les fonctions objectifs telles que le cout ou la consommation en fuel, sont presque linéaires en les variables de conception et l'ensemble des contraintes peut être approché par un polyèdre convexe. Ainsi en linéarisant la fonction f par rapport aux variables x de l'optimisation et en remplaçant le domaine admissible par un polyèdre dont la construction est détaillée dans [142], le problème (7.11) peut être approché par un programme linéaire incertain de la forme:

$$\min_{x\in\mathbb{R}^n} c^\top x+d \quad \text{sous:} \quad Ax\leq b, \qquad x_{min}\leq x\leq x_{max}. \tag{7.12}$$

où les incertitudes sur les coefficients (A,b,c,D) sont supposées connues (données par le savoir-faire des ingénieurs ou bien par des méthodes de propagation des incertitudes). Notons $\mathcal{U}$ l'ensemble des incertitudes décrit par ces coefficients. Suivant le formalisme de A. Ben-Tal, L. El Ghaoui et A. Nemirovski [16], on suppose que $\mathcal{U}$ admet un paramétrage affine de la forme:

$$\mathcal{U}=\left\{D=\begin{bmatrix} c^\top & d\\ A & b\end{bmatrix}\in\mathbb{R}^{(1+m)\times(1+n)}\ :\ D=D^0+\sum_{k=1}^{L}\zeta_k D^k,\ \zeta\in\mathcal{Z}\subset\mathbb{R}^L\right\},$$

où $\mathcal{Z}$ est l'ensemble des perturbations, D^0 la valeur nominale des incertitudes et D^k la base des variations de ces incertitudes. En première approche, nous avons choisi une situation pire-cas dans laquelle: $L=(1+m)(1+n)$ et:

$$D^k_{i,j}=\begin{cases}1 & \text{si } l=(n+1)(i-1)+j\\ 0 & \text{sinon.}\end{cases}$$

L'ensemble des perturbations est alors choisi de la forme: $\mathcal{Z}=\bigotimes_{k=1}^{L}\left[\zeta_k^{inf},\zeta_k^{sup}\right]$ conduisant vraisemblablement à une sur-estimation de l'ensemble des incertitudes. En suivant la méthodologie décrite dans [16, Chapitre 1], le Problème (7.12) est équivalent au problème:

$$\min_{(x,t)\in\mathbb{R}^n\times\mathbb{R}} t \quad \text{sous:} \quad c^\top x+d\leq t,\ Ax\leq b, \qquad x_{min}\leq x\leq x_{max}. \tag{7.13}$$

Par définition, une solution robuste du Problème (7.13) est une solution optimale de sa contre-partie robuste définie par:

$$\min_{(x,t)\in\mathbb{R}^n\times\mathbb{R}}\left(\sup_{(A,b,c,d)\in\mathcal{U}} t\right)=t \quad \text{sous:} \quad c^\top x+d\leq t,\ Ax\leq b,\ \forall(A,b,c,d)\in\mathcal{U},$$

$$x_{min} \leq x \leq x_{max}.$$

soit ici:

$$\min_{(x,t)\in\mathbb{R}^n\times\mathbb{R}} t \quad \text{sous:} \quad c^\top x + d \leq t,\ Ax \leq b,\ \forall (A,b,c,d) \in \mathcal{U} \qquad (7.14)$$
$$x_{min} \leq x \leq x_{max}.$$

En introduisant des variables d'écart comme expliqué dans [16, Chapitre 1], le problème (7.14) est équivalent à un problème de programmation linéaire déterministe à $2n+1$ variables, $2n+m+1$ contraintes d'inégalités et n contraintes de boites que l'on peut résoudre à l'aide d'outils classiques de la programmation linéaire:

$$\min_{X\in\mathbb{R}^{2n+1}} \widetilde{C}^\top X \quad \text{sous:} \quad \widetilde{A}X \leq \widetilde{b},\ X_{min} \leq X \leq X_{max}. \qquad (7.15)$$

Considérons maintenant deux exemples respectivement en dimension 2 et 3 d'optimisation de la conception robuste d'avion. La fonction objectif et les contraintes sont définies dans les Tables 7.1 et 7.2.

	Dénomination	Unité	Sigle	$[x_{min}, x_{max}]$
x_1	Surface de la voilure	m^2	WingArea	$[100, 170]$
x_2	Poussée statique au niveau de la mer	daN	SLSThrust	$[9000, 13000]$
x_3	Mach de croisière	mach		$[0.65, 0.76]$

Table 7.1: Variables de l'optimisation: (x_1, x_2) si $n = 2$ et (x_1, x_2, x_3) si $n = 3$.

Objectif	f	Cout d'exploitation au comptant (en \$/vol)	COC		
Contraintes	g_1	Longueur de piste au décollage 1 (au niveau de la mer)	TOFL1	$\leq$	2000 m
	g_2	Longueur de piste au décollage 2 (in High & Hot conditions)	TOFL2	$\leq$	2500 m
	g_3	Vitesse verticale de montée	CLBVZ	$\geq$	500 ft/min
	g_4	Vitesse verticale de croisière	CRZVZ	$\geq$	300 ft/min
	g_5	Vitesse à l'atterrissage	LDSPEED	$\leq$	130 kt

Table 7.2: Fonctions objectif et contraintes.

Pour chaque exemple, le démarche est la suivante:

1. Construction du problème linéaire approché (7.12) par linéarisation de la fonction objectif et des contraintes.

2. Quantification et propagation des incertitudes pour obtenir les boites $\mathcal{L}_\infty$ sur les ζ par une méthode de propagation basée sur le développement de Taylor d'ordre 1.

3. Détermination des coefficients $(\widetilde{A}, \widetilde{b}, \widetilde{c}, \widetilde{d})$ associés pour obtenir le problème (7.15).

4. Résolution du problème (7.15) à l'aide de l'algorithme du simplexe (fonction *linpro* sous Scilab).

Dans le cas $n = 2$ par exemple et pour $m = 25$ contraintes d'inégalités, on obtient la solution suivante du problème (7.15):

$$X_{sol} = \left(10292 \text{ daN}, 115.6 \text{ m}^2\right) \text{ , pour un cout optimal: } COC = 4285 \text{ \$/pax.}$$

Cette solution est alors comparée à la solution (*a priori* non robuste X_{sol}^{det} du problème d'optimisation déterministe initial:

$$X_{sol}^{det} = \left(10121 \text{ daN}, 114.3 \text{ m}^2\right) \text{ , pour un cout optimal: } COC^{det} = 4279 \text{ \$/pax.}$$

Les deux solutions sont représentées sur la Figure 7.8. Sans surprise, le prix à payer pour la robustesse de la solution est une augmentation de la valeur du cout optimal.

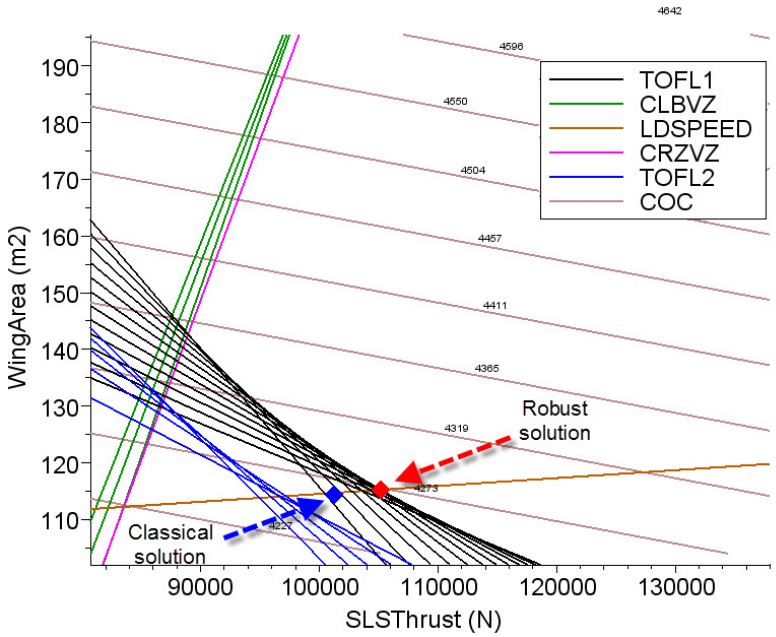

Figure 7.8: Solutions déterministe et robuste du problème de conception 2D robuste d'avion.

Pour terminer, nous avons conclu notre étude en vérifiant la robustesse de la solution X_{sol} vis-à-vis du domaine admissible initial (avant linéarisation).

7.4 Conclusion

Le premier objectif de cette thèse était d'établir, d'investiguer et de résoudre le problème hautement multidisciplinaire et multi-objectif de la conception d'un avion et de ses opérations. Cet objectif a été atteint en appliquant une méthode pas à pas. La première contribution est d'avoir incorporé minutieusement et progressivement des nouveaux modèles de propulsion, du profil de la mission et d'impact climatique, aux modèles basiques usuels.

Nous avons validé chaque ajout de modèle en comparant les résultats de la simulation à des avions existants.

La seconde contribution a été d'intégrer de nouvelles variables de conception dans le processus d'optimisation de la conception d'avions. Aux deux degrés de liberté de base, la surface de l'aile et la poussée statique au niveau de la mer des moteurs (représentatif de la taille du moteur et de sa puissance), nous avons ajouté l'allongement de la voilure pour la cellule avion, le taux de dilution pour système de propulsion, l'altitude de croisière et le Mach pour la trajectoire, et enfin des vitesses de montée et de descente. Nous avons validé les résultats de l'optimisation par une intégration étape par étape de ces nouveaux degrés de liberté.

Un autre objectif de cette thèse était de résoudre le problème de la conception d'avions plus écologiques. Nous avons incorporé un modèle d'impact climatique dans les processus. A partir de ce modèle, nous avons sélectionné une mesure représentative de l'impact climatique, qui a été ajouté comme nouveau critère de l'optimisation de la conception d'avions. Dans ce but de réduction d'impact environnemental, nous avons proposé une configuration d'un avion non conventionnel: un avion à propulsion hybride électrique-carburant. Cet avion est composé d'un fan électrique sur son fuselage arrière, des générateurs électriques sur les moteurs thermiques, et des batteries supplémentaires. Le concept a été modélisé accompagné d'une gestion précise et efficace de l'utilisation des batteries, du fan et des générateurs tout au long de la mission. Nous avons ensuite optimisé à la fois la conception de la configuration classique et celle de l'avion hybride, à cahier des charges équivalent. Pour cela, nous avons appliqué l'intégration étape par étape des degrés de liberté. De plus, nous avons comparé l'optimisation en termes d'impact climatique, de coûts d'exploitation et d'un critère représentatif de l'efficacité globale de l'avion, à savoir la masse maximal au décollage. L'analyse des résultats finaux a mis en évidence l'impact de chaque groupe de degrés de liberté sur l'avion optimisé. Nous avons également observé que le coût et l'impact climatique sont deux critères contradictoires. Un autre résultat intéressant était l'efficacité en termes d'impact environnemental de la configuration hybride. Enfin, nous avons proposé de tirer tous les bénéfices de la configuration hybride en travaillant sur les synergies offertes par le fan électrique et les batteries. Nous avons observé que ce travail sur les synergies était nécessaire pour obtenir un avion hybride concurrentiel.

Les autres contributions de cette thèse sont les suivantes :

1. l'intégration d'une méthode de différenciation automatique aux outils numériques existants, en surchargeant tous les opérateurs et fonctions de base incluses dans le processus. Cela a permis d'atteindre une précision meilleure que celle des méthodes de différences finies classiques lors du calcul de gradients et Hessiens. De plus, cela peut entraîner une amélioration significative au niveau de la convergence des méthodes d'optimisation à base de gradient.

2. La comparaison et la sélection de méthodes d'optimisation bien adaptées au problème de la conception d'avions. Dans un premier temps, les méthodes à base de gradients ont été utilisées en utilisant les gradients fournis par l'outil de différentiation automatique. Cependant, certains points de l'espace de conception n'étaient pas calculables. Ceci est la raison pour laquelle nous avons eu recours à des techniques d'optimisation sans-dérivés. Les algorithmes génétiques (NSGA II) ont été testés pour résoudre le problème d'optimisation mono-objectif ainsi que l'optimisation multi-objectifs. Les algorithmes à Evolution Différentielle ont été modifiés pour gérer les contraintes, et

appliqués dans certaines études. Une mise en œuvre de l'algorithme MADS compilé à partir du C++ s'est également avéré avoir de bonnes propriétés de convergence dans nos études. Enfin, le nombre croissant de degrés de liberté a motivé l'utilisation de méta-modèles avec les outils d'optimisation.

3. Le développement et l'utilisation d'une nouvelle famille de distribution de probabilité ayant quatre paramètres, nommée la distribution Beta-Mystique, qui couvre un large spectre de distribution unimodales.

4. Une étude détaillée et une comparaison des méthodes de propagation d'incertitude, en fonction des critères de précision, du coût de calcul et des connaissances sur les modèles. La comparaison est faite entre les méthodes de type Monte-Carlo, les méthodes d"expansion de Taylor, les méthodes d'expansion en polynôme du chaos, et les méthodes de quadrature. Une attention particulière est portée aux méthodes basées sur les moments, qui ont des applications pratiques puissantes pour résoudre des problèmes de conception sous incertitudes.

5. Une approche d'optimisation de la conception d'avions sous incertitude. Pour cela, une approche sous contraintes en probabilités a été proposée. Nous avons apporté des améliorations à une méthode numérique d'optimisation robuste, à savoir la méthode séquentielle nommée SORA. En utilisant une technique qui calcule les bornes sur les mesures de probabilité, la méthode SORA est capable de gérer une grande variété de distributions.

6. L'application de tous les outils mentionnés précédemment à la conception sous contraintes en probabilités d'un avion non conventionnel. Nous avons résolu le problème suivant : trouver l'année à partir de laquelle l'avion hybride sera compétitif par rapport à l'avion conventionnel avec une probabilité de 0,95.

7. Les premiers pas vers une autre approche de l'optimisation robuste de la conception d'avions. Le résultat est un avion optimal qui satisfait à toutes les réalisations des contraintes à l'intérieur une certaine zone d'incertitude. Une attention particulière a été accordée à la modélisation d'une telle approche.

Enfin, cette thèse contribue à sensibiliser le bureau des avant-projets à la gestion des incertitudes en utilisant les distributions de probabilité. Elle a également permis le développement et l'amélioration de certains outils numériques internes, à savoir SiMCAD et OCCAM, utilisés pour résoudre le problème de la conception d'avions. Tous les modèles développés dans le cadre de cette thèse - l'impact climatique, l'avion hybride, le moteur thermodynamique et le profil de mission détaillé - ont été incorporés dans ces outils, et validés par les études présentées. Dans le cadre de certains projets internes, cette thèse a permis des études de sensibilité sur les paramètres de conception d'avions hybrides, et a permis de présenter une étude complète de ce concept novateur. En outre, cette thèse conduit à l'intégration des méthodes de propagation des incertitudes aux outils de conception numériques. En particulier, le premier ordre, le second ordre, les méthodes de quadrature URQ et BRQ.

Les résultats obtenus dans cette thèse donnent les perspectives suivantes.

La première est de poursuivre l'approche d'optimisation robuste menée dans le Chapitre 4. En effet, l'application de la méthode a bien fonctionné pour les cas en deux et trois dimensions, et devrait être généralisé en dimension supérieure.

Un autre point de vue a été soulevé par l'approche d'optimisation robuste, par rapport à la propagation des incertitudes. Il pourrait être intéressant d'étudier l'impact de la précision de la sortie incertaine sur la mesure du risque sélectionnée, ou même sur la borne de la mesure du risque. Cela permettrait d'être conscient de l'erreur qui est faite lorsque la mesure est calculée et ensuite de connaître la vraie robustesse de la solution du problème. Par exemple, dans l'optimisation sous contraintes en probabilités proposée, nous utilisons les moments de l'incertitude de sortie pour calculer la borne de la mesure de probabilité. L'impact de l'erreur du calcul du moment sur la limite devrait être évalué.

Un autre point pourrait être d'automatiser l'étude d'une solution dans le cas des études déterministes. Le voisinage de la solution est intéressant pour les différents acteurs du transport aérien. La sensibilité des résultats à la variable de conception est importante, par exemple la sensibilité au nombre de Mach en croisière et l'altitude de croisière, qui sont des données extrêmement importantes pour les opérations des compagnies aériennes.

En outre, l'intégration de tous les outils et méthodes aux outils numériques internes apportent la possibilité d'étudier d'autres concepts d'avions, en particulier d'autres configurations hybrides. Cela a déjà commencé avec un stage sur l'optimisation d'un nouveau concept d'appareil hybride, en le comparant à d'autres concepts plus classiques.

Un autre point de vue qui pourrait apporter d'importants bénéfices dans l'optimisation de la conception robuste est l'étude du cas de probabilités jointes. Il pourrait être utile, pour les praticiens de la conception robuste, de construire une probabilité jointe avec des méthodes de réduction de dimensions. Dans le cadre de cette thèse, l'étude des copules, qui sont un outil intéressant pour représenter des variables aléatoires multidimensionnelles, n'a malheureusement pas pu être menée. Cela pourrait être une prochaine étape.

Enfin, des méthodes très récentes dans le domaine de la conception robuste pourraient avoir un intérêt, en particulier quand un grand nombre d'entrée incertaines sont impliquées. Celles-ci couplent des méthodes adaptatives de quantification des incertitudes et des algorithmes d'optimisation par recherche directe [44]. Ces méthodes ont montré des propriétés de convergence très intéressantes, avec des temps de calcul raisonnables.

Appendix A

Turbofan engine modeling

This appendix is dedicated to a more detailed presentation of the thermodynamic engine modeling process that we propose to replace the simple thermodynamic engine.

The simple thermodynamic engine model was computing fast enough to be used within the overall aircraft sizing loop as long as the Breguet-Leduc based mission simulation was involved. In that case, the computation time for one single design point was a tenth of seconds and the optimization of Wing Area and Engine Size took a few minutes. These performances were acceptable for first runs with this limited number of degrees of freedom where only airframe and engine size design are involved. It was also sufficient for various useful sensitivity studies. However, it was clearly not acceptable for a global optimization involving the engine, the airframe and the trajectory, especially when a complete time dependent mission simulation is computed.

A short profiling study of the code reveals that the engine model was the major time consuming model block.

For this reason, an even simpler engine model has been set up on the following specifications.

A.0.1 Engine model Specifications

Ideally the engine model should satisfy the following specifications:

1. The EM (Engine Model) must has two levels of parameterization:
   (a) At design level, its output will have to vary consistently versus:
      i. required overall maximum thrust (driving of the engine size),
      ii. By Pass Ratio (BPR).
   (b) At simulation level, it will have to vary its output according to current flying condition:
      i. Altitude,
      ii. Temperature,
      iii. Speed,
      iv. Selected rating (i.e. engine power level, see below).
2. The EM must run quickly enough to be able to compute one single analysis, including mission simulation versus time, in at most a few seconds.

3. The EM must take account of the general behavior of the consumption versus required current thrust and particularly, the phenomenon of the bucket (the existence of a minimum of specific fuel consumption versus thrust).

4. The EM must incorporate calibration factors so that the EM can match as closely as possible any arbitrary given engine data pack. A data pack is a big set of pre-computed engine data into which it is possible to interpolate engine thrust and consumption versus any flying conditions. The data pack is in fact a tabulated engine model.

These specifications are actually quite ambitious regarding the state of art of such simple models in the literature [151, 165, 150]. The following expression shows a common formula that can be found with various adaptations in many sources.

$$Fn = Kfn_{rating} \times SLST \times \sqrt{\frac{\rho}{1.225}} \times (1 - Mach + 0.5Mach^2) \times Kfn, \tag{A.1}$$

$$SFC = Constant, \tag{A.2}$$

where the variables can be defined as follows:

- Fn is the resulting maximum thrust in the condition defined by the following variables,
- $SLST$ is the Sea Level Static Thrust. it is considered as the maximum thrust that an engine can delivered. This maximum thrust is supposed to be obtained at sea level and zero speed.
- Kfn_{rating} is a constant lower than 1 defining the ratio of the SLST which is available in the given flying phase. There is a specific rating for each flight phase:
  - Take off: Max Take Off rating (MTO),
  - In case of engine failure: Maxi Continuous rating (MCN),
  - Climb: Max Climb rating (MCL),
  - Cruise: Max Cruise rating (MCR),
  - In case were no thrust is required in flight (idle): Flight Idle (FID),
  - In case were no thrust is required on ground: Ground Idle (GID).
- ρ is the current air density (kg/m^3), and the air density at sea level ρ_0 is equal to 1.225 kg/m^3,
- $Mach$ is the current Mach number (the ratio between Air Speed and Sound Speed),
- Kfn is a calibration factor to match with any given data,
- SFC is the Specific Fuel Consumption. It is the amount of fuel required to produce a thrust unit during a time unit (usually in $kg/daN/h$).

We can see that this model is addressing the requirements (1(a)i), (1(b)i), (1(b)iii), (1(b)iv), (2) and partially (4) through the Kfn factor and the choice of the constant SFC.

Nevertheless, the requirements (1(a)ii), (1(b)ii) and (3) are not covered whilst being very important for our purpose.

After some discussions with experts and various attempts, we have followed the approach detailed below.

A.0.2 Modeling approach

The approach will be based on the use of the "mini engine" presented in [15] as it was very easy with this model to vary the design in term of engine size and bypass ratio and then to submit the obtained model to various flying conditions. Validation has been done afterward versus real aircraft information.

A.0.2.1 Thrust Model

The guide lines to build this model were:

- Keep $SLST$ as the overall scale factor for the engine thrust.
- Keep the rating factor Kfn_{rating} and identify it using regressions versus all available existing aircraft data. This factor will capture the main part of rating balance (see below).
- Keep the Kfn factor to be able to match with a given engine.
- Keep the term $\sqrt{(\rho/1.225)}$ but incorporate a correction factor as a power to better match the behavior of given engine versus altitude. The term becomes $(\rho/1.225)^{(0.5Kp)}$ where Kp can be adapted for each rating. Used in conjunction with Kfn, these two factors will allow matching a given engine rating at sea level as well as thrust evolution versus altitude.
- Merge the Mach effect and the BPR effect into a polynomial formula. This is justified by the fact that thrust variation versus speed for a given rating is highly coupled with BPR.

Rating factors will have the role to capture "the global picture" of power balance between Take off, drift down, climb cruise and descent while calibration factor Kfn and Kp will be used to match with a particular engine implementation

The proposed modeling approach for thrust is based on the assumption that effects of altitude (mainly with ρ) from one side and BPR and speed from another side are independent enough so that their contribution in the expression of the model can be inserted as the product of two independent terms. In practice, this assumption reveals to be acceptable as it produces a behavior that is consistent with real engine data packs but further investigation would be necessary to quantify the validity of this assumption and eventually to merge both effects into one single expression.

Another important point is that the available data concerning real engines are given at specific conditions of altitude and speed that can be different from an engine to another. This engines being also of different by pass ratio. As a result of this, the engine model must be built in a given order:

- First with BPR and Speed effect,
- Secondly, with altitude effect,
- Finally, with rating factor identification.

A consequence of this step by step implementation is that step 1 and 2 cannot be done by looking for absolute values of thrust but rather relative ones. The final step only will give to the model its absolute output.

A.0.2.2 Consumption Model

The guidelines for this model were:

- Look for a simple law to take account of the dependency of fuel consumption versus altitude, temperature and speed,
- Look for a parametric formula that could reproduce the behavior of the bucket with the minimum set of tuning parameter.

Thermodynamic approach will be used to propose a formulation for altitude, temperature and speed dependency but after some tests, theoretical approach had to be modified to incorporate more empiricism to better match observed data.

Concerning thrust dependency, a pure statistical approach has been selected because any attempt to make something simpler than the "mini engine" failed.

The implemented of each step of the approach are presented below followed by the final model obtained.

A.0.3 Development

A.0.3.1 Thrust Model

Speed-BPR Effect

The coupling between speed (quantified by Mach number) and By Pass Ratio has been quantified using the "mini engine" [15] as it was very easy to vary the design in term of BPR while keeping constant the maximum sea level static thrust.

We performed sampling by varying bypass ratio in the interval $[5, 9]$ and Mach number in the interval $[0.25, 0.95]$ for various values of $SLST$ and altitude $ZpRef$ and we observed a quite robust behavior of the variation of the ratio $\eta_{TS} = Thrust/SLST$ versus BPR and $Mach$.

The function:

$$\eta_{TS}^{(SLST,ZpRef)} := (BPR, Mach) \mapsto \eta_{TS}^{(SLST,ZpRef)}(BPR, Mach), \tag{A.3}$$

is robust to the variation of $SLST$ and $ZpRef$ which confirms the assumption of independence explained above. The graph from Figure A.1 shows the behavior of the function that has been selected. The expression of the function is a polynomial function of the two variables BPR and $Mach$:

$$\eta_{TS} = \begin{bmatrix} Mach^2 & Mach & 1 \end{bmatrix} \cdot \left(MC \cdot \begin{bmatrix} BPR^2 \\ BPR \\ 1 \end{bmatrix} \right), \tag{A.4}$$

where:

$$MC = \begin{bmatrix} -0.0017 & 0.0562 & 0.1693 \\ 0.0043 & -0.1269 & -0.1914 \\ -0.001 & 0.0279 & 1.0354 \end{bmatrix}. \tag{A.5}$$

The error brought by this model is lower than about 5% in the whole flight domain which is quite accurate at this stage. However, this result has been figured out using the "mini engine" [15]. Further validations using real data have been done for one engine and have given similar result.

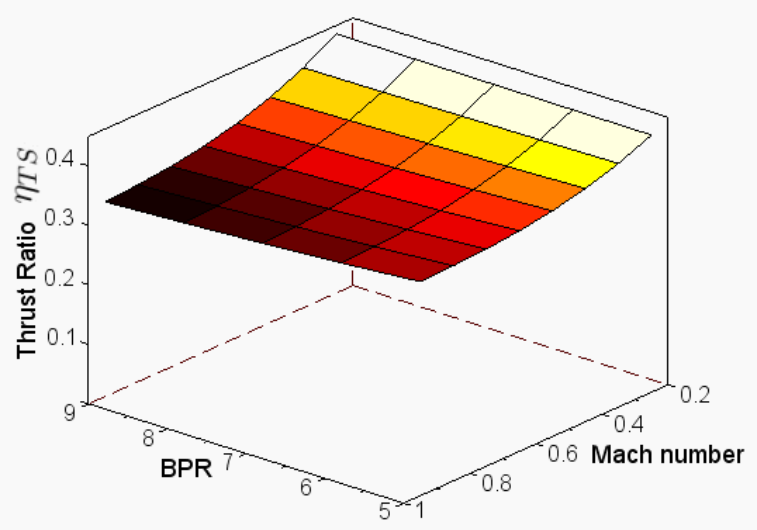

Figure A.1: Thrust Ratio Versus BPR and Mach number.

Altitude Effect

We are here dealing with the following term function of ρ:

$$\left(\frac{\rho}{\rho_0}\right)^{0.5Kp}, \text{ with } \rho_0 = 1.225\ kg/m^3. \tag{A.6}$$

In the context of model identification the Kp factor disappears and the question is to adjust, eventually, the power of 0.5. After several tests on existing engine data packs, it appears that a power of 0.75 instead of 0.5 seems to better represent the behavior of modern engines with high bypass ratio.

Subsequently, we put the following term for the altitude effect:

$$\left(\frac{\rho}{\rho_0}\right)^{0.75Kp}. \tag{A.7}$$

After this step, the expression of the function is:

$$\eta_{TS} = \begin{bmatrix} Mach^2 & Mach & 1 \end{bmatrix} \cdot \left(MC \cdot \begin{bmatrix} BPR^2 \\ BPR \\ 1 \end{bmatrix} \right), \tag{A.8}$$

$$\rho = \frac{P_{amb}}{287.05 \times T_{amb}}, \tag{A.9}$$

$$Fn_{basic} = SLST \times \eta_{TS} \times \left(\frac{\rho}{\rho_0}\right)^{0.75Kp}, \tag{A.10}$$

where:

$$MC = \begin{bmatrix} -0.0017 & 0.0562 & 0.1693 \\ 0.0043 & -0.1269 & -0.1914 \\ -0.001 & 0.0279 & 1.0354 \end{bmatrix}, \tag{A.11}$$

$$Kp = 1. \tag{A.12}$$

In the last expressions:

- Fn_{basic} is the nominal thrust computed by the function,
- P_{amb} is the ambient pressure,
- P_0 is the pressure at the seal level, $P_0 = 101325$ Pa.

All is now in place to perform the final step which consists in calibrating each rating.

Rating factor identification

For turbofans, ratings are level of thrust that are predefined at design stage. They are fraction of the maximum available thrust of the engine. The Thrust that can deliver a turbofan is mainly driven by its architecture and the temperature of the gas resulting from fuel combustion. It is used to deal with the temperature at the exhaust of the combustion chamber, called $T4$, as a physical indicator of the level of power, i.e. the level of thrust. The $T4$ temperature is constrained by material resistance and is tightly driven by engine internal systems. Ratio between rating thrust and maximum thrust is in fact driven by $T4$ temperature and more specifically by the margin between current value of $T4$ and its maximum value. So, thrust rating of the engine corresponds physically to $T4$ margins versus maximum $T4$ value.

There exist as many different engine ratings as specific flight phases. This is due to the fact that each flight phases has specific requirements in term of power and duration. From the most power demanding to the less one, we have:

- Take off phase: very short (a few minutes) but requires very high thrust. Rating is MTO (Max Take Off). This level of power cannot be sustained more than a few minutes without damaging the engine. Time period in between inspection visits takes count of the cumulated time when MTO has been run.
- Drift down: No time limit (except available fuel). In case of engine failure, remaining working engines are set to most powerful regime that can be sustained. Rating is MCN (Maxi Continuous). This level of power can be sustained as long as necessary to fly the aircraft safely to a destination. Time period in between inspections takes count of the cumulated time when MCN has been run.
- Climb: No time limit (except available fuel). Rating is MCL (Max Climb). Corresponding level of power may be a little bit lower than for MCN to save maintenance cost.
- Cruise: No time limit (except available fuel). Rating is MCR (Max Cruise). Except for very short missions (less than $500NM$) for which cruise segment may be shorter in time than climb segment, this is the nominal level of power. In fact, most of the time, the required thrust is lower than MCR.
- Descent: No time limit (except ground level). Rating is FID (Flight Idle). This level of power is adjusted to ensure energy for airplane systems (avionics, hydraulics, air conditioning), thrust is no longer driven but is an outcome of the required power.

This level of power is the most unpredictable one as it is not driven by flight mechanics considerations, in compensation, it has very limited effects on global fuel consumption.

The balance between these different ratings is driven by engine architecture which has been selected to satisfy airplane requirements. For a given set of requirements and implemented technology, this balance has a direct effect on engine component life and thus on maintenance costs. As said previously, rating factors will have the role to capture "the global picture" of power balance between Take off, drift down, climb cruise and descent while calibration factor Kfn and Kp will be used to match with a particular engine implementation. To identify rating factors, we have used existing aircraft data in the department data base in order to find regressions for the following ratios:

- MTO thrust versus SLST at sea level ISA conditions,
- MCN thrust versus Max thrust in specific airplane conditions,
- MCL thrust versus Max thrust in specific top of climb conditions,
- MCR thrust versus Max thrust in specific top of climb conditions.

Flight conditions are given for each aircraft consistently with the engine thrust. Rating factors have been computed by least square minimization of the differences between data base values and model values for the whole population of aircraft. For each rating, we give below the value resulting from the least-square optimization and the corresponding scatter plot showing the performance of the resulting factor in term of error. Data Base values are plotted on horizontal axis whilst Model values are plotted on vertical axis.

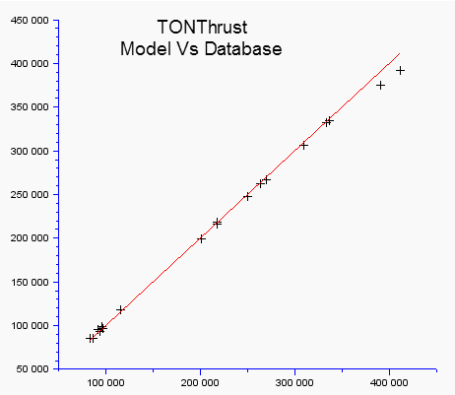

Figure A.2: MTO rating factor = 0.835.

The FID rating factor is arbitrary put at a value of 0.01 as no data were available in the data base. Globally, we can observe a quite good robustness of this part of the model within the range of values even if in some cases, the discrepancy between data base value and model value can reach about 10%. The shape of the error which increases accordingly to the value itself indicates an extensive behavior of the model (the bigger the engine, the larger the prediction error). This behavior about complex systems such as engine or aircraft is not surprising. It is often coupled with the increase of the number of degrees of

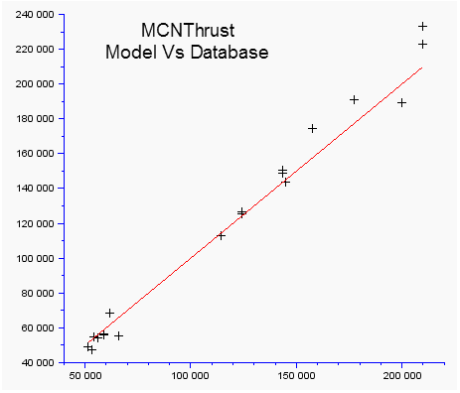

Figure A.3: MCN rating factor = 0.720.

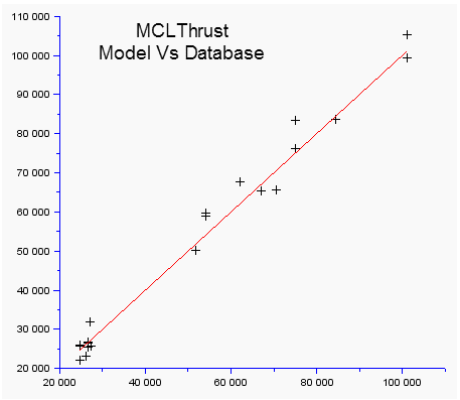

Figure A.4: MCL rating factor = 0.650.

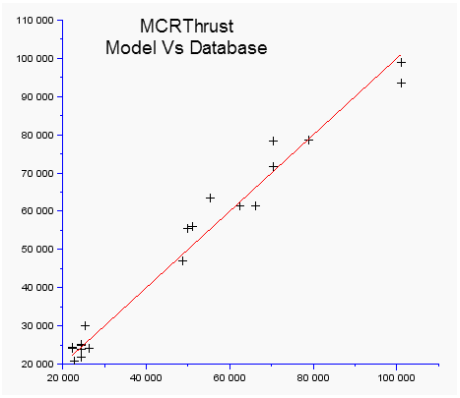

Figure A.5: MCR rating factor = 0.590.

freedom for design increases parallel to the size of the object. In this case, the capacity of a simple model to predict a quantity related to the overall system decreases when the number of undetected degrees of freedom increases. Nevertheless, such error is acceptable

as this stage. The final expression of the model is:

$$\eta_{TS} = \begin{bmatrix} Mach^2 & Mach & 1 \end{bmatrix} \cdot \left(MC \cdot \begin{bmatrix} BPR^2 \\ BPR \\ 1 \end{bmatrix} \right), \tag{A.13}$$

$$\rho = \frac{P_{amb}}{287.05 \times T_{amb}}, \tag{A.14}$$

if rating== 'MTO',

$$Fn = 0.835 \times SLST \times \eta_{TS} \left(\frac{\rho}{1.225} \right)^{(0.75 Kp_{TON})}, \tag{A.15}$$

elseif rating=='MCN',

$$Fn = 0.720 \times SLST \times \eta_{TS} \left(\frac{\rho}{1.225} \right)^{(0.75 Kp_{MCN})}, \tag{A.16}$$

elseif rating=='MCL',

$$Fn = 0.650 \times SLST \times \eta_{TS} \left(\frac{\rho}{1.225} \right)^{(0.75 Kp_{MCL})}, \tag{A.17}$$

elseif rating=='MCR',

$$Fn = 0.590 \times SLST \times \eta_{TS} \left(\frac{\rho}{1.225} \right)^{(0.75 Kp_{MCR})}, \tag{A.18}$$

elseif rating=='FID',

$$Fn = 0.010 \times SLST \times \eta_{TS} \left(\frac{\rho}{1.225} \right)^{(0.75 Kp_{FID})}, \tag{A.19}$$

end.

(A.20)

where:

$$MC = \begin{bmatrix} -0.0017 & 0.0562 & 0.1693 \\ 0.0043 & -0.1269 & -0.1914 \\ -0.001 & 0.0279 & 1.0354 \end{bmatrix}. \tag{A.21}$$

In the last expressions:

- Fn is the nominal thrust,
- factors Kp_{TON}, Kp_{MCN}, Kp_{MCL}, Kp_{MCR}, Kp_{FID} are equal to 1 except when matching with specific engine is required.

A.0.3.2 The phenomenon of the bucket

The bucket is the point of Thrust where the Specific Fuel Consumption is minimal. Physically, the existence of this minimum results from a balance between engine propulsive and thermal efficiency. It can be observed in the example of Figure A.6 which presents the variation of SFC versus the thrust Fn for two different real engines.

Several characteristics of the bucket phenomenon appear in these graphs:

- the bucket is a flat minimum but can be more or less flat depending on the engine,

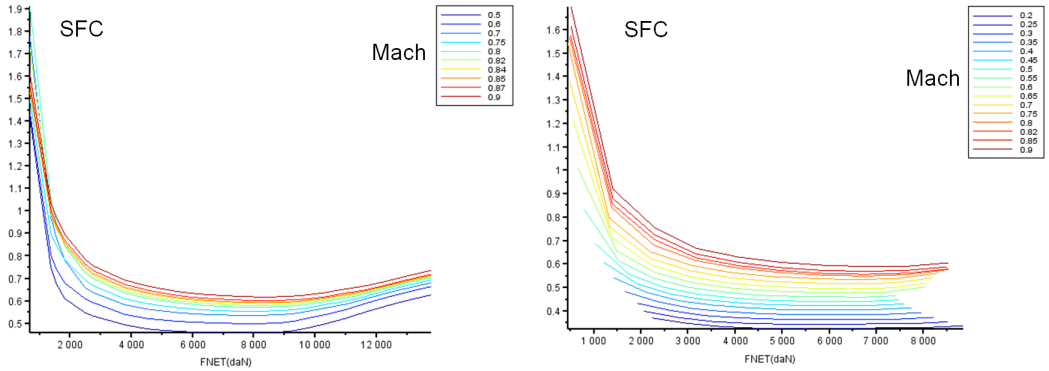

Figure A.6: Illustration of the existence of the bucket SFC for two different engines. Graphs are presenting SFC as a function of the thrust Fn at different Mach numbers.

- its location within the thrust ladder is not fixed from an engine to an other,
- the left part of the SFC curve is more or less looking like an hyperbole. However, the SFC behavior at very low thrust is not necessarily accurate.
- the right part of the SFC curve can be modeled as an oblique asymptote.

To these characteristics, we have to add that:

- the most important point is the couple (Fn, SFC) corresponding to the cruise design point which is common to engine and airframe design,
- this couple of values is generally well known for a given aircraft.

Here also, we will assume that the effect on SFC of flying conditions (altitude $ZpRef$ and $Mach$) from one side and thrust level from the other side can be modeled independently. This assumption will be confirmed on the way.

Identification of the variation of bucket SFC versus By Pass Ratio

Looking for a correlation between BPR and best cruise SFC (named $Bucket_{SFC}$), we found that the following simple affine function is able to predict the Bucket SFC with a precision of about 5% according to the available set of 48 engines. This is quite satisfactory. The graph from Figure A.7 shows the distribution of the calibration factor $kSFC$ that allows to match with the set of available engines.

$$Bucket_{SFC} = kSFC \times 1.03 \times \frac{-0.026 \times BPR + 0.76}{36000}. \tag{A.22}$$

Identification of bucket behavior versus flying conditions

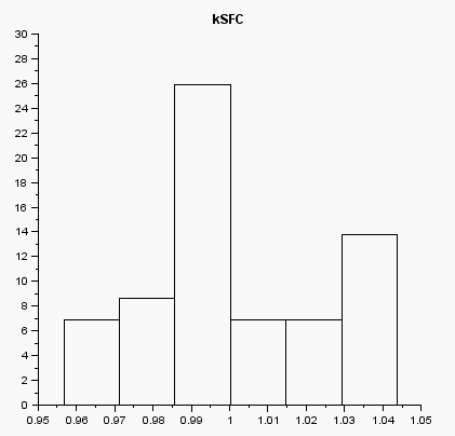

Figure A.7: Probability distribution of the calibration factor $kSFC$ over the database of available engines.

From propulsion experts, we obtained that the variation of the SFC versus flying conditions can be captured by the term:

$$SFC_{factor} = \left(\frac{T_{amb}}{T_0} \left(1 + 0.2 \times Mach^2 \right) \right)^n, \tag{A.23}$$

where:

- T_{amb} is the ambient temperature,
- T_0 is equal to 288.15 Kelvin,
- n is a power that is theoretically 0.5, but is more likely to be 0.6 in practice.

This term is defined so that the ratio SFC/SFC_{factor} becomes more or less independent from flying conditions. Note that the term $T_{amb}(1+0.2\times Mach^2)$ is what aerodynamics experts call the total temperature. Another advise was to use an expression of the SFC_{factor} enriched with the contribution of total pressure as follows:

$$SFC_{factor} = \frac{\left(\frac{T_{amb}}{T_0} \left(1 + 0.2 \times Mach^2 \right) \right)^{0.5}}{\left(\frac{P_{amb}}{P_0} \left(1\check{}0.2 \times Mach^2 \right) \right)^{3.5}}, \tag{A.24}$$

The term $P_{amb}(1\check{}0.2 \times Mach^2)^{3.5}$ is the total pressure. Various experiments have shown that the best expression seems to be the following compromise between the two formulas:

$$SFC_{factor} = \left(\frac{T_{amb}}{T_0} \right)^{0.6} \left(1 + 0.2 \times Mach^2 \right)^{4.1}. \tag{A.25}$$

By best expression, we mean the expression that gives the most physical results, i.e. the results which offer the best matching with real data. Note that the exponent 4.1 corresponds to $0.6 + 3.5$.

Graphs from Figure A.8 are presenting on the left side the SFC variation at a given altitude versus Mach number and thrust. On the right side it presents the SFC_{factor} variations versus the same input. We can see that the variations versus Mach number are very well damped for thrust values higher than about 30% of its range which corresponds to main using domain. Only flight idle is in the domain where Mach effect is not very well damped but this also corresponds to the domain where only a very limited amount of fuel is burnt.

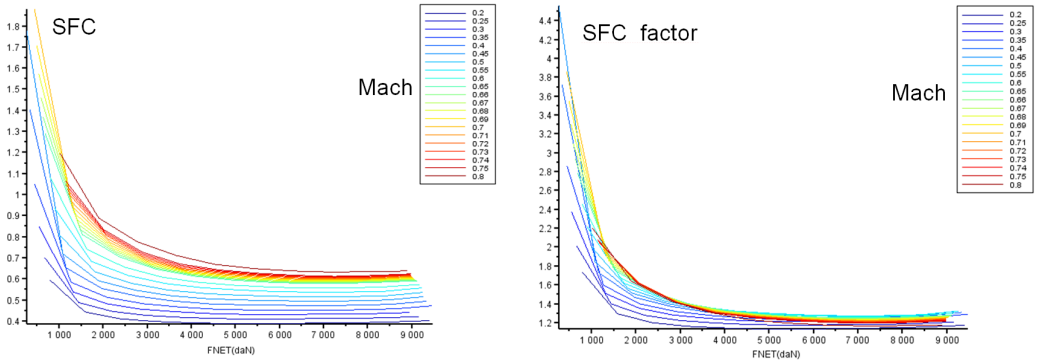

Figure A.8: Graph presenting SFC (on the left) and SFC_{factor} (on the right) as a function of the $Thrust$ at different Mach numbers.

The same graphs when altitude is varying are showing the same behavior as illustrated in Figure A.9 for the SFC and in Figure A.10 for the SFC_{factor} .

Identification of the SFC behavior versus thrust

A first physical analysis of the phenomenon of the bucket has been done during the development of the "mini engine" model [15]. This analysis shown that the existence of a minimum of specific fuel consumption versus thrust is due to a balance between:

- propulsive efficiency, which is high at low thrust and low at high thrust,
- thermodynamic efficiency which is low at low thrust and high at high thrust.

Propulsive and thermodynamic efficiencies are the consequence of all assumptions and choices taken during the engine design. However, a simple formula that would be parameterized by a limited number of main drivers can not capture these efficiencies. So, it has been decide to set up an arbitrary functional expression with the minimum required parameters to be able to match the shape of the curve with most frequent real evolutions of SFC versus the thrust.

By analyzing the main characteristics of the shape and how it changes from an engine to another, a minimum of four parameters have been selected as presented in Figure A.11.

Function expression selection

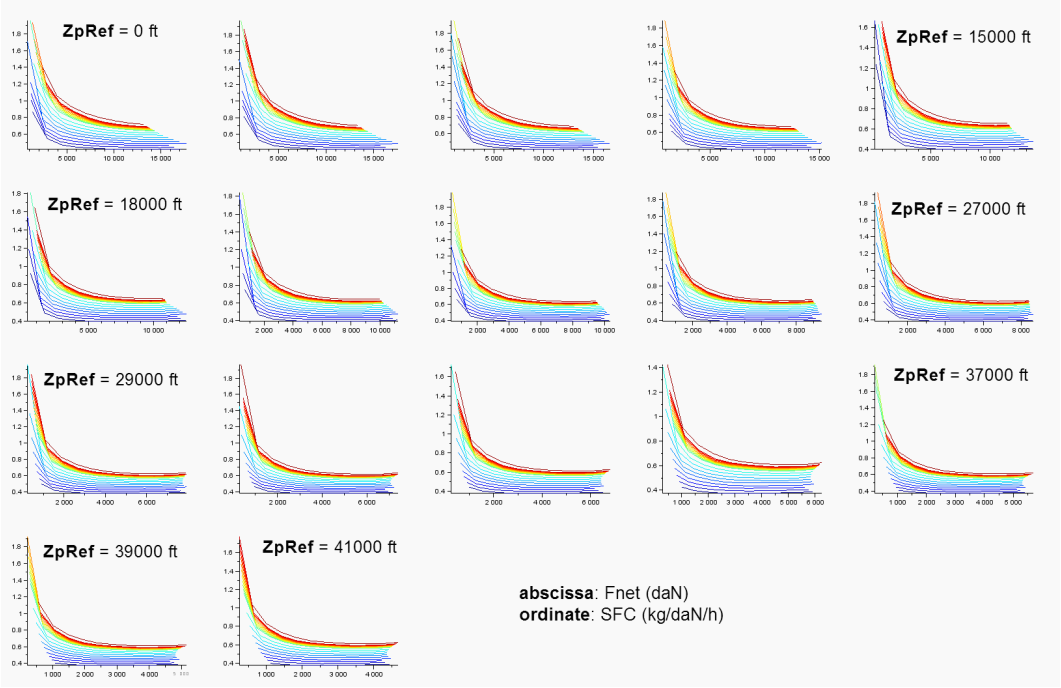

Figure A.9: Graphs presenting SFC as a function of the thrust Fn at different Mach numbers for various altitude $ZpRef$.

The behavior at the left of the bucket looks more or less as an arc of hyperbole and the behavior at the right can be matched by an oblique asymptote, so we selected a rational function to merge those two effects in one single expression:

$$SFC = \frac{1 + k_1 \left(\frac{Fn}{k_0} + k_2 \left(\frac{Fn}{k_0} \right)^2 \right)}{1 + \frac{Fn}{k_0}}, \tag{A.26}$$

where:

- k_0 is the parameter that controls the bucket thrust,
- k_1 is the parameter that controls the bucket SFC,
- k_2 is the parameter that controls the flatness (by the way of the oblique asymptote).

In addition, the SFC at zero thrust has been anchored to 1 as this part of the curve has poor contribution to the final result. This choice simplifies the expression of the function. In reality, only the evolution of $Bucket_{SFC}$ and $Bucket_{Thrust}$ are known, so only two parameters can be tuned. This is not a problem because flatness is an arbitrary characteristic that can be adjusted a posteriori. As a result of this, the parameter k_2 will be fixed to the default value of 0.001 which seems to fit with quite a lot of engines. The parameter k_1 will control the level of SFC at the bucket and the parameter k_0 will control the bucket thrust. Following formulas are giving the expressions of these parameters:

$$k_0 = 0.001, \tag{A.27}$$

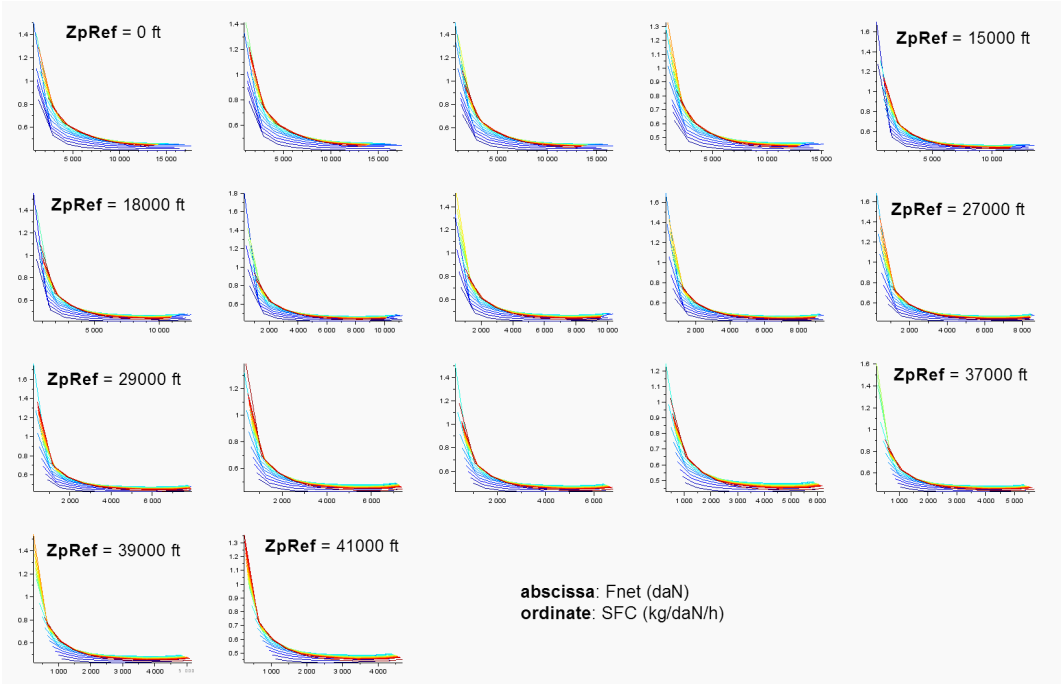

Figure A.10: Graphs presenting SFC_{factor} as a function of the $Thrust$ at different Mach numbers for various altitude.

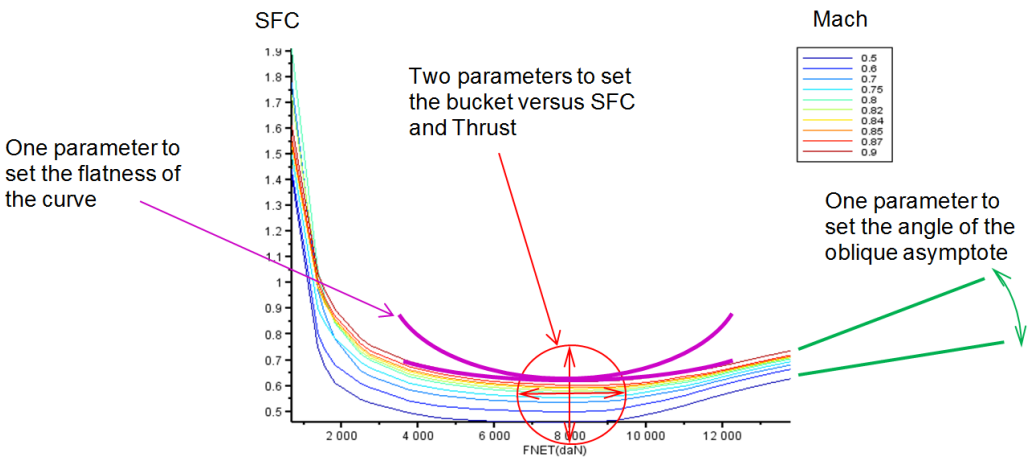

Figure A.11: Selection of the parameters driving the SFC behavior as a function of the Thrust.

$$k_1 = Bucket_{SFC} - 2\sqrt{k_0(1 - Bucket_{SFC})}, \tag{A.28}$$

$$k_2 = \frac{Bucket_{Thrust}}{\sqrt{1 + \frac{(1-k1)}{k_0}} - 1}. \tag{A.29}$$

The graph from Figure A.12 shows the contribution of different terms when $Bucket_{Thrust} =$

20000 N and $Bucket_{SFC} = 0.6$. By gathering all the components described above, we

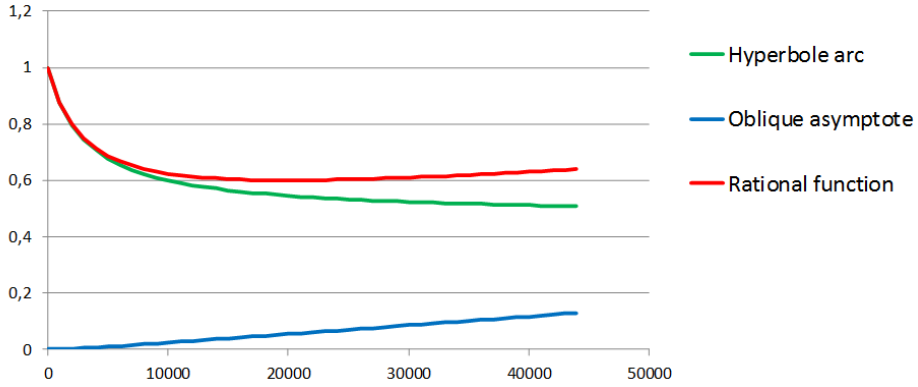

Figure A.12: Contribution of the hyperbole and the asymptotic term in the expression of SFC versus the thrust.

obtain the final model for Specific fuel consumption:

Equation	**Name & Goal**
$Bucket_{SFC}^{(Ref)} = 1.03 \times \dfrac{-0.026 \times BPR + 0.76}{36000} \times kSFC^{(Ref)},$	Reference bucket SFC
$[P_{std}, T_{std}] = f_{atmosphere}(0, ZpRef),$	Cruise altitude standard conditions
$[P_{amb}, T_{amb}] = f_{atmosphere}(0, Zp),$	Current altitude conditions
$SFC_{factor}^{(0)} = \left(1 + 0.2 \times CruiseMach^2\right)^{4.1} \times \left(\dfrac{T_{std}}{T_0}\right)^{0.6},$	Reference cruise SFC factor
$SFC_{factor}^{(1)} = \left(1 + 0.2 \times Mach^2\right)^{4.1} \times \left(\dfrac{T_{amb}}{T_0}\right)^{0.6},$	Current SFC factor
$SFC_{factor} = \dfrac{SFC_{factor}^{(1)}}{SFC_{factor}^{(0)}},$	Factor capturing Zp & Mach dependencies
$Bucket_{SFC} = \left(Bucket_{SFC}^{(Ref)} \times SFC_{factor}\right) \times kSFC,$	Bucket SFC in current conditions
$Bucket_{Thrust} = Bucket_{Thrust}^{(Ref)} \times \dfrac{P_{amb}}{P_{std}},$	Bucket thrust in current conditions
$Ksi = 0.001,$	Flatness $(0 < Ksi < 1)$
$\zeta = Bucket_{SFC} - 2\sqrt{Ksi \times (1 - Bucket_{SFC})},$	Adapt level of SFC
$k_0 = \dfrac{Bucket_{Thrust}}{\sqrt{1 + \dfrac{1-\zeta}{Ksi}} - 1},$	Adapt bucket thrust
$SFC = \dfrac{1 + \zeta\dfrac{Fn}{k_0} + Ksi\left(\dfrac{Fn}{k_0}\right)^2}{1 + \dfrac{Fn}{k_0}},$	Rational function

In the last expressions:

- T_0 is equal to 288.15 Kelvin,

- T_{amb} is the ambient temperature,
- T_{std} is the standard temperature at cruise altitude,
- P_{amb} is the ambient pressure,
- P_{std} is the standard pressure at cruise altitude,
- $f_{atmosphere}(\Delta_{isa}, Z)$ is the function computing the pressure and the temperature at a given altitude Z and in Δ_{isa} conditions (see [22]),
- $CruiseMach$ is the reference cruise Mach,
- $Mach$ is the current Mach,
- Fn is the current nominal thrust,
- $ZpRef$ is the reference cruise altitude,
- Zp is the current cruise altitude,
- BPR is the engine by-pass ratio,
- SFC is the Specific Fuel Consumption,
- $kThrust^{(Ref)}$, $kSFC^{(Ref)}$, $kSFC$ and Ksi are calibration factors which are used to match a given engine model.

The shape of SFC curve evolves as presented in Figure A.13: when altitude, Mach and thrust vary, this behavior is very similar to what can be observed on most of real turbofans.

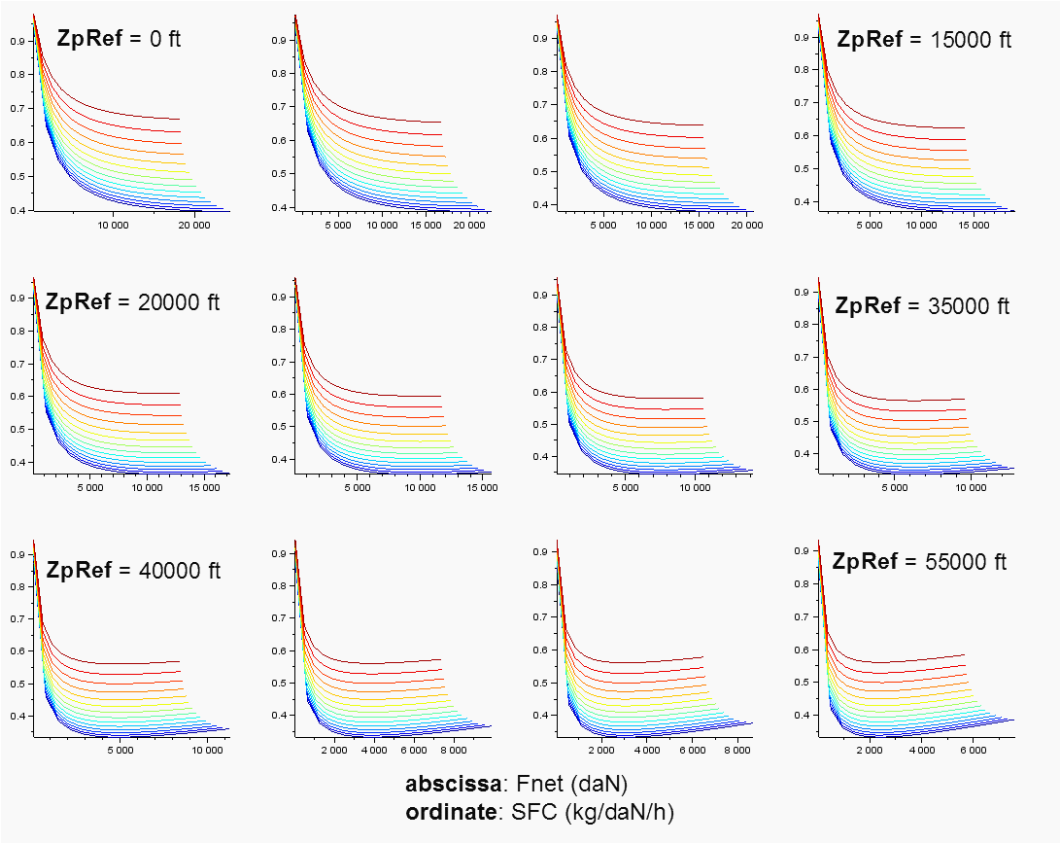

Figure A.13: Graphs presenting SFC as a function of the $Thrust$ at different Mach numbers for various altitude.

Appendix B

Preliminary aircraft design deterministic optimization

This appendix presents the numerical results of the following approach of the deterministic optimization of the hybrid aircraft. The first step is to observe the impact of the additional synergies on the optimization of the basic hybrid aircraft (with the first 7 dofs), which is presented in the first section. The second step is to observe the increasing number of dofs on the hybrid aircraft with all the synergies, which is presented in the second section.

B.0.4 Impact of the synergies on the 7 design variables optimized aircraft

The result of this approach are presenting in the table from Figure B.1 and graph from Figure B.2.

	Unit	Number of synergies			
		0	1	2	3
WingArea	m2	172,1	169,5	166,5	167,4
SLSThrust	daN	9 341	9 036	9 359	9 367
ElecRatio	no_dim	***0,01***	***0,01***	0,03	0,04
eFanPower	MW	***2***	***2***	***2***	***2***
eFanSize	m	***1***	***1***	***1***	***1***
OWE	kg	44 807	43 667	43 355	43 384
DesignMTOW	kg	75 198	74 126	73 537	73 184
StepMisFuelBlock	kg	9 149	9 266	8 994	8 722
CashOpCost	$/trip	7 588	7 556	7 542	7 464
APGWP	1e-6.W/m2/km/year	0,228	0,218	0,224	0,212
Tofl1	m	1 749	1 776	1 752	1 736
ExtTofl1	m	737	750	745	731
LdSpeed1	kt	120	120	120	120
ClbVz1	ft/min	433	385	438	426
CrzVz1	ft/min	149	100	151	138
TimeToClimb	min	22,4	23,7	22,1	22,4
eTONthrust	daN		*1 077*	*1 077*	*1 077*

Figure B.1: Design variables and performances of the optimized hybrid aircraft for the 7 dofs optimization, with the increasing number of synergies, with respect to the MTOW.

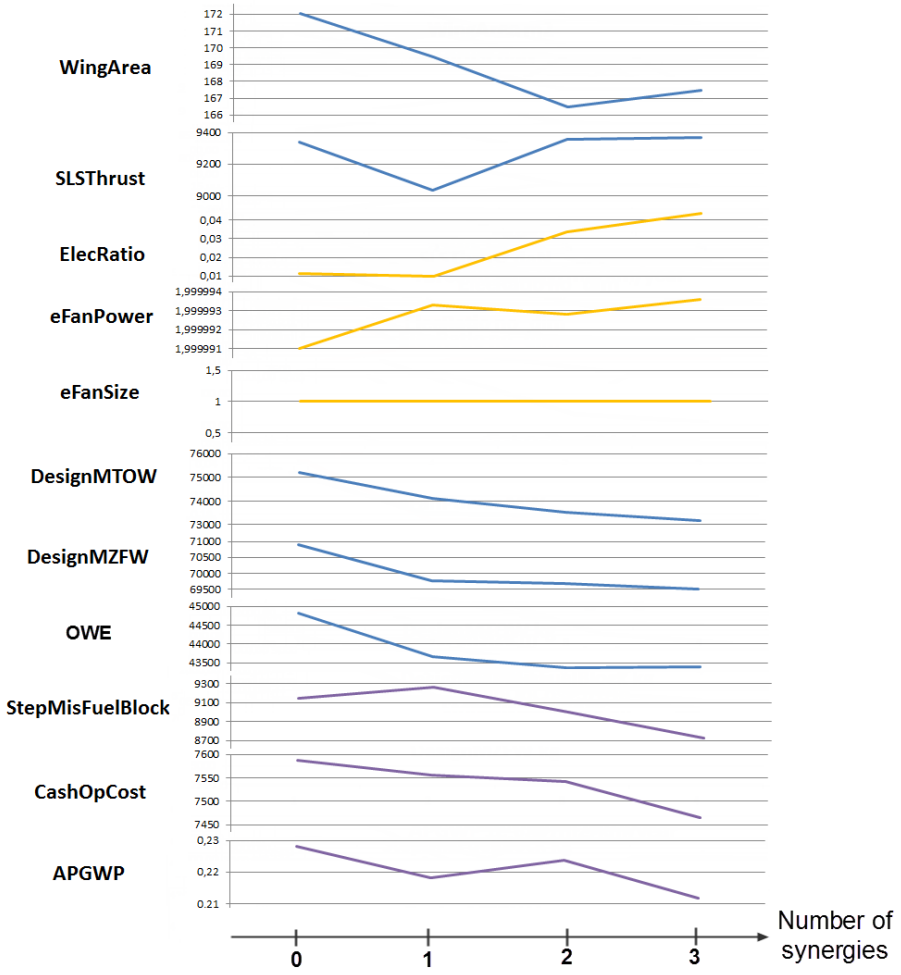

Figure B.2: Hybrid aircraft optimization graphs with the increasing number of synergies, for the 7 dofs optimization, with respect to the MTOW.

B.0.5 Impact of the increasing number of design variables on the all-synergies optimized aircraft

The result of this approach are presenting in the table from Figure B.3 and graph from Figure B.4.

	Unit	Number of degrees of freedom			
		7	9	11	16
WingArea	m2	167,4	160,1	132,7	130,8
SLSThrust	daN	9 367	8 868	8 180	8 198
WingAR	no_dim	9	12,49	15,96	14,98
BPR	no_dim	9	***12***	***12***	***12***
ZpRef	ft	35 000	35 000	25 175	25 095
CruiseMach	mach	0,76	0,76	0,65	0,65
StepMisVcas0	kt	250	250	250	***250***
StepMisVcas1	kt	250	250	250	264
StepMisVcas2	kt	250	250	250	240
StepMisVcas3	kt	270	270	270	***200***
StepMisVcas4	kt	250	250	250	***200***
ElecRatio	no_dim	0,04	***0,01***	***0,01***	***0,01***
eFanPower	MW	2	1,54	1,54	1,54
eFanSize	m	***1***	1,45	1,45	1,45
OWE	kg	43 384	43 129	40 591	40 102
DesignMTOW	kg	73 184	70 750	67 102	66 610
StepMisFuelBlock	kg	8 722	7 025	6 266	6 248
CashOpCost	$/trip	7 464	7 162	7 476	7 492
APGWP	1e-6.W/m2/km/year	0,212	0,192	0,189	0,187
Tofl1	m	1 736	1 751	2 000	2 000
ExtTofl1	m	731	697	791	808
LdSpeed1	kt	120	120	120	120
ClbVz1	ft/min	426	407	1074	1100
CrzVz1	ft/min	138	105	729	758
TimeToClimb	min	22,4	22,9	20,1	18,6

Figure B.3: Design variables and performances of the optimized hybrid aircraft with all synergies, with the increasing number of dofs, with respect to the MTOW.

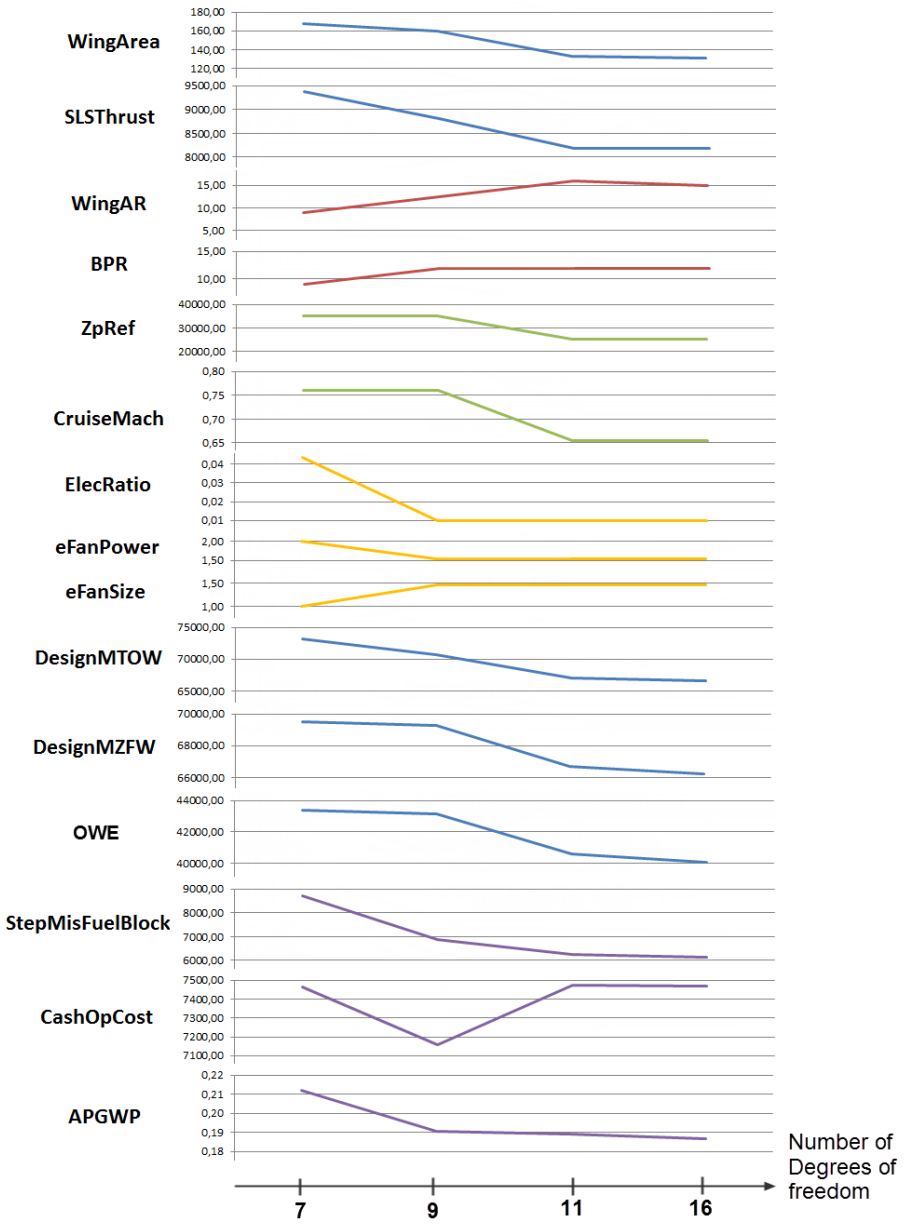

Figure B.4: Hybrid aircraft all-synergies optimization graphs with increasing number of dofs, with respect to the MTOW.

Appendix C

Robust counterpart of the uncertain optimization problem

This appendix is dedicated to the conversion of the uncertain optimization problem to its equivalent robust counterpart. Let us define: $P_k = \frac{\zeta_k^{sup} - \zeta_k^{inf}}{2}$. We have the following equivalences:

$$
\begin{aligned}
&\forall (A,b,c,d) \in \mathcal{U}\text{:} \begin{cases} \forall i = 1,\dots,m,\ a_i^\top X \leq b_i, \\ c^\top X - t \leq -d, \end{cases} \\
&\Leftrightarrow \forall (A,b,c,d) \in \mathcal{U}\text{:} \begin{cases} \forall i = 1,\dots,m,\ \sum_{j=1}^n a_{i,j} \cdot x_j \leq b_i, \\ \sum_{j=1}^n c_j \cdot x_j - t \leq -d, \end{cases} \\
&\Leftrightarrow \forall \xi \in [-1,1]^L\text{:} \begin{cases} \forall i = 1,\dots,m,\ \sum_{j=1}^n \hat{a}_{i,j}^{(0)} \cdot x_j + \sum_{j=1}^n P_{i,j}^{(a)} \cdot \xi_{i,j} \cdot x_j \leq \hat{b}_i^{(0)} + P_i^{(b)} \cdot \xi_b, \\ \sum_{j=1}^n \hat{c}_j^{(0)} \cdot x_j + \sum_{j=1}^n P_j^{(c)} \cdot \xi_j \cdot x_j - t \leq -\hat{d}^{(0)} - P^{(d)} \cdot \xi_d, \end{cases} \\
&\Leftrightarrow \forall \xi \in [-1,1]^L\text{:} \begin{cases} \forall i = 1,\dots,m,\ \sum_{j=1}^n \xi_{i,j} \cdot P_{i,j}^{(a)} x_j - \xi_b \cdot P_i^{(b)} \leq \hat{B}_i^{(0)}, \\ \xi_d \cdot P^{(d)} + \sum_{j=1}^n \xi_j \cdot P_j^{(c)} x_j \leq \hat{D}^{(0)}, \end{cases} \\
&\Leftrightarrow \begin{cases} \forall i = 1,\dots,m,\ \sum_{j=1}^n \max\limits_{-1 \leq \xi_{i,j} \leq 1} \left[\xi_{i,j} \cdot P_{i,j}^{(a)} x_j \right] - \min\limits_{-1 \leq \xi_b \leq 1} \left[\xi_b \cdot P_i^{(b)} \right] \leq \hat{B}_i^{(0)}, \\ \max\limits_{-1 \leq \xi_d \leq 1} \left[\xi_d \cdot P^{(d)} \right] + \sum_{j=1}^n \max\limits_{-1 \leq \xi_j \leq 1} \left[\xi_j \cdot P_j^{(c)} x_j \right] \leq \hat{D}^{(0)}, \end{cases} \\
&\Leftrightarrow \begin{cases} \forall i = 1,\dots,m,\ \sum_{j=1}^n P_{i,j}^{(a)} \left| x_j \right| + P_i^{(b)} \leq \hat{B}_j^{(0)}, \\ P^{(d)} + \sum_{j=1}^n P_j^{(c)} \left| x_j \right| \leq \hat{D}^{(0)}, \end{cases} \\
&\Leftrightarrow \exists u \in \mathbb{R}^n\text{:} \begin{cases} \forall j = 1,\dots,n,\ \left| x_j \right| \leq u_j, \\ \forall i = 1,\dots,m,\ \sum_{j=1}^n P_{i,j}^{(a)} u_j + P_i^{(b)} \leq \hat{B}_i^{(0)}, \\ \sum_{j=1}^n P_j^{(c)} u_j + P^{(d)} \leq \hat{D}^{(0)}, \end{cases} \\
&\Leftrightarrow \begin{cases} \forall j = 1,\dots,n,\ x_j - u_j \leq 0, \\ \forall j = 1,\dots,n,\ -x_j - u_j \leq 0, \\ \forall i = 1,\dots,m,\ \sum_{j=1}^n P_{i,j}^{(a)} u_j + P_i^{(b)} \leq \hat{B}_i^{(0)}, \\ \sum_{j=1}^n P_j^{(c)} u_j + P^{(d)} \leq \hat{D}^{(0)}, \end{cases}
\end{aligned}
$$

$$
\begin{aligned}
&\Leftrightarrow \begin{cases} \forall j = 1, \dots, n,\ x_j - u_j \leq 0, \\ \forall j = 1, \dots, n,\ -x_j - u_j \leq 0, \\ \forall i = 1, \dots, m,\ \sum_{j=1}^{n} P_{i,j}^{(a)} u_j + \sum_{j=1}^{n} \hat{a}_{i,j}^{(0)} \cdot x_j + P_i^{(b)} - \hat{b}_i^{(0)} \leq 0, \\ \sum_{j=1}^{n} P_j^{(c)} u_j + \sum_{j=1}^{n} \hat{c}_j^{(0)} \cdot x_j - t + P^{(d)} + \hat{d}^{(0)} \leq 0, \end{cases} \\
&\Leftrightarrow A\tilde{X} \leq b.
\end{aligned}
$$

In the above equations we have: $\tilde{\mathbf{X}} = \left(X^\top, t, \mathbf{u}^\top\right)^\top$, and:

$$
\begin{aligned}
&\forall i = 1, \dots, m\ ,\ \hat{B}_i^{(0)} = \hat{b}_i^{(0)} - \sum_{j=1}^{n} \hat{a}_{i,j}^{(0)} \cdot x_j, \\
&\hat{D}^{(0)} = -\hat{d}^{(0)} - \sum_{j=1}^{n} \hat{c}_j^{(0)} \cdot x_j + t, \\
&\mathbf{C}' = (0, \dots, 0, 1, 0, \dots, 0)^\top \in \mathbb{R}^{2n+1}, \\
&\mathbf{A} = \begin{pmatrix} I_n & 0_n & -I_n \\ -I_n & 0_n & I_n \\ \hat{A^{(0)}} & 0_m & P^{(a)} \\ \hat{\mathbf{C}^{(0)}}^\top & -1 & \mathbf{P^{(c)}} \end{pmatrix} \in \mathbb{R}^{(2n+m+1)\times(2n+1)}, \\
&\mathbf{b} = \left(0_{1\times 2n}, \hat{\mathbf{b}}^{(0)} - \mathbf{P^{(b)}}, -P^{(d)} - \hat{d}^{(0)}\right)^\top \in \mathbb{R}^{(2n+m+1)}, \\
&\hat{\mathbf{A}^{(0)}} = \begin{pmatrix} \hat{a}_{1,1}^{(0)} & \dots & \hat{a}_{1,n}^{(0)} \\ \vdots & \dots & \vdots \\ \hat{a}_{m,1}^{(0)} & \dots & \hat{a}_{m,n}^{(0)} \end{pmatrix}\ ,\ \mathbf{P^{(a)}} = \begin{pmatrix} P_{1,1}^{(a)} & \dots & P_{1,n}^{(a)} \\ \vdots & \dots & \vdots \\ P_{m,1}^{(a)} & \dots & P_{m,n}^{(a)} \end{pmatrix}, \\
&\hat{\mathbf{C}^{(0)}} = (\hat{c}_1^{(0)}, \dots, \hat{c}_n^{(0)})\ ,\ \mathbf{P^{(c)}} = (P_1^{(c)}, \dots, P_n^{(c)})^\top, \\
&\hat{\mathbf{b}^{(0)}} = (\hat{b}_1^{(0)}, \dots, \hat{b}_m^{(0)})\ ,\ \mathbf{P^{(b)}} = (P_1^{(b)}, \dots, P_m^{(b)}).
\end{aligned}
$$

Bibliography

[1] R. Abgrall, P. M. Congedo, G. Geraci, and G. Iaccarino. Decomposition of high-order statistics. Research Report v1, hal-00766853 RR-8193, `https://hal.inria.fr/hal-00766853`, Dec. 2012.

[2] M. Abramowitz and I. A. Stegun. *Handbook of mathematical functions: with formulas, graphs, and mathematical tables*. Number 55. Courier Dover Publications, 1972.

[3] M. A. Abramson and C. Audet. Convergence of mesh adaptive direct search to second-order stationary points. *SIAM Journal on Optimization*, 17(2):606–619, 2006.

[4] W. V. Ackooij and R. Henrion. Gradient formulae for nonlinear probabilistic constraints with gaussian and gaussian-like distributions. *SIAM Journal on Optimization*, (24):1864–1889, 2014.

[5] F. O. S. . L. A. Airbus. Getting to grips with aircraft performances. `http://www.skybrary.aero/bookshelf/books/2263.pdf`, 2002.

[6] G. Airbus. Flying on demand, airbus global market forecast 2014–2033. *Toulouse*, 2014.

[7] A. Andriy, K. Antti, and M. P. et al. Simple approach for distribution selection in the pearson system. *Helsinki School of Economics*, 2005.

[8] C. Annis. Why the "most probable point" isn't. `http://www.statisticalengineering.com/limit_state.htm`. 2014.

[9] P. Artzner, F. Delbaen, J.-M. Eber, and D. Heath. Coherent measures of risk. *Mathematical finance, Wiley Online Library*, 9(3):203–228, 1999.

[10] S. W. M. Au-yeung. Finding probability distributions from moments. Technical report, MSc Degree in Computing Science of the University of London, 2003.

[11] C. Audet and J. E. Dennis Jr. Mesh adaptive direct search algorithms for constrained optimization. *SIAM Journal on optimization*, 17(1):188–217, 2006.

[12] C. Badufle. *Définition conceptuelle d'avions: vers une optimisation multi-objectif, robuste et incertaine*. PhD thesis, University of Toulouse III - Paul Sabatier, 2007.

[13] A. Bassi and S. De Marchi. A scilab radial basis functions toolbox. `http://www.openeering.com/sites/default/files/RBF_toolbox_Scilab.pdf`, 2012. Universita degli Studi di Padova.

[14] S. L. Baughcum, T. G. Tritz, S. C. Henderson, and D. C. Pickett. *Scheduled civil aircraft emission inventories for 1992: Database development and analysis*. National Aeronautics and Space Administration, Langley Research Center, 1996.

[15] M. Belleville. Simple hybrid propulsion model for hybrid aircraft design space exploration. `https://hal.archives-ouvertes.fr/hal-01120080`, MEA 2015, Feb. 2015. hal-01120080 v1.

[16] A. Ben-Tal, L. El Ghaoui, and A. Nemirovski. *Robust optimization*. Princeton University Press, 2009.

[17] A. Ben-Tal and A. Nemirovski. *Lectures on modern convex optimization: analysis, algorithms, and engineering applications*, volume 2. MPS-SIAM Series on Optimization, 2001.

[18] D. Bertsimas, G. J. Lauprete, and A. Samarov. Shortfall as a risk measure: properties, optimization and applications. *Journal of Economic Dynamics and Control, Elsevier*, 28(7):1353–1381, 2004.

[19] H.-G. Beyer and B. Sendhoff. Robust optimization–a comprehensive survey. *Computer methods in applied mechanics and engineering, Elsevier*, 196(33):3190–3218, 2007.

[20] H.-G. Beyer and B. Sendhoff. Robust optimization–a comprehensive survey. *Computer methods in applied mechanics and engineering, Elsevier*, 196(33):3190–3218, 2007.

[21] J. R. Birge and F. Louveaux. *Introduction to stochastic programming*. Springer, 2011.

[22] J. Birman. *Uncertainty quantification and propagation in Conceptual Aircraft Design: from deterministic optimization to chance constrained optimization*. PhD thesis, University of Toulouse III - Paul Sabatier, september 2013.

[23] C. H. Bischof, P. D. Hovland, and B. Norris. On the implementation of automatic differentiation tools. *Higher-Order and Symbolic Computation, Springer*, 21(3):311–331, 2008.

[24] L. Blackmore, M. Ono, and B. C. Williams. Chance-constrained optimal path planning with obstacles. *Robotics, IEEE Transactions on*, 27(6):1080–1094, 2011.

[25] G. Blatman. *Adaptive sparse polynomial chaos expansions for uncertainty propagation and sensitivity analysis*. Phd thesis, Clermont-Ferrand 2, 2009.

[26] T. Bonk. A new algorithm for multi-dimensional adaptive numerical quadrature. In *Adaptive Methods—Algorithms, Theory and Applications*, pages 54–68. Springer, 1994.

[27] J.-F. Bonnans, J. C. Gilbert, C. Lemaréchal, and C. A. Sagastizábal. *Numerical optimization: theoretical and practical aspects*. Springer, 2006.

[28] A. J. Booker, J. Dennis Jr, P. D. Frank, D. B. Serafini, V. Torczon, and M. W. Trosset. A rigorous framework for optimization of expensive functions by surrogates. *Structural optimization, Springer*, 17(1):1–13, 1999.

[29] G. E. Box and D. R. Cox. An analysis of transformations. *Journal of the Royal Statistical Society. Series B (Methodological), JSTOR*, pages 211–252, 1964.

[30] H. Brass and K. Petras. *Quadrature Theory: The Theory of Numerical Integration on a Compact Interval*. Mathematical surveys and monographs. American Mathematical Society, 2011.

[31] F. P. Bretherton, R. E. Davis, and C. Fandry. A technique for objective analysis and design of oceanographic experiments applied to mode-73. *Deep Sea Research and Oceanographic Abstracts*, 23(7):559 – 582, 1976.

[32] M. D. Buhmann. Radial basis functions. `http://journals.cambridge.org/article_S0962492900000015`, Acta Numerica 2000, 1 2000.

[33] K. Bury. *Statistical Distributions in Engineering*. Cambridge University Press, cambridge books online edition, 1999.

[34] R. H. Byrd, M. E. Hribar, and J. Nocedal. An interior point algorithm for large-scale nonlinear programming. *SIAM Journal on Optimization*, 9(4):877–900, 1999.

[35] R. Byrne, A. Charnes, W. W. Cooper, and K. Kortanek. A chance-constrained approach to capital budgeting with portfolio type payback and liquidity constraints and horizon posture controls. *Journal of Financial and Quantitative Analysis, Cambridge Univ Press*, 2(04):339–364, 1967.

[36] J. Čerbáková. Worst-case var and cvar. In *Operations Research Proceedings 2005*, pages 817–822. Springer, 2006.

[37] G. Chamberlain. A characterization of the distributions that imply mean—variance utility functions. *Journal of Economic Theory, Elsevier*, 29(1):185–201, 1983.

[38] A. Charnes and W. W. Cooper. Chance-constrained programming. *Management science, INFORMS*, 6(1):73–79, 1959.

[39] J. Clément. *Optimisation multidisciplinaire: étude théorique et application à la conception des avions en phase d'avant projet*. PhD thesis, ISAE Toulouse, 2009.

[40] C. W. Clenshaw and A. R. Curtis. A method for numerical integration on an automatic computer. *Numerische Mathematik, Springer*, 2(1):197–205, 1960.

[41] M. Clerc and P. Siarry. Une nouvelle métaheuristique pour l'optimisation difficile: la méthode des essaims particulaires. *J3eA, EDP Sciences*, 3:007, 2004.

[42] E. Commission et al. Flightpath 2050. europe's vision for aviation. Report of the High Level Group on Aviation Research, Publications Office of the European Union, Luxembourg, 2011.

[43] P. M. Congedo, R. Abgrall, and G. Geraci. On the use of the Sparse Grid techniques coupled with Polynomial Chaos. Research Report, inria-00579205 v1 RR-7579, `https://hal.inria.fr/inria-00579205`, Mar. 2011.

[44] P. M. Congedo, J. Witteveen, and G. Iaccarino. A simplex-based numerical framework for simple and efficient robust design optimization. *Computational Optimization and Applications, Springer*, 56(1):231–251, 2013.

[45] A. R. Conn, K. Scheinberg, and L. N. Vicente. *Introduction to derivative-free optimization*, volume 8. Siam, 2009.

[46] H. Cramér. *Mathematical methods of statistics*. Asia Publishing House, 1946.

[47] N. Cressie. Fitting variogram models by weighted least squares. *Journal of the International Association for Mathematical Geology, Springer*, 17(5):563–586, 1985.

[48] J. Dahn. Electrically rechargeable metal-air batteries compared to advanced lithium-ion batteries. *Dalhousie University, Canada*, 2009.

[49] G. B. Dantzig. Linear programming under uncertainty. *Management science, INFORMS*, 1(3-4):197–206, 1955.

[50] K. Deb. *Multi-objective optimization using evolutionary algorithms*, volume 16. John Wiley & Sons, 2001.

[51] K. Deb, A. Pratap, S. Agarwal, and T. Meyarivan. A fast and elitist multiobjective genetic algorithm: Nsga-ii. *Evolutionary Computation, IEEE Transactions on*, 6(2):182–197, 2002.

[52] B. J. Debusschere, H. N. Najm, P. P. Pébay, O. M. Knio, R. G. Ghanem, and O. P. Le Maître. Numerical challenges in the use of polynomial chaos representations for stochastic processes. *SIAM Journal on Scientific Computing*, 26(2):698–719, 2004.

[53] J. Dennis and V. Torczon. Managing approximation models in optimization. *Multidisciplinary design optimization: State-of-the-art, Philadelphia, PA: SIAM*, pages 330–347, 1997.

[54] J. Dréo, A. Pétrowski, P. Siarry, and E. Taillard. *Métaheuristiques pour l'optimisation difficile, Eyrolles*. 2003. Paris.

[55] X. Du and W. Chen. A most probable point-based method for efficient uncertainty analysis. *Journal of Design and Manufacturing Automation, Taylor & Francis*, 4(1):47–66, 2001.

[56] X. Du and W. Chen. Sequential optimization and reliability assessment method for efficient probabilistic design. *Journal of Mechanical Design*, page 126(2):225, 2004.

[57] J. Dupačová. Applications of stochastic programming under incomplete information. *Journal of Computational and Applied Mathematics, Elsevier*, 56(1):113–125, 1994.

[58] R. Duvigneau, M. Martinelli, P. Chandrashekarappa, et al. Uncertainty quantification for robust design. *Multidisciplinary Design Optimization in Computational Mechanics*, 2010.

[59] M. S. Eldred. Desing under uncertainty employing stochastic expansion methods. *International Journal for Uncertainty Quantification*, 1(2):119–146, 2011.

[60] M. S. Eldred and J. Burkardt. Comparison of non-intrusive polynomial chaos and stochastic collocation methods for uncertainty quantification. *Proceedings of* 47^{th} *AIAA Aerospace Sciences Meeting and Exhibit*, (AIAA-2009-0976), 2009.

[61] S. L. Ellison, M. Rosslein, A. Williams, et al. Quantifying uncertainty in analytical measurement. In *Quantifying uncertainty in analytical measurement*. Eurachem/CITAC Guide CG4, 2012.

[62] D. H. Evans. Statistical tolerancing: the state of the art, part 2. *Journal of Quality Technology*, 7(1):1–12, 1975.

[63] V. D. F. and P. Y. I. Improvement of the unilateral 3σ-rule for unimodal distributions. *Dokl. Akad. Nauk Ukr. SSR, Ser. A., no. 1, pp. 6-8.*, 1985.

[64] W. Gautschi. Orthogonal polynomials: applications and computation. *Acta numerica, Cambridge Univ Press*, 5:45–119, 1996.

[65] W. Gautschi and S. E. Notaris. Gauss–kronrod quadrature formulae for weight functions of bernstein–szegö type. *Journal of Computational and Applied Mathematics, Elsevier*, 25(2):199–224, 1989.

[66] W. Gautschi and T. J. Rivlin. A family of gauss-kronrod quadrature formulae. *Mathematics of computation*, 51(184):749–754, 1988.

[67] A. Geletu, M. Klöppel, H. Zhang, and P. Li. Advances and applications of chance-constrained approaches to systems optimisation under uncertainty. *International Journal of Systems Science, Taylor & Francis*, 44(7):1209–1232, 2013.

[68] A. Geletu, M. Klöppel, H. Zhang, and P. Li. Advances and applications of chance-constrained approaches to systems optimisation under uncertainty. *International Journal of Systems Science, Taylor & Francis*, 44(7):1209–1232, 2013.

[69] A. Geletu, M. Klöppel, H. Zhang, and P. Li. Advances and applications of chance-constrained approaches to systems optimisation under uncertainty. *International Journal of Systems Science, Taylor & Francis*, 44(7):1209–1232, 2013.

[70] A. Gelman. Method of moments using monte carlo simulation. *Journal of Computational and Graphical Statistics, Taylor & Francis*, 4(1):36–54, 1995.

[71] T. Gerstner. Sparse grid quadrature methods for computational finance. *Habilitation, University of Bonn*, 2007. Citeseer.

[72] T. Gerstner and M. Griebel. Numerical integration using sparse grids. *Numerical algorithms, Springer*, 18(3-4):209–232, 1998.

[73] T. Gerstner and M. Griebel. Dimension–adaptive tensor–product quadrature. *Computing, Springer*, 71(1):65–87, 2003.

[74] P. Goovaerts. *Geostatistics for natural resources evaluation*. Oxford university press, 1997.

[75] A. Griewank et al. On automatic differentiation. *Mathematical Programming: recent developments and applications, Amsterdam*, 6:83–107, 1989.

[76] B. Hamma. Local and global behavior of moving polytope algorithms. *CERFACS, Toulouse, France, Tech. Report TR/PA/97/39*, 1997.

[77] M. A. Hanson. On sufficiency of the kuhn-tucker conditions. *Journal of Mathematical Analysis and Applications, Elsevier*, 80(2):545–550, 1981.

[78] B. Hegerty, C.-C. Hung, and K. Kasprak. A comparative study on differential evolution and genetic algorithms for some combinatorial problems. In *Proceedings of 8th Mexican International Conference on Artificial Intelligence*, 2009.

[79] M. Hegland. Adaptive sparse grids. *Anziam Journal*, 44:C335–C353, 2003.

[80] J. Heinrich. A guide to the pearson type iv distribution. *University of Pennsyl-vania*, 2004.

[81] R. Henrion. Introduction to chance-constrained programming. *Tutorial paper for the Stochastic Programming Community Home Page*, 2004.

[82] R. Henrion. Some remarks on value-at-risk optimization. *International Journal of Management Science and Engineering Management, Taylor & Francis*, 1(2):111–118, 2006.

[83] R. Henrion. Gradient estimates for gaussian distribution functions: Application to probabilistically constrained optimization problems. *Humboldt-Universität zu Berlin, Mathematisch-Naturwissenschaftliche Fakultät II, Institut für Mathematik*, 2012.

[84] R. Henrion, P. Li, A. Möller, M. C. Steinbach, M. Wendt, and G. Wozny. *Stochastic optimization for operating chemical processes under uncertainty.* Springer, 2001.

[85] R. Henrion and W. Römisch. Metric regularity and quantitative stability in stochastic programs with probabilistic constraints. *Mathematical Programming, Springer*, 84(1):55–88, 1999.

[86] M. Holtz. Sparse grid quadrature. In *Sparse Grid Quadrature in High Dimensions with Applications in Finance and Insurance*, volume 77, pages 51–76. Springer Berlin Heidelberg, 2011. Lecture Notes in Computational Science and Engineering.

[87] R. Hooke and T. A. Jeeves. Direct search solution of numerical and statistical problems. *J. ACM*, 8(2):212–229, 1961.

[88] C. Hu and B. D. Youn. Adaptive-sparse polynomial chaos expansion for reliability analysis and design of complex engineering systems. *Structural and Multidisciplinary Optimization, Springer-Verlag*, 43(3):419–442, 2011.

[89] C. Hume. Leea: Low emissions effect aircrat final report. Internal Airbus, 2008.

[90] W. Hurlimann. Analytical bounds for two value-at-risk functionals. *Astin bulletin*, 32(2):235–265, 2002.

[91] P. Jäckel. A note on multivariate gauss-hermite quadrature. `http://www.pjaeckel.webspace.virginmedia.com/ANoteOnMultivariateGaussHermiteQuadrature.pdf`, 2005.

[92] L. Jaeger. *Optimisation multidisciplinaire sous incertitude en phase conceptuelle avion.* PhD thesis, University of Toulouse III - Paul Sabatier, 2013.

[93] R. Jin, X. Du, and W. Chen. The use of metamodeling techniques for optimization under uncertainty. *Structural and Multidisciplinary Optimization, Springer*, 25(2):99–116, 2003.

[94] P. Jorion. *Value at risk: the new benchmark for managing financial risk*, volume 2. McGraw-Hill New York, 2007.

[95] K. L. Judd. *Numerical methods in economics*. MIT press, 1998.

[96] Z. Kajee-Bagdadi. *Differential evolution algorithms for constrained global optimization*. PhD thesis, Faculty of Science, University of the Witwatersrand, Johannesburg, 2007.

[97] P. Kali and S. W. Wallace. *Stochastic programming*. Springer, 1994.

[98] N. Karmarkar. A new polynomial-time algorithm for linear programming. In *Proceedings of the sixteenth annual ACM symposium on Theory of computing*, pages 302–311. ACM, 1984.

[99] S. Kirkpatrick, M. Vecchi, et al. Optimization by simmulated annealing. *Science, Washington*, 220(4598):671–680, 1983.

[100] D. G. Krige. *A Statistical Approach to Some Mine Valuation and Allied Problems on the Witwatersrand*. Journal of Chemical, Metallurgical, and Mining Society of South Africa, 1951.

[101] J. C. Lagarias, J. A. Reeds, M. H. Wright, and P. E. Wright. Convergence properties of the nelder–mead simplex method in low dimensions. *SIAM Journal on optimization*, 9(1):112–147, 1998.

[102] J. Laurenceau and P. Sagaut. Building efficient response surfaces of aerodynamic functions with kriging and cokriging. *AIAA journal*, 46(2):498–507, 2008.

[103] S. Lee and W. Chen. A comparative study of uncertainty propagation methods for black-box-type problems. *Structural and Multidisciplinary Optimization, Springer-Verlag*, 37(3):239–253, 2009. `http://dx.doi.org/10.1007/s00158-008-0234-7`.

[104] T. W. Lee and B. M. Kwak. A reliability-based optimal design using advanced first order second moment method. *Journal of Structural Mechanics, Taylor & Francis*, 15(4):523–542, 1987.

[105] Y.-z. Lei, W.-s. Wang, Y.-h. Yin, and H.-z. DAI. Wind power penetration limit calculation based on chance constrained programming [j]. *Proceedings of the Csee*, 5:006, 2002.

[106] P. Lewis and E. McKenzie. *Simulation methodology for statisticians, operations analysts, and engineers*, volume 1. CRC press, 1988.

[107] R. M. Lewis, V. Torczon, and M. W. Trosset. Direct search methods: then and now. *Journal of Computational and Applied Mathematics*, 124(1–2):191 – 207, 2000. Numerical Analysis 2000. Vol. IV: Optimization and Nonlinear Equations.

[108] D. S. M. Basil, C. Papadopoulos and H. Yeung. Application of probabilistic uncertainty methods (monte-carlo simulation) in flow measurement uncertainty estimation. *Flow Measurement international conference*, 2001.

[109] H. Markowitz. Portfolio selection*. *The journal of finance, Wiley Online Library*, 7(1):77–91, 1952.

[110] R. T. Marler and J. S. Arora. Survey of multi-objective optimization methods for engineering. *Structural and multidisciplinary optimization, Springer*, 26(6):369–395, 2004.

[111] K. Marti. *Stochastic optimization methods*. Springer, 2005.

[112] G. Matheron. Principles of geostatistics. *Economic geology, Society of Economic Geologists*, 58(8):1246–1266, 1963.

[113] M. G. Morgan and M. Henrion. Uncertainty: A guide to dealing with uncertainty in quantitative risk and policy analysis. *Cambridge University Press*, 1990.

[114] W. J. Morokoff and R. E. Caflisch. Quasi-monte carlo integration. *Journal of Computational Physics*, 122(2):218 – 230, 1995.

[115] J. A. Nelder and R. Mead. A simplex method for function minimization. *The computer journal, Br Computer Soc*, 7(4):308–313, 1965.

[116] A. Nemirovski and A. Shapiro. Convex approximations of chance constrained programs. *SIAM Journal on Optimization*, 17(4):969–996, 2006.

[117] H. Niederreiter. *Random number generation and quasi-Monte Carlo methods*, volume 63. SIAM.

[118] T. Nilsen and T. Aven. Models and model uncertainty in the context of risk analysis. *Reliability Engineering & System Safety, Elsevier*, 79(3):309–317, 2003.

[119] T. Nilsen and T. Aven. Models and model uncertainty in the context of risk analysis. *Reliability Engineering & System Safety, Elsevier*, 79(3):309–317, 2003.

[120] E. Novak and K. Ritter. High dimensional integration of smooth functions over cubes. *Numerische Mathematik, Springer*, 75(1):79–97, 1996.

[121] W. L. Oberkampf, T. G. Trucano, and C. Hirsch. Verification, validation, and predictive capability in computational engineering and physics. *Applied Mechanics Reviews, American Society of Mechanical Engineers*, 57(5):345–384, 2004.

[122] S. Oladyshkin and W. Nowak. Data-driven uncertainty quantification using the arbitrary polynomial chaos expansion. *Reliability Engineering & System Safety*, 106(0):179 – 190, 2012.

[123] M. J. Orr et al. Introduction to radial basis function networks. Technical Report, Center for Cognitive Science, University of Edinburgh, 1996.

[124] M. Padulo. Computational engineering design under uncertainty: an aircraft conceptual design perspective. *Cranfield University*, 2009.

[125] M. Padulo, M. S. Campobasso, and M. D. Guenov. Novel uncertainty propagation method for robust aerodynamic design. *AIAA Journal*, 49(3):530–543, 2011.

[126] M. Padulo, M. S. Campobasso, M. D. Guenov, et al. Comparative analysis of uncertainty propagation methods for robust engineering design. *Guidelines for a Decision Support Method Adapted to NPD Processes*, 2007.

[127] M. Padulo and J. Delbove. A risk-based approach to aircraft design optimization. page Internal Airbus number PR1416492. 4th International Conference on Engineering Optimization, 2014.

[128] M. Padulo and M. D. Guenov. Worst-case robust design optimization under distributional assumptions. *Int. J. Numer. Meth. Engng.*, 88:797–816, 2011.

[129] M. Padulo and M.-S. Liou. A minmax framework for robust design optimization. 10^{th} *World congress on structural and multidisciplinary optimization, Orlando (FL)*, 2013.

[130] K. Pearson. Contributions to the mathematical theory of evolution. ii. skew variation in homogeneous material. *Philosophical Transactions of the Royal Society of London, JSTOR*, pages 343–414, 1895.

[131] K. Pearson. Method of moments and method of maximum likelihood. *Biometrika, JSTOR*, pages 34–59, 1936.

[132] J. E. Penner. *Aviation and the global atmosphere: a special report of IPCC Working Groups I and III in collaboration with the Scientific Assessment Panel to the Montreal Protocol on Substances that Deplete the Ozone Layer*. Cambridge University Press, 1999.

[133] I. Pinelis. Between chebyshev and cantelli. *ArXiv e-prints 1011.6065*, nov 2010.

[134] A. Plas, M. Sargeant, V. Madani, D. Crichton, E. Greitzer, T. Hynes, and C. Hall. Performance of a boundary layer ingesting (bli) propulsion system. 45th American Institute of Aeronautics and Astronautics Aerospace Sciences Meeting and Exhibit, Reno, NV, (pp. 8-11), January 2007.

[135] I. Popescu. A semidefinite programming approach to optimal-moment bounds for convex classes of distributions. *Mathematics of Operations Research, INFORMS*, 30(3):632–657, 2005.

[136] W. P.P. and F. P. *Gas Turbine Performance, Second Edition*. Blackwell Science Limited, 2004.

[137] A. Prékopa. A class of stochastic programming decision problems. *Statistics: A Journal of Theoretical and Applied Statistics, Taylor & Francis*, 3(5):349–354, 1972.

[138] A. Prékopa. Logarithmic concave measures and related topics. In *Stochastic Programming*. Citeseer, 1980.

[139] A. Prékopa. *Stochastic Programming*. Mathematics and Its Applications. Springer Netherlands, 1995.

[140] A. Prékopa. On the concavity of multivariate probability distribution functions. *Operations research letters, Elsevier*, 29(1):1–4, 2001.

[141] S. Prigent, M. Belleville, T. Druot, A. Rondepierre, and P. Maréchal. Chance constrained business case of a three-engines hybrid aircraft. 10^{th} *World congress on structural and multidisciplinary optimization, Orlando (FL)*, 2013.

[142] S. Prigent, P. Maréchal, A. Rondepierre, T. Druot, and M. Belleville. A robust optimization methodology for preliminary aircraft design. *Engineering Optimization*, 2015.

[143] H. Putter, G. A. Young, et al. On the effect of covariance function estimation on the accuracy of kriging predictors. *Bernoulli Society for Mathematical Statistics and Probability*, 7(3):421–438, 2001.

[144] N. V. Queipo, R. T. Haftka, W. Shyy, T. Goel, R. Vaidyanathan, and P. K. Tucker. Surrogate-based analysis and optimization. *Progress in aerospace sciences, Elsevier*, 41(1):1–28, 2005.

[145] S. Rahman and D. Wei. A univariate approximation at most probable point for higher-order reliability analysis. *International Journal of Solids and Structures*, 43(9):2820 – 2839, 2006.

[146] S. Rahman and H. Xu. A univariate dimension-reduction method for multi-dimensional integration in stochastic mechanics. *Probabilistic Engineering Mechanics*, 19(4):393 – 408, 2004.

[147] L. B. Rall. *Automatic differentiation: Techniques and applications*, volume 120. Springer, 1981.

[148] R. T. Rockafellar and S. Uryasev. Optimization of conditional value-at-risk. *Journal of risk*, 2:21–42, 2000.

[149] R. T. Rockafellar, S. Uryasev, and M. Zabarankin. Optimality conditions in portfolio analysis with general deviation measures. *Mathematical Programming, Springer*, 108(2-3):515–540, 2006.

[150] J. Roskam. *Airplane Design: Part 2 - Preliminary Configuration Design and Integration of the Propulsion System*. DARcorporation, 1985.

[151] E. Roux. *Modèles Moteurs: réacteurs double flux civils et réacteurs militaires à faible taux de dilution avec Post-Combustion*. INSA-ISAE-ONERA, 2002.

[152] T. W. Ruefli. Mean-variance approaches to risk-return relationships in strategy: Paradox lost. *Management Science*, 36(3):368–380, 1990.

[153] S. Samson. *Performance based decisions under uncertainty and risk*. ProQuest, 2008.

[154] P. A. Samuelson. The fundamental approximation theorem of portfolio analysis in terms of means, variances and higher moments. *The Review of Economic Studies, JSTOR*, pages 537–542, 1970.

[155] Scilab Enterprises. *Scilab: Le logiciel open source gratuit de calcul numérique*. Scilab Enterprises, Orsay, France, 2012.

[156] T. M. Sellke and S. H. Sellke. Chebyshev inequalities for unimodal distributions. *The American Statistician, Taylor & Francis*, 51(1):34–40, 1997.

[157] S. Shan and G. Wang. Survey of modeling and optimization strategies to solve high-dimensional design problems with computationally-expensive black-box functions. *Structural and Multidisciplinary Optimization, Springer-Verlag*, 41(2):219–241, 2010.

[158] P. Simon. Storage technologies including trends for batteries and super-capacitors for power quality and energy management improvement. *Technology Watch Energy Battery Topic, Airbus*, 2012.

[159] T. Simpson, J. Poplinski, P. N. Koch, and J. Allen. Metamodels for computer-based engineering design: Survey and recommendations. *Engineering with Computers, Springer-Verlag*, 17(2):129–150, 2001.

[160] S. Smolyak. Quadrature and interpolation formulas for tensor products of certain classes of functions. *Soviet Mathematics, Doklady*, 4:240–243, 1963.

[161] G. Taguchi. Performance analysis design. *The international journal of production research, Taylor & Francis*, 16(6):521–530, 1978.

[162] M. Tari and A. Dahmani. Refined descriptive sampling: A better approach to monte carlo simulation. *Simulation Modelling Practice and Theory*, 14(2):143 – 160, 2006.

[163] M. Tichỳ. First-order third-moment reliability method. *Structural Safety, Elsevier*, 16(3):189–200, 1994.

[164] V. Torczon. On the convergence of pattern search algorithms. *SIAM Journal on optimization*, 7(1):1–25, 1997.

[165] E. Torenbeek. *Synthesis of subsonic airplane design: an introduction to the preliminary design of subsonic general aviation and transport aircraft, with emphasis on layout, aerodynamic design, propulsion and performance*. Springer Science & Business Media, 1982.

[166] B. Trahmer. Overall aircraft preliminary design training. *Airbus, Toulouse*, 2012.

[167] L. N. Trefethen. Is gauss quadrature better than clenshaw-curtis? *SIAM review*, 50(1):67–87, 2008.

[168] S. Uryasev. Derivatives of probability functions and some applications. *Annals of Operations Research, Springer*, 56(1):287–311, 1995.

[169] S. Uryasev. *Probabilistic constrained optimization: methodology and applications*, volume 49. Springer Science & Business Media, 2000.

[170] S. Uryasev. Var vs cvar in risk management and optimization. CARISMA conference, 2010.

[171] M. H. van der Vlerk. Stochastic programming bibliography. *World Wide Web, http://www.eco.rug.nl/mally/spbib.html*, 2007.

[172] I. Vanderplaats Research & Development. Dot - design optimization tools. `https://www.vrand.com/DOT.html`.

[173] H. Wackernagel. *Multivariate geostatistics*. Springer, 2003.

[174] A. Waechter, C. Laird, F. Margot, and Y. Kawajir. Introduction to ipopt: A tutorial for downloading, installing, and using ipopt, 2009.

[175] G. G. Wang and S. Shan. Review of metamodeling techniques in support of engineering design optimization. *Journal of Mechanical Design, American Society of Mechanical Engineers*, 129(4):370–380, 2007.

[176] A. Wächter and L. T. Biegler. On the implementation of an interior-point filter line-search algorithm for large-scale nonlinear programming. *Mathematical Programming, Springer-Verlag*, 106(1):25–57, 2006.

[177] M. Wendt, P. Li, and G. Wozny. Nonlinear chance-constrained process optimization under uncertainty. *Industrial & engineering chemistry research, ACS Publications*, 41(15):3621–3629, 2002.

[178] M. Wendt, P. Li, and G. Wozny. Nonlinear chance-constrained process optimization under uncertainty. *Industrial & engineering chemistry research, ACS Publications*, 41(15):3621–3629, 2002.

[179] N. Wiener. The homogeneous chaos. *American Journal of Mathematics, JSTOR*, pages 897–936, 1938.

[180] D. Xiu. Fast numerical methods for stochastic computations: a review. *Communications in computational physics*, 5(2-4):242–272, 2009.

[181] D. Xiu and G. Em Karniadakis. Modeling uncertainty in steady state diffusion problems via generalized polynomial chaos. *Computer Methods in Applied Mechanics and Engineering, Elsevier*, 191(43):4927–4948, 2002.

[182] H. Xu and S. Rahman. A generalized dimension-reduction method for multidimensional integration in stochastic mechanics. *International Journal for Numerical Methods in Engineering, John Wiley & Sons, Ltd*, 61(12):1992–2019, 2004.

[183] X. Yin and W. Chen. Enhanced sequential optimization and reliability assessment method for probabilistic optimization with varying design variance. *Structures and Infrastructure Engineering, Taylor & Francis*, 2(3-4):261–275, 2006.

[184] J. L. Zhou and A. L. Tits. User's guide for fsqp version 3.0 c: A fortran code for solving constrained nonlinear (minimax) optimization problems, generating iterates satisfying all inequality and linear constraints. 1992.

AUTHOR: Sylvain Prigent

TITLE: Innovated and integrated approach for environmentally efficient aircraft design and operations

SUPERVISORS: Pierre Maréchal and Aude Rondepierre

PLACE AND DATE OF THE DEFENSE: INSA de Toulouse (France), 17/09/2015

ABSTRACT: The objective of this PhD work is to pose, investigate, and solve the highly multidisciplinary and multiobjective problem of environmentally efficient aircraft design and operation. In this purpose, the main three drivers for optimizing the environmental performance of an aircraft are the airframe, the engine, and the mission profiles. The figures of merit, which will be considered for optimization, are fuel burn, local emissions, global emissions, and climate impact (noise excluded). The study will be focused on finding efficient compromise strategies and identifying the most powerful design architectures and design driver combinations for improvement of environmental performances. The modeling uncertainty will be considered thanks to rigorously selected methods. A hybrid aircraft configuration is proposed to reach the climatic impact reduction objective.

KEYWORDS: Modeling, Optimization, Aircraft Design, Uncertainty Propagation, Chance Constrained Optimization, Robust Optimization.

ADMINISTRATIVE FIELD: Applied Mathematics (Optimization, Aeronautics)

AUTEUR : Sylvain Prigent

TITRE : Approche novatrice pour la conception et l'exploitation d'avions écologiques

DIRECTION DE THESE : Pierre Maréchal et Aude Rondepierre

LIEU ET DATE DE SOUTENANCE : INSA de Toulouse (France), le 17/09/2015

RESUME : L'objectif de ce travail de thèse est de poser, d'analyser et de résoudre le problème multidisciplinaire et multi-objectif de la conception d'avions plus écologiques et plus économiques. Dans ce but, les principaux drivers de l'optimisation des performances d'un avion seront: la géométrie de l'avion, son moteur ainsi que son profil de mission, autrement dit sa trajectoire. Les objectifs à minimiser considérés sont la consommation de carburant, l'impact climatique et le coût d'opération de l'avion. L'étude sera axée sur la stratégie de recherche de compromis entre ces objectifs, afin d'identifier les configurations d'avions optimales selon le critère sélectionné et de proposer une analyse de ces résultats. L'incertitude présente au niveau des modèles utilisés sera prise en compte par des méthodes rigoureusement sélectionnées. Une configuration d'avion hybride est proposée pour atteindre l'objectif de réduction d'impact climatique.

MOTS CLES : Modélisation, Optimisation, Conception avion, Propagation des incertitudes, Optimisation sous contraintes en probabilités, Optimisation robuste.

DISCIPLINE ADMINISTRATIVE : Mathématiques Appliquées (Optimisation, Aéronautique)